ABSTRACT

Title of Document:	CHARACTERIZATION AND INVESTIGATION OF BENZYLIC CARBENIUM ION AND CARBANION ION-DIRADICAL INTERMEDIATES WITH 3,5-DISUBSTIUTED π–DONORS/ACCEPTORS
	Raffaele Romano Perrotta, Doctor of Philosophy, 2012
Directed by:	Professor Daniel E. Falvey Department of Chemistry & Biochemistry

High-spin magnetic materials have been based on monomeric units that contain metals. Far less research has been done to develop and characterize alternative high-spin building blocks consisting of mostly organic subunits. To date, there exists a small class of known high-spin organomagnetic building blocks. These organic building blocks are comprised of neutral intermediates such as diradicals, nitrenes, and carbenes. The work presented in this text will show that a novel class of high-spin intermediates also exists that derives from ionic rather than neutral intermediates.

Previous density functional theory (DFT) computations by Winter and Falvey identified a number of ion-diradicals that have favorable triplet ground states. For instance, the 3,5-bis(dimethylamino)benzyl carbenium ion, and 2-(3,5-dinitrophenyl)-1,3-dithiane carbanion, have singlet-triplet energy gaps (ΔE_{ST}s) of +1.9 and +0.3 kcal/mol, respectively.

Ion-diradicals are based on a general framework whereby either an electron deficient or electron rich exocyclic center is attached to a benzene ring that contains two π-electron withdrawing or donating groups *meta* with respects to this site. The objective of chapter 2 is to identify the electronic spin state of the 3,5-bis(dimethylamino)benzyl carbenium ion. We have shown that this carbenium ion can be generated from C-O bond heterolysis of 3,5-bis(dimethylamino)benzyl esters and alcohols when photolyzed in polar protic solvents (e.g. methanol, 2-propanol, 2,2,2-trifluoroethanol). Our product studies show that indeed the 3,5-bis(dimethylamino)benzyl ethers are formed from this process, however an unexpected reduction product (3,5-bis(dimethylamino)toluene) is also observed. The reduction product here aptly demonstrates how an ion-diradical could be generated. Formal one electron transfer from a NMe_2 group to the exocyclic benzylic carbenium ion center, creates a triplet cation diradical (ion-diradical) intermediate, which eventually leads to the formation of the 3,5-bis(dimethylamino)toluene product observed in all photolysis experiments.

Chapters 4-6 investigates whether ion-diradicals can be generated from anionic exocyclic centers that have *meta* π-acceptor groups (e.g. NO_2, CN, CO_2R). Computations, NMR, UV-Vis, chemical trapping, H/D exchange, and Evans method magnetic susceptibility experiments demonstrate that the 2-(3,5-dinitrophenyl)-1,3-dithiane carbanion is a persistent and paramagnetic species. Chapters 5 and 6 focuses primarily on characterizing the electronic spin-states to similar anionic systems such as the 3,5-dinitroanilide anion, and 3,5-dinitrobenzyl methoxy ether carbanion.

CHARACTERIZATION AND INVESTIGATION OF BENZYL
CARBENIUM ION AND CARBANION ION-DIRADICAL
INTERMEDIATES WITH 3,5-DISUBSTIUTED π–DONORS/ACCEPTORS

By

Raffaele Romano Perrotta

Dissertation submitted to the Faculty of the Graduate School of the
University of Maryland, College Park, in partial fulfillment
of the requirements for the degree of
Doctor of Philosophy
2012

Advisory Committee:
Professor Daniel E. Falvey, Chair
Professor Phillip DeShong
Professor Lyle Isaacs
Professor Herman Sintim
Professor Ray Phaneuf (Dean's representative)

Dedication

The research presented in this dissertation is dedicated to my

mom (Brenda Perrotta), my dad (Victor Perrotta), and brothers

and sister Orlando, Emanuelle (Manny), and Giulietta. Without

all of your love and support throughout the years, this work

would not be possible.

Acknowledgements

      First and foremost, I would like to thank and acknowledge my advisor Dr. Daniel Falvey. For the past 5+ years I have been fortunate enough to work in his research group. Dr. Falvey's patience, constant positive feedback, and his easygoing attitude towards running his research group, has both allowed me to excel at doing my research and learning Organic chemistry. His "open door" policy when it comes to talking to his students has enabled me to talk with him about anything chemistry related. Dr. Falvey is an exceptional teacher. Thank you Dr. Falvey for teaching me so much about physical organic chemistry, especially when I was your student in Chem 641. Since I am very independent, self-motivated, and initiative orientated person/researcher, Dr. Falvey's "hands off" approach has given me the opportunity to do research at my own pace. There have been many difficult and frustrating days in the lab or doing research throughout my Ph. D career. However, Dr. Falvey always finds a way to make a negative situation like this better and for that I am very thankful.   He is always willing to talk about an interesting research project/problem or move a project in a different direction when necessary.

      I would like to give a special thanks to the Falvey group members past and present.   I appreciate and have benefited from the advice, support, and guidance provided to me over the years by former group members: Drs. Becky Vieira, Wei-Ho Huang, Brian Borak, and Art Winter. I would also like to further thank Dr. Art Winter for his immense help in collaborating on two research papers which were published out of our group recently and for helping us run some important computations. I want give a big special thanks to my current fellow graduate student group members Romina Heymann, and Derek Denning. Both of you have been good friends and collegues throughout my time in the Falvey group. Thank you guys for listening and sitting through countless practice talks for my second year seminar, candidacy, and research presentations.   Furthermore, thank you for editing and providing me feedback and advice on all my research papers, job applications, presentations, posters, my dissertation, and candidacy paper.   I am very thankful that you guys have always made the lab a pleasant place to work in and have always been there to support me in the good days and bad days. I will really miss you guys (Romina and Derek)!! I would like to thank and acknowledge all the undergraduates that have worked in our lab which I have had the pleasure of working with throughout the past 6 years. Thank you David Kunsburg, Melissa Aplan, Lok-Man Yeung, and Bill Coldren. I am extremely thankful for working with Bill Coldren who worked as an undergraduate for over 2+ years in our lab. He was immensely helpful in putting together many of the calculations performed in my research and would occasionally help out in lab as well. I learned so much about computations than I ever could imagine from you. Thanks again Bill for all your hard work through the years!

      I want to also take this opportunity to thank and acknowledge my fellow graduate students who I have got to know through my 6 years here at Maryland. I would like to first thank Dr. Max Ratnikov, Dr. Jason Nichols, and Dr. Emily McLaughlin for their help in using the Doyle group GC-MS. Moreover, I want to

Dean's representative on my committee and Dr. Sintim for teaching me so much about organic synthesis over the years.

Table of Contents

List of Tables

List of Figures[*]

_____

[*] Note: These figure titles are in some cases abbreviated or shortened titles from the lengthy captions given throughout the text.

Chapter 4, Figures.

Chapter 5, Figures.

Chapter 6, Figures.

Chapter 7, Figures.

List of Schemes

Chapter 1, Schemes.

Chapter 2, Schemes.

Chapter 3, Schemes.

Chapter 1: Introduction

1.1. The Purpose of Investigating High-Spin Ion Diradicals

The vast majority of organic compounds and intermediates are diamagnetic in nature, viewing that they have no net magnetic moment.   Benzylic carbenium ions and carbanion intermediates are just two examples of organic reactive intermediates, which have been shown to behave as ground state singlets. Since most of these intermediates are ground state singlets that are overall diamagnetic, they would not be useful in the design of new high-spin organic materials.

Currently, there exist a small class of neutral organic intermediates that have been shown to have high-spin states, such intermediates are of interest because they could be used as high-spin building blocks to develop organomagnetic materials. Diradical, carbene, and nitrene intermediates have all been previously identified as potential high-spin building blocks. In the later sections of this introduction, we will discuss these reactive intermediates in more detail.

The main objective of the work presented in this dissertation, is to identify and characterize ionic, organic reactive intermediates, which could serve as a new source of high-spin building blocks. We will show computational and experimental results, which demonstrate that several ion-diradicals have favorable triplet ground states. The ion-diradicals that we have identified and characterized as having kinetically favorable triplet ground states broadly consist of benzylic carbenium ions and carbanions. It should be clarified that the purpose of this dissertation is not to

demonstrate the direct application of these ion-diradicals into existing magnetic

materials.   Indeed, it is the purpose of this project to show that certain ion-diradical

intermediates have triplet ground states and could therefore be used as a potential new

source of high-spin, organic building blocks.   Moreover, several experimental

methods for generating and characterizing benzylic carbenium ions and carbanions

will be described in the following sections.

1.2. Generation and Characterization of Singlet Benzylic Carbenium Ions

A. Photolysis and Solvolysis of Ar-CH$_2$-X and Ar-CH$_2$-OR's

Traditionally, substituted benzyl cations have been generated and characterized

using a variety of different methods. For example, benzyl carbenium ions can be

generated through the thermal solvolysis of benzylic chlorides to yield benzylic ether

and alcohol adducts (Scheme 1.1).[1] The solvolysis reaction shown in Scheme 1.1

represents the typical behavior for most ground state singlet benzyl carbenium ions.

Scheme 1.1. Solvolysis of substituted benzylic halides
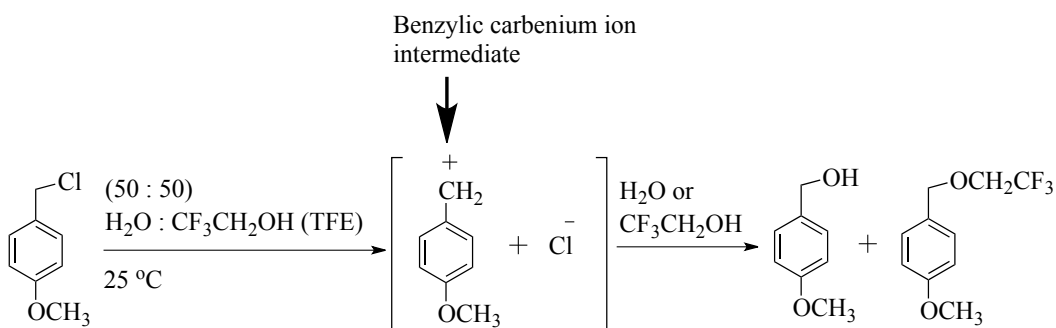
The mechanism of this reaction consists of the loss of the leaving group (Cl⁻) and the

formation of a benzyl carbenium ion intermediate. Nucleophilic trapping by the polar

protic solvent, results in effective substitution of the leaving group with the incoming

nucleophile at the benzylic position. Benzylic carbenium ions have been familiar

intermediates to all organic chemists in the past 20th century. The chemistry of

benzylic carbenium ions is described in most advanced organic chemistry textbooks,

in terms of their use in defining substituent parameters (σ^+).[2,3]

Olah, *et al.* has characterized a variety of aryl substituted benzyl carbenium

ions by ^{13}C NMR and X-ray crystallography using low temperature superacid

conditions (SbF_6, -78 $^\circ$C or below).[4,5] Again these benzylic carbenium ions are

predicted to be ground state singlets.

Another technique for generating benzylic or aryl substituted carbenium ions

Scheme 1.2. Generation of diphenylmethyl carbenium ions by photolysis of
diaryldiazomethanes
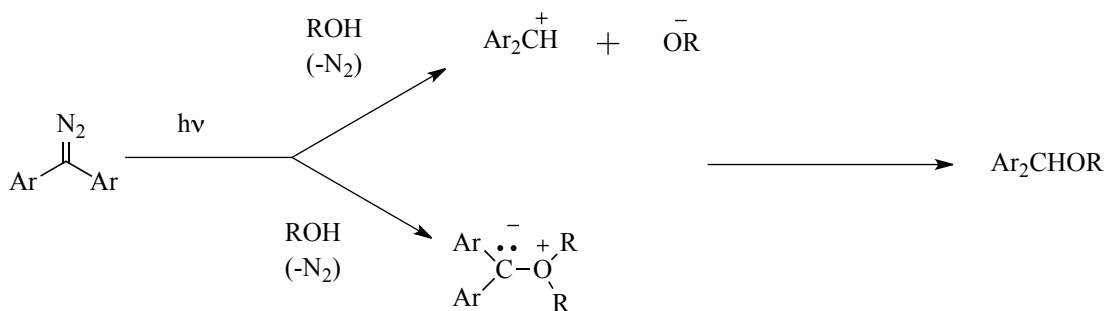
is through photolysis or laser flash photolysis (LFP). This can be done through the

photolysis of the corresponding benzylic halides, alcohols or diazo precursors.[6,7] For

instance, Bartl *et al.* are shown that the photolysis of diphenylmethyl halides,

acetates, and ethers at 254 nm results in the generation of both the diphenylmethyl

carbenium ion and the diphenylmethyl benzyl radical intermediates.[6] Kirmse and co-workers have shown similar results (Scheme 1.2) from the photolysis of diazodiarylmethanes, that directly yields the diphenylmethyl carbenium ion intermediate by LFP.[7]   There are two challenges that face most investigators when studying benzylic carbenium ions by LFP. First, most benzylic carbenium ions are generated in protic solutions (H_2O, TFE,1,1,1,3,3,3-hexafluoro-2-propanol (HFIPA)) have short lifetimes of *ca.* 1 ns making their characterization by LFP methods very challenging for most investigators.[6] Secondly, as demonstrated in work done by Bartl, *et al.* and others, the photolysis of benzyl or aryl halides yield mixtures of photoproducts and intermediates associated with competing C-X bond heterolysis and homolysis.[6]

B. The "Meta Effect"

One of the major breakthroughs in both physical organic chemistry and organic photochemistry, came in the early 1960s by Howard Zimmerman at the University of Wisconsin, Madison. The cornerstone of Zimmerman's research was the development and application of the term "*meta* effect." The general definition of the "*meta* effect" can be described by the noticeable difference in chemical reactivity between ground state chemistry and excited state chemistry. Normally, an electron deficient group attached to an aromatic ring (e.g. CH_2^+, NH^+, O^+ groups), are stabilized in the ground state through resonance, by electron donating groups (e.g. NH_2, OCH_3, etc.) in the *ortho* and/or *para* positions. Similarly, electron rich groups (e.g. NH^-, CH_2^-, O^-) adjacent to an aromatic ring are directly stabilized through resonance by electron withdrawing groups (e.g. NO_2, CN) in the *ortho* and/or *para* positions.[8-9]

Surprisingly, Zimmerman's work showed that an electron deficient group attached to an aromatic ring (e.g. CH_2^+, NH^+, O^+ groups) is stabilized in the excited state by π-electron donating groups (e.g. NH_2, OCH_3, etc.) in the *meta* position rather than in the *ortho/para* positions. The same was determined for electron rich groups adjacent to the aromatic ring which were further stabilized in the excited state by π-

Scheme 1.3. General difference in ground state vs. excited state chemical reactivity of monosubstituted nitrobenzyl carbanions

Ground state stabilization   Excited state destabilization

para

no stabilization of
exocyclic anion

Ground state stabilization   Excited state destabilization

ortho

no stabilization of
exocyclic anion

Ground state destabilization   Excited state

meta

not much stabilization in the ground state

stabilization in the excited state

5
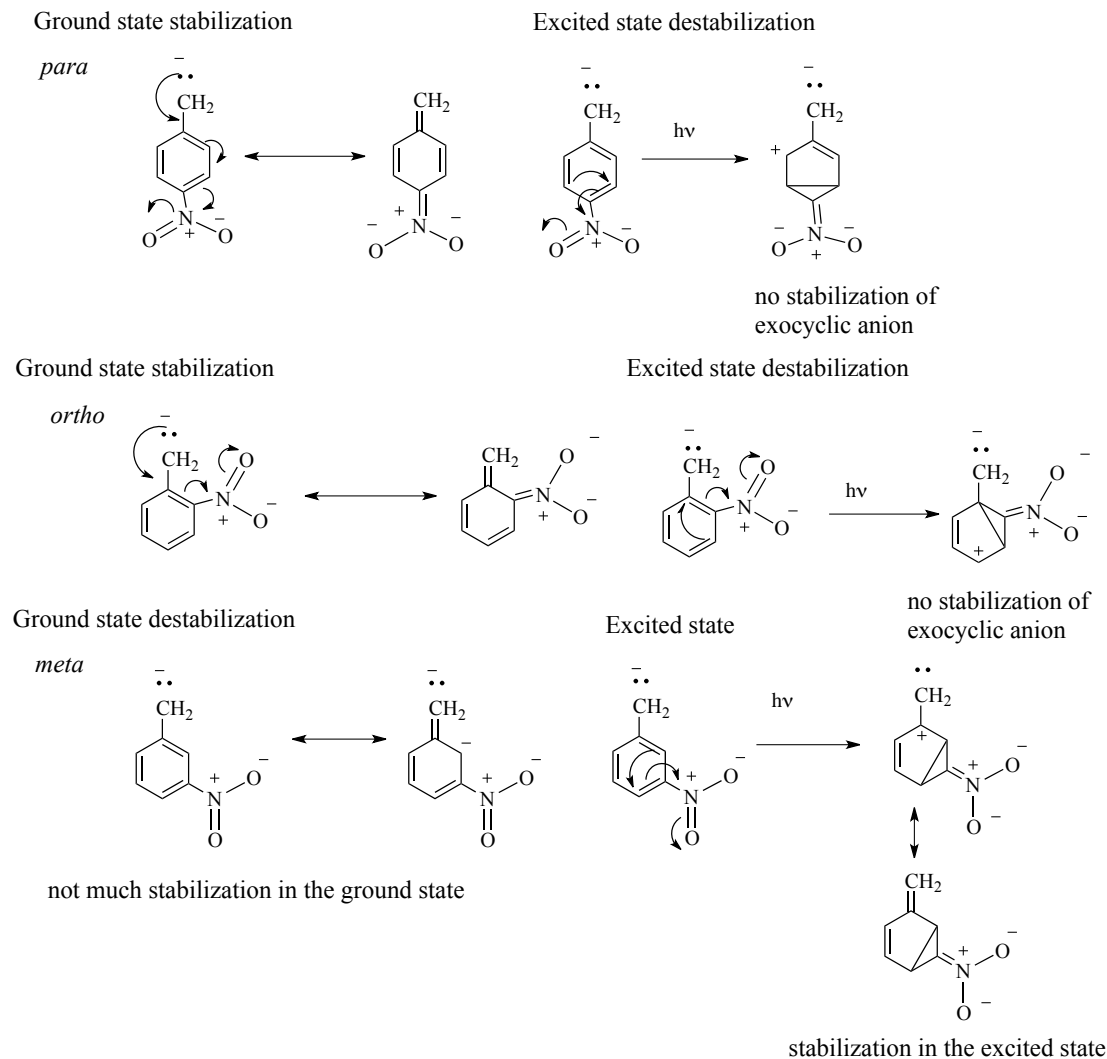
electron withdrawing groups at the *meta* position. This transmission stabilization of the charge density in the excited state by groups *meta* to the center in question, is what was coined by the scientific community as the term "*meta* effect." Zimmerman showed through both computational chemistry and photoproduct studies that the "*meta* effect" could be applied to several aromatic systems with groups that contained a *meta* relationship. The contrast between the reactivity of monsubstituted *ortho*, *meta*, and *para* benzene derivatives, with exocyclic anionic groups, is shown in Scheme 1.3.

The best illustration of the "*meta* effect" was observed by Zimmerman when comparing the products associated with the photosolvolysis of *m*-methoxybenzyl acetate, *p*-methoxybenzyl acetate, and 3,5-dimethoxybenzyl acetates. Scheme 1.4 summarizes the photoproducts observed by Zimmerman for the *m*-methoxybenzyl acetate **1**, 3,5-dimethoxybenzyl acetate **2**, and *p*-methoxybenzyl acetate **3**, in aqueous dioxane.[8-10] As one can see from Scheme 1.4, the *p*-methoxy benzyl acetate **3** gives exclusively photoadducts that resulted from C-O bond homolysis and thus yielded mostly radical products. The *m*-methoxybenzyl acetate **1** yields primarily C-O bond heterolysis products such as the *m*-methoxybenzyl alcohol. However, some radical photoproducts were observed, but only in trace amounts. The photolysis of 3,5-dimethoxybenzyl acetate **2** yielded the 3,5-dimethoxybenzyl alcohol as the only major adduct, thus indicating that C-O bond heterolysis is the major pathway from these results.

Scheme 1.4. Different photoproducts observed from the photolysis of various substituted methoxybenzyl acetates
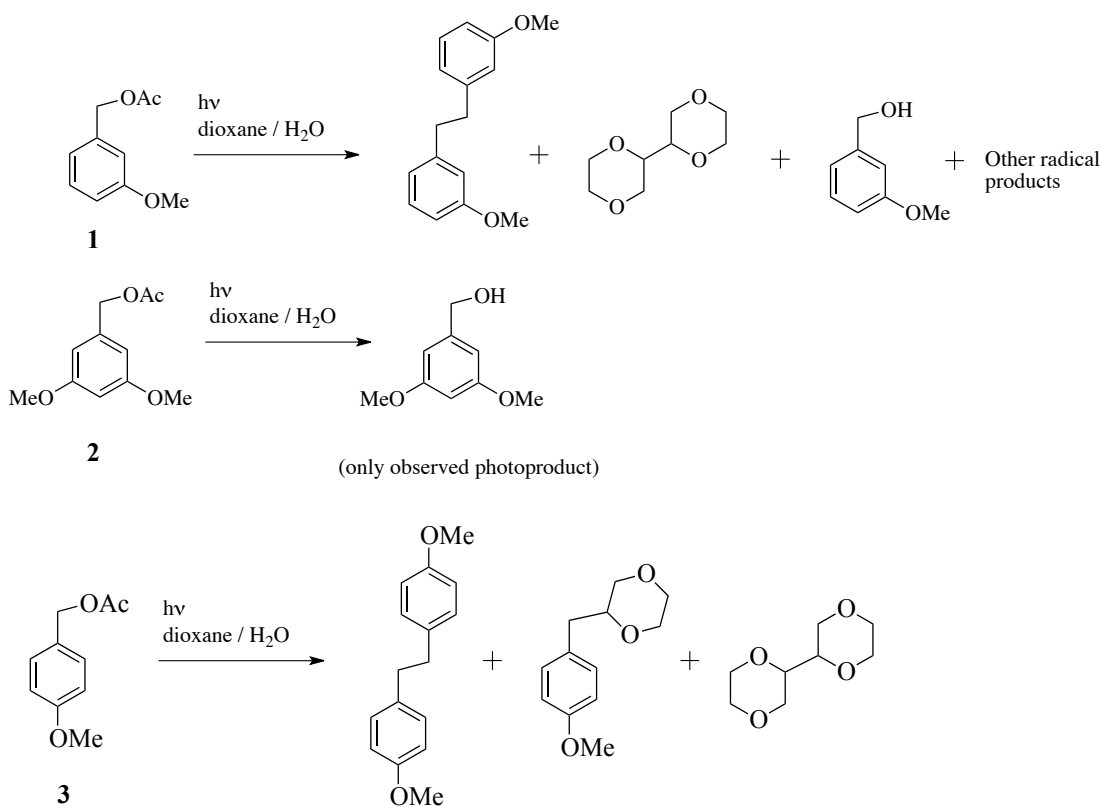
Zimmerman's findings, therefore demonstrates that the transmission effect ("*meta* effect") shown for the excited state stabilization in Scheme 1.4, must play a pivotal role in the direct stabilization of a benzylic carbenium ion intermediate, with this *meta* substitution pattern.

The research done by Zimmerman and others on the "*meta* effect" provided us with a convenient method for generating benzylic carbenium ions photochemically and will be described briefly in the context of benzylic ion-diradical intermediates later in this chapter (section 1.5), and in chapters 2 and 3.

As one might expect, carbanions like carbenium ions behave as ground state singlets. The electron rich nature of carbanions generally defines their overall chemical reactivity. Similar to most anionic species, carbanions can either act as bases or nucleophiles in substitution reactions (i.e. S_N2 reactions). Generally, carbanions are generated through deprotonation of the corresponding hydrocarbon with an appropriate strong base such as lithium diisopropyl amide (LDA), *n*-butyllithium (*n*-BuLi), methyllithium (MeLi), or *tert*-butyllithium (*t*-BuLi). Scheme 1.5 shows the prototypical behavior of a fairly simple benzylic carbanion. In the first step of the two reactions shown in Scheme 1.5, the benzylic C-H bond of the dithiane is quantatively deprotonated with *n*-BuLi. A different electropile (E^+) is then added in the second step of each of the two reactions shown in Scheme 1.5.[11] The first

Scheme 1.5. Chemical reactions of simple benzylic carbanions
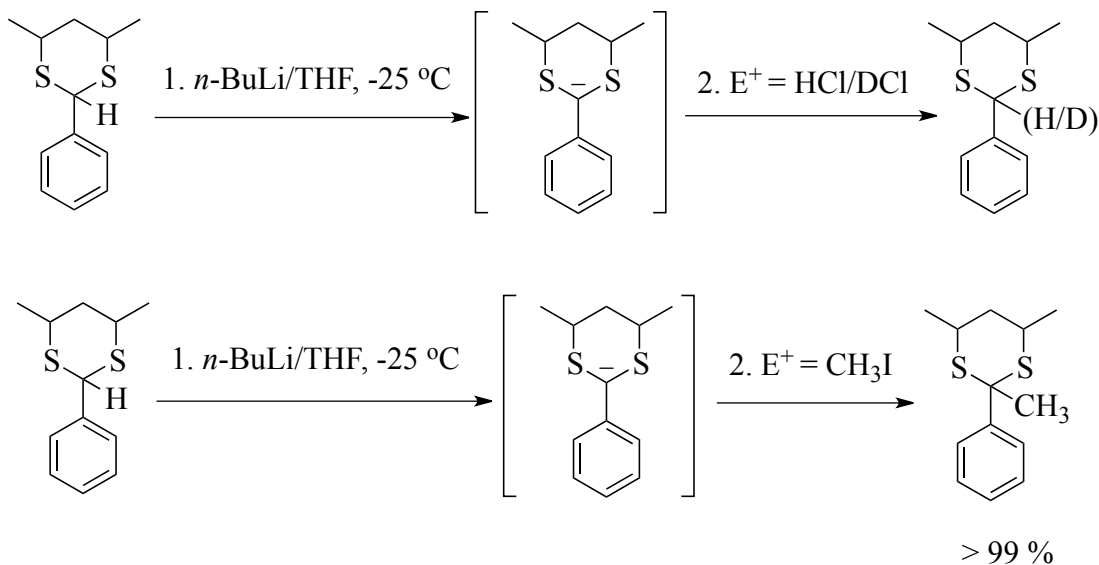
reaction in Scheme 1.5 effectively results in the replacement of the benzylic hydrogen

attached to the 1,3-dithiane ring with a deuterium atom, thereby illustrating the acid-

base chemistry associated with this carbanion. The benzylic hydrogen in the second

reaction is essentially replaced with a CH_3 group (Scheme 1.5).[11] Consequently, this

reflects how simple benzylic carbanions can also behave as nucleophiles in a S_N2

reaction. Scheme 1.5 shows an example of the chemical reactivity of only one

carbanion. It is important to note that it is beyond the scope of this dissertation, and

this section, to adequately discuss and provide a thorough review of the chemistry of

carbanion intermediates. For a more extensive review of carbanions see Moss, R. A.;

Platz, M. S.; Jones, Jr., M. *Reactive Intermediate Chemistry*, chapter 3, pp. 69-120,

Wiley and Sons: Hoboken, New Jersey, 2004.

1.4 Traditional Organic Based High-Spin Building Blocks

Presnetly, there are three main classes of neutral, organic based high-spin

building blocks that have been extensively studied by chemists in the development of

novel magnetic materials. These high-spin building blocks consist of diradicals,

triplet carbenes, and nitrenes. The sections below provide a brief introduction and

overview of each of these high-spin organic building blocks. There are two major

challenges that one must face when studying high-spin reactive intermediates such as

diradicals, carbenes, and nitrenes. The first is how to accurately identify and

characterize the electronic ground state of the intermediate, which is being

investigated. The second challenge is that most of these high-spin intermediates tend

to be very reactive. The reactive intermediates discussed in the next few sections are

similar and in some ways different from the ion-diradicals that will be discussed later in this dissertation.

A. Diradicals

The study and development of organic building blocks with high-spin states (triplet or higher) has gained wide interest in the chemistry and material science community due to their potential applications into the design of new electronic and magnetic polymeric materials.[12a-j] Nevertheless, identifying and characterizing these high-spin building blocks has proven challenging for most investigators computationally and experimentally, due to their high chemical reactivity.

Diradicals and polyradicals have been one of the most widely researched and studied class of organic high-spin building blocks in the past century. These diradicals are considered non-Kekulé structures that are defined as being π-conjugated molecules that are unable to satisfy standard valency. A few of these compounds are shown in Figure 1.1. The non-Kekulé compounds shown in Figure 1.1 (with the exception of **7** and **8**), are suitable high-spin building blocks because of the simple fact that they are all open-shell species, where the radicals in each structure can never fully achieve complete valency.

The Schlenk-Brauns hydrocarbon shown in Figure 1.1, was one of the first diradicals to be synthesized and studied by ESR spectroscopy. It was also shown to have a triplet ground state.[13,14] Accurately assigning the electronic spin states (singlet, triplet, or higher) to the compounds shown in Figure 1.1 has proven elusive

for organic chemists studying these reactive intermediates. Fortunately, advances in

electron paramagnetic (EPR) spectroscopy, rigid matrix isolation techniques, and
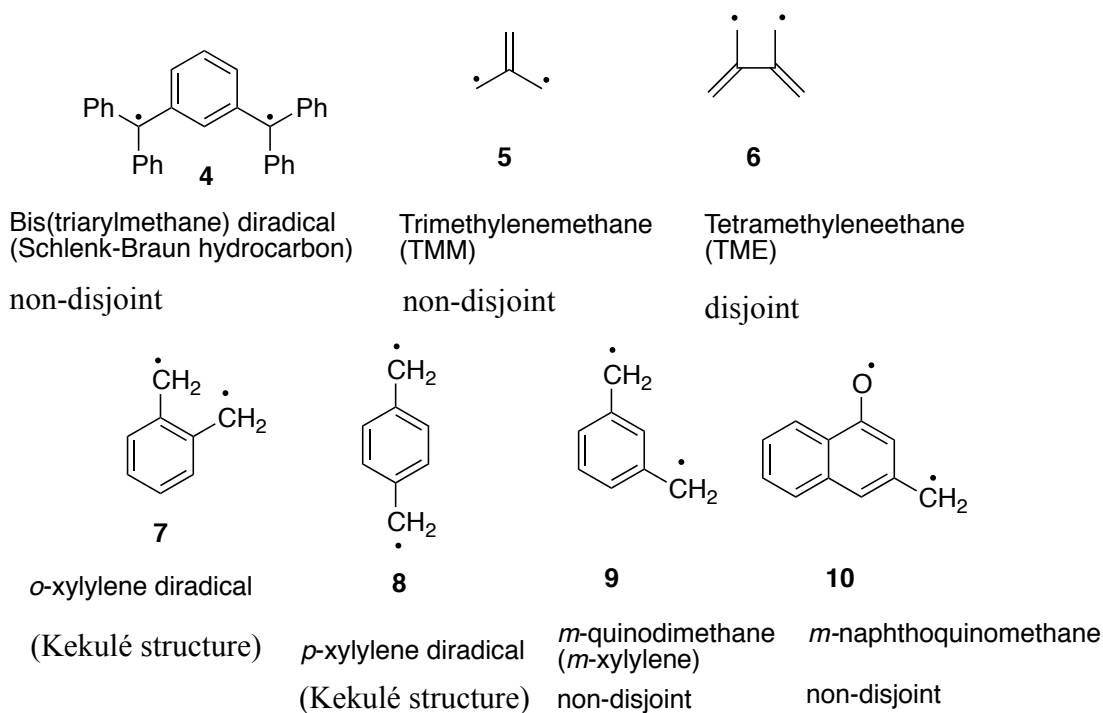
Figure 1.1. Some examples of non-Kekulé and Kekulé diradicals.

modern computational methods, have allowed chemists to accurately identify their

spin states. How does one determine the spin state of these diradicals? Diradicals fall

into two main classes. A diradical can be classified as either *disjoint* or *non-disjoint*.

Non-disjoint, non-Kekulé diradicals are defined as having electron density from the

non-bonding molecular orbitals (NMBOs) located on the same atoms. Whereas

disjoint diradicals have NBMO electron density located on different atoms.[12] Non-

disjoint diradicals such as trimethylenemethane (TMM) **5**[15], and the *m*-xylylene

diradical **9**[16,17] (Figure 1.1) are predicted to have triplet ground states because the

electron interaction of the NBMOs according to Hund's rule, would be minimized if the spins are unpaired. On the other hand, *disjoint* diradicals such as tetramethyleneethane (TME),[18] and *o*- and *p*-xylylene diradicals[19,20] are predicted to have degenerate singlet and triplet energies, due to the fact that these systems have small or close to zero electron exchange interactions for their NBMOs.

In addition to the use of molecular orbital (MO) theory to determine if a diradical is disjoint or non-disjoint, a valence bond (VB) approach can also be used for the same purpose. Valence bond (VB) theory involves the use of parity in the conjugated diradical system. A non-disjoint diradical, as a rule of thumb, has an *odd number* of π-conjugated electrons between the unpaired spin centers. If there is an *even number* of π electrons between the portion of the diradical containing the unpaired centers, then the diradical is considered to be disjoint. For instance, TMM contains 1 electron between each radical center.[21] Therefore, VB theory correctly predicts that TMM is in fact non-disjoint and a ground state triplet. For TME, there are 2 electrons between the radical centers and therefore VB theory again correctly predicts that TME is a disjoint diradical.[21]

Similar heteroatom based diradical systems have been shown to be non-disjoint and posses high-spin states. For example, *m*-quinomethane was determined to be a ground state triplet by both EPR and chemical trapping experiments.[22] Recently, Rajca, *et al.* has shown that the aza-*m*-xylylene diradical derivative in Figure 1.2 is a ground state triplet and is a persistent diradical at room temperature.[23]

The diradical in Figure 1.2 is simply an extension of the *m*-xylylene diradical, **9** described in Figure 1.1. Interestingly, the stability of the diradical in Figure 1.2 can be attributed to the steric bulk of the alkyl groups surrounding the diradical nitrogens, which efficently shields the diradical centers from readily reacting with itself or other species that might be present once it is generated.
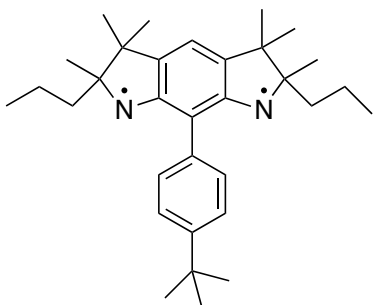
$\Delta E_{ST} = +10$ kcal/mol

Figure 1.2. A heteroatom based *m*-xylylene diradical that is persistent at room temperature.

B. Triplet Carbenes

Carbenes have been extensively investigated as reactive intermediates both experimentally and computationally. The facile generation of both singlet and triplet carbenes by the photolysis or thermolysis of their corresponding alkyl diazo or aryl diazo precursors, allows one the ability to conduct extensive studies on these reactive intermediates. Carbenes can exist in two possible electronic states. These two states consist of the singlet state where the electron spins are paired in an empty *p*–orbital on the divalent carbon center, and the triplet state, where the electron spins are each unpaired in two vacant *p*-orbitals that are orthogonal to one another. Both types of carbenes have different chemical reactivities. Singlet carbenes are known to react

stereoselectively with olefins, which makes them very useful in synthetic

methodologies. Triplet carbenes have two unpaired electron spins, and are therefore

mostly utilized in the development of new organic, high-spin, magnetic building

blocks.   As with most other reactive intermediates discussed in the previous sections,

identifying and characterizing the ground state electronic structure of carbenes is

carried out either through computational methods, laser flash photolysis (LFP), or by

low temperature EPR studies.[24]

The electronic structure and steric effects of substituents at the carbene center,

both contribute in determining its ground state configuration. Herein these concepts

will be briefly discussed.
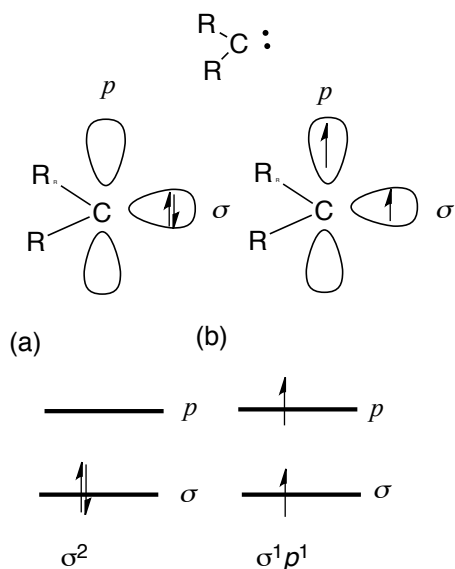
(a) Singlet configuration (b) Triplet configuration

Figure 1.3. The electronic structures of carbenes

Electronic Structure of Carbenes

Simple methylene carbenes (R = H, Figure 1.3) tend to be ground state triplets. Molecular orbital (MO) theory can be used to explain why this carbene adopts a triplet electronic configuration. Filling the MOs of the methylene carbene, we see that according to Hund's rule, the nearly degenerate non-bonding p-orbitals of the carbene (Figure 1.3a and b) would rather be occupied with a single electron of the same spin in each orbital. The filling of the MOs in this fashion, consequently leads to a triplet ground state configuration (Figure 1.3b). The electronic state and thus the relative energies of the non-bonding p-orbitals that reside on the carbene center, changes when one replaces the H attached to the carbene center with a π-electron donating group (e.g. R = OCH_3, OH, NH_2, etc.). Initially, the two electrons on the carbene center each occupy a non-bonding p-orbital with the same spin (triplet configuration). However, the addition of one or two π-electron donating group(s) results in raising the relative energy of the singly occupied p-orbital, which is in the same plane as the π-donating substituent. This is mainly due to the electron-electron repulsion between the half-filled p-orbital on the carbene and non-bonding electrons on the π-electron donating group. As a result, the p-orbitals are destabilized in the triplet state (Figure 1.3b) when π-electron donors are bonded to the carbene center.[24] The electronic destabilization of the non-bonding p-orbital in the triplet state here, causes one of the p-orbital electrons to spin flip and results in intersystem crossing from the triplet state to the singlet state (Figure 1.3a). Addition of a π-electron withdrawing group(s) (e.g. R = NO_2, CN, C(O)R', etc.) to the carbene center, consequently has the opposite electronic effect on the carbene non-bonding p-orbitals.

The energy of the non-bonding *p*-orbital in the triplet state (Figure 1.3b) is lowered when π-electron withdrawing groups are bonded to the carbene center. Therefore, the triplet state (Figure 1.3b) is favored when π-electron withdrawing groups are placed on the carbene center, whereas the singlet electronic configuration (Figure 1.3a) is destabilized by π-electron withdrawing groups on the carbene.[24]

Knowing the ground state electron configuration is crucial in determining the reactivity of the carbene. What has been discussed up to this point has been purely qualitative in nature. A more quantative approach can be achieved by looking at the relative energy difference between the singlet and triplet state of the carbene. Hence, the singlet-triplet energy gap (ΔE_{ST}) is defined as $E_S - E_T$ in this section and throughout this dissertation. Negative values for ΔE_{ST} means the singlet is the favored ground state, whereas positive values for ΔE_{ST} signifies that the triplet is the ground state.

Figure 1.4 depicts a few representative aryl substituted carbenes. As expected, π-electron donating groups that are bonded to a carbene center such as intermediate **11**, has a ground state energy gap that is close to degenerate between that of the singlet and triplet state (ΔE_{ST} = +0.7 kcal/mol, B3LYP/6-311+G**//B3LYP/6-31G*).[20] Likewise, **13** (Figure 1.4) is clearly a ground state triplet by DFT computations (ΔE_{ST} = +10.3 kcal/mol).[24] The computational results presented here, demonstrates the large electronic effects that substituents have on

predicting the overall ground state energy and the ΔE_{ST} value associated with a specific carbene intermediate.
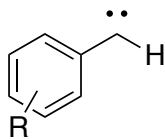
11 R = *p*-NH$_2$, ΔE_{ST} = +0.7 kcal/mol
12 R = H, ΔE_{ST} = +5.4 kcal/mol
13 R = *p*-NO$_2$, ΔE_{ST} = +10.3 kcal/mol

Figure 1.4. Some aryl substituted carbenes.

Steric Effects

The addition of bulky alkyl substituents increases the C-C-C bond angles at the carbene center and destabilizes the singlet state through steric repulsion and creates more *p* character associated with the occupied *sp²* orbital. For instance, the strained cyclopropyl carbene **14**, has bond angles of <70° and thus favors the singlet state as the ground state by a ΔE_{ST} value of -12.9 kcal/mol (Figure 1.5).[24] The addition of bulky *tert*-butyl groups destabilizes the singlet state and stabilizes the triplet state, by increasing the carbon bond angles around the carbene center. The di-*tert*-butyl carbene **15**, consequently is a ground state triplet by +5.2 kcal/mol with

14   **15**
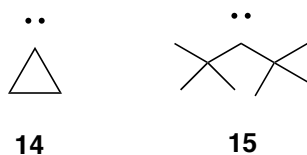
ΔE_{ST} = -12.9 kcal/mol ΔE_{ST} = +5.16 kcal/mol

Figure 1.5. Steric effects on ΔE_{ST} for carbenes.

bond angles of 125.1° for the singlet carbene, and 141.9° for the triplet, according to

computational methods.[24]

<u>Key Examples of High-Spin Carbenes</u>

Several groups have utilized the combined concepts of electronic effects of π-

electron withdrawing and bulky alkyl substituents adjacent to the carbene center, to

effectively design stabilized triplet carbene intermediates. The use of sterically bulky

alkyl groups to essentially stabilize and protect the reactivity of the triplet carbene

center was reported in work done by Tomioka, *et al.*[25,26]   EPR, LFP, UV-Vis, and

product studies were all used to identify the electronic states of **16-17** as triplets

(Figure 1.6).[25,26] Carbene **16** and **17** demonstrate how one can use large alkyl groups

16 R = Me, R' = Me   **17**

18

Figure 1.6. Some examples of high-spin (triplet or higher) carbenes.

to shield this carbene center from significantly reacting or polymerizing.   Moreover,

Itoh *et al.* has extended the concept of using carbenes as high-spin building blocks by

generating and characterizing dicarbene **18** (Figure 1.6), which is a ground state

18

quintet by ESR spectroscopy.[27] The mixed *meta*/*para* relationship of the biphenyl

rings between the 2 carbene centers of **18**, creates a fascinating effect on the

electronic structure of this dicarbene. One carbene center is *para* substituted at the

biphenyl ring, which allows the electron spins of this carbene, to be fully delocalized

throughout both the phenyl and biphenyl rings.   However, the second carbene center

is *meta* substituted to the phenyl and biphenyl rings that separates the two carbenes,

and is therefore in essence, more localized on the two phenyl rings directly adjacent

to the carbene center.

The high-spin aryl carbenes developed by Tomioka and Itoh, are just a few

examples of yet another class of persistent, organic, high-spin building blocks that

could be used to construct bulk magnetic materials.

C. Nitrenes

Electronic Structure

The third class of neutral, organic high-spin building blocks is comprised of

nitrene intermediates. Most nitrenes are generated by the photolysis of the

corresponding azide precursors. The behavior of nitrenes is generally similar to that

of carbenes. However, there are a few key differences in their chemistry compared to

that of carbenes. Nitrenes are monovalent, and thus have different MO energies

compared to that of carbenes. For example, Figure 1.7 shows the singlet and triplet

states of a typical nitrene. The nitrene has a single paired set of electrons in a

(a)

(b)

singlet nitrene

triplet nitrene
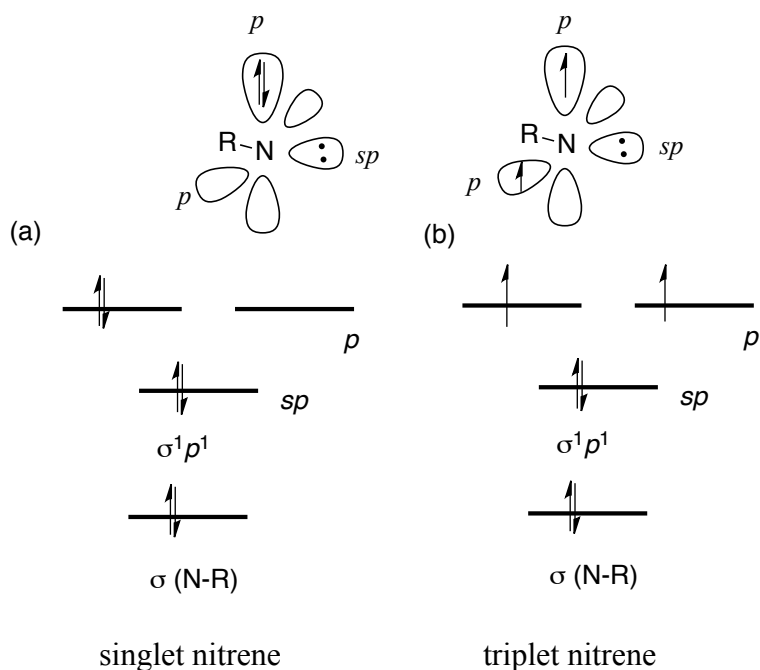
Figure 1.7. The electronic states of nitrenes.

sp orbital that is orthoganol to the other non-bonding electron pair. The other orbital

consists of either a set of paired electrons (singlet), or each electron with unpaired

spins in different orbitals (triplet). Since the nitrene is *sp* hybridized, the lowest

energy electronic state is that of the triplet (Figure 1.7b), which minimizes the

electron-electron Coulombic repulsion. This has a direct impact on the ΔE_{ST} of

nitrenes. When for instance the R group bound to the nitrene is H, the

$\Delta E_{ST} = +36$ kcal/mol, and for R = CH$_3$ the energy gap is $+31.2$ kcal/mol.[24] These

nitrenes however are typically not useful either synthetically or in the design of

magnetic materials, because it is necessary to generate them at very low temperatures

or in the gas-phase, due to their high reactivity.

For simple phenylnitrenes, the value for ΔE_{ST} drops substantially to about

+18.5 kcal/mol and starts to favor the singlet state.[28,29] The lowered singlet-triplet

energy gap is a result of one of the non-bonding electron pairs being able to

delocalize into the adjacent phenyl ring, resulting in a quinodal resonance structure.

Although the singlet-triplet energy gap is decreased for phenylnitrenes, like most

nitrenes it is still large in comparison to that of similar carbenes. As a result of this

large energy gap, most nitrenes have excess vibrational or thermal energy when they

are formed from the corresponding azides. The excess energy from the generation of

the phenylnitrene, results in a variety of different intermediates and products being

19A   **19B**
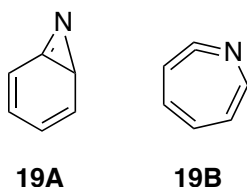
Figure 1.8. Intermediates generated from singlet nitrenes.

formed from aryl or phenylnitrenes. Two intermediates that are formed from singlet

nitrenes are azirine **19A** and ketenimine **19B** (Figure 1.8).[30]

Through photoproduct studies and laser flash photolysis (LFP), Platz, *et al.*

has shown that singlet nitrenes can be generated from the photolysis of the

corresponding 2-fluoro, 4-fluoro, 3,5-difluoro, 2,6-difluoro, and 2,3,4,5,6-pentafluoro

phenylazides.[31] Like carbenes, nitrenes are predicted to have a triplet ground state

electronic configuration. The only significant difference, is that the singlet state for

nitrenes tends to possess so much excess thermal energy, that under most conditions, it rapidly reacts before the triplet state can be observed experimentally. Most nitrenes are generated from the room temperature photolysis of the corresponding azide precursors. This initially results in the formation of a singlet nitrene, which in turn forms several rearrangement products. In certain cases, reactions from the singlet state or any rearrangement products thereof can be avoided by the photolysis of such azide precursors at cryogenic temperatures in rigid matrices. At low temperatures, one slows down most of the possible reactions caused from the initial generation of the singlet nitrene intermediate, and as a result intersystem crossing to the triplet becomes more favorable. Hence, most investigators observe products and intermediates associated the singlet state rather than those of the triplet state.

Triplet and higher spin nitrenes are more widely observed in the form of phenyl substituted dinitrenes. EPR, LFP, and product studies, have been used to identify and characterize many of these triplet nitrenes. Wasserman, *et al.* has shown that simple *m*-phenylenedinitrene **20**, is a ground state quintet by ESR spectroscopy (Figure 1.9).[32] Furthermore, Lahti and co-workers, Tomioka, *et al.* and even Sander, *et al.*, have shown EPR and spectroscopic data for many ground state quintet dinitrenes (Figure 1.9).[33-35] These are just a few key examples of how coupling two nitrene centers to aryl moieties (as with carbenes), results in the generation and design of new high-spin building blocks.
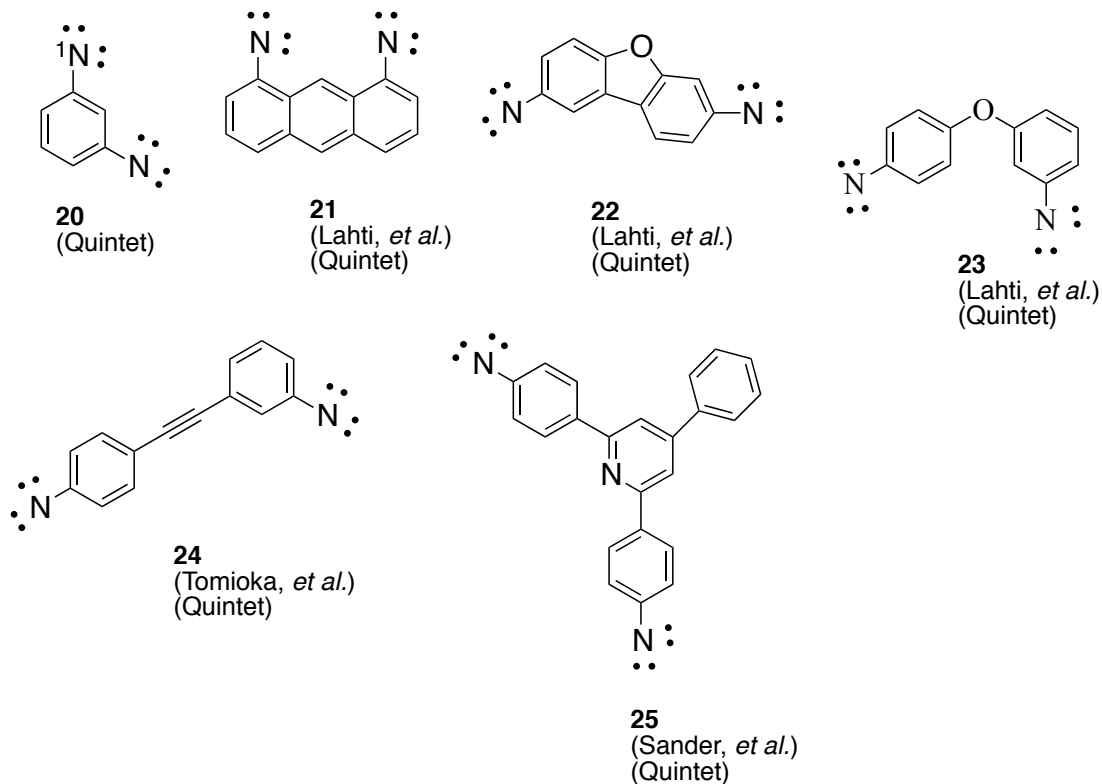
Figure 1.9. Some examples of high-spin dinitrenes.

In summation, diradicals, triplet carbenes, and nitrenes, consist of the fundamental classes of reactive intermediates in which one can develop new organic, high-spin building blocks, and thus materials. However, little research has been done to find other neutral, or non-neutral organic high-spin building blocks. The following sections will demonstrate how ion-diradicals can be used as a new source of high-spin building blocks. It should also be noted that the examples presented earlier in this introduction section, represents only a brief survey of a few significant examples of high-spin diradicals, carbenes, and nitrenes.

A. Benzylic Carbenium Ions and Carbanions

Normally, simple benzylic carbanions, carbenium ions, and other heteroatom

ions adjacent to aromatic rings are traditionally closed-shell singlet species. The

reaction chemistry of these simple reactive intermediates (benzyl carbenium ions

discussed earlier in this chapter) is known to either proceed through nucleophilic

addition to the cationic center or electrophilic additions if it is an anionic center. In

contrast, placement of strong π-donating groups or accepting groups at the *meta*

positions with respects to the cationic and anionic centers, dramatically affects the

singlet-triplet energy gaps for these simple ions. One can think of electron accepting

exocyclic groups on **26** such as carbenium, nitrenium or oxenium ions (Scheme 1.6).

For ion **28** where the substituents are switched, one can envision having analogous

exocyclic anionic groups such as carbanions, amides, and phenolates. Formal

electron transfer from the π-donating group to a vacant *p*-orbital on the acceptor

Scheme 1.6. Effect of *meta* disubstituted π-acceptors and donors on exocyclic
cationic and anionic centers

A = $^+CR_2$, ^+NR, ^+O
D = NMe_2, NH_2, OMe, OH, SCH_3

D = $^-CR_2$, ^-NR, ^-O
A = NO_2, C(O)R, CN
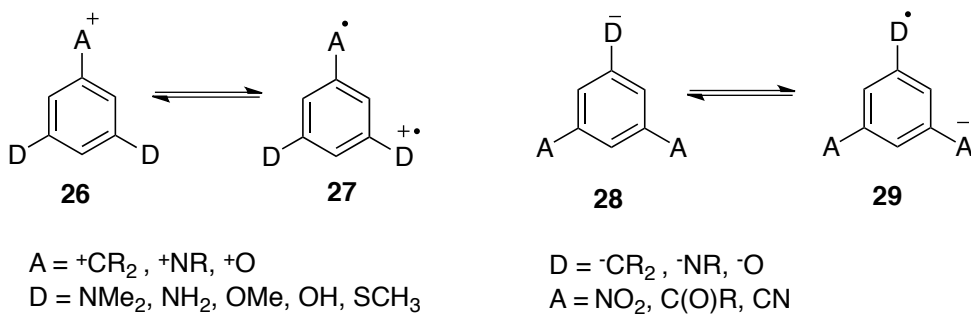
group results in a *meta* diradical cationic intermediate (**27**). Similarly, if a donating

group with excess electron density is placed at the exocyclic position and is coupled

to strong π-acceptors that are placed at the *meta* positions, formal electron transfer

can occur from the exocyclic donor to the acceptor (**29**).   In this case, structure **29**

represents an anion diradical intermediate that results from a formal one electron

transfer from the exocyclic donor group (D) to a π-acceptor group (A) at the *meta*

position. Structures **27** and **29** closely resemble that of the well-known *m*-xylylene

diradical, which is predicted to be a ground state triplet computationally by as much

as +9.6 kcal/mol.[36-39]   Evidence for this phenomenon is currently being investigated

computationally and experimentally.   Recent work by Winter *et al.* has identified

several phenylnitrenium ions,[40] and benzylic carbenium ions[41] with *meta* disubstituted

π-electron donors (e.g. NH_2, NMe_2), that are computed to be ground state triplet

diradicals.   Vinyl cations with beta π-electron donating groups, are also predicted to

be ground state triplets.[42]

   B. Triplet Nitrenium Ions

        Further examples of reactive intermediates that have been shown

computationally and experimentally as being triplet ion-diradicals, are aryl nitrenium

ions. Though most of these nitrenium ions do not appear to be similar in the

substitution pattern at the phenyl ring directly attached to the nitrenium ion center, as

that of the ion-diradicals discussed in the previous section, they do however show

some triplet diradical character. For instance, the photolysis of anthranilium ion **30**

shown in Scheme 1.7, yields products associated both with the singlet and triplet

states.[43-48]   The triplet adduct (**33**) arises through hydrogen atom abtraction from the

solvent. The nitrenium ion triplet state is generated from the photolysis of **30**, results

from intersystem crossing from the singlet state to the triplet state *via* the use of a sensitizer.

Scheme 1.7. Examples of triplet nitrenium ions generated through photolysis

Singlet adducts

Triplet adduct
(from addition of a triplet sensitizer)

Triplet nitrenium ion
intermediate
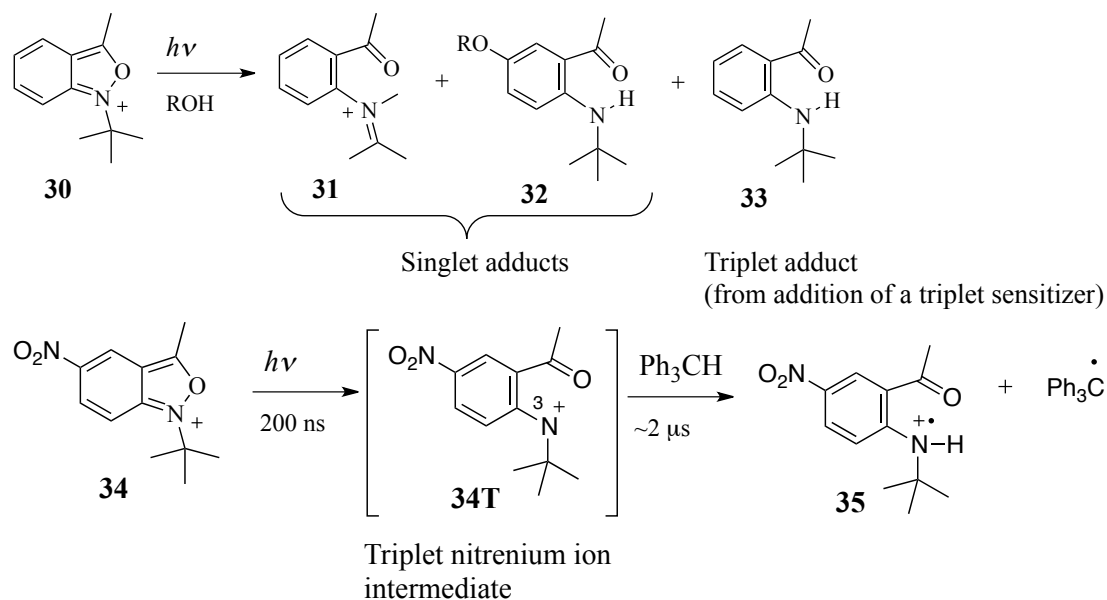
Interestingly, when the nitro anthranilium ion derivative **34** was photolyzed (Scheme 1.7), only triplet adducts were obtained from hydrogen atom abstraction from triphenylmethane.[49] Falvey and co-workers proposed that the nitrenium ion intermediate from the photolysis of **34**, resulted directly from the formation of a ground state triplet nitrenium ion (**34T**) intermediate.[49]

As one can see from the examples in Scheme 1.7, there are currently only a few examples in the literature of comprehensive experimental studies in which a number of these ion-diradicals have been directly identified or observed. One reason for the lack of experimental findings on ion-diradicals, is that the reaction chemistry associated with these intermediates is largely unknown. More specifically, other than

nitrenium ions, there has been no attempt to determine if there are other types of similar ion-diradical systems that have triplet ground states. Indeed, preliminary computational results show that in fact some *meta* disubstituted ion-diradical carbenium ions have triplet ground states.[41] Subsequently, we sought out to investigate if ion-diradicals with triplet ground states could be characterized and generated experimentally, for *meta* disubstituted benzylic carbenium ions and carbanions.

1.6 Computational Methods for Ion-Diradicals

Computational chemistry is a very useful tool for the physical organic chemist to predict the structural properties and reactivity of a target intermediate. For example, computational chemistry can be used to predict or generate the lowest energy geometries, bond dissociation energies, solvation energies, thermodynamic properties, infared, UV-Vis , NMR, EPR (electron pair resonance), Raman spectra, and electronic energy gaps for a variety of reactive intermediates. One of the most accurate yet inexpensive computational method used to predict these theoretical properties for small molecule reactive intermediates, is density functional theory (DFT). As a result, computations using some form of DFT calculations will be used to describe many of the reactive intermediates presented throughout this dissertation. DFT has been shown to accurately predict the electron states[50-54], spectroscopic[50], and thermodynamic[55,56] properties of high-spin diradicals.[54-60] It should also be noted that since the body of work presented in this manuscript is largely experimental in nature, a comprehensive discussion of DFT and related computational methods as a whole, is beyond the scope of this dissertation.

One of the main aspects of computational chemistry that has aided in the discovery of ion-diradicals used throughout this dissertation, is the use of DFT to predict various singlet-triplet energy gaps (ΔE_{ST}). The singlet state configuration is generally the ground state for most compounds/intermediates. Generally, the singlet electronic state consists of a species that is diamagnetic and has all electron spins paired either in the same orbital (the S_o state) or in two different orbitals (the S_1 state). The triplet state consists of two electron pairs that reside in different atomic or molecular orbitals with unpaired spins. Both singlet states (S_o and S_1) are commonly referred to using the DFT B3LYP/6-31G(d,p) basis sets, as the restricted (R) or closed-shell and the unrestricted (U) or open-shell singlet states, respectively. The two unpaired electron spins must reside in different atomic or molecular orbitals according to Hund's rule. Usually, the triplet state is therefore higher in energy

A   **B**
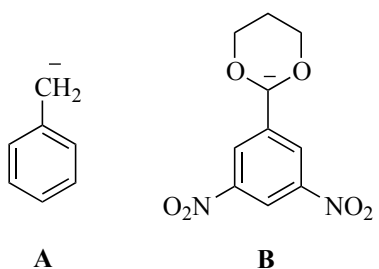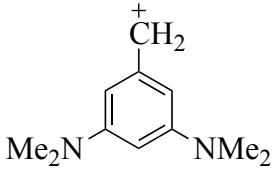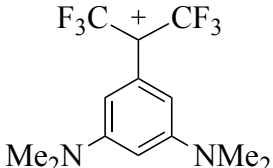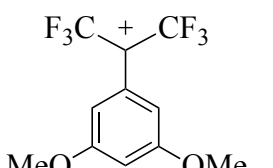
(ΔE_{ST} = -42.0 kcal/mol)   (ΔE_{ST} = +6.2 kcal/mol)

Figure 1.10. Two typical computed gas-phase ΔE_{ST} values predicted using DFT (U)B3LYP/6-31+G(d,p) basis sets.

compared to the singlet state. A typical computation is shown in Figure 1.10 whereby the singlet-triplet energy gaps were calculated for 2 different carbanions.

Unless otherwise specified, all of the DFT ΔE_{ST} values were computed using the sum of all the electronic and zero point vibrational energies (ZVPEs) and the values were converted from Hartree's to kcal/mol. We also defined the ΔE_{ST} value as being equal to the difference between the E_S (energy of the singlet) – E_T (energy of the triplet) in kcal/mol. Therefore, a negative value for ΔE_{ST} indicates that the singlet state is lower in energy (i.e. the ground state) compared to that of the triplet state. A positive value for ΔE_{ST} indicates that the triplet state is the ground state. Structure **A** in Figure 1.10 represents a simple benzyl carbanion. The gas-phase DFT computations clearly suggest (as one might predict), that this anion is a ground state singlet. However, the carbanion for structure **B** in Figure 1.10 has a positive value for ΔE_{ST}. DFT computations therefore predict that this anion should be a ground state triplet diradical, according to the definition for the ΔE_{ST} values described above. In some cases, the value for ΔE_{ST} largely favors the singlet state (i.e. a large $-\Delta E_{ST}$ value, usually < -10 kcal/mol). For these instances, the calculated differences between the electronic energies of the restricted and unrestricted singlet states does not produce a substantial effect on the overall ΔE_{ST} value, when computed. Most of the DFT computations for ΔE_{ST} values presented in this dissertation, on a select few ion-diradical intermediates, were already previous done by Dr. Arthur Winter (Ph. D thesis 2007, Department of Chemistry and Biochemistry, University of Maryland). Similar computations to those presented in this section of chapter 1, will appear to some extent throughout this dissertation.
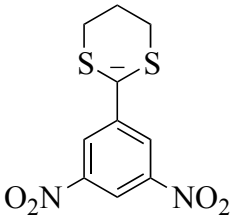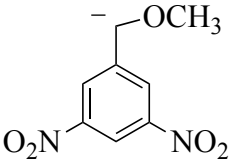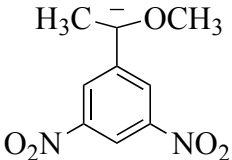
Table 1.1. Predicted DFT ΔE_{ST} Values For a Few Carbenium Ion Intermediates (BLYP/6-31G(d,p)).

Intermediate	ΔE_{ST} value (kcal/mol)[a]
$\overset{+}{C}H_2$ ring with Me_2N and NMe_2	$+1.9$[41]
$F_3C\,\overset{+}{}\,CF_3$ ring with Me_2N and NMe_2	$+12.2$[41]
$F_3C\,\overset{+}{}\,CF_3$ ring with MeO and OMe	$+1.65$

[a]Values indicated here include all zero-point vibrational energies (ZVPEs) and electronic energies.

Table 1.1 and 1.2 shows a few carbanion and carbenium ion intermediates, which are predicted to be ground state triplets by DFT. Thus, some of the intermediates described in Tables 1.1 and 1.2, will be encountered in later chapters of this dissertation.

Table 1.2. Predicted DFT ΔE_{ST} Values For a Few Carbanion Intermediates (BLYP/6-31+G(d,p)).

Intermediate	ΔE_{ST} value (kcal/mol)[a]
	+0.3
	+2.81
	+2.13

[a]Values indicated here include all zero-point vibrational energies (ZVPEs) and electronic energies.

1.7 Experimental Methods for Identifying and Characterizing High-Spin Ion-Diradicals: Magnetic Susceptibility

There are currently a number of different ways in which a physical organic chemist can effectively identify and characterize the behavior of a reactive intermediate. Some of these methods include: product studies, NMR, EPR, FT-IR, UV-Vis, H/D exchange experiments, chemical trapping experiments, and magnetic susceptibility measurements. A few of these methods will be brief described in this section of the introduction.

An indirect experimental method for identifying a reactive intermediate is through product studies. Identification and/or isolation of a specific product from a reaction mixture, provides an investigator some hints about what mechanism might be occurring to yield these products. Additionally, once some of the details associated with the possible mechanism is postulated by the investigator, he or she can begin to explore various intermediates that would indirectly be consistent with both the mechanism of that chemical reaction and the products that are formed from the reaction. Therefore, the information obtained from product studies, is an important piece of information for those studying a particular reactive intermediate and will be discussed throughout this text.

Another example of a method that is commonly used to identify reactive intermediates, is nuclear magnetic resonance (NMR) spectroscopy. NMR provides crucial structural information associated with the intermediate generated. For instance, organic anions typically show upfield proton shifts in the ^{1}H NMR spectrum, due to the shielding of the effective charge density that develops at or near the anionic center.[11,61] In contrast, organic carbenium ion proton resonances show downfield chemical shifts in the ^{1}H NMR, because of the deshielding effect near or at the cationic center.[62,63] For anionic organic or organometallic compounds, NMR also provides some information about the solute's magnetic character. Most organic compounds have all paired electron spins and thus are equally opposed to the applied magnetic field in the NMR. Thus, diamagnetic materials have essentially no net magnetic moment. Paramagnetic materials in contrast, are compounds that contain

one or more unpaired electron spins. The electron spins in paramagnetic compounds

tend to align with or reinforce the applied magnetic field, therefore creating a net

magnetic moment. In the proton NMR spectrum, a paramagnetic species tends to

exhibit either NMR silent behavior or peak broadening behavior. Highly broadened

peaks and/or NMR silent behavior might also be a result of either chemical exchange,

aggregation, or precipitation effects.

There are several methods to quantitatively determine: 1. whether a reactive

intermediate is paramagnetic or diamagnetic or 2. the assignment of the electronic

ground state of the desired reactive intermediate (i.e. singlet, triplet, quartet, etc.).

Electron pair resonance (EPR) or electron spin resonance (ESR) spectroscopy is the

main method used to determine both structural and electronic state information for

paramagnetic radical species. An EPR singal is generally obtained from the

excitation of electron spins. We have seen in section 1.4 A-C, many high-spin

reactive intermediates such as diradical[12a-b,13-17,22-24], carbenes[25-27], and nitrenes[32-35],

have been characterized by EPR spectroscopy. As a result, EPR spectroscopy is a

useful experimental technique used to elucidate the electronic spin states of high-spin

reactive intermediates at low temperatures or in rigid matrices.

There are some limitations to the use of EPR spectroscopy to determine

structural information and/or the electronic state of radical/diradical species. First, a

paramagnetic species must show a linear Curie-Weiss law plot. The Curie law states

that $I = C/T$ where I is the intensity of the absorption lines in the EPR spectrum, T is

the absolute temperature, and C is a constant. One can usually plot I vs. 1/T to obtain

hopefully a linear Curie plot. Secondly, one assumes that the equilibrium between

the singlet state and triplet state is rapid, and as a result would not show a substantial

effect on the Curie plot except at possibly low temperatures.[24] However, in the case

where the singlet-triplet energy gap is small ($< \sim 2$ kcal/mol) or close to degenerate,

the amount of triplet present in the EPR spectrum would be too small to detect.[64]

Obtaining an EPR spectrum even at cryogenic temperatures for solutions, can be

challenging due to motion of viscous solvents, and rapid tumbling which would cause

line shape distortion.[24] The line distortion would not make extraction of zero-field

splitting parameters possible.

paramagnetic solute + NMR solvent
(e.g. C_6D_6, d_8-THF, etc.)

pure NMR solvent only
(e.g. C_6D_6, d_8-THF, etc.)
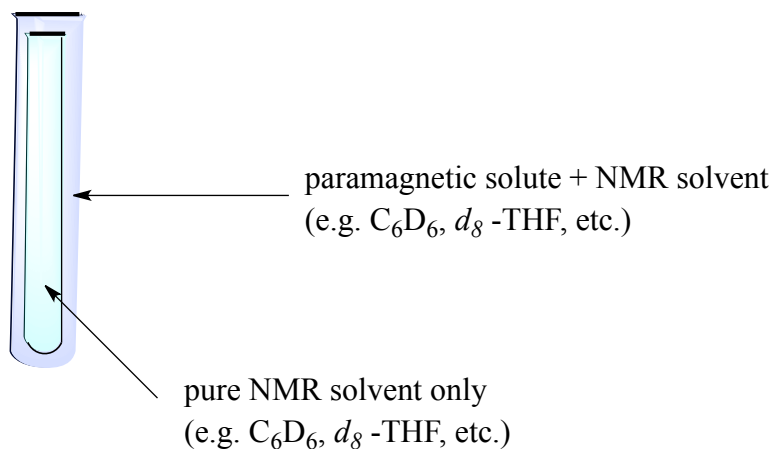
Figure 1.11. Typical Evans method setup.

Alternative methods for identifying and quantifying the paramagnetic

character of a reactive intermediate, includes either the use of a Guoy balance[64] or by

using the Evans method.[66-74] The latter method has been used to identify and

characterize various paramagnetic species in solution. In fact, the Evans method has

been used in a variety of undergraduate level physical chemistry courses, to quantitatively determine the amount of paramagnetic character in transition metal complexes. Figure 1.11 shows a typical Evans method setup. The Evans method consists of a 2 compartmental NMR tube system. The sealed inner tube consists of pure NMR solvent only (Figure 1.11). This inner tube is fully immersed into a larger, sealed outer tube that contains the paramagnetic solute that is dissolved in the same NMR solvent (Figure 1.11). If the solute in the outer tube solution is paramagnetic, then two different NMR solvent peaks should be observed in the NMR spectrum. One solvent peak should be observed for the outer tube, and another for the inner tube solvent. This is due to the 2 different magnetic environments present in this Evans method setup. The NMR solvent inner tube is diamagnetic, and is interacting with the NMR solvent in the paramagnetic environment of the outer NMR tube, thus producing 2 distinct solvent peaks in the NMR spectrum. If the solute in the outer tube is diamagnetic in nature (as are most organic compounds), then a single solvent peak should be observed for both solvents. A simple qualitative comparison can be made from these Evans method experiments. The amount (i.e. concentration) of the paramagnetic solute in the outer tube will be proportional to the peak separation between the inner and outer tube solvent peaks. That is to say, the higher the concentration of paramagnetic species in the outer tube, the larger the solvent peak separation.

One can in fact obtain quantitative data from these Evans method experiments. Grant, *et al.*[75] and Schubert*, et al.*[76] have determined a relatively simple

set of equations that provides the % singlet character from the Evans method shifts

obtained in any given NMR experiment. Equations 1.1 and 1.2 below demonstrates

how one can calculate the amount of singlet and triplet from an Evans method

experiment. The magnetic moment is defined in the equations by μ, $\Delta\delta$ represents the

difference between solvent peaks (Evans shift) in ppm, T is the temperature in

degrees Celsius, and N_{anion} is the number of moles of paramagnetic solute. There are

a few assumptions made with using these equations. First, N_{anion} assumes that full

deprotonation of the corresponding conjugate acid occurs. Secondly, temperature T

must be fairly constant. Lastly, the diamagnetic contributions from the solvent and

other additives in the solution, do not have a large contribution to the value of μ, and

can therefore be ignored.

$$\% \text{ singlet} = 100 \left[1 - \frac{\mu^2}{3.3^2} \right] \qquad \text{(Eq. 1.1)}$$

$$\mu = 2.84 \left[\frac{-3\Delta\delta N_{anion}T}{4\pi 10^6} \right]^{1/2} \qquad \text{(Eq. 1.2)}$$

Overall, EPR spectroscopy and Guoy balances tend to give important and

reliable magnetic susceptibility information for solids, and rigid matrices that have

large singlet-triplet energy gaps. The Evans method however provides a useful

solution phase, experimental alternative, for quantitatively identifying and

characterizing paramagnetic species that have close to degenerate singlet-triplet

electronic states.

The next chapter entitled "Chapter 2: Photoheterolysis of 3,5-Bis(dimethylamino)benzyl Esters and Alcohols" will discuss the first class of ion-diradicals mentioned earlier in section 1.5.

Chapter 2: Photoheterolysis of 3,5-Bis(dimethylamino)benzyl Alcohols and Esters

2.1 Computations on the 3,5-Bis(dimethylamino)benzyl Carbenium Ion

As with any project involving ion-diradical reactive intermediates, computational chemistry allows us the ability to identify viable targets. According to the DFT results presented in Chapter 1, *meta* disubstituted π-donors such as amines relative to a benzylic carbenium ion center should favor a triplet diradical ground state. Therefore, we computed various singlet-triplet energy gaps for *meta* mono and disubstituted amines to identify if any of these intermediates would have favorable triplet ground states (Figure 2.1). As stated in Chapter 1, if the singlet-triplet energy gap (ΔE_{ST}) has a negative value, then the singlet state is the ground state and is lower in energy relative to the triplet state. Similarly, if the singlet-triplet energy gap has a positive value, then the triplet state is the ground state.

39
ΔE_{ST} = -11.1 kcal/mol
DFT B3LYP/6-31G(d,p)

40
ΔE_{ST} = -0.48 kcal/mol
DFT B3LYP/6-31G(d,p)

41
ΔE_{ST} = -4.4 kcal/mol[41]
DFT B3LYP/6-31G(d,p)

42
ΔE_{ST} = +1.9 kcal/mol[41]
DFT B3LYP/6-31G(d,p)
ΔE_{ST} = +1.9 kcal/mol[41]
CASPT2/cc-pVDZ
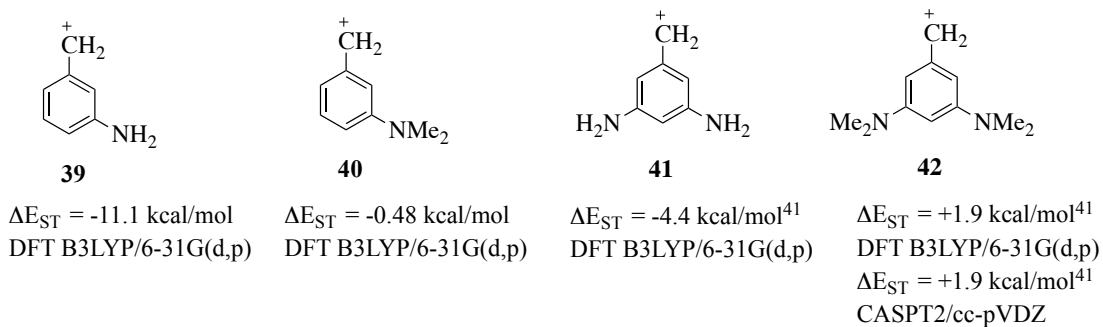
Figure 2.1. Computed singlet-triplet energy gaps for various *meta* substituted amino benzylic carbenium ions.

The computations in Figure 2.1 demonstrates a fascinating and compelling trend. The 3-aminobenzyl carbenium ion, **39** is clearly a ground state singlet by -11.1 kcal/mol. However, if 2 methyl groups are placed on the amino group at the *meta* position (**40**), the singlet-triplet energy gap almost becomes nearly degenerate ($\Delta E_{ST} =$ -0.48 kcal/mol). Addition of two strong π-donors at the 3 and 5 positions relative to the benzylic carbenium ion center (**41**), still favors the singlet state by -4.4 kcal/mol.[41] DFT computations on the 3,5-bis(dimethylamino)benzyl carbenium ion **42**, predicts that the ground state for this benzylic carbenium ion should be that of a triplet by +1.9 kcal/mol. Although **42** only has a small energy gap that favors the triplet state as the ground state, it should be noted that it is the only benzylic carbenium ion intermediate

42S   **42T**
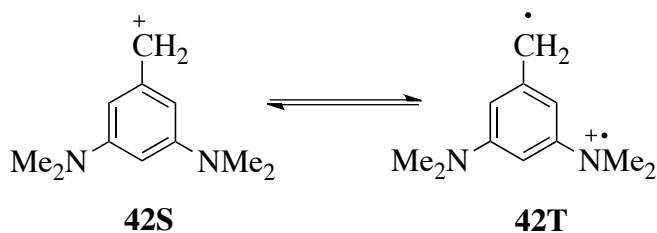
Figure 2.2. Singlet and triplet structures for the 3,5-bis(dimethylamino)benzyl carbenium ion.

shown in Figure 2.1, that is expected to have this ground state configuration by DFT. We also performed a higher level CASPT2/cc-pVDZ computation on **42**, which showed that the 3,5-bis(dimethylamino)benzyl carbenium ion might actually have an essentially degenerate singlet and triplet states of $\Delta E_{ST} = $ -0.1 kcal/mol (Figure 2.1).[41] Furthermore, the triplet state of **42** can be generated from formal electron transfer from one of the dimethyl amino groups to the vacant *p*-orbital on the benzylic carbenium ion center (Figure 2.2).

In summation, our DFT computations on *meta* mono and disubstituted benzylic carbenium ions with amino π-donors suggests that if the 3,5-bis(dimethylamino)benzyl carbenium ion can be generated, then it should have a thermally accessible triplet state. As a result, in the following sections of this chapter, we will attempt to identify suitable precursors to this benzylic carbenium ion, and show which methods could be used to generate this desired intermediate.

2.2. Synthesis of 3,5-Bis(dimethylamino)benzyl Alcohol and Ester Photoprecursors

Finding suitable precursors for the 3,5-bis(dimethylamino)benzyl carbenium ion **42** was inspired in part from the results presented in Zimmerman's work. (see section 1.2). Recall Zimmerman showed that 3,5-dimethoxybenzyl acetate esters, yielded exclusively the 3,5-dimethoxybenzyl alcohol when photolyzed in aqueous dioxane. Zimmerman reasoned that the initial 3,5-dimethoxybenzyl carbenium ion intermediate (not shown in section 1.2), resulted from C-O bond heterolysis of the corresponding benzyl acetate ester, and would ultimately lead to the formation of solvolysis products. Moreover, if the 3,5-dimethoxybenzyl carbenium ion was generated from the photolysis of a 3,5-dimethoxybenzyl acetate ester, then by the same logic, similar benzyl acetates or esters with 3,5-bis(dimethylamino) groups should result in the formation of the corresponding benzyl carbenium ion if photolyzed in polar protic media.

Benzyl esters with 3,5-bis(dimethylamino) groups were synthesized from the commercially available 3,5-diaminobenzoic acid, **43** as shown in Scheme 2.1. Initial Fischer esterification affords the ethyl-3,5-diaminobenzoate ester **44**. The two amino groups of **44** were selectively methylated through the use of 37 % formalin/3 M H_2SO_4 followed by $NaBH_4$ to yield the 3,5-bis(dimethylamino)ethyl benzoate, **45**. Reduction of ester **45** with $LiAlH_4$/THF results in the formation of the 3,5-bis(dimethylamino)benzyl alcohol **46**, which itself can serve as a photoprecursor. However, alcohol **46** in itself would not be a suitable photoprecursor, since photolysis of **46** could result in either C-O bond homolysis resulting in the formation of a $^\bullet$OH and the 3,5-bis(dimethylamino)benzyl radical, or C-O bond heterolysis which would lead to the formation of $^-$OH and the 3,5-bis(dimethylamino)benzyl carbenium ion.

Scheme 2.1. Synthesis of 3,5-bis(dimethylamino)benzyl alcohol and ester photoprecursors
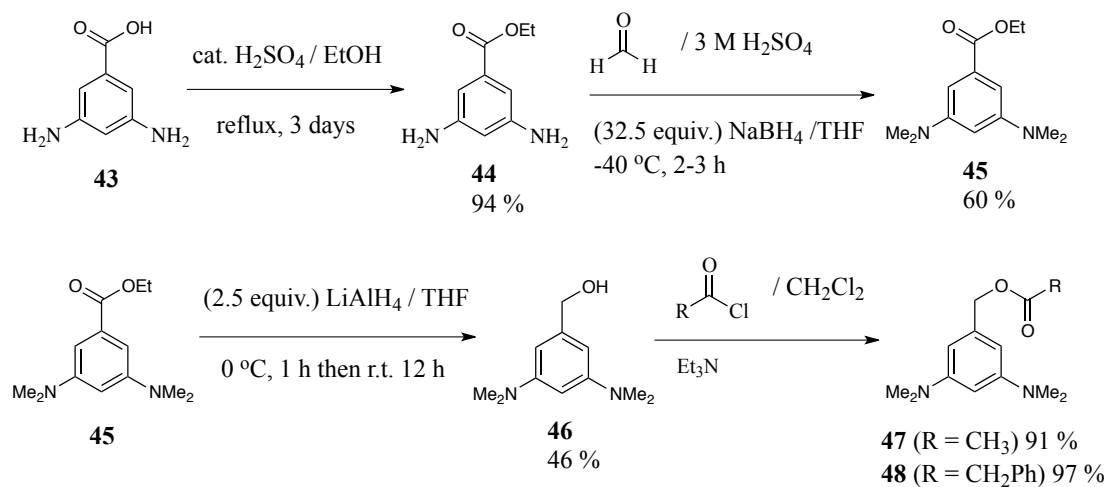
Consequently, we also synthesized the 3,5-bis(dimethylamino)benzyl acetate, **47** and 3,5-bis(dimethylamino)benzyl phenyl acetate **48**. Benzyl esters **47** and **48** as we will see shortly in this chapter, the carboxylate leaving groups generated from the

41

photolysis of these precursors, will provide valuable evidence for determining if the

target 3,5-bis(dimethylamino)benzyl carbenium ion intermediate is generated, and will

assist in characterizing the nature of other possible photoproducts.

2.3 Photoproduct Studies

      Based on the computations shown in Figure 2.1, and Zimmerman's findings

on the photochemistry associated with *meta* disubstiuted methoxy benzyl acetate

Scheme 2.2. Photoheterolysis vs. photohomolysis mechanisms for 3,5-bis(dimethylamino)benzyl alcohols and esters, **46-48** in alcoholic solvents

46 (X = OH)
47 (X = OAc)
48 (X = OC(O)CH$_2$Ph)

49 (R = Me)
50 (R = CH$_2$CF$_3$)
51 (R = CH(CH$_3$)$_2$)
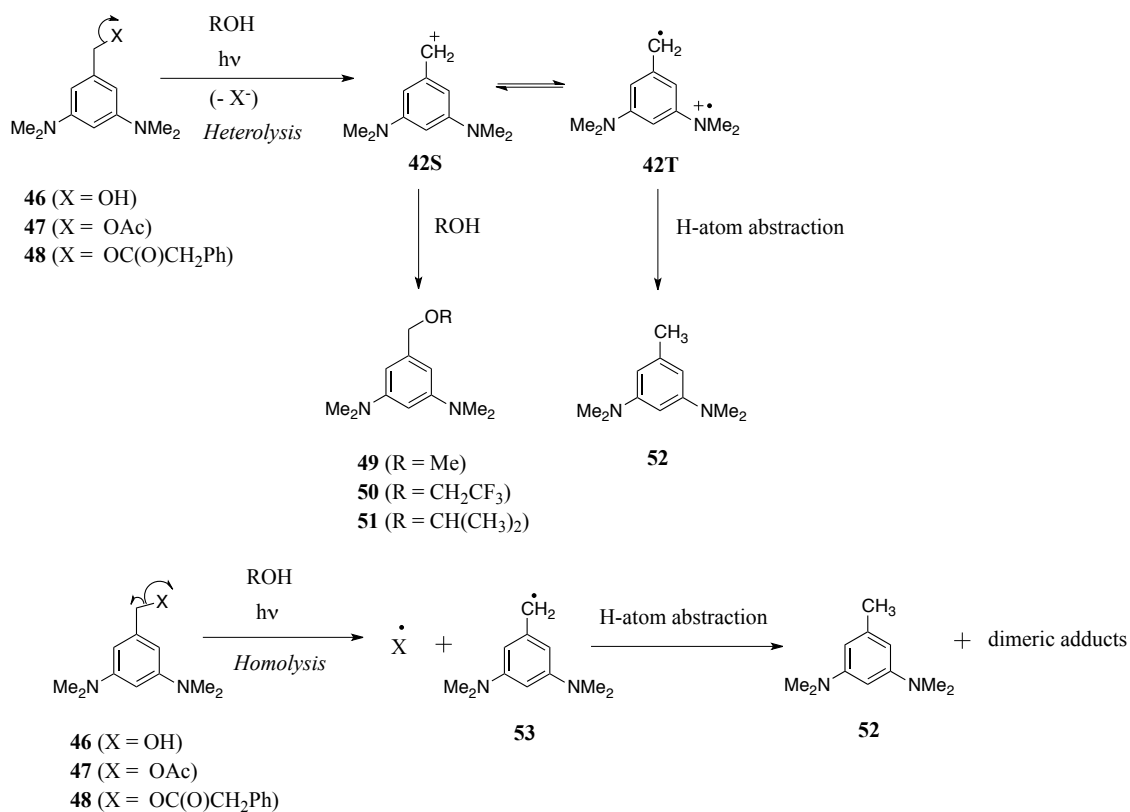
Where X = OAc and/or OC(O)CH$_2$Ph

$\overset{\bullet}{X} \xrightarrow{\text{Fast}} \overset{\bullet}{CH_3}$ or $\overset{\bullet}{CH_2}Ph$ + CO$_2$

PhCH$_3$ + PhCH$_2$CH$_2$Ph or CH$_3$CH$_3$
(not observed)   (not observed)

42
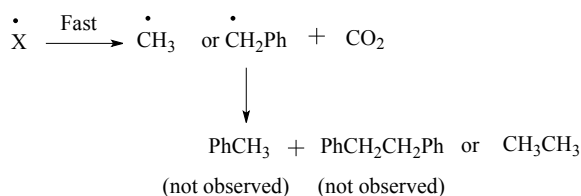
esters, we formulated two possible mechanistic pathways in which alcohol **46** and esters **47-48** could, in principle, lead to the formation of photoproducts upon irradiation in alcoholic solvents. These two mechanistic pathways are benzylic C-O bond homolysis and heterolysis, respectively (Scheme 2.2).

The heterolysis pathway depicted in Scheme 2.2, initially yields 3,5-bis(dimethylamino)benzyl carbenium ion **42S**, which is either trapped by alcoholic solvents to yield benzyl ethers (**49-51**) or can undergo intersystem crossing to form the triplet diradical **42T**. Diradical **42T** can subsequently abstract a H-atom from a solvent molecule to eventually lead to the formation of the 3,5-bis(dimethylamino)toluene product, **52**. Alternatively, if C-O bond homolysis were to occur, then the first intermediates that would be generated from this process, are the 3,5-bis(dimethylamino)tolyl radical **53**, and the acetoxy, phenyl acetoxy, or hydroxyl radicals. Tolyl radical **53**, would also yield the 3,5-bis(dimethylamino)toluene product **52**, as well as other radical products (such as homodimers or heterodimers of tolyl radical, **53**). The acetoxy and phenyl acetoxy radicals shown in Scheme 2.2, which are generated from initial C-O bond homolytic scission of precursors **46-48**, undergo rapidly decarboxylation to ultimately yield ethane and bibenzyl as byproducts, respectively. Therefore, from the hypothesized mechanisms from the photolysis of **46-48** shown in Scheme 2.2, we can anticipate that the two major products one might observe in any given photolysis experiment, are benzyl ethers **49-51**, and the 3,5-bis(dimethylamino)toluene, **52**.

Benzyl ethers **49** and **50** were isolated from exhaustive photolysis of the 3,5-bis(dimethylamino)benzyl alcohol, **46** in MeOH and 2,2,2-trifluorethanol (TFE) respectively (Scheme 2.3). The 3,5-bis(dimethylamino)toluene adduct **52** was synthesized by a Ni-catalyzed borohydride reduction of acetate **47** similar to a previous procedure developed for the reduction of aromatic benzyl acetates to aryl toluenes by He, *et al.*[77]   Unfortunately, we were unable to isolate benzyl isopropyl ether adduct **51**, since its GC retention time (R_T) was very similar to all of the photoprecursors (**46-48**).

Scheme 2.3. Synthesis of photoproduct standards **49**, **50**, and **52**
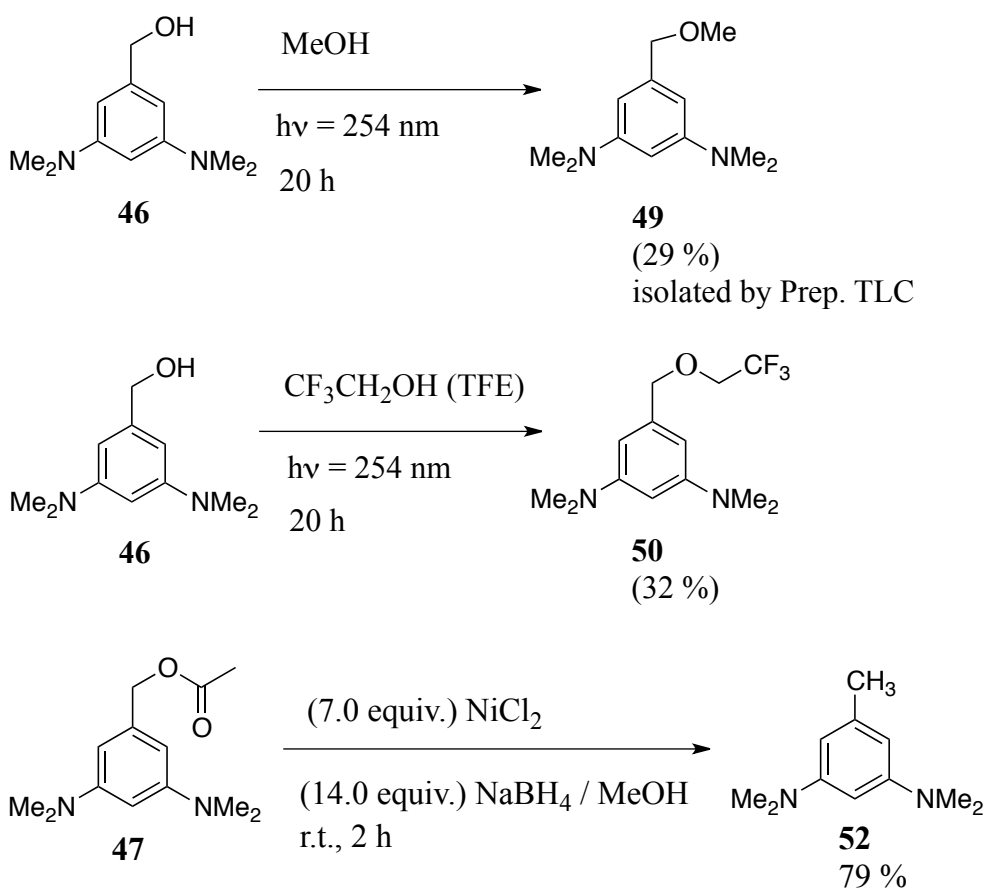
With photoprecursors **46-48** and standards **49**, **50**, and **52** in hand, we initially

attempted to photolyze **47** using a 254 nm light source in MeOH for 1 hour (Scheme

2.4) to see if any photoproducts could be observed. The photolysis mixture at this

time of irradiation consisted of two major photoproducts (in addition to some of the

starting ester **47**), which were observed by GC and GC-MS. The two products had a

GC retention time of 7.7 and 8.5 minutes. GC-MS analysis of this photoproduct

mixture enabled us to identify the mass of one of the major products as having a mass

to charge ratio (m/z) of 208. As predicted by Zimmerman and our hypothesized

mechanisms described in Scheme 2.2, one of the major products obtained by the

"*meta* effect" of the photolysis of benzyl acetates should be the corresponding

solvolysis product. In the case of **47**, the photosolvolysis product should be the

methoxy ether **49**, which is consistent with an observed m/z of 208 and thus

corresponds nicely to the mass determined by our GC-MS analysis in this particular

Scheme 2.4. Example of the photolysis of 3,5-bis(dimethylamino)benzyl acetate **47**
in MeOH for 1 hour using a 254 nm light source
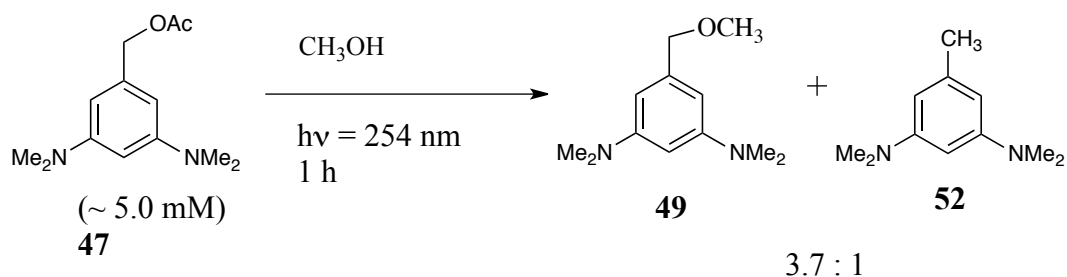
photolysis mixture. Interestingly, another minor product was observed in this

photolysis mixture. Unfortunately, the GC-MS analysis of this second photoproduct

peak (presumably the reduction product **52**) observed by GC, was either below the

detection limit of the instrument, or failed to adequately ionize in the mass

spectrometer. As discussed in section 2.1 of this chapter, the 3,5-

bis(dimethylamino)benzyl carbenium ion **42**, is predicted to have a triplet ground state or has a nearly degenerate ground state by DFT. Thus, the observed 3,5-bis(dimethylamino)benzyl methoxy ether **49** from this experiment, seems expected from the photochemical heterolysis of acetate **47** and trapping of the resulting singlet benzylic carbenium by MeOH. However, the 3,5-bis(dimethylamino)benzyl carbenium ion **42** is also predicted to have an accessible triplet diradical state, and we thus considered that this second photoproduct could have resulted from the formation of the triplet diradical **42T**.

Radical intermediates generated chemically or photochemically can lead to the formation of several potential products depending on the reaction conditions. Some typical products formed from radical intermediates include complex polymers, dimers, and H-atom abstraction products that results from the abstraction of a single hydrogen atom from the solvent. If dimeric or polymeric photoproducts were not formed from the 3,5-bis(dimethylamino)benzyl ion-diradical **42T**, then it is most likely that the second product peak obtained by GC (R_T = 7.7 minutes) is in fact the 3,5-bis(dimethylamino)toluene product **52**, based on the hypothesized mechanism shown in Scheme 2.2. Hence, we considered that this photoadduct was consequently produced from H-atom abstraction from the solvent, MeOH (Scheme 2.4). If this was the case, the resulting photoadduct would be **52**, the 3,5-bis(dimethylamino)toluene (Scheme 2.4). To verify the accumulation of **52** in the photolysis mixture depicted in Scheme 2.4, we co-injected a small amount of the

Table 2.1. Summary of Photoproducts Observed from the Photolysis (254 nm) of 3,5-Bis(dimethylamino)benzyl Alcohols and Esters (5-6 mM) in Alcoholic Solvents.

46 (R = H)
47 (R = Ac)
48 (R = C(O)CH$_2$Ph)

49 (R' = Me)
50 (R' = CH$_2$CF$_3$)
51 (R' = CH(CH$_3$)$_2$)

52

Entry	Substrate	Products	GC R$_T$ (min.)	Product Ratio (**49, 50, 51** : **52**)[a]	GC/MS (m/z)
1	**46**	**49**	8.5	6.7 : 1*	208
		52	7.7		----
2	**47**	**49**	8.5	3.7 : 1*	208
		52	7.7		----
3	**48**	**49**	8.5	3.5 : 1*b	208
		52	7.7		----
4	**46**	**50**	8.2	2.8 : 1*	276
		52	7.7		----
5	**47**	**50**	8.2	5.3 : 1	276
		52	7.7		----
6	**48**	**50**	8.2	3.2 : 1	276
		52	7.7		----
7	**46**	**51**	8.8	2.8 : 1*c	236
		52	7.7		----
8	**47**	**51**	8.8	5.3 : 1*c	236
		52	7.7		----
9	**48**	**51**	8.8	2.7 : 1*c	236
		52	7.7		----
10	**46**+10.5 mM CHD/TFE	**50** 52	8.2 7.7	2 : 1	NM
11	**47**+10.5 mM CHD/TFE	**50** 52	8.2 7.7	2 : 1	NM

[a]With the exceptions of entries **10** and **11**, all photolysis GC ratios were determined when the reduction adduct **52** became detectable by GC and was not based on the amount of photolysis conversion of the starting materials (**46-48**).   All GC-MS masses were obtained using electron impact ionization method (EI).   *Authenticity was verified by co-injection of GC standard. [b]Co-injection with 5.7 mM bibenzyl in CH$_2$Cl$_2$. [c]Photolysis product ratios were solely based on GC peak areas.

authentic standard of **52**, which was synthesized previously (see Scheme 2.3), into one of our photolysis GC samples.

As a result, several photolysis experiments similar to that shown in Scheme 2.4, were carried out on benzyl cation precursors **46-48** in various alcoholic solvents. Table 2.1 shows a summary of our photolysis experiments and results. Further analysis of the data in Table 2.1, shows that there is no discernible trend in the photoproduct ratios of the benzyl ether adducts **49-51** to reduction product, **52**. It should also be noted that all product ratios were obtained directly from standard calibration curves for entries 1-6 and 10-11 in Table 2.1 (see Chapter 7, Supporting Information for GC calibration curves).

In MeOH, we obtained the largest ratio of benzyl ether adducts from solvent incorporation to that of reduction adduct (6.7 :1). Interestingly, the addition of a small amount of a strong H-atom donor like 1,4-cyclohexadiene (Table 2.1, Entry 10-11), results in the largest observed ratio of 3,5-bis(dimethylamino)toluene **52**, to benzyl ether adducts (1 : 2). Other than benzyl ether **51**, the only potential adducts that we could not characterize efficiently and accurately by GC/GC-MS is the corresponding carboxylate ion or carboxylic acid leaving groups associated with benzyl esters **47** and **48**. In the case of 3,5-bis(dimethylamino)benzyl alcohol **46**, it would be difficult to accurately distinguish the extent of C-O bond heterolysis from homolysis to yield $^{\bullet}OH$ or ^{-}OH as both would be expected to produce H_2O. Section 2.4 will discuss how we determined both the mechanism whereby the photolysis of

48

benzyl alcohols and esters **46-48** occurs, and how we identified the presence of the corresponding leaving group byproducts (acetic acid and phenyl acetic acid respectively) from the photolysis of **47** and **48** by ^{1}H NMR.

The accumulation of a small amount of the 3,5-bis(dimethylamino)toluene adduct **52**, might result from the formation of the 3,5-bis(dimethylamino)benzyl radical **53** (Scheme 2.2) or 3,5-bis(dimethylamino)benzyl triplet diradical, **42T**. However, the generation of the 3,5-bis(dimethylamino)benzyl radical seems to be unlikely since benzyl methoxy ether **49** was formed as the major photoproduct observed from photoheterolysis of the C-O bond of benzyl acetate ester **47**. From this reasoning, the generation of the 3,5-bis(dimethylamino)benzyl carbenium ion **42**, would certainly lead to the formation of benzyl methoxy ether **49** from nucleophilic trapping by MeOH. Also, we wanted to determine whether similar or different photoproducts could be observed from the photolysis of benzyl alcohol and ester precursors **46-48** using several different polar protic solvents such as MeOH, 2,2,2-trifluoroethanol, and 2-propanol (Table 2.1). In all cases two major products were observed by GC/GC-MS. One photoproduct, was the corresponding benzyl ether formed from the presumed photosolvolysis of the benzyl alcohol/esters (**46-48**), and the correct masses for each of the benzyl ethers (**49-51**) were observed accordingly. The other photoadduct's mass that could not be determined directly from GC-MS, but was observed in all photolysis mixtures by GC to have a $R_T = 7.7$ min. To confirm and quantify the products generated in the photolysis experiments shown in Table 2.1, we synthesized 2 of the benzyl ether adducts, the 3,5-bis(dimethylamino)benzyl

methoxy ether, **49** and the 3,5-bis(dimethylamino)benzyl-2,2,2-trifluoethyl ether, **50**,

and the reduction photoproduct the 3,5-bis(dimethylamino)toluene, **52** (Scheme 2.3).

The data from Table 2.1 led us to investigate a few other important aspects to

the photochemistry associated with 3,5-bis(dimethylamino)benzyl alcohols and

esters. First, we wanted to determine if photoirradiation was a necessary requirement

for producing solvolysis adducts from polar protic solvents when any of the benzyl

Scheme 2.5. Thermal, and solvent control experiments conducted on benzyl esters
47 and **48**[*]

48
(5-6 mM)
(3 % conversion by GC)

48
(5-6 mM)
(13 % conversion by GC)

47
(5-6 mM)
(22 % conversion by GC)
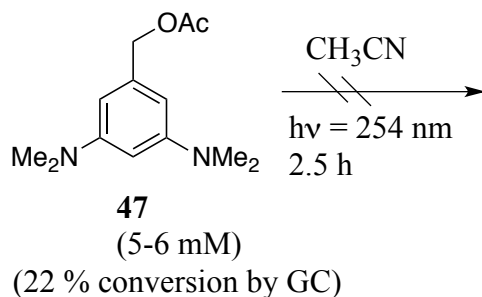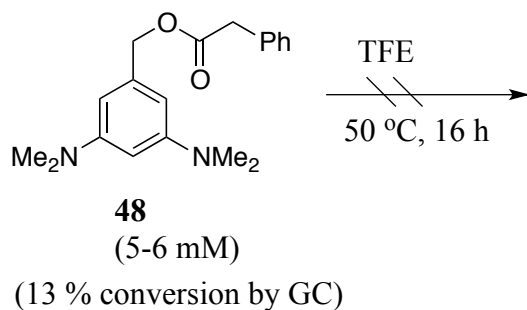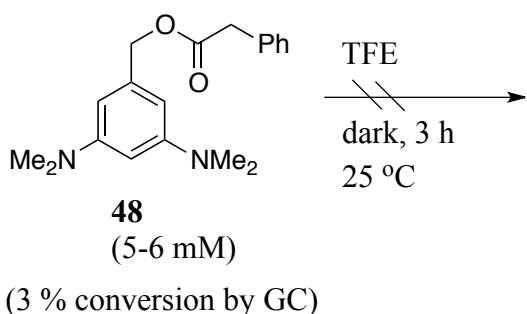
[*]Conversion was determined from GC calibration curves for **47** and **48** respectively (see Chapter 7, Supporting Information for calibration curves). No other products were detected by GC/GC-MS.

cation precursors **46-48** were used. Secondly, we wanted to examine whether thermal conditions could also result in the formation of similar products to that which we had previously observed from photoirradiation of benzyl cation precusors **46-48** in alcoholic solvents. Third, we wanted to determine whether polar aprotic solvents conditions could also result in the formation of similar products to that which we had previously observed from photoirradiation of benzyl cation precursors **46-48** iis necessary for a photochemical reaction to occur between any of the benzyl cation precursors **46-48**, and the solvent. Some of these results are shown in Scheme 2.5.

Extensive heating of ester **48** to *ca.* 50 $^{\circ}$C in 2,2,2-trifluoroethanol (TFE), results in only 13 % conversion of **48** by GC with no other clearly identifiable products (Scheme 2.5). Additionally, a dark control consisting of a *ca.* 5-6 mM solution of **48** in TFE was carried out for 3 hours at room temperature and showed minimal conversion by GC (Scheme 2.5). Prolonged irradiation (~ 2.5 h.) of ester **47** in anhydrous CH_3CN resulted in only 22 % conversion of the starting ester by GC and showed no formation of any new photoproducts during the course of the photolysis experiment. It is unclear to us at this time what additional products where formed from the photolysis of **47** in CH_3CN. Therefore, from the control experiments shown in Scheme 2.5, two important conclusions can be made concerning the 3,5-bis(dimethylamino) esters **47** and **48**. The first conclusion is that thermal decomposition of 3,5-bis(dimethylamino) esters is not a facile process and that similar products from C-O bond homolysis or heterolysis of the benzylic bond could

not be observed under these conditions. Lastly, preliminary photoirradiation of 3,5-bis(dimethylamino)benzyl alcohols and esters in polar aprotic solvents does not appear to result in the formation of any appreciable photoproducts. Further study into the thermal and photochemical reactivity of benzyl alcohol and benzyl esters **46-48** should be conducted in the future.

2.4 Investigation of the Mechanism of Photoheterolysis vs. Photohomolysis of 3,5-Bis(dimethylamino)benzyl Alcohols and Esters

It is important to note that the photolysis experiments discussed throughout section 2.3 were performed under neutral conditions (neither acidic nor basic conditions). The use of strong acids such as H_2SO_4, HCl, HBr, etc. would most certainly result in protonation of the leaving group at the benzylic position and would cause C-O bond heterolysis to be more facile than if the analogous chemical reaction was performed under neutral conditions (Scheme 2.6). Heterolysis of the benzylic C-O bond would consequently form the target 3,5-bis(dimethylamino)benzylic carbenium ion and the conjugate acid of the leaving group (Scheme 2.6). However, under strongly acidic conditions, protonation of one or both of the dimethylamino

Scheme 2.6. The consequences of using strongly acidic conditions on 3,5-bis(dimethylamino)benzyl alcohols and esters

46 (R = H)
47 (R = Ac)
48 (R = C(O)CH$_2$Ph)

42S/T

(undesired intermediates)
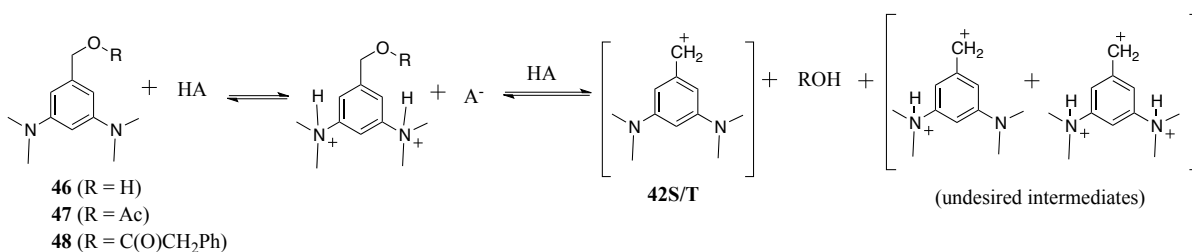
groups (pK_a of the *N,N*-dimethylanilinium ion is estimated to be 2.45 in DMSO at 25 °C)[78] must also be considered. Protonation of one or both of the dimethylamino groups could diminish the ability of the amino group(s) to act as an electron donor once the desired 3,5-bis(dimethylamino)benzyl carbenium ion is formed. Thus, generating the target 3,5-bis(dimethylamino)benzyl carbenium ion **42** cleanly in strong or mildly acidic media might not be feasible, since several other unwanted intermediates could also be formed under these conditions.

All indications from our product studies suggests that heterolysis of the C-O benzyl bond must be occurring and is the major pathway in which products are formed from the photolysis of 3,5-bis(dimethylamino)benzyl alcohols and esters. In hopes of identifying and possibly quantifying the amount of all the photoproducts formed (including that of leaving groups of **47** and **48**), we conducted ^{1}H NMR experiments whereby benzyl cation precursors **47** and **48** were photolyzed in a solution of CD_3OD with 3.0 mM methyl *tert*-butyl ether (MTBE) as an internal standard (Figure 2.3). For comparison purposes, pure standards of 3,5-bis(dimethylamino)toluene **52**, 3,5-bis(dimethylamino)benzyl methoxy ether **49**, and

(e)

(d)

54

(c) _____

(b)

t = 0
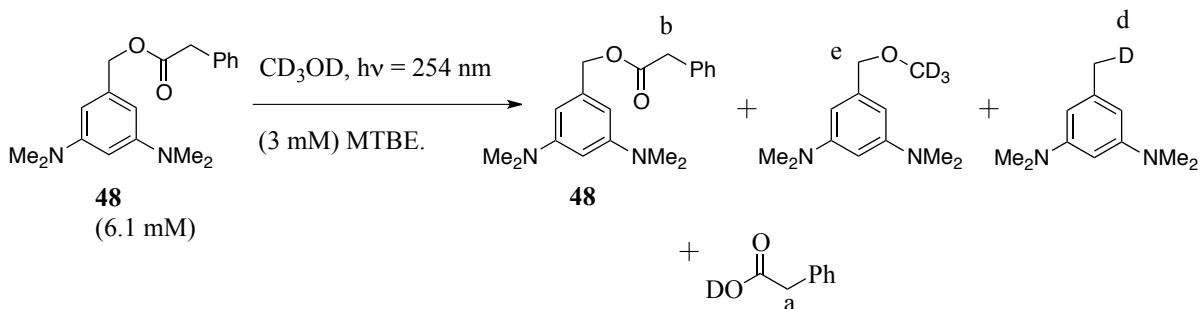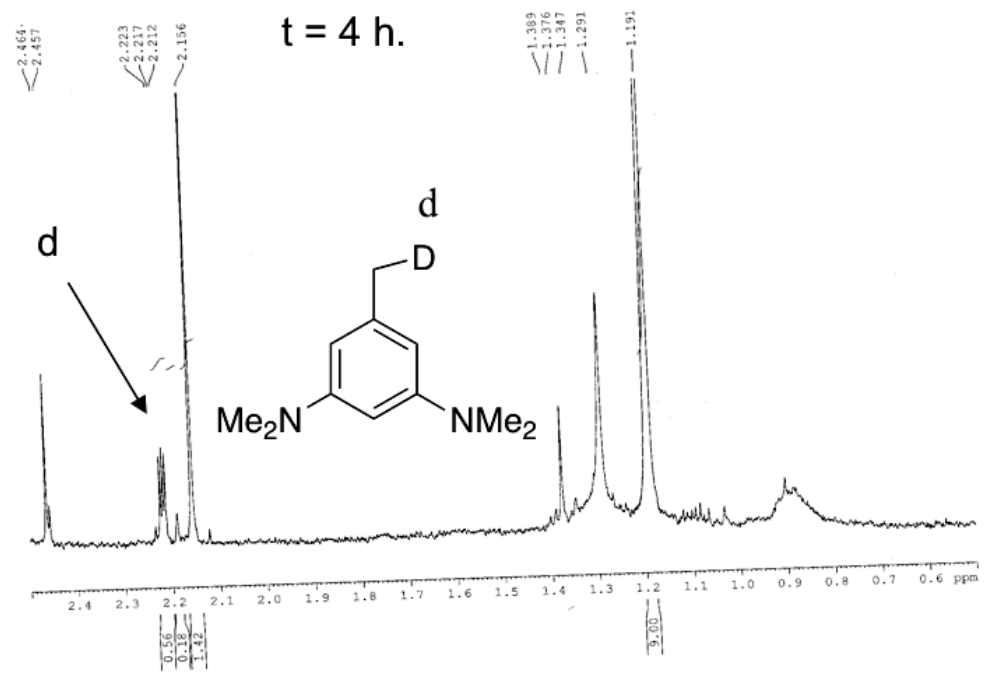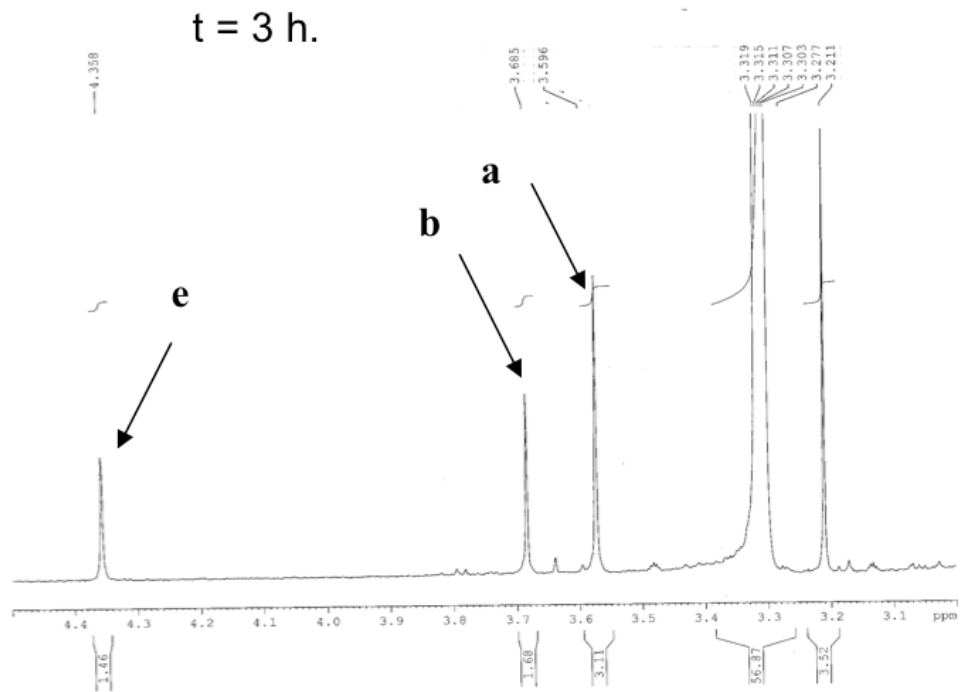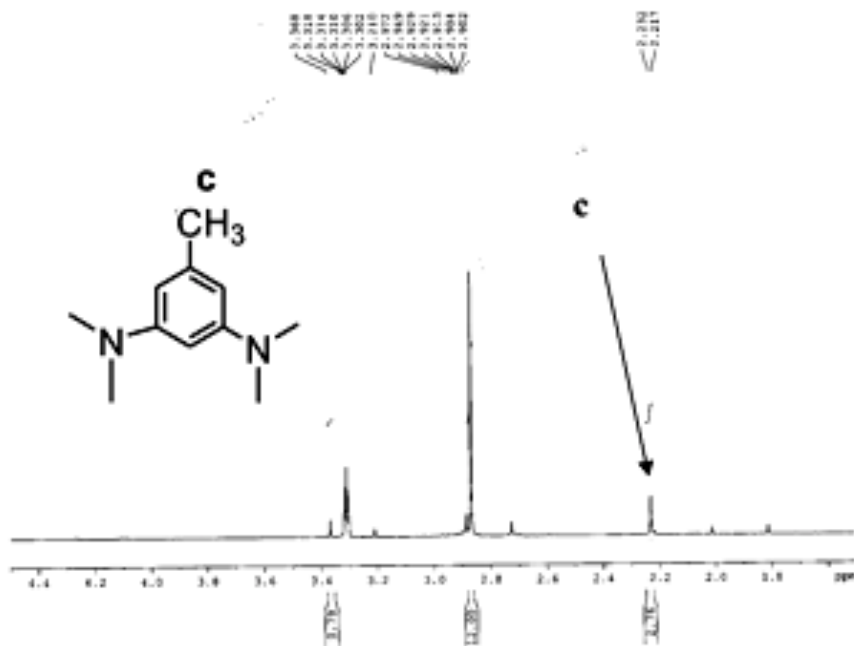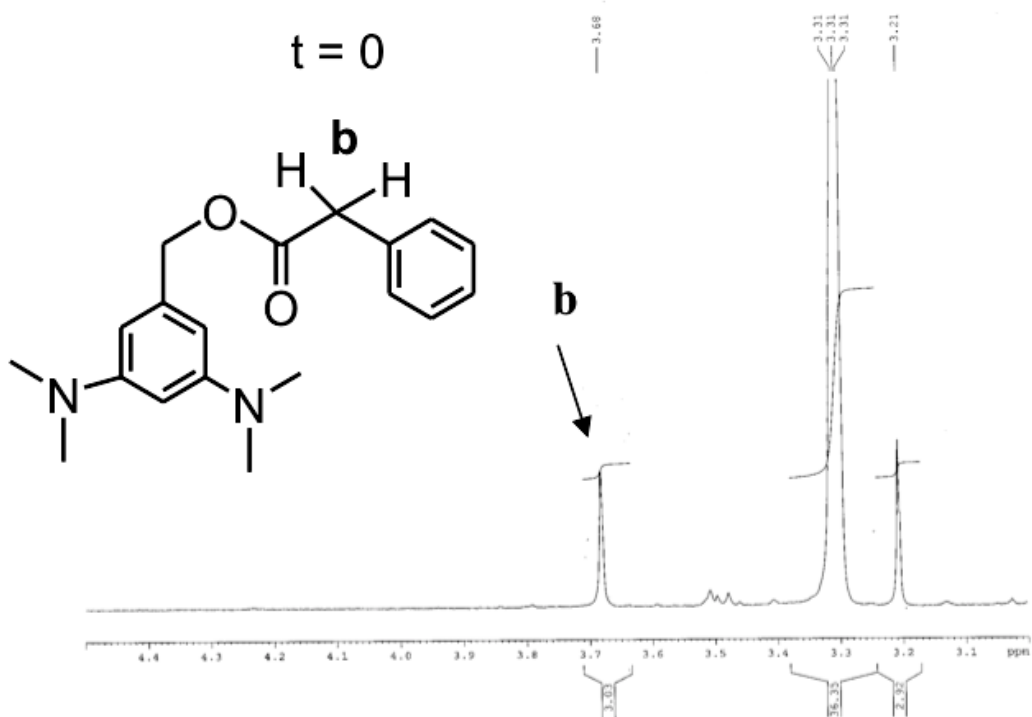
(a)
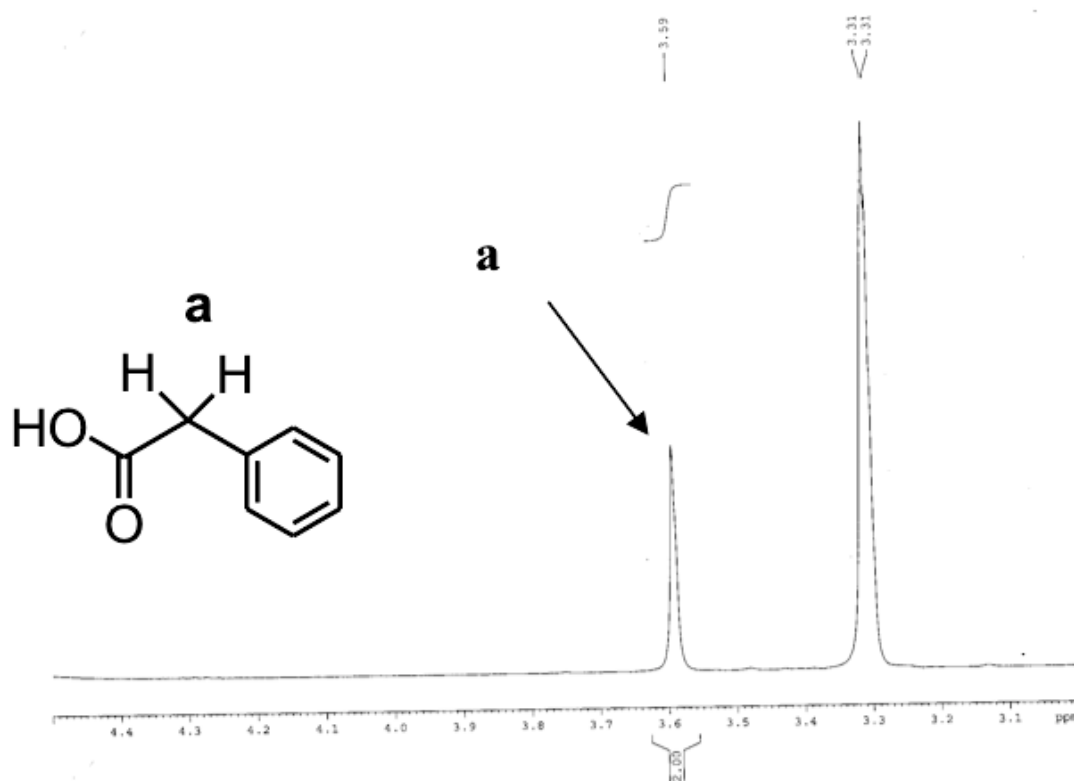
Figure 2.3. Photolysis (at 254 nm) of 3,5-bis(dimethylamino)benzyl phenyl acetate, **48** in CD$_3$OD/3 M MTBE ^{1}H NMR (400 MHz) spectra. (a) ^{1}H NMR spectrum (400 MHz) phenyl acetic acid standard in CD$_3$OD/MTBE, 4.5-3.0 ppm region. (b) ^{1}H NMR spectrum (400 MHz) 6.1 mM solution of 3,5-bis(dimethylamino)benzyl phenyl acetate, **48**/CD$_3$OD/3 M MTBE at t = 0 (no photolysis), 4.5-3.0 ppm region. (c) ^{1}H NMR spectrum (400 MHz) 3,5-bis(dimethylamino)toluene, **52** photoproduct standard in CD$_3$OD/MTBE. (d) ^{1}H NMR spectrum (400 MHz) 6.1 mM solution of 3,5-bis(dimethylamino)benzyl phenyl acetate, **48**/CD$_3$OD/3 M MTBE at t = 3 h. (λ = 254 nm), 4.5-3.0 ppm region. (e) ^{1}H NMR spectrum (400 MHz) 6.1 mM solution of 3,5-bis(dimethylamino)benzyl phenyl acetate, **48**/CD$_3$OD/3 M MTBE at t = 4 h. (λ = 254 nm), 2.5-0 ppm region.

phenyl acetic acid NMRs were taken in CD$_3$OD (Figure 2.3, a and c, for the NMR

spectrum data for **49** see Chapter 7, Supporting Information, section 7.3).   All

photolysis NMR peak integrations shown in Figure 2.3d-e, were calibrated towards the 9H's of the *tert*-butyl group of the internal standard (MTBE).

As seen in Figure 2.3a, the benzylic CH_2s indicated by "a", appear at *ca.* 3.59 ppm. Figure 2.3b shows the region between 4.5-3.0 ppm for phenyl acetate benzyl cation precursor, **48** in CD_3OD/MTBE prior to photolysis (t = 0) and shows that the resonance assigned to the phenyl acetate benzylic protons (b), resonate slightly downfield at δ = 3.68 ppm relative to the phenyl acetic acid standard (Figure 2.3a). Also, since we anticipated that the 3,5-bis(dimethylamino)toluene adduct **52** will be formed from the photolysis of **46-48**, we obtained an authentic NMR of the pure toluene standard **52**, in CD_3OD (Figure 2.3c). Upon photolysis of ester **48** in CD_3OD at 254 nm (t = 3 h), several new peaks appear in the region between 4.5-3.0 ppm (Figure 2.3d). One peak that grows in, is that of the benzylic resonance at ~3.59 ppm for that of phenyl acetate ion or phenyl acetic acid (Figure 2.3d). Over the course of photolysis at 254 nm, the singlet peak for phenyl acetic acid/phenyl acetate ion at 3.59 ppm increases while the benzylic peak for that of the starting ester at ~3.68 ppm, decreases in its relative NMR peak integration (Figure 2.3d).

Thus, we can conclude that during photolysis of ester **48**, phenyl acetic acid/phenyl acetate ion is being produced, and that **48** is consumed and is converted to its respective photoproducts (**49**, **50**, **51**, and **52**) upon photolysis. Additionally, Figure 2.3d shows a downfield singlet peak at *ca.* 4.36 ppm (indicated by e) which closely corresponds to that of the authentic CH_2 benzylic resonances of the 3,5-

bis(dimethylamino)benzyl methoxy ether's ^{1}H NMR resonance at *ca.* 4.29 ppm (spectrum not shown for 3,5-bis(dimethylamino)benzyl methoxy ether **49**, see Chapter 7, Supporting Information, section 7.3 for NMR characterization data). Further irradiation of ester **48** for 4 hours at 254 nm, results in the formation of a three line pattern resonance at *ca.* 2.2 ppm (Figure 2.3e). The observed three line splitting pattern in this region of the proton NMR spectrum, is due to the germinal H/D coupling indicated for deuterium (labeled as d in Figure 2.3e). Secondly, the chemical shifts for these protons closely resembles that of the authentic 3,5-bis(dimethylamino)toluene **52**, obtained in CD_3OD/MTBE, which appears at ~2.2 ppm for the tolyl protons in the NMR spectrum (Figure 2.3c). Similar results to that shown in Figure 2.3 were also seen from the analogous photolysis of 3,5-bis(dimethylamino)benzyl acetate ester **47** in CD_3OD/MTBE (see Chapter 7, Supporting Information, section 7.4 for spectra). Irradiation of benzyl acetate **47** under similar conditions resulted in the accumulation of comparable photoproducts by NMR and the production of either acetic acid or the acetate ion as a byproduct was also observed (see Chapter 7, Supporting Information for spectra).

2.5 Summary and Conclusions

  Considering all our previously discussed photoproduct studies and proton NMR experiments on 3,5-bis(dimethylamino)benzyl alcohols and ester **46-48**, we can make a few mechanistic conclusions. Our experimental results suggest that C-O bond photoheterolysis is the major mechanistic pathway in which alcohol and esters **46-48** lead to the accumulation of their respective photoproducts (see Scheme 2.2). The heterolysis pathways is favored for the following reasons:

(1)   Lack of radical products from the leaving group(s). As shown in Scheme 2.2, homolysis of the benzyl C-O bond would result in the formation of the acetoxy and phenyl acetoxy radicals, were not detected by GC/GC-MS or ^{1}H NMR. These radical intermediates are shown to decarboxylate on a subnanosecond time scale by Hilborn and Pincock[79] and are reported to have rate constants of *ca.* $1.3 \times 10^9 \, s^{-1}$ for the acetoxy radical and *ca.* $5 \times 10^9 \, s^{-1}$ for the phenylacetoxy radical. Therefore, it is highly unlikely that these species would be trapped in simple alcohol solvents.   We would expect that benzyl cation precursor **48** would yield substantial amounts of bibenzyl (PhCH$_2$CH$_2$Ph). Standard addition of bibenzyl to our GC photolysis mixtures, showed that < 1 % of this byproduct was formed. Furthermore, no heterocoupled products (PhCH$_2^{\bullet}$ + solvent or **53**) could be detectected by GC-MS. Our ^{1}H NMR analysis showed that a substantial amount of phenyl acetic acid or acetic acid was formed.   The peak integrations showed that these byproducts accounted for all of the consumed ester, within the experimental uncertainty.

(2)   Weak to no dependence on product ratios on the solvent. The heterolysis process, which creates two ion pairs from a neutral excited state, should be accelerated in polar solvents and inhibited in less polar solvents. In contrast, the homolysis process is expected to show a negligible dependence on the solvent. We would therefore predict consistently higher yields of the solvolysis product in TFE (E$_T$(30) = 61.1 kcal/mol) than in *i*-PrOH (E$_T$(30) = 48.6 kcal/mol) and MeOH (E$_T$(30) = 55.5 kcal/mol) would have intermediate values.[80]

(3)   Precedence for the photochemical *meta* effect. According to work done by Zimmerman, *et al.*, benzylic esters with a single moderate π-electron-donating group

(MeO) at the *meta* position, gives a mixture of heterolysis and homolysis products.[8-10] However, the addition of two *meta* MeO groups relative to a benzylic ester, yields clean heterolysis photoproducts.[10] Extrapolating from this, we feel that increasing the potency of the electron donor should favor heterolysis. Thus, we view the substitution of two MeO groups with two NMe_2 groups that are *meta* relative to the benzylic ester center, would be unlikely to favor the homolysis pathway.[81]

Chapter 3: A Critical Reexamination of the Photochemical "*Meta* Effect": Photolysis of the 3,5-Dimethoxy-α,α'-Bis(trifluoromethyl)benzyl Acetate

3.1 Computations on α-Trifluoromethyl and α-Fluoro Substituted Benzyl Carbenium Ions

Recent work by Winter, *et al.* has shown that the placement of σ-electron withdrawing groups directly adjacent to a benzylic carbenium ion center, increases the singlet-triplet energy gap in favor of the triplet state.[41] Coupling the destabilizing effect of σ-electron withdrawing groups (e.g. CF_3, CCl_3, F, etc.) directly adjacent to the carbenium ion center with strong *meta* π-donors such as amines and methoxy groups, results in a benzylic carbenium ion intermediate that strongly favors the triplet state as the ground state. Consequently, Winter *et al.* as well as myself investigated a few of these intermediates computationally (Figure 3.1).[41] All but one (**56**) of the benzyl carbenium ions in Figure 3.1 are predicted to be ground state triplets by DFT with ΔE_{ST}s > 1 kcal/mol. It is important to note that the largest ΔE_{ST} value of all of the benzyl carbenium ions in Figure 3.1 is +12.2 kcal/mol for the 3,5-bis(dimethylamino)-α,α'- bis(trifluoromethyl)benzyl carbenium ion **55**, and that most

54	**55**	**56**	**57**
ΔE_{ST} = +5.1 kcal/mol[41]	ΔE_{ST} = +12.2 kcal/mol[41]	ΔE_{ST} = -7.8 kcal/mol[41]	ΔE_{ST} = +1.65 kcal/mol
DFT B3LYP/6-31G(d,p)	DFT B3LYP/6-31G(d,p)	DFT B3LYP/6-31G(d,p)	DFT B3LYP/6-31G(d,p)
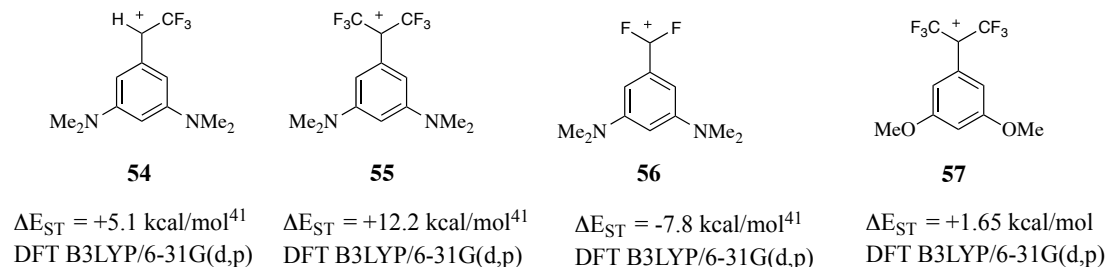
Figure 3.1. Computed singlet-triplet energy gaps (ΔE_{ST}) for various α-mono and disubstituted fluorinated benzyl carbenium ions with *meta* π-donors.

of these predicted values are much higher than that of the 3,5-

bis(dimethylamino)benzyl carbenium ion **42**, which we encountered in chapter 2.

Therefore, based on these computations we were confident that if we were able to

generate either carbenium ions **54**, **55** or **57**, that these intermediates would show

triplet diradical behavior in solution.

3.2 Synthesis of α,α'-Bis(trifluoromethyl)benzyl Carbenium Ion Precursors

　　　　In order to test the computations described in section 3.1, we set out to

synthesize a suitable photoprecursor that might lead to the formation of benzyl

carbenium intermediate **55**, since this intermediate is predicted by DFT to have the

Scheme 3.1. Synthesis of 3,5-bis(dimethylamino)-α,α'-bis(trifluoromethyl)benzyl carbinol and esters[‡]
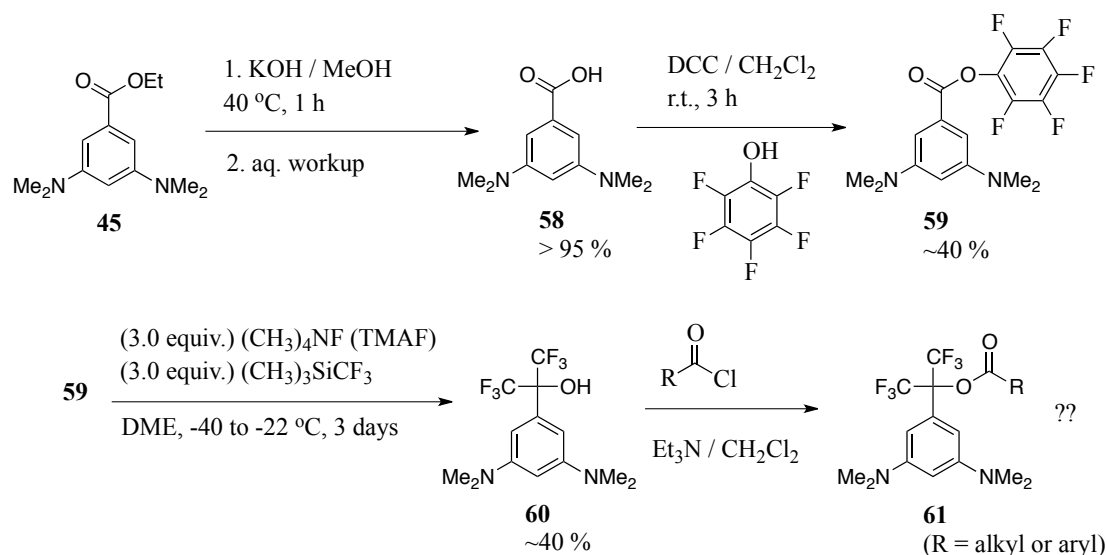
largest singlet-triplet energy gap as shown in Figure 3.1. The initial synthesis is fairly straightforward. The first two steps of this synthesis is identical to that shown previously in Scheme 2.1. 3,5-Diaminobenzoic acid, **43** is esterified under acidic conditions, then the amino groups are methylated to yield ester **45** (see Scheme 2.1). Ester **45** is quantitatively hydrolyzed to yield the 3,5-bis(dimethylamino)benzoic acid **58** (Scheme 3.1). Benzoic acid **58** is then activated by dicyclohexyl carbodiimide (DCC) and then acylated with pentafluorophenol to yield the 3,5-bis(dimethylamino)pentafluoro ester **59** in a yield of ~40 %. Subsequently, pentafluoroester **59** was then combined with trifluoromethyltrimethylsilane (TMS-CF$_3$, Ruppert's reagent), and tetramethylammonium fluoride (TMAF), in 1,2-dimethoxyethane (DME) generating the 3,5-bis(dimethylamino)-α,α'-bis(trifluoromethyl)benzyl carbinol in a yield of *ca.* 40 % (Scheme 3.1).[82] This carbinol can be in principle acylated to generate various esters (Scheme 3.1).

There are several crucial drawbacks to the synthesis of carbinol **60** and its corresponding ester derivatives, **61**. One major problem with this synthesis, is not in the steps that lead to the formation of the 3,5-bis(dimethylamino)benzoic acid, **58**, but rather this synthesis suffers immensely from two low yielding steps (no higher than 40-50 % yield) from **58** to the pentafluoro ester **59** and the reaction that leads to the formation of carbinol **60**. Secondly, even if one could quantitatively synthesize carbinol **60**, as discussed in section 2.3, there most likely would be no clear method of testing (unambiguously) whether C-O bond heterolysis or homolysis is occurring. Thus, we turned our attention to the 3,5-dimethoxy-α,α'-bis(trifluoromethyl) carbinol and acetates since aryl methoxy groups are more robust under a variety of synthetic

conditions (i.e. aryl methoxy compounds are stable under most oxidation-reduction

conditions, acid-base conditions, etc.). Likewise, the synthesis of these derivatives is

more facile than their respective 3,5-bis(dimethylamino) substituted counterparts.

Scheme 3.2 shows the synthesis we developed for the 3,5-dimethoxy-α,α'-

bis(trifluoromethyl)benzyl carbinol **64**, and acetate ester **65** (for characterization and

Scheme 3.2. Synthesis of the 3,5-dimethoxy-α,α'-bis(trifluoromethyl)benzyl
carbinol and acetate
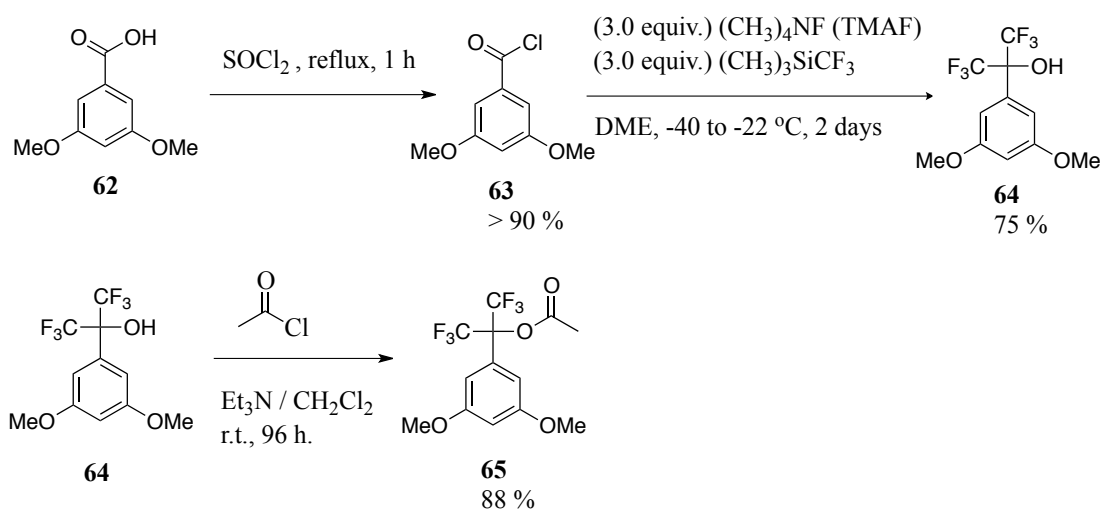
experimental procedures for these compounds see Chapter 7, Supporting

Information). Several benefits arise from the synthetic scheme above. Two such

benefits are fewer synthetic steps (3-4 steps only) to make either the carbinol **64** or

acetate ester **65**. Higher yields for each step were generally observed from this

synthetic route. Hence, one in principle can easily make substantially more of

carbinol **64** and several *O*-acylated leaving group derivatives at the benzylic position,

quantitatively from this proposed synthetic scheme.

The photochemical *meta* effect has been well documented by Zimmerman, *et al.* to yield C-O bond heterolysis of 3,5-dimethoxy benzyl acetates.[10] However, far less research has been done to adequately characterize the photochemical mechanistic pathway that 3,5-dimethoxy-α,α'-bis(trifluoromethyl)benzyl carbinols or acetates would follow. It was our hope at the onset of the project that either **64** or **65** would undergo C-O bond heterolysis, similar to what Zimmerman had observed to occur for 3,5-dimethoxy benzyl acetates. If C-O bond heterolysis is the major photochemical mechanistic pathway for either **64** or **65**, then one would expect that C-O bond heterolysis would yield the 3,5-dimethoxy-α,α'-bis(trifluoromethyl)benzyl carbenium ion **57**, which is predicted to be a ground state triplet by our DFT computations (ΔE_{ST} = +1.65 kcal/mol).

We initially chose to photolyze **64** in several polar protic solvents such as MeOH, TFE, 2-propanol, and ethanol. Prolonged photolysis (at 254 nm) of carbinol **64** for several hours (3-5 hrs. or longer) resulted in minimal conversion of the starting carbinol, **64**. On the other hand, photolysis at 254 nm of carbinol **64** in EtOH yielded some very interesting results. Scheme 3.3 shows our findings for this experiment. We expected that in EtOH, expulsion of the $^-$OH group would lead to the formation 3,5-dimethoxy-α,α'-bis(trifluoromethyl)benzyl ethoxy ether. This however was not the case. Instead, one actually observes the substitution of one or both of the CF_3 groups with either OH or EtOH. Also, the carbinol **64** appears to yield several products where either one or two ethanol molecules are to some extent incorporated

into the overall 3,5-dimethoxy benzene structure. As one can see from Scheme 3.3,

we did not expect that the loss of ⁻OH would compete with that of ⁻CF₃.   These three

photoproducts were assumed to be present in the photolysis mixture from the masses

observed in the GC-MS analysis in which we performed.   Mass to charge

Scheme 3.3. Possible photolysis (hν = 254 nm) products from the irradiation of 3,5-dimethoxy-α,α'-bis(trifluoromethyl)benzyl carbinol in EtOH
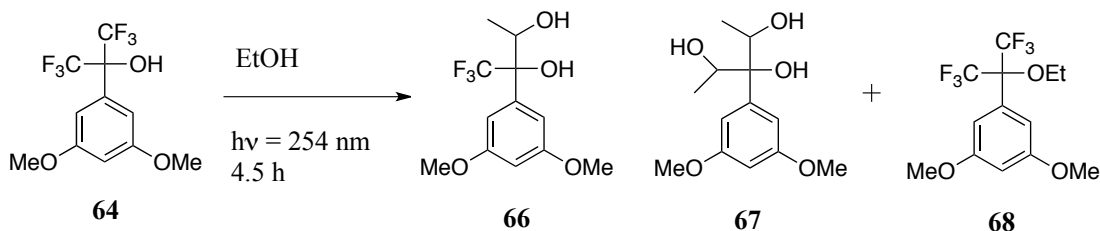
ratios of 282, 258, and 336 were observed in equal amounts by GC-MS. Although

the observed masses for **66-68** (predicted m/z = 282, 256 and 332 respectively) are

slightly higher than that in which we observed in this GC-MS photolysis mixture, we

assumed that this was due to instrumental error. Another important feature of the

results found in Scheme 3.3, is that carbinol **64** is not very photolabile and thus must

be exposed to UV irradiation for several hours (>3-4 hours) in order to observe

substantial decomposition to any respective photoproducts.   Carbinol **64** also showed

a lack of substantial conversion to photoproducts in other polar protic solvents such

as MeOH, 2-propanol, and TFE.

Since carbinol **64** failed to sufficiently generate the correct photosolvolysis

products from substitution of the benzyl alcohol to the corresponding ethers, we

determined that we might be able to facilitate more efficient cleavage of the C-O

benzyl bond by transforming the OH group into a better leaving group. Hence, we

synthesized benzyl acetate **65**.   Photolysis of a 5-6 mM solution of acetate **65** in

EtOH using a 254 nm light source for 2 hours, yields a complex mixture of 6 products

that were detected by GC-MS (Scheme 3.4). Careful analysis of each product,

showed that one product had the same mass trace, but appeared as two peaks in the

gas chromatogram. The m/z of these two closely eluting peaks was *ca.* 304. These

Scheme 3.4. Possible photoproducts identified by GC-MS[a] from the irradiation (hν = 254 nm) of acetate ester **65** (5-6 mM) in EtOH and 2-propanol[b]
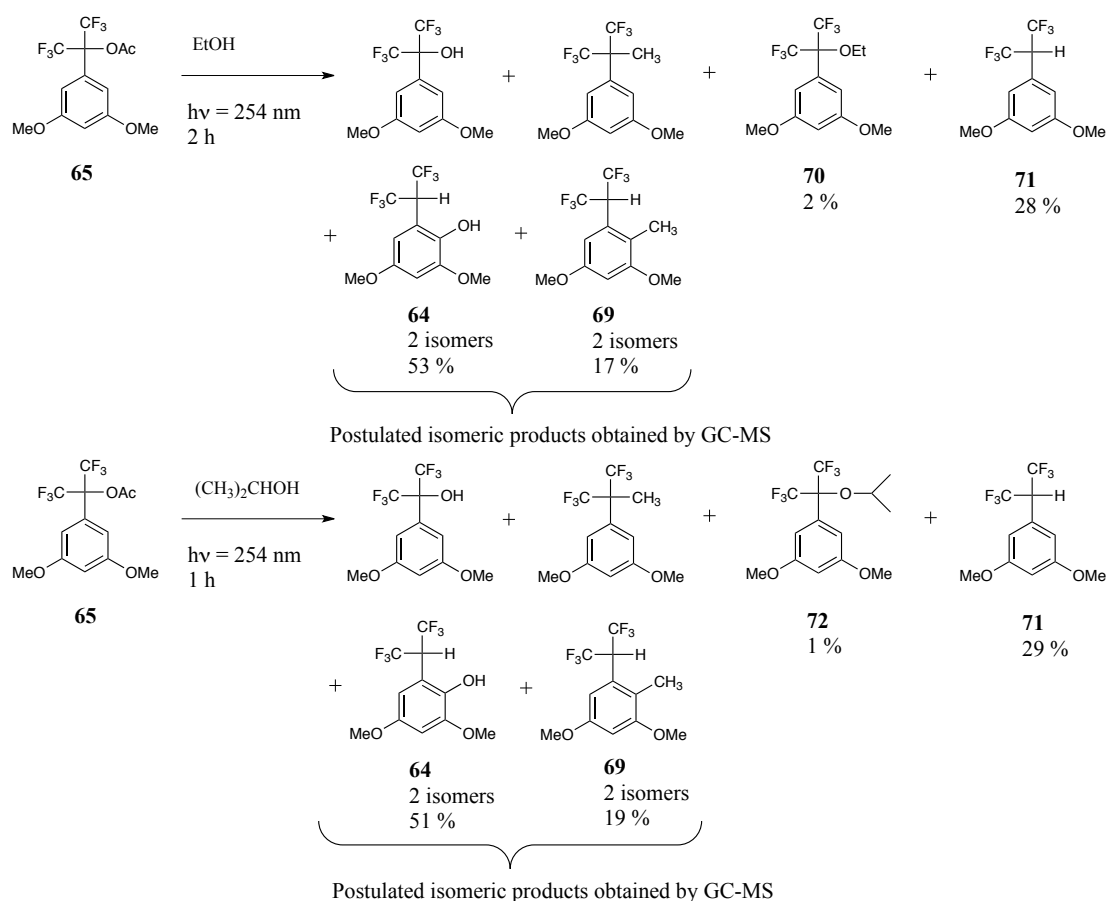
Postulated isomeric products obtained by GC-MS

Postulated isomeric products obtained by GC-MS

[a]GC-MS masses were all conducted using an electron impact (EI) method. For further specifications on the GC-MS instrument and the method used to analyze these and other photolysis mixtures see Chapter 7, Supporting Information. [b]All product ratios were exclusively based on GC peak areas in the GC-MS trace.

GC peaks closely match the retention time (R_T) for carbinol **64**. As a result, this lead

us to reason that these two peaks were 2 isomeric photoproducts of carbinol **64** and

that these 2 isomeric products consisted of roughly 53 % of the overall photoproduct

mixture (Scheme 3.4). Additionally, 2 other GC peaks also had similar m/z

chromatograms, but slightly different GC R_Ts. The mass associated with these two

isomeric products was 302. We believe that this product might be methylated product

69, and was present in ~17 % of the photolysis mixture by GC-MS (Scheme 3.4).

Only 2 % of the photolysis mixture (by GC-MS) consisted of what we believe is the

photosolvolysis product, ethoxy ether **70** (Scheme 3.4) which had the correct nominal

GC-MS mass of 332. The remaining product that was present in ~28 % had a m/z =

288, and thus matches that of the H-atom abstraction product **71** (Scheme 3.4). To

determine whether these products were exclusively formed in only EtOH, we

conducted several photolysis experiments in which we photolyzed (at hν = 254 nm)

acetate **65** in MeOH, 2-propanol, and TFE. In fact, similar products and product

ratios were found in all of these solvents with the exception of TFE. Scheme 3.4

shows that similar results for both products and product ratios can be seen for the

photolysis of **65** in 2-propanol.

Based on the experimental findings obtained from the photolysis of acetate

ester **65**, we can make some preliminary conclusions. First, it appears that **65** does

not give a clean mixture of 1 or 2 major photoproducts. Rather a complex mixture is

observed even if performed in various alcoholic solvents under similar photolysis

conditions. Secondly, the same mixture of products and product ratios is observed in

almost all alcoholic solvents (with the exception of TFE). One of the major products

is likely 2 isomers of carbinol **64** which can either arise from photoinduced

hydrolysis/transesterification of acetate **65** or from nucleophilic trapping by H_2O of

the 3,5-dimethoxy-α,α'-bis(trifluoromethyl)benzyl carbenium ion formed from C-O

bond heterolysis. We are unable to distinguish which process is occurring at the

present time. In addiiton, the 2 isomeric methylated products we observed in all

photolysis mixtures of acetate **65** in EtOH, MeOH, 2-propanol, etc. is likely the

consequence of initial C-O bond homolysis of the acetate leaving group followed by

"in cage" radical coupling of a CH_3 from the resulting acetoxy radical that would be

generated from this process. This pathway would ultimately lead to the loss of CO_2

from the generation of an initial acetoxy radical.

Scheme 3.5. Possible photoproducts identified by GC-MS[a] from the irradiation (hν = 254 nm) of acetate ester **65** (5-6 mM) in 2,2,2-trifluoroethanol (TFE)[b]
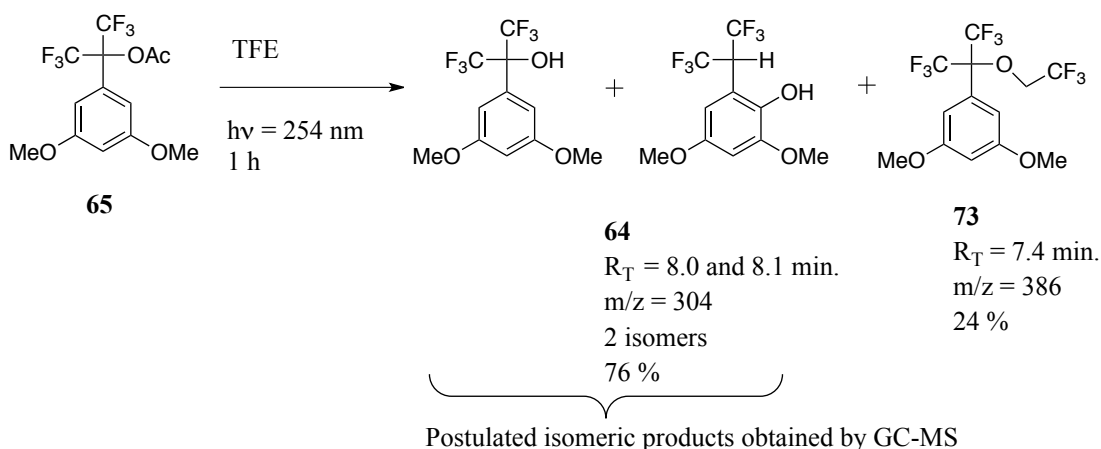
Postulated isomeric products obtained by GC-MS

[a]GC-MS masses were all conducted using an electron impact (EI) method. For further specifications on the GC-MS instrument and the method used to analyze these and other photolysis mixtures see Chapter 7, Supporting Information. [b]All product ratios were based exclusively on GC peak areas in the GC-MS trace.

From the small yield of ether adducts (**70** and **72**), we can only conclude that C-O bond homolysis must be occurring, thereby diminishing any nucleophilic trapping from the solvent that would produce either **70** or **72**. Because we believe the first step of this mechanism to the photolysis of **65** in alcoholic solvents must be homolysis (from the formation of methylated product **69**), then unfortunately it is unlikely that the H-atom abstraction product **71**, would be formed from a 3,5-dimethoxy-α,α'-bis(trifluoromethyl)benzyl triplet diradical intermediate. Instead we can only infer that any H-atom abstraction products observed in these experiments must come from the formation of the 3,5-dimethoxy-α,α'-bis(trifluormethy)benzyl radical intermediate from this reasoning.

Surprisingly, different results were observed for the photolysis of **65** in TFE (Scheme 3.5). We had expected to find homolysis products similar to **69** and **71**. However, no such products were observed by GC-MS even after at least 2-3 repetitions of the experiment in TFE (Scheme 3.5). Once again 2 isomers of carbinol **64** (m/z = 304) were detected by GC-MS and consisted of both 38 % each of the total product mixture (not including the amount of starting acetate **65** that was still present). The remaining 24 % of the photolysis mixture, consisted of what we assumed to be attributed to the TFE ether adduct (m/z = 386) **73** (Scheme 3.5). This was the only instance where a strong case can be made that C-O bond heterolysis may be occurring. Again C-O bond heterolysis would imply formation of the target 3,5-dimethoxy-α,α'-bis(trifluoromethyl)benzyl carbenium ion **57**. No further attempts to isolate or investigate the photochemistry of carbinol **64** and acetate **65** was pursued

due to that fact that under most conditions, the desired 3,5-dimethoxy- α,α'-bis(trifluoromethyl)benzyl carbenium ion intermediate **57**, could not be generated with the exception of performing the photolysis in TFE.

3.4 Future Work

From some of our preliminary results on *meta* disubstituted benzyl carbenium ions with α,α'-bis(trifluoromethyl) groups strongly suggests that Zimmerman's hypothesis for C-O bond heterolysis of benzyl acetates with 2 *meta* substituted MeO groups must be modified. Thus, Zimmerman's findings it seems can be only applied when there are simply hydrogens attached to the benzylic carbon bearing the acetate leaving group to promote efficient C-O bond heterolysis. Substitution of both H's with CF_3 groups at the benzylic carbon bearing the acetate leaving group, tends to promote more homolysis rather than heterolysis from the preliminary data that has been presented throughout this chapter. Therefore, careful steady-state NMR experiments should be conducted to identify some of the unusual photoproducts from the photolysis of **64** and **65** in the same alcoholic solvents presented throughout this chapter. The synthesis and isolation of some of the products observed in our photolysis mixtures of **64** and **65** (Scheme 3.3-3.5), must also be investigated in the near future.

Following our preliminary results from the phtolysis of **64** and **65** in various alcoholic solvents, it is clear that a variety of photoproducts are observed by GC/GC-MS. As a result, one potential solution to obtaining a less complex mixture of

photoproducts, is to slightly modify the photoprecursor leaving group.   Moreover,

one can increase the probability for C-O bond photoheterolysis to yield the target 3,5-

dimethoxy-α,α'-bis(trifluoromethyl)benzyl carbenium ion **57**, by changing the

hydroxyl or acetate at the benzylic carbon, to a better leaving group. Good leaving

groups that would most certainly lead to C-O bond heterolysis, are the *p*-toluene

sulfonyl or methylsulfonyl groups. The pK$_a$'s of the conjugate acids of these leaving

groups are *ca.* -2.8 and -1.9 respectively. Consequently, future work must be done to

synthesize and investigate the photochemistry of sulfonyl esters **74** and **75** (Figure

3.2).
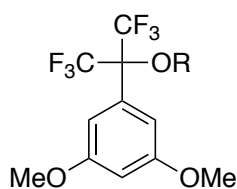
74
R = Ts or SO$_2$-C$_6$H$_4$-4-Me or
75
R = Ms or SO$_2$Me

Figure 3.2. Potential photoprecursors that could lead to the generation of the 3,5-
dimethoxy-α,α'-bis(trifluoromethyl)benzyl carbenium ion **57**.

Chapter 4: The 2-(3,5-Dinitrophenyl)-1,3-Dithiane Carbanion: A Benzyl Anion with a Low Lying Triplet State

4.1 Introduction

In chapter 2, we have seen that a strong case can be made that 3,5-bis(dimethylamino)benzyl carbenium ion intermediates have degenerate singlet and triplet ground states. Recent computations have identified a new class of ion-diradicals (Scheme 1.6, chapter 1), wherein a cationic acceptor group (e.g. O^+, NR^+, CR_2^+) is placed on a benzene ring *meta* with respect to one or two strong neutral π-electron donors (e.g. NMe_2, NH_2).[41] In some favorable cases, the cationic species can have a π,π^*-triplet ground state. This can be viewed as resulting from a formal transfer of a single electron from the donor substituent to the cationic center.

This chapter and the next chapters will explore if the same reasoning could be applied to anionic species. Recall in Scheme 1.6 in chapter 1, we hypothesized that an anionic center that possessed two strong π-acceptor groups (e.g. NO_2, CN, C(O)R) that are *meta* with respect to the formally anionic center, could have a triplet diradical state. This anion diradical state can be generated by the transfer of an electron from the anionic donor group to one of the π-acceptor groups.   To test this, we have generated and characterized a benzylic carbanion having two *meta* disubstituted nitro groups. Furthermore, the main focus of this chapter will center on comparing the differences in the chemical and electronic properties associated with the 2-phenyl-1,3-dithiane carbanion (which is predicted to behave as a ground state singlet by our computations) and the 2-(3,5-dinitrophenyl)-1,3-dithiane carbanion (which we

believe to have a thermally accessible triplet ground state).   Density functional theory (DFT) calculations suggests that the 2-(3,5-dinitrophenyl)-1,3-dithiane carbanion has a diradical ground state. Proton NMR, UV-Vis, H/D exchange experiments, as well as chemical trapping experiments provides evidence that the 2-(3,5-dinitrophenyl)-1,3-dithiane carbanion is both a persistent and paramagnetic species.

4.2 DFT Computations on Benzyl Anions With Meta π-Acceptors

Previously in chapters 2 and 3, we have seen that computations of singlet-triplet energy gaps has provided us a useful starting point in determining which species may have low energy, open-shell and/or triplet electronic states. Therefore, we approached anionic species in the same fashion. Scheme 4.1 shows the computed gas-phase DFT ΔE_{ST} values of 9 carbanions and 2 neutral salts.   We investigated various anions of which included benzylic carbanions with no electron acceptors **76**, the 3,5-dicyano **77**, and 3,5-dinitro **78** derivatives (Scheme 4.1). Also, we computed singlet-triplet energy gaps for several benzyl anions that possessed either two sulfur atoms **79**, **82-83**, two oxygen atoms **80**, or one of each **81**. Each of the anion's geometries of the singlet and triplet states were optimized at the (U)B3LYP/6-31+G(d,p) level and the reported geometries were verified as local minima based on the vibrational energy calculations which showed no imaginary frequencies. All of ΔE_{ST} values were corrected for zero-point vibrational energy (ZPVE) and negative values indicate that the singlet is the ground state.

Simple benzyl anions without strong π-acceptors in the *meta* positions (**76** and

82) are as expected ground state singlets having negative ΔE_{ST} values. Placement of

modest π-acceptors at the *meta* positions (**77**, **78**, and **86**) has a small effect of

lowering the ΔE_{ST} values in favor of the triplet state. Interestingly, dicarboxylate

trianion **86** still has a singlet-triplet energy gap that favors the singlet state by -18.1

kcal/mol. In fact, the 3,5-dinitrobenzyl anion **78** is predicted to be a singlet by DFT,

Scheme 4.1. Predicted singlet-triplet energy gaps by DFT (B3LYP/6-31+G(d,p)) for
several benzylic carbanions

76	**77**	**78**	**79**
ΔE_{ST} = -42 kcal/mol	ΔE_{ST} = -21.5 kcal/mol	ΔE_{ST} = -1.3 kcal/mol	ΔE_{ST} = +0.3 kcal/mol

80	**81**	**82**	**83**
ΔE_{ST} = +6.2 kcal/mol	ΔE_{ST} = +2.7 kcal/mol	ΔE_{ST} = -45.4 kcal/mol	ΔE_{ST} = -10 kcal/mol

84	**85**	**86**
ΔE_{ST} = +26 kcal/mol	ΔE_{ST} = +12 kcal/mol	ΔE_{ST} = -18.1 kcal/mol
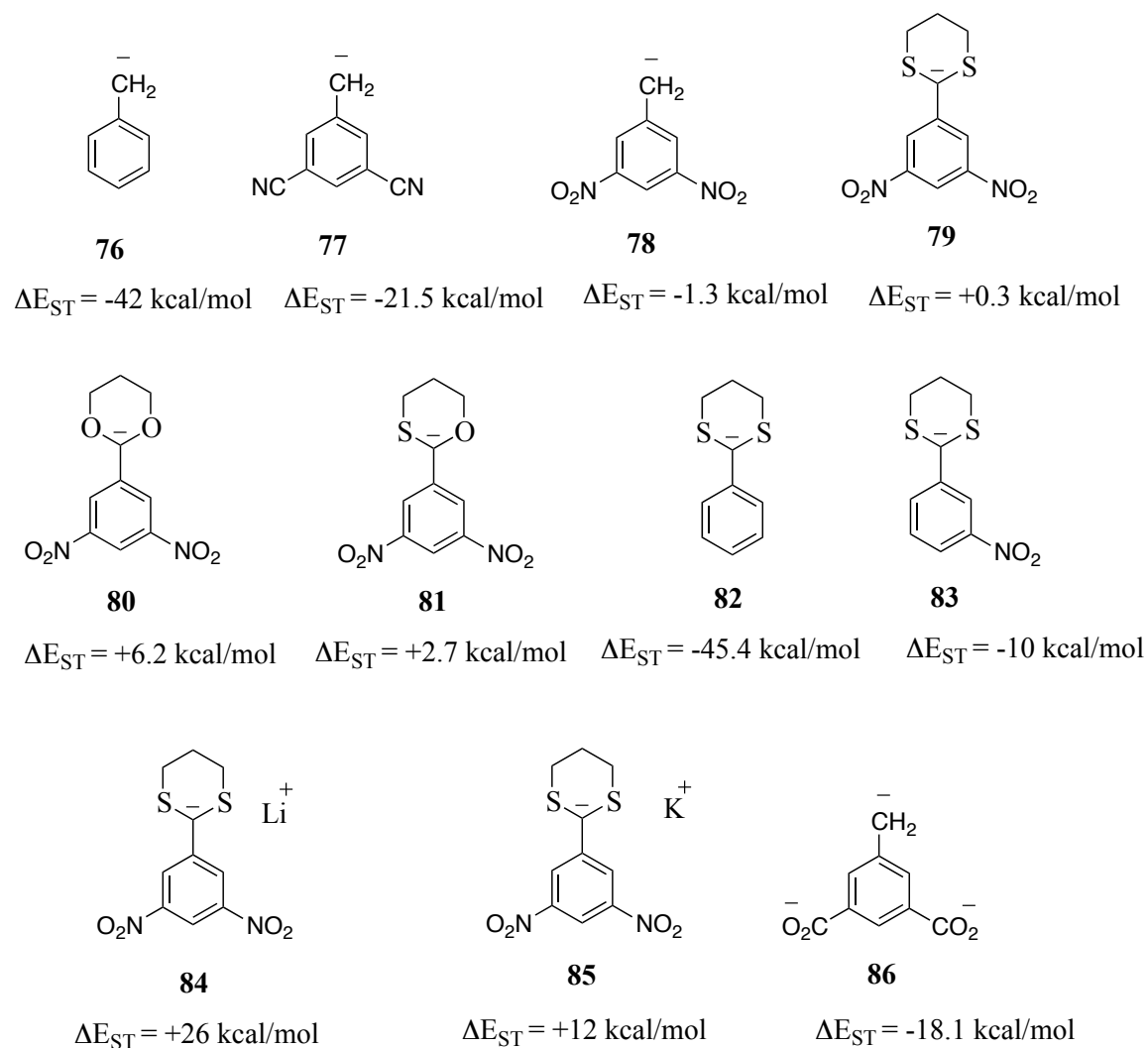
however the singlet-triplet energy gap is very small at this point. Only when *meta* π-electron donating groups are added adjacent to the anionic center (**79-81** and **84-85**) does DFT predict a triplet ground state (Scheme 4.1).

It should be noted that DFT is a single-reference method and so it does not explicitly account for nondynamical correlation in any rigorous way. Nondynamical correlation is usually important for the singlet state than the triplet state. Hence, DFT often underestimates the singlet stability relative to the triplet by several kcal/mol.

To evaluate the accuracy of (U)B3LYP/6-31+G(d,p) method we used for our computations, we computed the singlet-triplet energy gap for the parent benzyl anion **76** using both CASSCF and CBS-QB3 computational methods. CASPT2/cc-pVDZ and the CBS-QB3 methods yielded values of -46.3 and -44.0 kcal/mol respectively for anion **76**. These numbers are in reasonable agreement with previous calculations (Scheme 4.1). Although CBS-QB3 is also a single-reference method, it has been known to give extremely accurate energy values by accounting for both static and dynamic electron correlation as well as extrapolating to an infinite basis set limit.

From the computations shown in Scheme 4.1, we considered that ion pairing might effect ΔE_{ST}. More specifically, we calculated the charge distributions for **84S-Li$^+$/84T-Li$^+$** and **85S-K$^+$/85T-K$^+$** (Figure 4.1a and b). The singlet state favors more the negative charge at the benzylic carbon center, whereas the triplet state favors more accumulation of the negative charge at the nitro groups. This picture is

consistent with the general structure depicted in Scheme 1.6 in chapter 1. Moreover, it implies that differential counterion binding to these sites might effect ΔE_{ST}.

Therefore, DFT computations were carried out on the singlet and triplet states of ion pairs consisting of anion **79** with lithium and potassium cations. While several local minima were located with respects to the positioning of the cations, the lowest

(a)
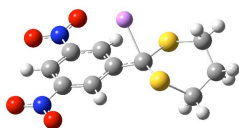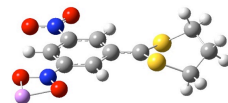
84S-Li$^+$ **84T-Li$^+$**

(b)
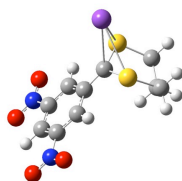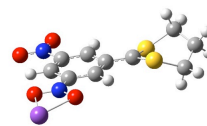
85S-K$^+$ **85T-K$^+$**

Figure 4.1. (a) Computed DFT (B3LYP/6-31+G(d,p)) geometries of the singlet **84S-Li$^+$** (left) and triplet **84T-Li$^+$** (right). (b) Computed DFT (B3LYP/6-31+G(d,p)) geometries of the singlet **85S-K$^+$** (left) and triplet **85T-K$^+$** (right).

energy minima for each spin state are depicted in Figure 4.1. As expected, the triplet state has the Li$^+$ or K$^+$ counterions associated with the nitro groups whereas in the singlet state the same counterions are associated with the benzylic carbon (Figure 4.1). For example, the value for ΔE_{ST} for the lithium increases to +26 kcal/mol as compared to nearly degenerate for the gas-phase free anion, **79** (ΔE_{ST} = +0.3 kcal/mol). The binding of potassium to benzyl anion **79** results in a smaller increase in the ΔE_{ST} value to +12 kcal/mol. The smaller increase in the ΔE_{ST} for the binding of benzyl anion **79** is presumably due to its weaker coordination to the anionic sites as a result of its larger ionic size compared to that of the lithium cation. Of course coordinating solvents like ethers would be expected to bind to the counterions competitively with the anions. Thus, we would expect the magnitude of the counterion effect on ΔE_{ST} to be diminished relative to what we previously calculated in the gas-phase. Reoptimization of the singlet benzyl anion **79S**, and the triplet diradical **79T** using the Polarizable Continium model (Integral Equation Formalism-PCM) at the 6-31+G(d,p) level with THF as solvent, showed a decrease in ΔE_{ST} to a value of +17 kcal/mol (including correction for ZPVEs). Nonetheless, it is reasonable to expect that either the lithium or potassium salts of benzyl anion **79**, will be a triplet or at least should have a thermally accessible triplet state if it is generated in solution.

*4.3 Synthesis of Benzyl Anion Precursor **89***

The 2-phenyl-1,3-dithiane **90** can fortunately be purchased from the Sigma-Alrich, Co. and was used without further purification. However, the 2-(3,5-dinitrophenyl)-1,3-dithiane benzyl anion precursor **89** was synthesized in two

straightforward steps from the commercially available benzyl alcohol **87** (Scheme 4.2). Initial PCC oxidation of the 3,5-dinitrobenzyl alcohol **87** affords the 3,5-dinitrobenzaldehyde **88** (Scheme 4.2). The dithiane benzyl anion precursor **89** is then synthesized by refuxing aldehyde **88** with a catalytic amount of *p*-toluenesulfonic acid (PTSA), 1,3-propanedithiol, in toluene and a Dean-Stark trap.

Scheme 4.2. Synthesis of dithiane benzyl anion precursor **89**
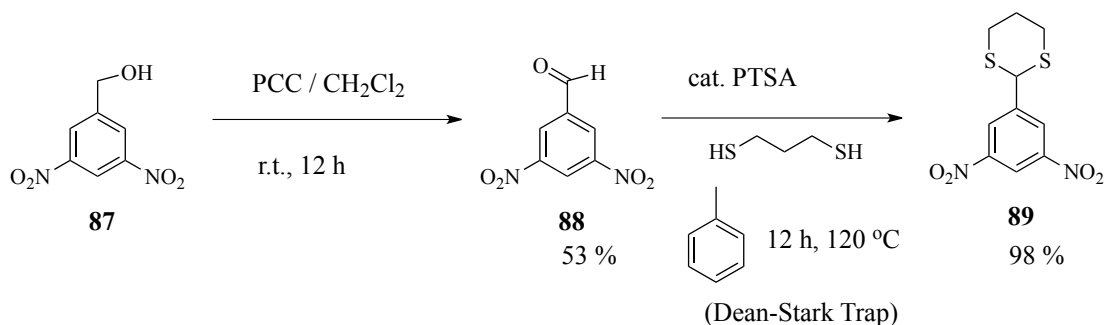
4.4 Generation of Benzyl Anions 79 and 82 (H/D Exchange Experiments)

Benzyl anions **79** and **82** were generated from simple deprotonation of their hydrocarbon precursors **89** and **90** using various strong alkyllithium bases. One method for determining whether an anion is formed from deprotonation of a carbon acid with a base, is through the replacement of the acidic hydrogen with that of a deuterium (H/D exchange).[11,83-88] For example, in a side by side experiment, dithianes **89** and **90** were allowed to react (separately) with a solution of excess KH/THF at room temperature for 1 hour (Scheme 4.3). The resulting reaction mixtures were then quenched with CD$_3$OD (Scheme 4.3). ^{1}H NMR analysis of each reaction mixture showed that deuterium was incorporated into the benzylic positions of both dithianes. Each of these two reaction mixtures yielded 86 % and 76 % H/D incorporation from the peak integrations for dithiane **89** and **90** respectively.

To verify whether H/D incorporation only occurs when KH in THF is used to deprotonate dithianes **89** and **90**, we conducted a few more of these experiments using different bases and various aprotic solvents. For instance, an experiment that showed similar H/D incorporation results can be seen in Scheme 4.4 and Figure 4.2. Here dithiane **89** was allowed to react with an excess of *n*-BuLi in THF at room temperature and the resulting red-purple mixture was subsequently quenched with

Scheme 4.3. H/D exchange experiment of dithiane **89** and **90** in anhydrous THF with excess KH at room temperature (1 hour) and quenching with excess CD$_3$OD

89 (X = NO$_2$)
90 (X = H)

89 X = NO$_2$ (86 % H/D incorporation)
90 X = H (76 % H/D incorporation)
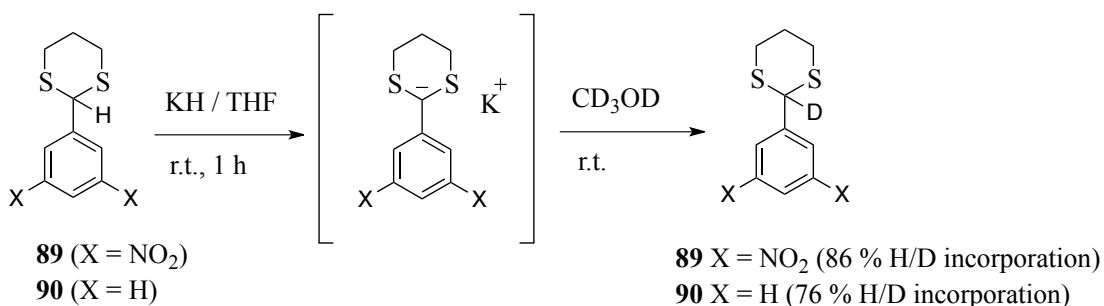
CD$_3$OD. The resulting mixture showed that 74 % H/D incorporation into the benzylic position of dithiane **89** was obtained from the NMR spectrum (Figure 4.2).

Scheme 4.4. H/D experiment conducted on dithiane **89**/THF with excess *n*-BuLi as base, which is quenched with CD$_3$OD

1. (1.7 equiv.) *n*-BuLi
r.t., 5 min.

2. excess CD$_3$OD, r.t., 3 min.

+ CD$_3$OLi

89

(74 % H/D incorporation)
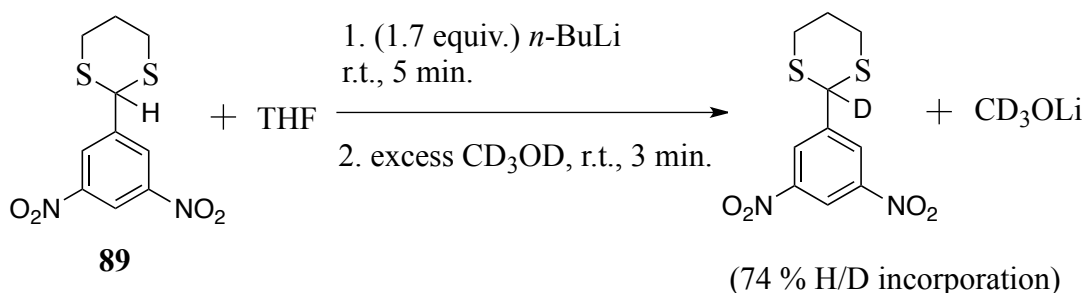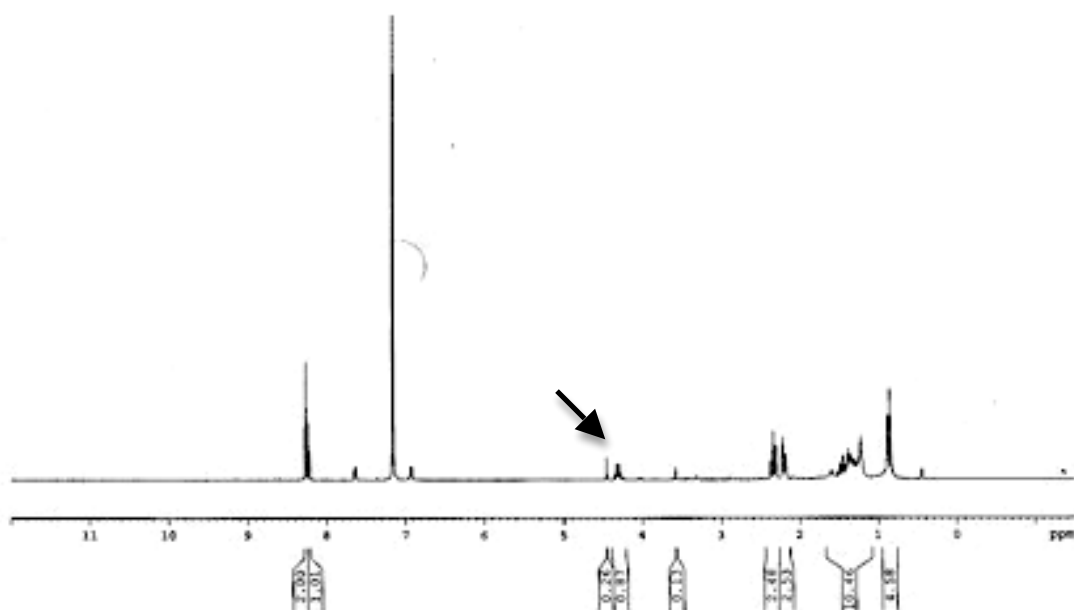
Figure 4.2. ^{1}H NMR (400 MHz) spectrum of the resulting reaction mixture shown in Scheme 4.4. NMR was performed in C_6D_6 and all peak integrations were calibrated to the 2 *ortho* aromatic protons of dithiane **89**. The arrow in the above spectrum indicates the location of the resonance associated with where the benzylic proton for dithiane **89** usually appears in C_6D_6. The arrow in the figure depicts a decrease in the NMR integration signal associated with the benzylic proton resonance of dithiane **89** at ~4.5 ppm.in the NMrR spectrum. Thereby demonstrating that significant H/D incorporation was achieved in this experiment.

Essentially similar results were obtained when different strong bases were used such as CH_3Li, and *n*-BuLi as well as with the use of other aprotic solvents including benzene, 1,4-dioxane, and THF (for NMR spectra for these and other experiments, see Chapter 7, Supporting Information for more details).

81

Carbanions derived from 1,3-dithanes are well known to carry out S_N2

reactions with primary alkyl halides.[89-99] In addition, the implementation of strong

electrophiles as an effective method for trapping anionic intermediates, is a useful

qualitative method of detecting the presence of this intermediate.[83,98] Deprotonation

of dithiane **90** with *n*-BuLi in 1,4-dioxane followed by addition of a suitable

electrophile such as 1-bromopropane resulted in modest alkylation (57 %) at the

benzylic position of dithiane **90** (Scheme 4.5). The alkylation product **91** formed in

this reaction was identified to be presented in the mixture by GC, mass spectroscopy

Scheme 4.5. Side by side chemical trapping experiment of dithianes **89** and **90** in
1,4-dioxane with addition of 2.5 M *n*-BuLi at room temperature followed by
treatment with 1-bromopropane
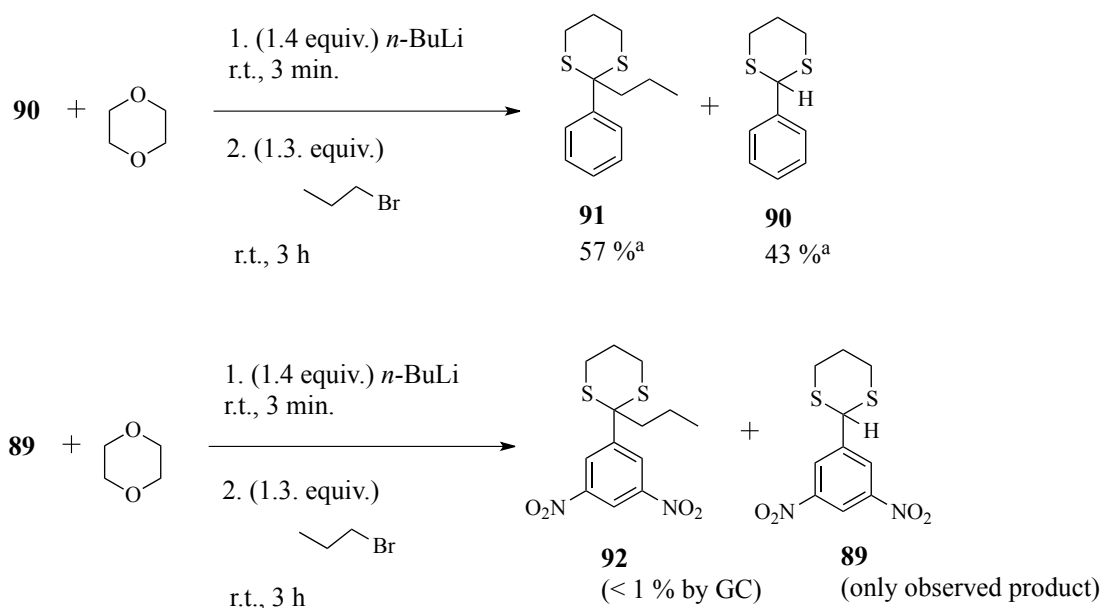
[a]Yields of **90** and **91** was determined by a 4-point GC calibration curve of **90**. The yield of **91** was
extrapolated from the yield of **90** determined from a GC calibration curve (see Chapter 7, Supporting
Information for calibration curve for **90**). Products **90** and **91** were the only products observed by GC,
DART (mass spectroscopy) and ^{1}H NMR. No attempt to isolate or optimize the conditions in which
alkylation products were generated under these experimental conditions.

and, ^{1}H NMR. Also, the only other product generated from this reaction was the

reprotonated dithiane **90**. Similarly, dithiane **89** was also allowed to react with *n*-

BuLi and 1-bromopropane under the exact same conditions, however < 1 % of

thealkylated product was observed from this process (Scheme 4.5). From this side by

side chemical trapping experiment, it appears that dithiane **90** can be alkylated (to

some degree). On the other hand, dithiane **89** seems to prefer reprotonation of the

benzylic C-H bond rather than S_N2 alkylation (Scheme 4.5).

Further attempts to alkylate dithianes **89** and **90** under similar reaction

conditions yielded consistently the same results as shown in Scheme 4.5. For

instance, both dithianes **89** and **90** were treated with *n*-BuLi in 1,4-dioxane followed

by methyl iodide (MeI) as an alkylating agent. Dithiane **90** resulted in roughly 60 %

of the alkylated adduct and 40 % of the original dithiane **90** was observed in this

reaction (see Chapter 7, Supporting Information for spectra data for this reaction).

Again, no effective alkylation of dithiane 8**9** (< 1 %) was observed under these

conditions (see Chapter 7, Supporting Information). Although the observations

descrbied above do not unambiguously determine the electronic states of dithiane

anions **89** and **90**, they do however show that the benzyl anions of **89/90** possess

qualitatively different chemical behavior.

4.6 UV-Vis Spectra of Anion **79**

Time-dependent Density Functional Theory (TD-DFT) has been used to

accurately predict the electronic ground state UV-Vis absorbance bands for various

reactive intermediates such as diradicals,[12a-b] carbenes,[100] nitrenium ions,[101] and

nitrenes.[102] As a result, we computed the TD-DFT UV-Vis absorbance bands for the

singlet and triplet states of benzyl anion **79**. The singlet state of benzyl anion **79** is

predicted to have strongests absorbance maxima (strongest oscillator strengths) at

1553, 481.9, 353.7, and 350.1 nm. The triplet diradical of benzyl anion **79** had only

three major UV-Vis peaks predicted by TD-DFT at 1662, 680, and 422.8 nm (for a

complete table of all TD-DFT computational data on benzyl anion **79**, see Chapter 7,

Supporting Information).

From the H/D and chemical trapping experiments used to generate benzyl

anions **79** and **82** (sections 4.4 and 4.5), we were able to determine under what

conditions these anions could be effectively studied in solution. Nonetheless, in these

two sections we were unable to unambiguously identify the electronic ground state of

dithiane anion **79**. Thus, we anticipated that the electronic configuration could be

elucidated through comparing UV-Vis spectra of anion **79** taken experimentally, with

the TD-DFT UV-Vis absorbance data that we obtained computationally. Obtaining

viable UV-Vis spectra of any carbanion in solution can be a very challenging task.

One challenge encountered in obtaining high quality UV-Vis spectra of carbanions, is

that in most cases one is working at very low concentrations (on the order of μM) of

the original conjugate acid. Therefore, most of the UV-Vis spectra for the

corresponding anion, is likely to be dominated from absorbances due to the solvent,

additives that might be present in solution, and impurities from the base being used to

generate the desired anion. To circumvent this, a control UV-Vis spectrum in which

excess base and solvent must be carefully subtracted from the UV spectrum obtained

for the target anion, which is taken with the same solvent and base.

Figure 4.3 shows a typical UV-Vis experiment involving the generation of

benzyl anion **79** from the deprotonation of dithiane **89**.   An inital UV-Vis spectrum
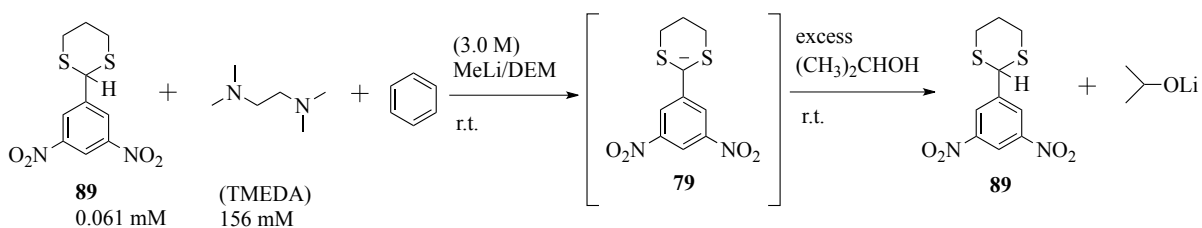
(b)
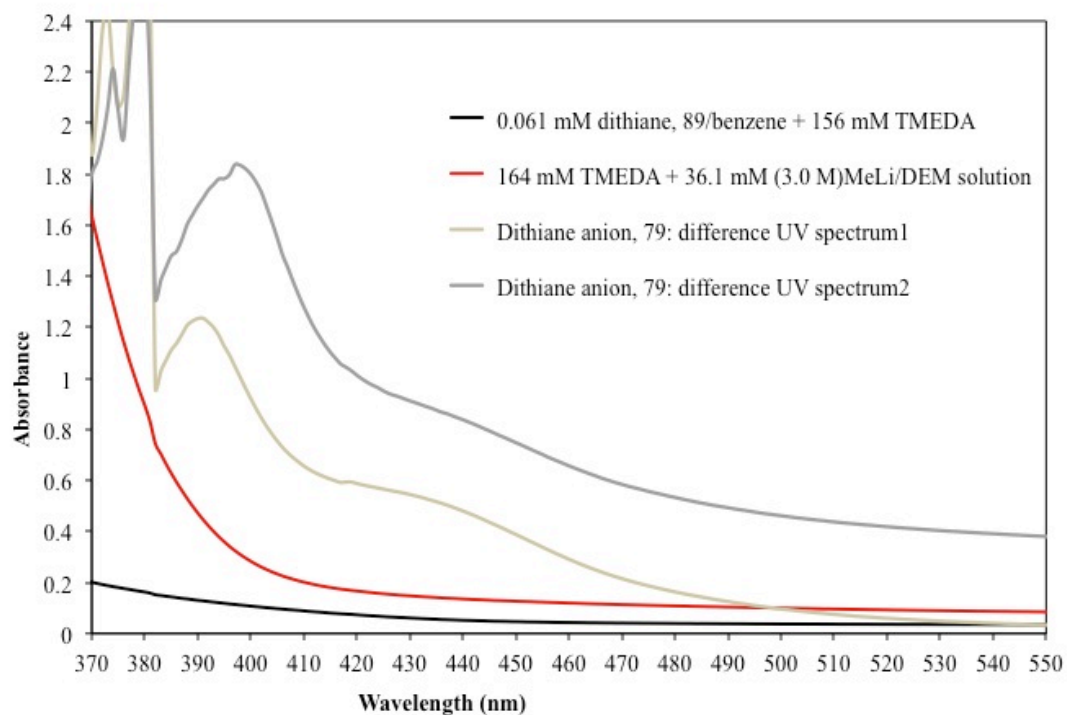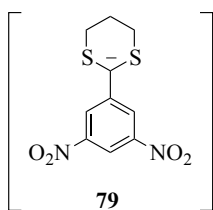
(a)
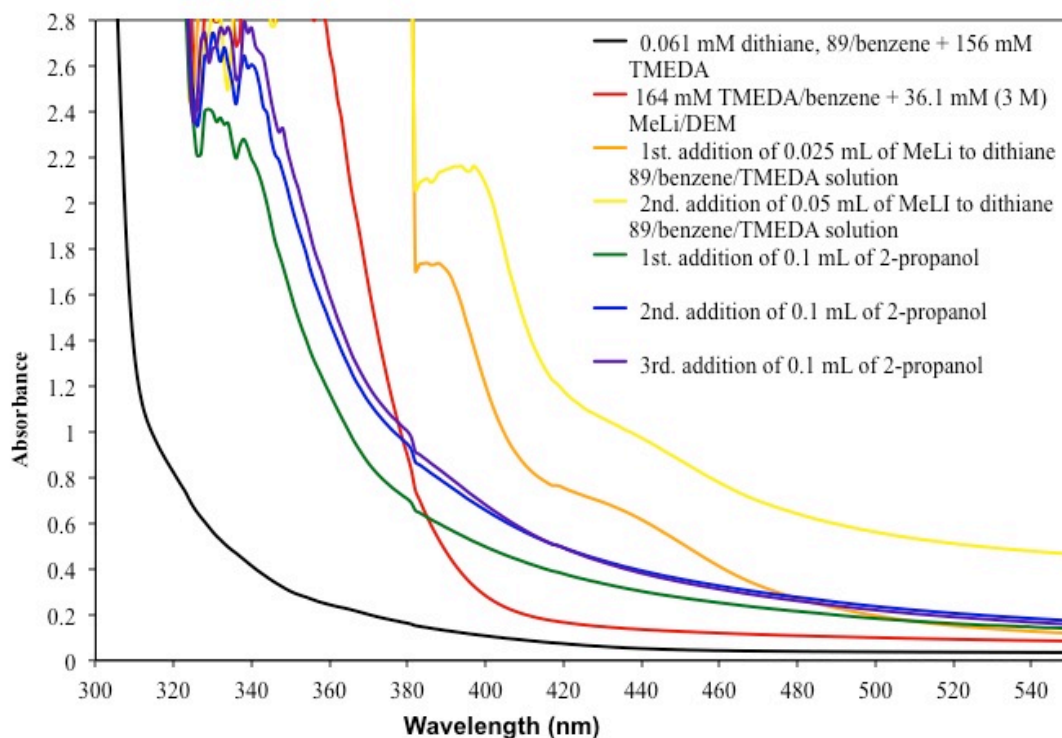
Figure 4.3. UV-Vis absorbance spectra for benzyl anion, **79** in benzene/TMEDA and MeLi. (a) 0.0610 mM dithiane**, 89**/benzene and 156 mM TMEDA (black). 164 mM TMEDA/benzene and 36.1 mM MeLi/DEM, background UV-Vis spectrum (red). 0.0610 mM dithiane**, 89**/benzene and 156 mM TMEDA with the first addition of 25.0 μL of 3.00 M MeLi/DEM (orange). 0.0610 mM dithiane**, 89**/benzene and 156 mM TMEDA with the second addition of 25.0 μL of 3.00 M MeLi/DEM (yellow). 0.0610 mM dithiane**, 89**/benzene and 156 mM TMEDA after additions of (50.0 μL total) MeLi/DEM, which is quenched with 0.100 mL of 2-propanol (green). 0.0610 mM dithiane**, 89**/benzene and 156 mM TMEDA after additions of (50.0 μL total) MeLi/DEM, which is quenched with a second aliquot of 0.100 mL of 2-propanol (blue). 0.0610 mM dithiane**, 89**/benzene and 156 mM TMEDA after additions of (50.0 μL total) MeLi/DEM, which is quenched with a third aliquot of 0.100 mL of 2-propanol (purple). (b) 0.0610 mM dithiane**, 89**/benzene and 156 mM TMEDA (black). 164 mM TMEDA/benzene and 36.1 mM MeLi/DEM, background UV-Vis spectrum (red). Difference spectrum1 of dithiane benzyl anion **79** (brown) obtained from the subtraction of MeLi + dithiane, **89** /benzene/TMEDA (orange) - MeLi/benzene/TMEDA control (red). Difference spectrum2 of dithiane benzyl anion **79** (grey) obtained from the subtraction of MeLi + dithiane, **89** /benzene/TMEDA (yellow) - MeLi/benzene/TMEDA control (red).

was taken of a 0.061 mM solution of dithiane **89** in 156 mM *N, N, N', N'*-tetramethylethylenediamine (TMEDA) as an additive in benzene (Figure 4.3a and b, black spectrum). Subsequently, MeLi was then added (in several portions) to the initial dithiane solution (Figure 4.3a, orange and yellow spectra).   The addition of excess base would presumably quantitatively deprotonate dithiane **89** to generate the resulting benzyl anion **79** spectrum. Two new absorbance bands clearly begin to grow in when base is added to the dithiane, **89**/benzene/TMEDA solution.   These two bands consists of shoulders at *ca*. 395 nm and λ_{max} = ~430 nm (Figure 4.3a, yellow and orange spectra).   As expected, when anion **79** is quenched with a protic source such as 2-propanol, the two maxima at 395 and ~430 nm become significantly blue shifted and diminish considerably in overall intensity in the UV-Vis spectrum (Figure 4.3a, green, blue, and purple spectra). To verify that the absorbance band at *ca.* 395 nm and the shoulder band at ~430 nm was not due to any significant absorbances from the base (MeLi) or the solvent/additive (benzene/TMEDA), a background control UV-Vis spectrum that only contained 164 mM TMEDA/benzene and 36.1 mM MeLi was taken (Figure 4.3a and b red spectrum). From this background spectrum (red), one can see that there is to a lesser degree an absorbance (< 0.3) due to MeLi or TMEDA/benzene in the UV spectrum. Nevertheless, the background spectrum that only contained MeLi, benzene, and TMEDA was subtracted from the spectra we obtained from the initial titrations of excess MeLi to the dithiane, **89**/benzene/TMEDA solution (Figure 4.3b, brown and grey spectra). In fact, the absorbances at λ_{max} = 395 and 430 nm clearly survived this background subtraction. As a result, we nominally assigned the benzyl anion **79** to have UV-Vis

peaks at 395 and ~430 nm under these experimental conditions. In general, both the

UV-Vis spectra seen in Figure 4.3a-b was reproduced several times and yielded

similar spectra.

Since we were able to generate and observe the UV-Vis spectra that we have

nominally assigned to benzyl anion, **79** with MeLi, benzene/TMEDA (Figure 4.3a

and b), we wanted to establish whether other bases, additives, and aprotic solvents

could be used to generate a UV-Vis spectrum for anion **79**. Thus, we elected to

generate benzyl anion **79** again in benzene/TMEDA but with the use of *n*-BuLi as

base. Similarly, we obtained UV-Vis spectra for benzyl anion **79** in THF as a solvent

and used excess *n*-BuLi as a base to deprotonate dithiane **89** at room temperature.

Both Figure 4.4a and b show several sets of subtracted UV-Vis spectra for benzyl

anion **79**, as well as the UV-Vis spectra for the background control UV-Vis spectra

that we obtained for the base + solvent (red spectrum), and the initial UV-Vis

spectrum that contained dithiane **89** + solvent (black spectrum). Not shown in either

Figure 4.4a or b is the detailed titration of excess base to the original dithiane

89/solvent solutions and the quenching of the resulting benzyl anion (**79**) solution

with a protic solvent (see Chapter 7, Supporting Information for the corresponding

spectra of Figure 4.4a and b). As with the difference spectra shown in Figure 4.3b,

each of the UV-Vis spectra shown brown, grey, and cyan respectively in Figure 4.4a-

b represents the subtracted spectra we obtained from each addition of base to dithiane

89 with again the corresponding base(s) + solvent(s) subtracted out.

Unfortunately, the subtracted UV-Vis spectra for benzyl anion **79** in Figure

4.4a and b are not as clean and well defined as seen in Figure 4.3b.   This may be

due to ion pairing or solvent aggegration effects, which could extensively broaden

some of the observed absorbances for anion **79**, in solution.[2] Figure 4.4a shows that

the background UV-Vis spectrum of 156 mM TMEDA/benzene and 119 mM *n*-BuLi

(red spectrum), has a significantly intense, tailing absorbance band starting at ~440

nm with an absorbance > ~0.4 which gradually increases to go off-scale below 440

nm. Analogously, the background UV-Vis spectrum of excess *n*-BuLi/THF (red

spectrum) shown in Figure 4.4b, shows a small band at ~420 nm, which again

increases in intensity (Abs. > ~0.2) below ~350 nm and proceeds to go off-scale.

Despite the substantial UV-Vis bands to the base in solution (Figure 4.4a and b, red

spectra), we were still able to observe some positive UV-Vis maxima for what we

attribute to be benzyl anion **79**, after the absorbances due to the respective bases and

solvents were carefully subtracted (Figure 4.4a cyan spectrum, and Figure 4.4b brown

and grey spectra).

The cyan UV-Vis difference spectrum for benzyl anion **79** in Figure 4.4a

shows that the anion has a broad absorbance band that starts at $\lambda_{max} = \sim 440$ nm and

extends to *ca*. 410 nm. Another maximum is also present in the benzyl anion **79**

difference spectrum (cyan) in Figure 4.4a at *ca*. 397 nm. Interestingly, benzyl anion

79 also has broad shoulder bands at ~430 and 375 nm, and a sharp and intense

absorbance at *ca*. 320 nm (grey and brown spectra) when generated in THF/*n*-BuLi

(Figure 4.4b). Although not all of the UV-Vis maxima for benzyl anion **79** are

always consistent in all of our UV-Vis experiments, there are still some key features

to point out from all the UV-Vis spectra we have obtained. It seems that broad bands

in the UV-Vis spectra throughout the region of 400-430 nm seems fairly consistent

(plus or minus about 10 nm) in MeLi/TMEDA/benzene (Figure 4.3b), *n*-BuLi/THF,

and *n*-BuLi/TMEDA/benzene (Figure 4.4a and b). Comparing some of our

experimental UV-Vis data with the TD-DFT results presented earlier in this section,

we can begin

(b)

79
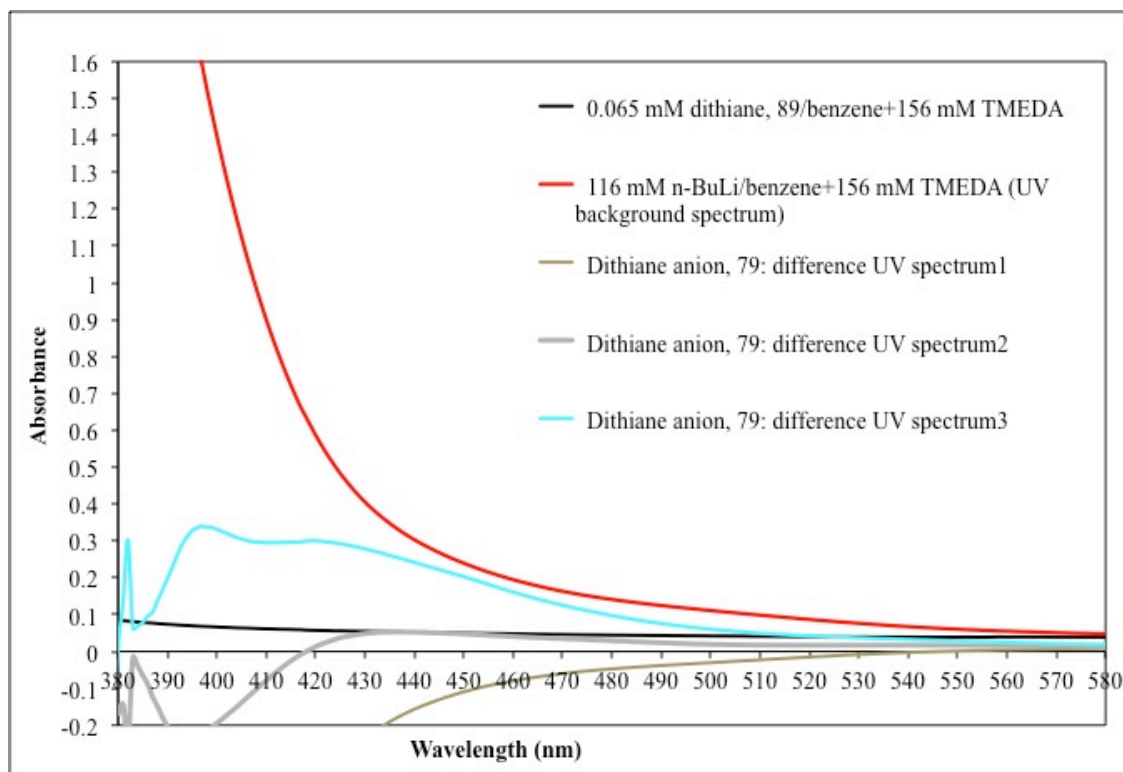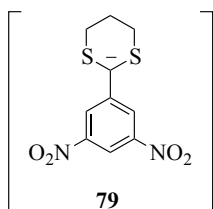
(a)
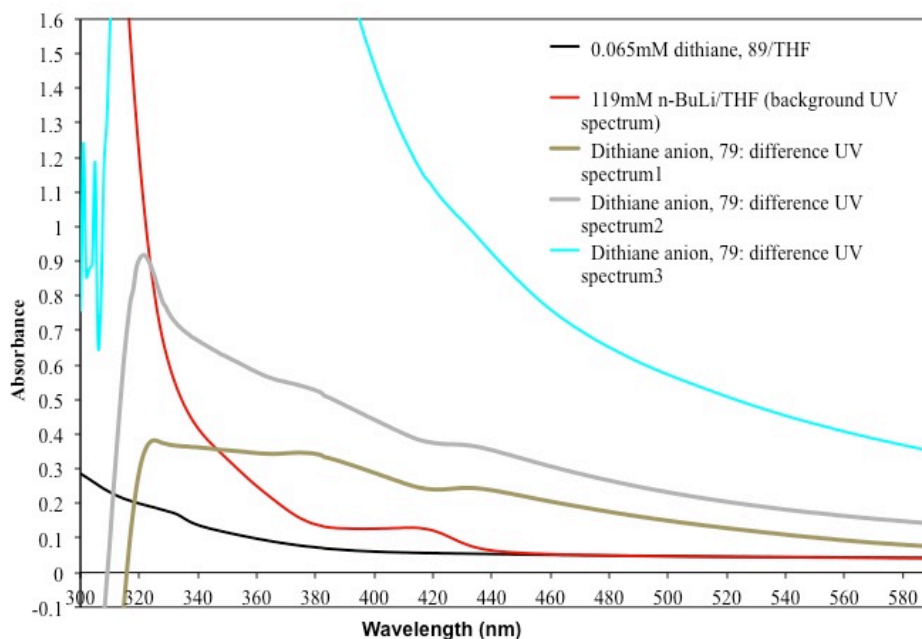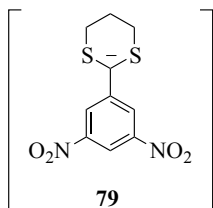
Figure 4.4. UV-Vis subtracted absorbance spectra for benzyl anion, 79 in benzene/TMEDA and *n*-BuLi and in THF/*n*-BuLi. (a) 0.0650 mM dithiane 89/benzene 156 mM TMEDA (black). 116 mM *n*-BuLi and 156 mM TMEDA/benzene (red). Difference spectrum1 of dithiane benzyl anion 79 (brown) obtained from the subtraction of the first addition of *n*-BuLi + dithiane, 89/benzene/TMEDA (not shown) – *n*-BuLi/benzene/TMEDA control (red). Difference spectrum2 of dithiane benzyl anion 79 (grey) obtained from the subtraction of the second addition of *n*-BuLi+dithiane, 89 /benzene/TMEDA (not shown) – *n*-BuLi/benzene/TMEDA control (red). Difference spectrum3 of dithiane benzyl anion 79 (cyan) obtained from the subtraction of the third addition of *n*-BuLi + dithiane, 89/benzene/TMEDA (not shown) – *n*-BuLi/benzene/TMEDA control (red). (b) 0.0650 mM dithiane 89/THF (black). 119 mM *n*-BuLi/THF background control spectrum (red). Difference spectrum1 of dithiane benzyl anion 79 (brown) obtained from the subtraction of the first addition of *n*-BuLi + dithiane, 89/THF (not shown) – *n*-BuLi/THF control (red). Difference spectrum2 of dithiane benzyl anion 79 (grey) obtained from the subtraction of the second addition of *n*-BuLi + dithiane,89/THF (not shown) – *n*-BuLi/THF control (red). Difference spectrum3 of dithiane benzyl anion 79 (cyan) obtained from the subtraction of third addition of *n*-BuLi + dithiane, 89/THF (not shown) – *n*-BuLi/THF control (red).

to attempt to identify the ground state electronic configuration of benzyl anion **79**. Recall that the benzyl anion **79** singlet is expected to have intense bands at 1553, 482, 354, and 350 nm. The TD-DFT UV-Vis bands for the benzyl anion triplet diradical **79** has key absorbances at 1662, 680, and 423 nm. If one only considers the relevant bands are 482, 354, and 350 nm for the singlet and 680 and 423 nm for the triplet respectively. In all of our experimental UV-Vis spectra presented in this section, there appears to be no significant absorbances at our around 481 nm. Furthermore, most of the broad bands we observed experimentally for benzyl anion **79** are present between *ca*. 390-440 nm. From this we can infer that the only band that is present within this region is that for the benzyl anion **79** triplet, which has one predicted UV-Vis maxima at 423 nm. Regrettably, we cannot explicitly explain why we do not observe a significant band experimentally at 680 nm, which is also predicted as an absorbance band for the benzyl anion **79** triplet in any of our UV-Vis spectra. It is important to note that the predicted TD-DFT UV-Vis bands are for the gas-phase benzyl anion **79** and not its gas-phase salt, **84** or **85**. Therefore, we acknowledge that solvent effects and ion pairing of benzyl anion **79** in solution might substantially change our assignment of the electronic ground state of benzyl anion **79** based on the predict TD-DFT values discussed earlier.

In summation, though our experimental UV-Vis results suggest that the absorbance maxima at *ca.* 390-440 nm are reasonably consistent with the computed band at 423 nm for the benzyl anion **79** triplet, we are unable to definitively

determine the ground state electronic configuration of benzyl anion **79** based solely

on the UV-Vis data. Thus, in sections 4.7 and 4.8, we will provide more definitive

NMR evidence that will assist in the elucidation of the electronic ground state of

benzyl anion **79**. This NMR evidence will show that the electronic configuration for

the benzyl anion **79** closely resembles that of the triplet diradical state.

4.7 ^{1}H NMR Spectra of Anions 79 and 82

Previous ^{1}H NMR studies done by Eliel, *et al.* demonstrated that the benzyl

anion **82** could be generated from deprotonation of the 2-phenyl-1,3-dithiane (**90**)

precursor, and could be detected and characterized by NMR spectroscopy.[11] As

shown by Eliel, *et al.* and our previous computations on benzyl anion **82** (section 4.2),

that this anion is in fact predicted to be a ground state, closed-shell singlet anion.[11]

Similar NMR experiments were carried out on dithiane **90** that is shown in Figure 4.5.

Chapter 1 briefly discussed the prototypical behavior associated with close-

shell anions more specifically ground singlet carbanions. Specifically, singlet

carbanions show upfield chemical shifts in the proton NMR spectrum.[24,11,61,84] The

upfield shift observed for carbanions in the ^{1}H NMR spectrum, is due directly to the

shielding effect on carbon atoms throughout the anion's structure that results from the

transmission of delocalized anionic charge (especially for highly conjugated systems)

over the entire π-framework. Therefore, the protons that are in the closest proximity

to the anionic center, will be the most shielded, and as a result will show the largest

upfield chemical shift in the NMR spectrum. Similar to Eliel's work, the *meta* and

para protons with respect to the anionic center shows a substantial upfield shift (Figure 4.5b) relative to its conjugate acid (Figure 4.5a), while the *ortho* protons show a downfield shift (Figure 4.5b). The latter is presumably due to the coordination of the lithium counterion at the benzylic site. Quenching with CD₃OD restores the original dithiane (Figure 4.5c). The broadening of the signals in the latter spectrum is attributed to the formation of insoluble lithium salts from the quenching reaction.

The 3,5-dinitro dithiane derivative **89**, instead shows qualitatively different behavior. Surprisingly, deprotonation of dithiane **89** using *n*-BuLi, in d_8-dioxane,
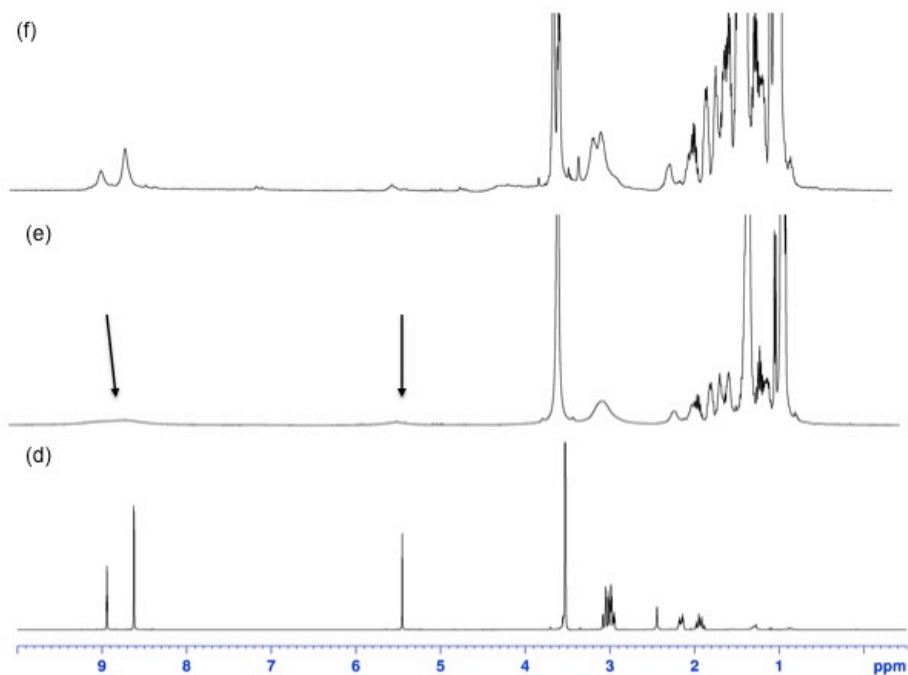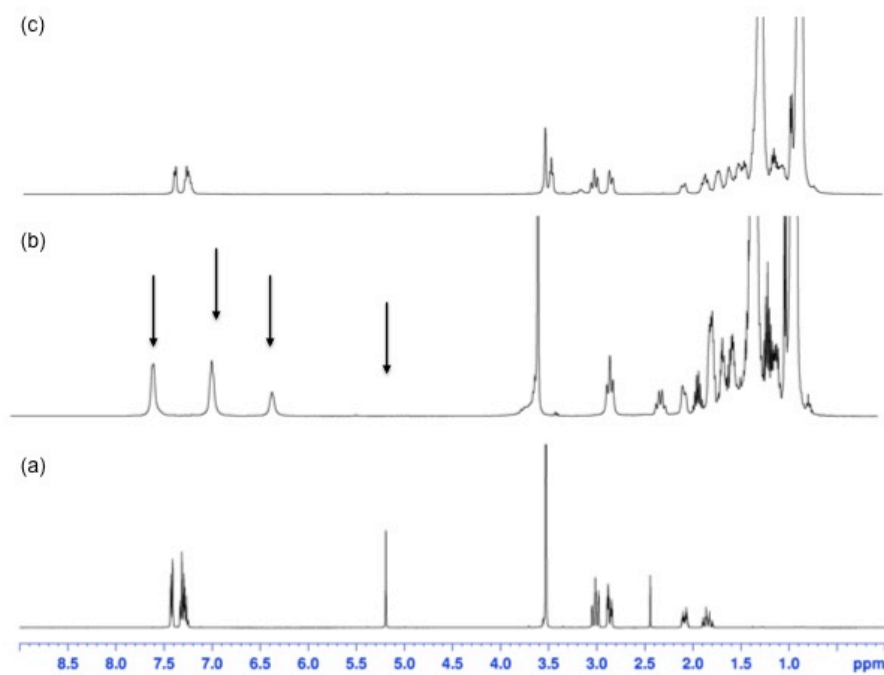
Figure 4.5. Room temperature ^{1}H NMR (400 MHz) spectra of the generation of the 2-phenyl-1,3-dithiane anion, **82** and the 2-(3,5-dinitrophenyl)-1,3-dithiane anion, **79** in d_8-dioxane in a sealed Yong tube under N_2, with *n*-BuLi as base . (a) 124 mM **90** in d_8-dioxane (no base added). (b) 124 mM **90** in d_8-dioxane after 0.450 mL of 2.50 M *n*-BuLi/hexanes was added. (c) 124 mM **90** in d_8-dioxane after 0.450 mL of 2.50 M *n*-BuLi/hexanes was added and quenched with 0.200 mL of CD_3OD. (d) 89.0 mM dithiane **89** in d_8-dioxane (no base added). (e) 89.0 mM dithiane **89** in d_8-dioxane after 0.200 mL of 2.50 M *n*-BuLi/hexanes was added. (f) 89.0 mM dithiane **89** in d_8-dioxane after 0.200 mL of 2.50 M *n*-BuLi/hexanes was added and quenched with 0.200 mL of CD_3OD.

Note that the arrow(s) in each figure indicates a significant change(s) for the dithiane anions **82/79** in the NMR spectra for the aromatic and benzylic proton resonances of the original dithianes **89/90**.

results in broadening of the aromatic resonances to the point where they disappear

(Figure 4.5e, indicated by the arrows in the figure). Similar to the deprotonation

experiment with dithiane **90**, quenching with CD_3OD restores the aromatic signals of

the dithiane (Figure 4.5f). Essentially analogous results to that shown for dithiane **89**

in Figure 4.5d-f, was observed when different bases such as CH_3Li (Figure 4.6)

and solvents (TMEDA/C_6D_6, data not shown, see Chapter 7, Supporting Information

for ^1H NMR spectra) were used. This behavior is consistent with what we would

expect for a paramagnetic species having significant spin density localized on the

phenyl ring. Generally, paramagnetic species show "NMR silent" peak broadening as

a result of rapid spin-spin relaxation. Other causes include chemical exchange,

aggregation, and the formation of precipitates could also explain this peak broadening

phenomenon. However, these causes would also have to be consistent with
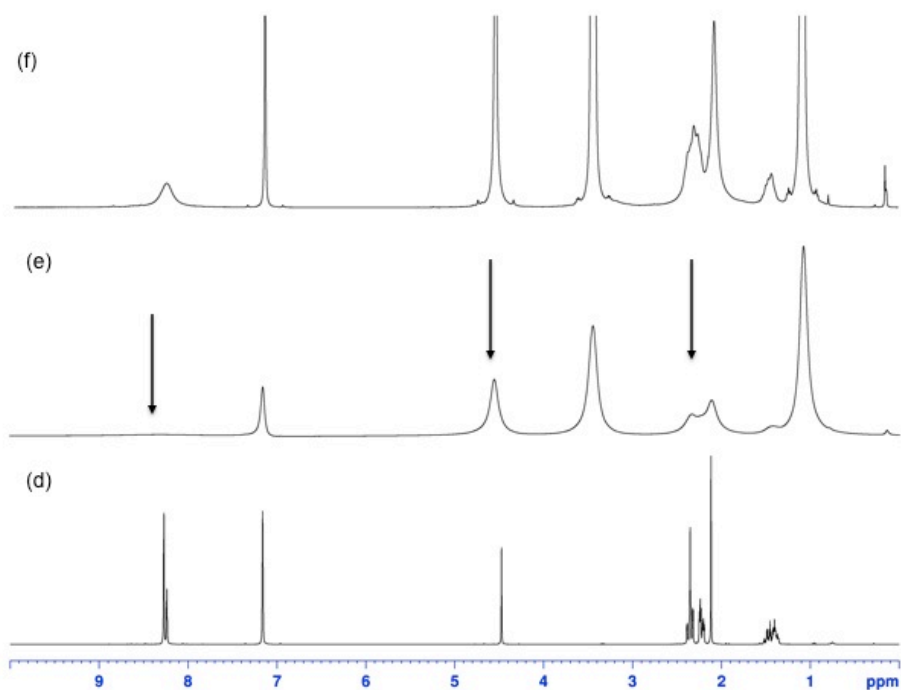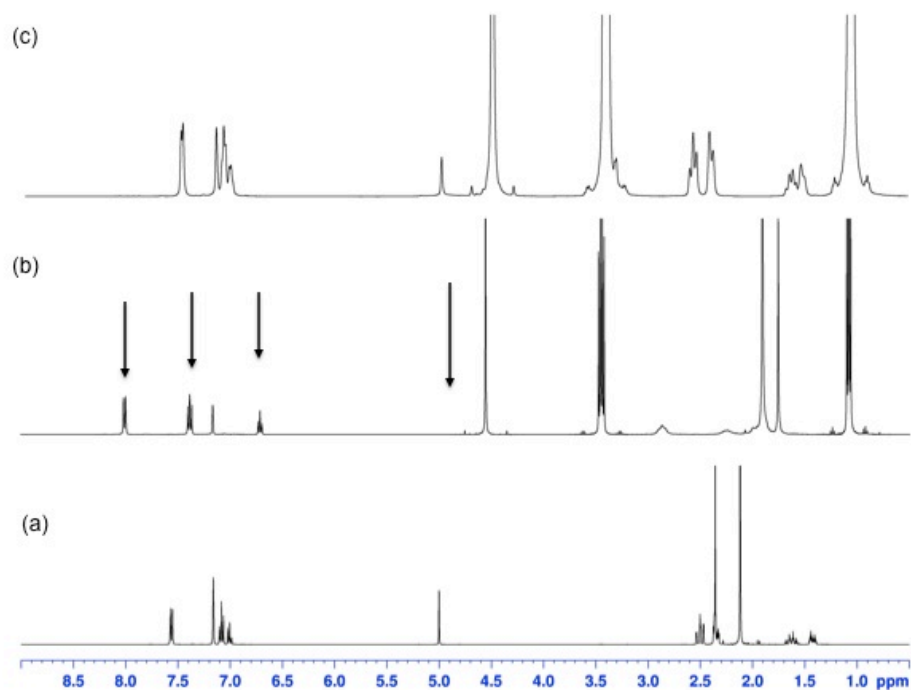
Figure 4.6. Room temperature ^{1}H NMR (400 MHz) spectra of the generation of the 2-phenyl-1,3-dithiane anion, **82** and the 2-(3,5-dinitrophenyl)-1,3-dithiane anion, **79** in C_6D_6/TMEDA in a sealed Yong tube under N_2, with MeLi as base. (a) 124 mM **90** in C_6D_6/164 mM TMEDA (no base added) (b) 124 mM **90** in C_6D_6/164 mM TMEDA after 0.15 mL of 3.0 M MeLi/DEM was added. (c) 124 mM **90** in C_6D_6/164 mM TMEDA after 0.15 mL of 3.0 M MeLi/DEM was added and quenched with 0.2 mL of CD_3OD. (d) 89.0 mM dithiane **89** in C_6D_6/164 mM TMEDA (no base added) (e) 89.0 mM dithiane **89** in C_6D_6/164 mM TMEDA after 0.30 mL of 3.0 M MeLi/DEM was added. (f) 89.0 mM dithiane **89** in C_6D_6/164 mM TMEDA after 0.30 mL of 3.0 M MeLi/DEM was added and quenched with 0.1 mL of CD_3OD.

Note that the arrow(s) in each figure indicates a significant change(s) for the dithiane anions **82/79** in the NMR spectra for the aromatic and benzylic proton resonances of the original dithianes **89/90**.

quantitative reformation of dithiane **89** when quenched with proton donors (Figure 4.5f and Figure 4.6f).

As we shall see in section 4.8, the peak broadening/"NMR silent" behavior of dithiane benzyl anion **79**, is mostly likely attributed to the presence of a paramagnetic species. Identifying and characterizing whether benzyl anion **79** will be done by performing the analogous NMR experiments used to generate benzyl anion **79**, but will employ the Evans method procedure.

4.8 Evans Method Magnetic Susceptibility Experiments on Anion 79

To determine whether the observed peak broadening was due to the formation of a paramagnetic species, several Evans method experiments were conducted on benzyl dithiane anion **79**. In addition to relaxation effects, paramagnetic additives can also cause deshielding of species that are in the same solution. By comparing the difference in chemical shifts of the solvent peak(s) in the absence and in the presence

paramagnetic solute + NMR solvent
(e.g. C_6D_6, d_8 -THF, etc.)

pure NMR solvent only
(e.g. C_6D_6, d_8 -THF, etc.)
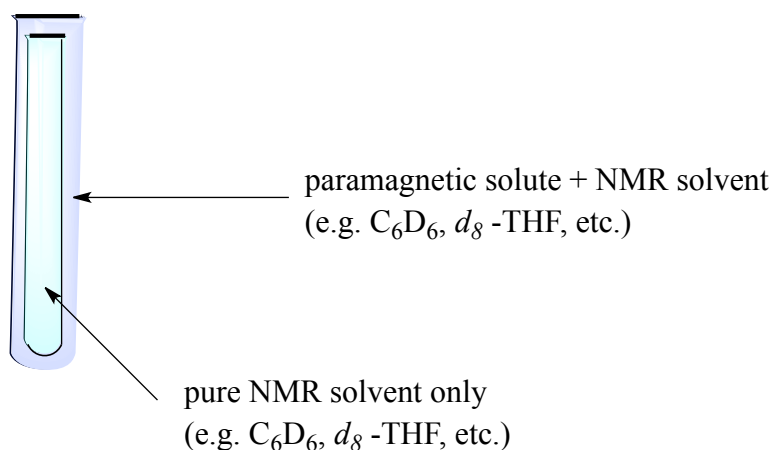
Figure 4.7. Typical Evans method setup. (This figure is the same as Figure 1.11 in chapter 1)

of a paramagnetic solute, it is possible to determine if the anion has some paramagnetic character. Recall from chapter 1 section 1.7, that the Evans method

utilizes a two compartment NMR tube setup. The two compartment system used for a typical Evans method experiment is shown above in Figure 4.7. In these experiments, the inner compartment was charged with only pure NMR solvent (C_6D_6), and the outer compartment contained a solution of the anion (**79**) and the same solvent. The original dithiane **89** in C_6D_6/TMEDA (i.e. in the absence of anion**79**) a single peak is observed for the solvent (Figure 4.8a). However, as the concentration of anion **79** increases (i.e. the concentration of the base and dithiane **89** increases), the solvent peaks begin to separate, signaling the formation of a paramagnetic species (Figure 4.8b-d, see Chapter 7, Supporting Information for full NMR spectra for these experiments). Furthermore, control experiments were conducted on dithiane **89** wherein *n*-BuLi/TMEDA in C_6D_6 but no dithiane (**89**) was added to the outer tube and showed no chemical shift change between the solvent peaks (data not shown, see Chapter 7, Supporting Information for spectra).

Figure 4.8 shows the ^{1}H NMR spectra of the region of 6.5-7.5 ppm from an Evans method experiment whereby anion **79** was generated in C_6D_6 with *n*-BuLI/TMEDA. The peaks shown in these figures correspond to the residual protonated solvent. Also, a summary of all our Evans method experiments on dithiane benzyl anion **79** is shown in Table 4.1. Table 4.1 shows a total of 7 Evans method experiments that were conducted on dithiane **89** which ranged in initial concentrations of dithiane **89** from as low as 54.8 mM, to as high as 130.0 mM. One point is particularly clear from analyzing both the data in Table 4.1 and Figure 4.8, which is that there seems to be a direct correlation between the initial concentration of
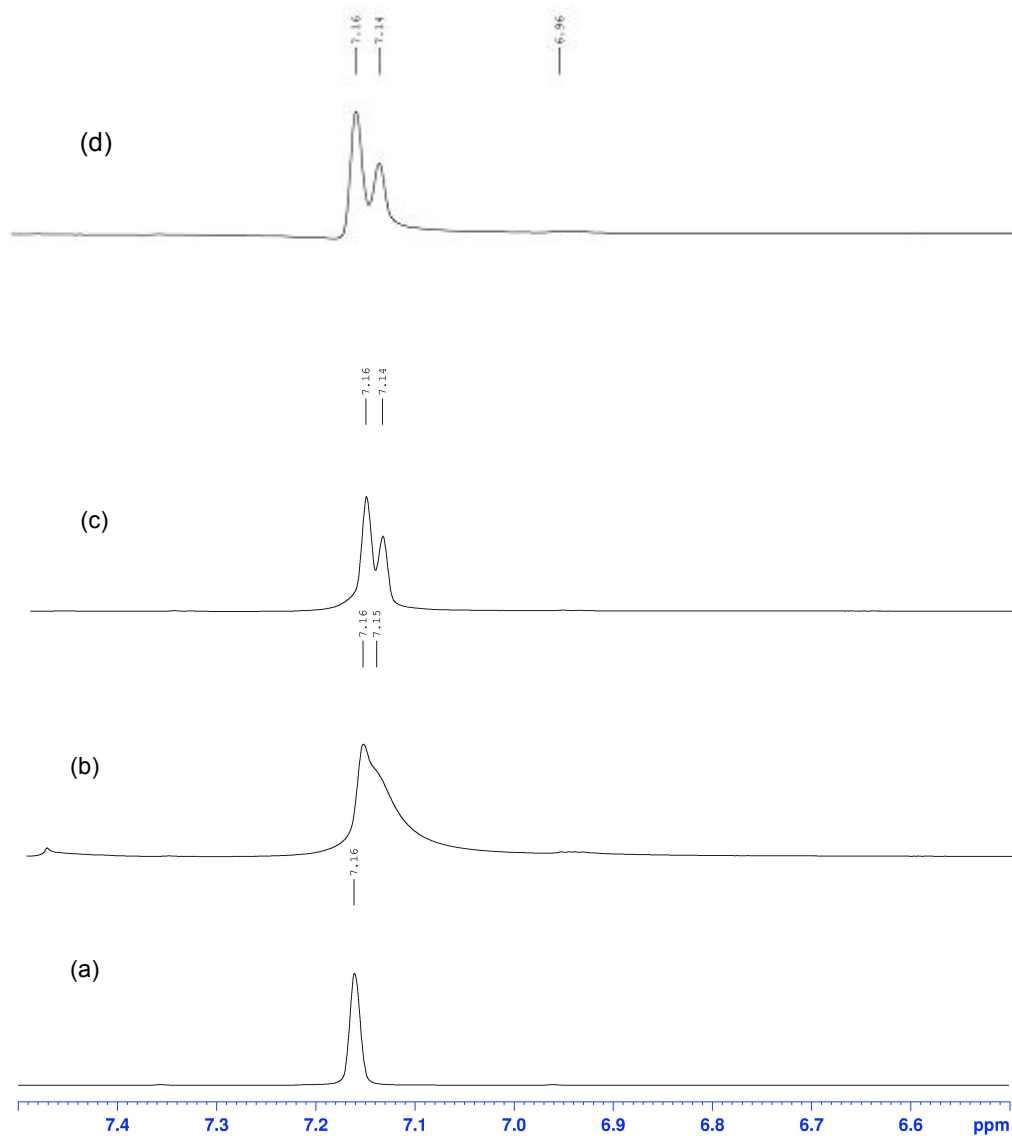
Figure 4.8. Representative ^{1}H NMR (400 MHz) Evans method experiments at room temperature expansions (7.5-6.5 ppm) of dithiane, **89**/C$_6$D$_6$/TMEDA, with the addition of *n*-BuLi as base. (a) 85.0 mM dithiane **89** in C$_6$D$_6$ with 132 mM TMEDA. (b) 54.8 mM dithiane **89** in C$_6$D$_6$ with 132 mM TMEDA and 94.3 mM *n*-BuLi/hexanes. (c) 85.0 mM dithiane **89** in C$_6$D$_6$ with 132 mM TMEDA and 117 mM *n*-BuLi/hexanes. (d) 114 mM dithiane **89** in C$_6$D$_6$ with 258 mM TMEDA and 219 mM *n*-BuLi/hexanes.

dithiane **89** in the outer Evans tube and the change in chemical shift ($\Delta\delta$) between the solvent peaks of the two compartments.

As anticipated from both of the results in Figure 4.8 and Table 4.1, as one increases the amount (i.e. concentration) of dithiane **89**, this therefore directly increases the concentration of the benzyl anion **79** (the paramagnetic species). Consequently, one observes a small, yet steady increase in the chemical shift ($\Delta\delta$) change between the inner/outer compartment solvent peaks.   Here the chemical shift change ($\Delta\delta$) between the two C_6D_6 peaks ranges from -0.010 to -0.20. Aside from one outlier value in Table 4.1 (Entry 3), the values for at least six of the concentrations of benzyl anion **79**, appears to show a very robust trend. Even if one does not entirely consider the lowest and highest concentrations for dithiane **89**

Table 4.1. Summary of Evans Method Experiments in C_6D_6/TMEDA.

Entry	Initial concentration of **89** (mM)	TMEDA initial concentration (mM)	Final concentration of 2.5 M n-BuLi/hexanes used (mM)	$\Delta\delta$ (ppm) of C_6D_6 peaks in anion spectrum (C_6D_6 - C_6D_6')
1	54.8	132	94.3	-0.010
2	68.2	132	223	-0.010
3	70.0	132	117	-0.030[a]
4	85.0	132	117	-0.020
5	113.5	258	219	-0.023
6	121.0	258	219	-0.080[*]
7	130.0	258	219	-0.200

[*]Averaged $\Delta\delta$ (ppm). This value was estimated by averaging 2 differences between the 2 C_6D_6 and C_6D_6' peaks. [a]An outlier value from the current trend shown in Table 4.1.

shown in Table 4.1 (Entry 1 and 7), due to the fact that at low concentrations some of dithiane **89** may not be fully deprotonated and at very high concentrations aggregation and precipitates may yield false positive results, there is clearly a small, paramagnetic effect that is observed in multiple Evans method experiments.   In all cases shown both in Figure 4.8 and Table 4.1, generally "NMR silent"/peak broadening was observed for all Evans method studies (see Chapter 7, Supporting Information for NMR spectra).

A more rigorous quantitative analysis of the data shown in both Table 4.1 and Figure 4.8, is accomplished by using equations 1.1 and 1.2 presented in section 1.7 of chapter 1 of this dissertation. Inserting some of the values found in Table 4.1 into each of the equations, we obtained a value of 1 % triplet and 99 % singlet respectively for benzyl anion **79**, from these Evans method experiments. This could indicate that the singlet is the ground state with a slightly higher energy triplet state or a lack of quantitative formation of benzyl anion **79**. As mentioned earlier in the introduction of equations 1.1 and 1.2 (section 1.7), that these equations tend to correct for the superconducting NMR magnet and neglects diamagnetic contributions from the solvent.[75,76] In calculating N_{anion} we assumed quantitative deprotonation of the benzyl anion precursor dithiane **89**, and furthermore neglected the diamagnetic contributions of the "ligands." The latter are extremely difficult to define, given the delocalization of anion **79**, as well as current uncertainties associated with the level of aggregation of the lithium salts and with the number of TMEDA or solvent molecules included in these organometallic complexes. With these assumptions aside, our data

from these Evans method experiments, provides an upper limit of 99 % singlet for benzyl anion **79**.

Also, we considered whether the peak broadening/NMR silent nature in our NMR and Evans method experiments could be due to the radical anion of dithiane **89**, which results from one electron reduction of one of the nitro groups. Moreover, we wanted to demonstrate that this peak broadening observed for benzyl anion **79** was not due to the dimer of dithiane **89** which is a very plausible product from the triplet diradical intermediate of anion **79**. Although it is possible that such an intermediate could in principle account for these observations it is difficult to reconcile with three observations.

First, the high level of deuterium incorporation at the benzylic position of dithiane **89** obtained in our H/D exchange experiments. Second, no products attributed to the anion radical were detected by GC or ^{1}H NMR.   Similar nitroarene anion radicals have been generated in aprotic media. These intermediates seem to decay by protonation on the nitro group to form hydroxylamines.[103] To qualitatively verify this we attempted to generate the radical anion of **89** and identify if any product(s) could be produced from this process. Samarium (II) diiodide (SmI$_2$) is known to carry out one electron reduction reactions with aliphatic and aromatic nitro groups to yield hydroxyamines, amines, and various other reduced adducts.[104,105] Therefore, dithiane **89** was combined with an excess of SmI$_2$/THF (*ca.* 6-10 equiv.) at reflux for 20.5 h. Following workup of the reaction mixture with CD$_3$OD, the

formation of 3-4 major products was observed by GC, GC-MS, and NMR (see the

Supporting Information document of Falvey, *et al.*[106] for this data). We did not

observe any of these products in the deprotonation experiments (Scheme 4.3 and 4.4).

While it is impossible to exclude trace formation of anion radical under these

conditions, we feel that our results are consistent with the formation of benzyl anion

79.

      Lastly, the same peak broadening and Evans shift effects are seen with a

variety of bases (MeLi, *n*-BuLi, etc.) as well as different solvents (THF,

benzene/TMEDA, 1,4-dioxane). From these three observations, we nominally feel

that the peak broadening/NMR silent behavior seen in our NMR and Evans method

experiments are due to a paramagnetic triplet diradical species of benzyl anion **79**.

Similarly, we excluded the possibility that the peak broadening in the NMR was due

to substantial formation of the dithiane dimer of **89**.[§] The dithiane dimer appears to

be soluble only in extremely polar aprotic solvents like DMSO, and CH_3CN. Also,

the NMR spectrum for this dimer (data not shown) in DMSO does not exhibit "NMR

silent" behavior nor are any of the chemical shifts in the NMR spectrum were similar

to that which was observed for the quenched dithiane benzyl anion **79** (Figure 4.2, 4.5

and 4.6).

[§] The dimer of dithiane **89** was previously isolated by Dr. Wei Ho-Huang a
previous post-doctorate associate in Dr. Falvey's research group (Department of
Chemistry and Biochemistry, University of Maryland, College Park, MD). No
rigorous attempts were made to characterize and synthesize the dimer of
dithane **89** other than what Dr. Ho-Huang had previous established.

Computations done on several substituted benzyl anions (Scheme 4.1) at the DFT, B3LYP/6-31+G(d,p) level, suggests that the lithium and potassium salts to dithiane benzyl anions **84** and **85** are predicted to be both ground state triplets by +26 and +12 kcal/mol respectively. Chemical trapping, H/D exchange, and UV-Vis experiments establishes that dithiane benzyl anion **79** can be generated in solution using different solvents (i.e. C_6D_6/TMEDA, THF, 1,4-dioxane) and various strong bases (i.e. KH, MeLi, *n*-BuLi) *via* deprotonation of the parent dithiane **89**. NMR and Evans method experiments demonstrate that dithiane benzyl anion **79** is a persistent and paramagnetic species at room temperature in solution. Future research will be conducted on possibly characterizing the dithiane benzyl anion **79** by X-ray crystallography, or EPR spectroscopy.

We define the *persistent* nature of a reactive intermediate throughout this dissertation and more specifically with respects to dithiane benzyl anion **79**, as a reactive intermediate that is sufficiently unreactive/stable for several minutes (~1-10 minutes) at room temperature unless the sample is exposed to either a proton source or oxygen. Therefore, the NMR silent/peak broadening signals associated with a long-lived, *persistent* intermediate such as dithiane benzyl anion **79**, are present for several minutes in solution, provided that this anion/triplet diradical is not subjected to an external reagent (e.g. CD_3OD, H_2O, oxygen, etc.). Our definition of the term *persistent* can be compared to the *m*-xylylene diradical, which is short-lived and decomposes at room temperature, in hundreds of nanoseconds.[23] Consequently, the *m*-xylylene diradical would not be a *persistent* triplet intermediate at room temperature, since it has been

shown to decompose very rapidly. On the other hand, the aza-*m*-xylylene diradical

(Chapter 1, Figure 1.2) reported by Rajca, *et al.* can be defined as a *persistent* triplet

diradical species, because its triplet EPR signal does not sufficiently decompose even

after a 10-20 minute time period at room temperature.[23]

Chapter 5: The 3,5-Dinitroaniline Anion: A Singlet Aniline Anion with a Low Lying, Thermally Accessible Triplet State

5.1 Introduction

As was seen in chapter 4 of this dissertation, work done by Falvey, *et al.* has shown computational and experimental evidence that exocyclic anionic donors, such as carbanions, with 2 strong *meta* π-acceptors (e.g. nitro groups) tend to yield ion-diradical intermediates with relatively stable triplet ground states.[106] Likewise, benzylic carbenium ions such as the 3,5-bis(dimethylamino)benzyl carbenium ion has also been shown to have a low lying triplet state (see chapter 2).[107] Based on these two previous studies, this chapter investigates a benzene system that combines two similar electronic properties as the former example. Therefore, we chose to study a benzene moiety that contained 2 strong π-accepting groups (i.e. NO_2 groups), and were in a *meta* relationship to a strong, anionic π-donor, in this case, an aniline anion. It was our hope at the onset of this project, that we might be able to combine the electron donating abilities of an amino group or amino anion with that of the electron withdrawing nature of a *meta* substituted nitro group in the same intermediate.

Currently, only a limited number of experimental studies have been conducted to characterize the spectroscopic properties of the anilide anion and its substituted derivatives. The bulk of the research that has been done on anilide anions has focused mainly on various theoretical properties[108] associated with these anions including their H-bonding ability in solution or in the gas phase,[109] and the solution phase acidity of the anilide anion's conjugate acid.[110-112] However, some recent

studies by Santos, *et al.*[113], and Pentin, *et al.*[114] have provided computational and structural evidence for the formation of various substituted anilide anions, using UV-Vis and resonance Raman spectroscopy.[113] Pentin, *et al.* reported both computational and IR spectroscopic data for the aniline anion, and the *meta*-fluoroaniline anion.[114] The most common method for generating and identifying aniline anions has been through the use of gas-phase photodetachment[115,116] or collision induced dissociation of anilines.[117] None of the recent studies demonstrates any concrete computational or experimental information regarding the electronic ground state configuration of aniline anions or its substituted derivatives. The lack of computational and experimental data in the literature for the ground state electronic configuration for various aniline anions, is likely due to the fact that most investigators assume that these anions are ground state singlets.

This chapter will present both computational and experimental studies designed to characterize the ground state electronic configurations for two anilide anions: the *p*-nitroanilide (PNA) anion, and 3,5-dinitroanilide (3,5-DNA) anion. NMR, UV-Vis, and Evans method magnetic susceptibility experiments will show that the 3,5-dinitroaniline anion (**94**) is a ground state singlet, but may have a thermally accessible triplet state. Furthermore, we have been able to generate these anilide anions from simple deprotonation of their corresponding aniline precursors (Scheme 5.1)

Scheme 5.1. General method for the generation of the 3,5-dinitroaniline anion **94** and *p*-nitroaniline anion **96**
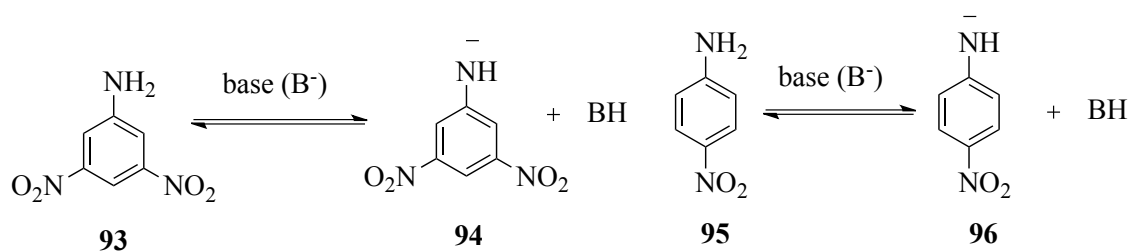
Base (B⁻) = NaNH$_2$, MeLi, *n*-BuLi, MeMgBr

5.2 DFT Computations on m-Nitro Substituted Heteroatom Derived Aromatic Anions

Initial gas-phase computations on the 3,5-dinitroanilide anion **94** suggests that

94

$\Delta E_{ST} = -12.5$ kcal/mol

94-Li⁺

$\Delta E_{ST} = -2.7$ kcal/mol

96

$\Delta E_{ST} = -35.9$ kcal/mol

97

$\Delta E_{ST} = -22.3$ kcal/mol
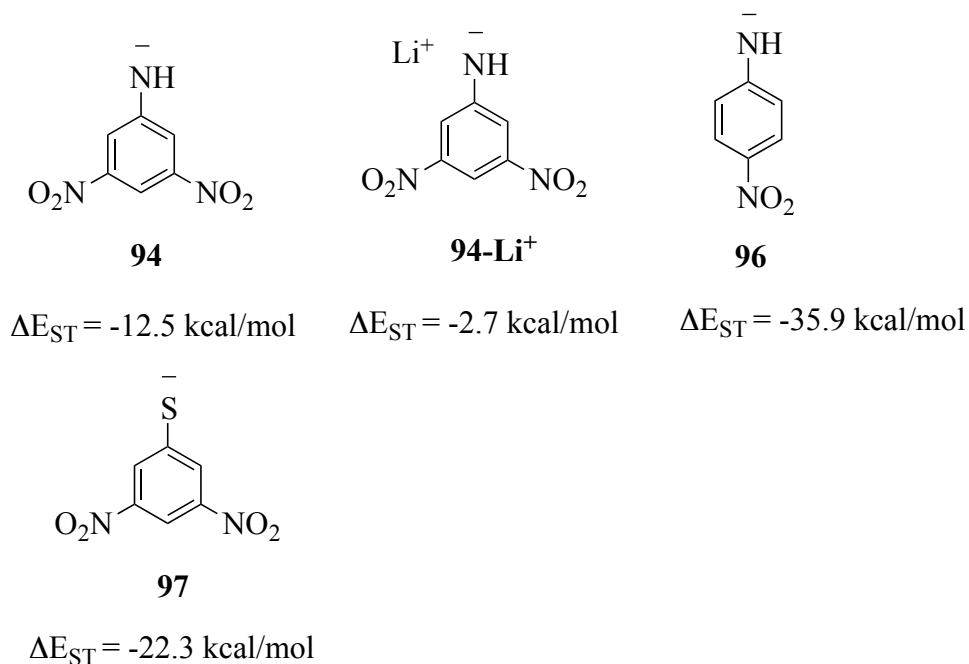
Figure 5.1. DFT computations on various nitro substituted heteroatom based aromatic anions. All computations were done using a B3LYP/6-31+G(d,p) basis set and the values that were computed here used the sum of the electronic and zero-point vibrational energies (ZVPEs) for both the restricted singlet and unrestricted triplet states.

the singlet state is clearly the ground state for this free anion by about -13.0 kcal/mol (Figure 5.1). Falvey, *et al.* have shown recently that the binding of cationic counterions to an anionic exocyclic center containing a benzene ring with strong π-acceptors, has a profound impact on the computed electronic ground state of that anion.[106] In this study, the authors demonstrated through DFT calculations that if a Li^+ ion binds to the anion center at the exocyclic position of the aromatic moiety, then the charge distribution favors the ground state to be that of the singlet. However, if the Li^+ ion is coordinated to the π-acceptor group (such as a nitro group), then the triplet state is preferred.[106] Consequently, we carried out similar gas-phase DFT computations on the Li^+ salts of 3,5-dinitroaniline anion **94** (Figure 5.2). The optimized structures shown in Figure 5.2, reflect a nominally consistent picture for exocyclic anionic donor groups that contain *meta* π-acceptors (i.e. similar to the dithiane benzyl anion lithium salt, **84**).

$94S\text{-}Li^+$ $94T\text{-}Li^+$
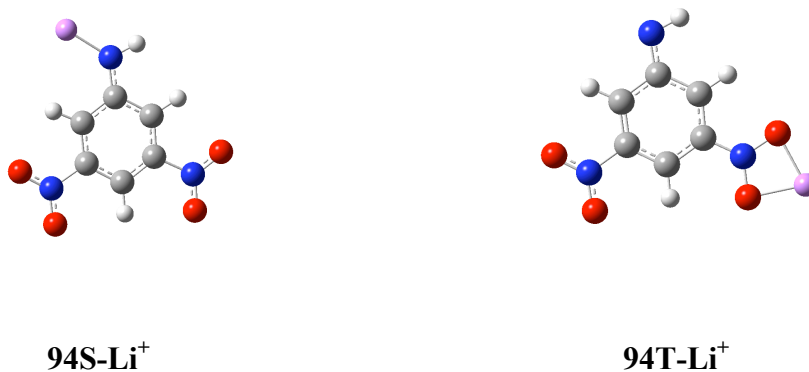
Figure 5.2. DFT B3LYP/6-31+G(d,p) optimized structures for the 3,5-dinitroaniline anion Li^+ salt singlet, **94S-Li$^+$** (left) and 3,5-dinitroaniline anion Li^+ salt triplet, **94T-Li$^+$** (right)

Our DFT computations on the Li^+ salt of 3,5-dinitroaniline anion **94**,

unfortunately shows that the singlet state is still the ground state by -2.7 kcal/mol for

this anion (Figure 5.1). This energy gap for the aniline anion salt **94-Li$^+$** is

nevertheless reasonably small relative to its free anion, **94**. From the computational

work shown in chapter 4, even the 3,5-dinitrotolyl benzyl anion **78** (Scheme 4.1) is a

ground state singlet computationally, with a ΔE_{ST} value of -1.3 kcal/mol, which is

only slightly lower than that of **94-Li$^+$** (ΔE_{ST} = -2.7 kcal/mol). By comparison, the *p*-

nitroaniline (PNA) anion **96** is obviously a ground state singlet by our computations

(ΔE_{ST} = -35.9 kcal/mol). Despite the fact that the lithium salt to the 3,5-dinitroaniline

anion possesses a small energy gap that still favors the singlet state, we wanted to

further investigate if this anion might have a thermally accessible triplet state if

generated in solution. Therefore, the next 3 sections will describe UV-Vis, NMR and

Evans method investigations of this question.

5.3 UV-Vis Spectra on Anion 94

We attempted to generate the 3,5-dinitroanilide anion **94**, by using a variety of

different solvents and bases, and observe its UV-Vis spectrum. Figure 5.3 shows

various UV-Vis spectra for the generation of the 3,5-dinitroaniline anion **94** in THF

with $NaNH_2$. The three subtracted spectra for anion **94** is shown in Figure 5.3b.

Initially, we obtained a UV-Vis spectrum that only contained the conjugate acid (**93**,

3,5-dinitroaniline) in THF (Figure 5.3a, black spectrum). The 3,5-dinitroaniline (3,5-

DNA), **93** has only one major absorbance in the UV-Vis spectrum at *ca.* 400 nm. As

one adds excess base to the 3,5-dinitroaniline/THF solution at room temperature, and

allows the heterogenous solution to equilibrate over time, a new shoulder band begins

to gradually develop at ~320 nm (Figure 5.3a, orange, yellow, and green spectra).

We attribute this small shoulder band at ~320 nm to be that of the 3,5-dinitroaniline

anion **94**. This shoulder at ~320 nm appears roughly in the region of *ca.* 300-320 nm

when the analogous experiment is conducted multiple times (data not shown).

Furthermore, to confirm that this band at 320 nm was in fact the result of the

formation of the target anilide anion **94**, we also obtained a background control

spectrum that contained an excess of $NaNH_2$/THF (Figure 5.3a, red spectrum).

Similar to other UV-Vis spectra, which we have obtained experimentally, several

difference spectra for anion **94** were calculated from the experiment in Figure 5.3a.

(b)
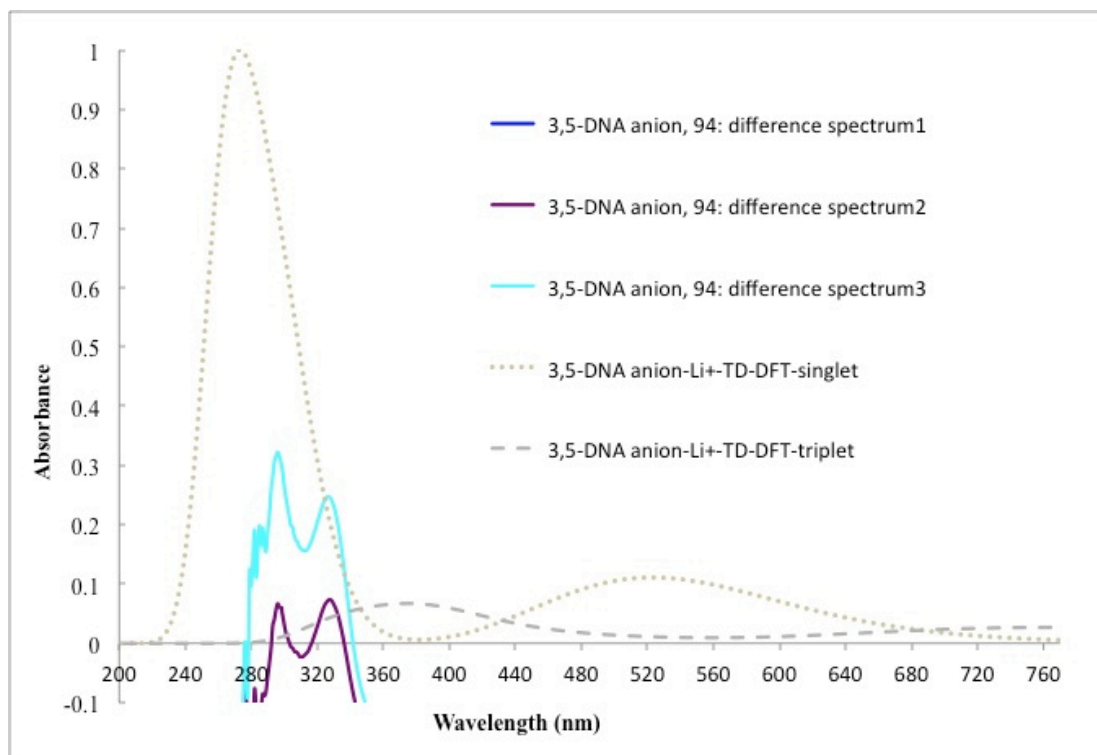
(a)
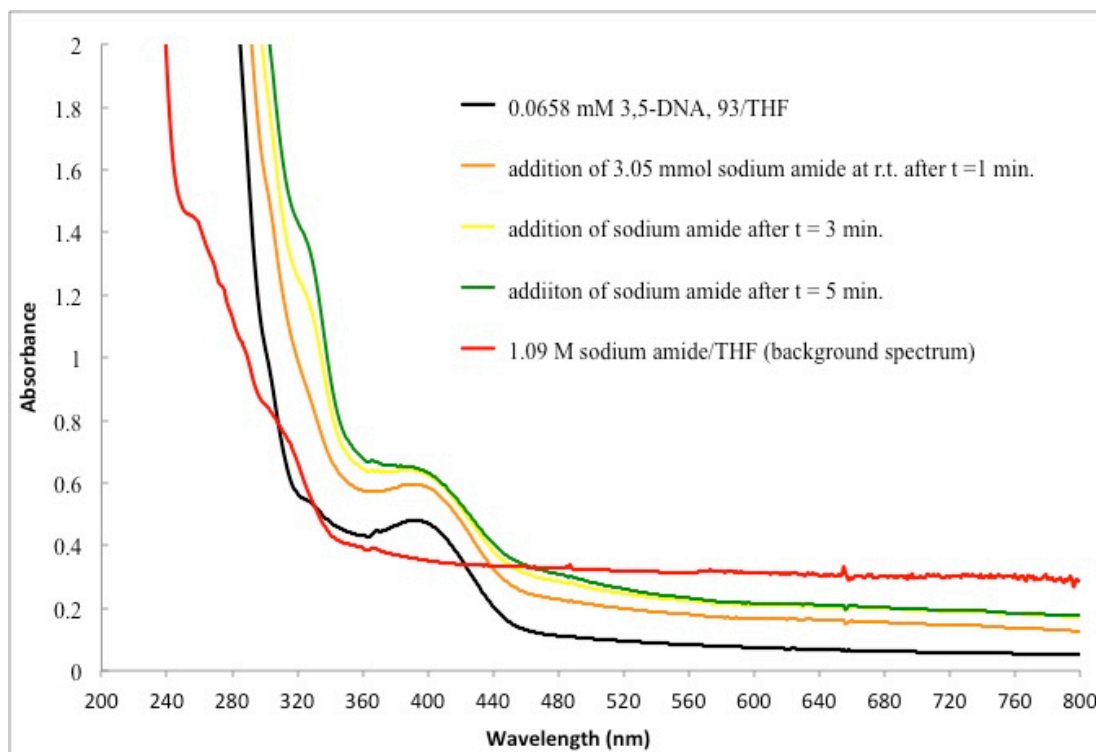
Figure 5.3. UV-Vis spectra of the 3,5-dinitroanilide (3,5-DNA) anion, **94** generated in NaNH$_2$/THF. (a) 0.0658 mM 3,5-dinitroaniline (3,5-DNA), **93**/THF (black spectrum). 0.0658 mM 3,5-dinitroaniline (3,5-DNA), **93**/THF and addition of 3.05 mmol NaNH$_2$ at room temperature after t = 1 min. of mixing (orange spectrum). 0.0658 mM 3,5-dinitroaniline (3,5-DNA), **93**/THF and addition of 3.05 mmol NaNH$_2$ at room temperature after t = 3 min. of mixing (yellow spectrum). 0.0658 mM 3,5-dinitroaniline (3,5-DNA), **93**/THF and addition of 3.05 mmol NaNH$_2$ at room temperature after t = 5 min. of mixing (green spectrum). 1.09 M NaNH$_2$/THF background control spectrum (red spectrum). (b) 3,5-Dinitroanilide (3,5-DNA) anion **94** difference spectrum1 (blue): orange spectrum (in Figure 5.3a) - 0.0658 mM 3,5-dinitroaniline (3,5-DNA), **93**/THF (black spectrum) - 1.09 M NaNH$_2$/THF background control spectrum (red). 3,5-Dinitroanilide (3,5-DNA) anion **94** difference spectrum2 (purple): yellow spectrum (in Figure 5.3a) - 0.0658 mM 3,5-dinitroaniline (3,5-DNA), **93**/THF (black spectrum) - 1.09 M NaNH$_2$/THF background control spectrum (red). 3,5-Dinitroanilide (3,5-DNA) anion **94** difference spectrum3 (cyan): green spectrum (in Figure 5.3a) - 0.0658 mM 3,5-dinitroaniline (3,5-DNA), **93**/THF (black spectrum) - 1.09 M NaNH$_2$/THF background control spectrum (red). Normalized 3,5-dinitroanilide anion-Li$^+$ singlet TD-DFT spectrum (brown dotted spectrum). Normalized 3,5-dinitroanilide anion-Li$^+$ triplet TD-DFT spectrum (grey dashed spectrum).

The purple and cyan spectra in Figure5.3b shows two out of a total of three

subtracted UV-Vis spectra for anilide anion **94** in THF/NaNH$_2$. These spectra were

generated from the subtraction of the original 3,5-dinitroaniline **93**, in THF and the

background spectrum from the base alone (red spectrum in Figure 5.3a), which was

subtracted from each successive spectra taken after the addition of NaNH$_2$ to the

solution of aniline **93**/THF (Figure 5.3a, orange, yellow, and green spectra).

Two significant absorbance bands at *ca.* 296 and 327 nm survive this rigorous

subtraction. As with dithiane benzyl anion **79**, we computed the TD-DFT UV-Vis

spectra for the singlet and triplet lithium salts of 3,5-dinitroaniline anion **94**. The

normalized TD-DFT spectra are also shown in Figure 5.3b.[**] The predicted singlet

spectrum (Figure 5.3b, brown dotted spectrum) has one highly intense absorbance at

ca. 272 nm and one low lying peak at 522 nm. On the other hand, the 3,5-

dinitroaniline anion lithium salt triplet has only a single maxima at *ca.* 376 nm

(Figure 5.3b, grey dashed spectrum). Careful analysis of each of the difference

spectra and the predicted TD-DFT spectra in Figure 5.3b, shows that the large

maxima at *ca.* 280 nm for the singlet overlaps considerably with the two absorbance

bands in our experimental difference spectra at *ca.* 296 and 327 nm (Figure 5.3b).

There is no significant overlap with the triplet band, which has a maximum at *ca.* 376

nm was observed. It is unclear to us why under these conditions we do not see the

---

[**] From the raw TD-DFT data, we normalized each value to the highest oscillator
strength value for both the 3,5-dinitroaniline anion lithium salt singlet and triplet. For
a complete list of TD-DFT oscillator strength vs. wavelength values for the 3,5-
dinitroaniline anion lithium salt, see Chapter 7, Supporting Information. The TD-
DFT computations on the 3,5-dinitroaniline anion lithium salt **94-Li$^+$**, was done by an
undergraduate in our lab, William Coldren.

predicted band for the singlet at *ca.* 522 nm. Nonetheless, we are confident from our results from the generation of the 3,5-dinitroanilide anion **94** in THF/NaNH$_2$, that the maxima at *ca.* 296 and 327 nm are in fact due to the target anion, **94**.

Several attempts were made to generate the 3,5-dinitroanilide anion **94** in other aprotic media (such as THF or 1,4-dioxane) and with various alkyllithium bases. However, these experiments either produced highly turbid UV-Vis solutions or resulted in a lack of distinguishable UV-Vis bands that could be attributed to the formation of any new species even after rigorous background subtraction. Furthermore, any quenching of the 3,5-dinitroanilide anion **94** with protic solvents (e.g. MeOH, 2-propanol, EtOH, H$_2$O) in any of the experiments that we have conducted, unfortunately results in also highly turbid solutions which therefore provided us with no viable UV-Vis data from these quenching reactions. Since aniline has been known to have a pK$_a$ of ~30.6[110-112] in DMSO, we are confident that the 2 electron withdrawing groups on 3,5-dinitroaniline **93**, should be able to inductively lower its ground state pK$_a$ below that of aniline (i.e. pK$_a$ < 30.6) in DMSO. In addition, if a suitably strong alkyllithium base were used in DMSO, it would almost certainly generate the dimsyl anion conjugate base to DMSO that has a pK$_a$ of ~35 for its parent conjugate acid.[118]

Thus, we obtained a UV-Vis spectrum for the 3,5-dinitroanilide anion **94** in DMSO with excess *n*-BuLi. Similar to generating the target anilide anion **94** with NaNH$_2$/THF, we obtained a UV-Vis spectrum for the 3,5-dinitroaniline (3,5-DNA)

93 in DMSO, and a background spectrum that contained only *n*-BuLi/DMSO (data

not shown, see Chapter 7, Supporting Information for spectra). As base is added in

small aliquots, a new broad band appears at *ca.* 508 nm. This band was not present

when the original 3,5-dinitroaniline (3,5-DNA)/DMSO UV-Vis spectrum was taken.

As a result, we tentatively assigned the broad shoulder band at *ca.* 508 nm to be that

of the 3,5-dinitroaniline (3,5-DNA) anion **94** in DMSO. Moreover, the broaden

shoulder band at *ca.* 508 nm was observed (to some extent) in other experiments

conducted in DMSO with *n*-BuLi. To determine if the peak at *ca.* 508 nm was the

only band present for anilide anion **94**, we again ran and obtained a few subtracted

spectra in which we have assigned to be that of the aniline anion **94** in DMSO. These

subtracted spectra (Figure 5.4, blue and purple spectra) were obtained by subtracting

the original 3,5-dinitroaniline, **93**/DMSO UV-Vis spectrum and the background UV-

Vis spectrum that only contained excess *n*-BuLi from each of the two aliquots of *n*-

BuLi additions to the 3,5-dinitroaniline, **93** solution in DMSO. Only the purple

difference spectrum in Figure 5.4 yielded positive absorbance bands after this

background subtraction was completed. Consequently, we tentatively assigned the

purple spectrum in Figure 5.4 to be that of anilide anion **94** in *n*-BuLi/DMSO.

Some key features to the purple difference spectrum in Figure 5.4, are a

maxima at $\lambda = 328$, 508, and a broad absorbance at 640 nm. Notice that the band at

ca. 328 nm is very similar to one of the maxima observed for the generation of the

3,5-dinitroaniline anion **94**, in NaNH$_2$/THF at *ca.* 327 nm. Thus, the UV-Vis data

that we have obtained of the 3,5-dinitroanilide anion **94**, in both *n*-BuLi/DMSO and

NaNH$_2$/THF shows consistent absorbances at *ca.* 326-328 nm. Our only explanation

for the lack of the observed band at *ca.* 508 nm in our NaNH$_2$/THF experiment, is that

the experiment shown is Figure 5.3 reflects the generation of the Na$^+$ salt to **94**,

whereas in the UV-Vis spectrum in Figure 5.4 is of the Li$^+$ salt to **94**.
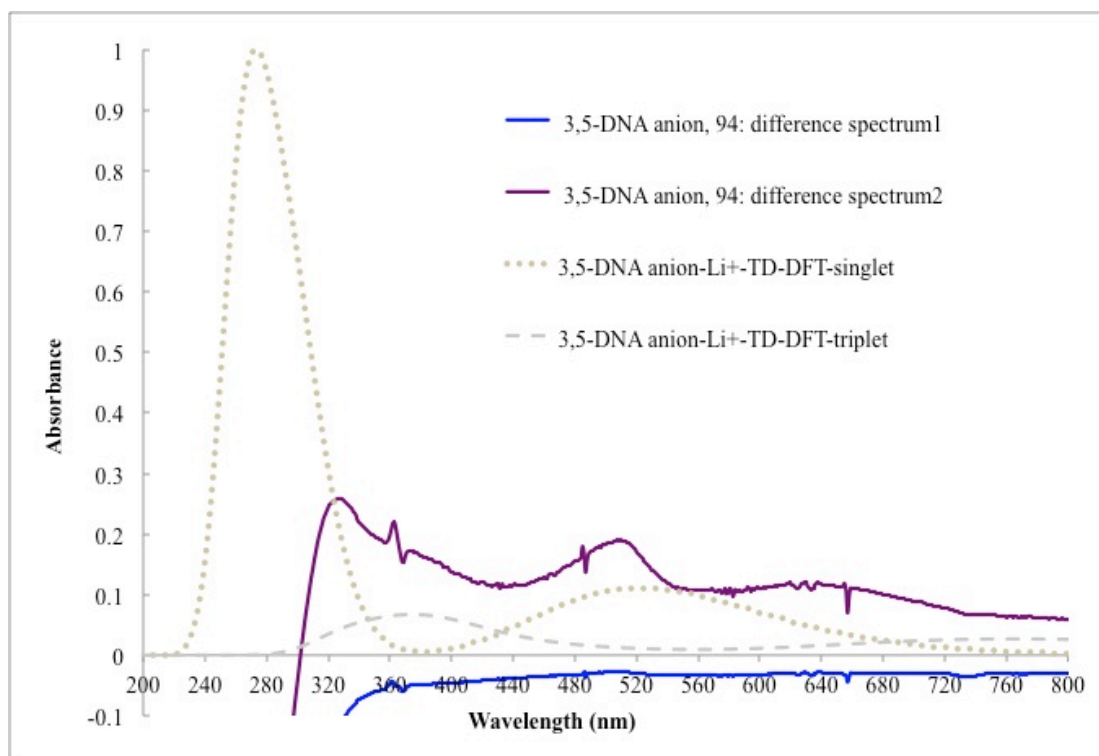
Figure 5.4. UV-Vis difference spectra of the 3,5-dinitroanilide (3,5-DNA) anion, **94** generated in *n*-BuLi/DMSO. 3,5-Dinitroanilide (3,5-DNA) anion, **94** difference spectrum1 (blue). 3,5-Dinitroanilide (3,5-DNA) anion, **94** difference spectrum2 (purple). Normalized 3,5-dinitroanilide anion-Li$^+$ singlet TD-DFT spectrum (brown dotted spectrum). Normalized 3,5-dinitroanilide anion-Li$^+$ triplet TD-DFT spectrum (grey dashed spectrum).

Nevertheless, we feel that this maybe one possible reason why the band at 508 nm is

only present in the latter UV-Vis spectrum. Also, plotted in the UV-Vis spectra in

Figure 5.4, are the analogous TD-DFT spectra for the singlet and triplet anion Li$^+$

salts to **94** (Figure 5.4, brown dotted spectrum and grey dashed spectrum

respectively). Comparing the TD-DFT predicted spectra for the lithium salts of anion

94 with that of the difference spectrum in Figure 5.4 (purple), we see that there is

more significant overlap with the singlet bands at λ_{max} = 272 and 522 nm than that of

the triplet. Although these maxima do not directly match up with the bands for either

the singlet or the triplet explicitly, we tentatively have assigned the ground state

electronic configuration of the 3,5-dinitroanilide anion **94** to be that of the singlet

state based on our UV-Vis results.

5.4 NMR Spectra of the 3,5-Dinitroaniline (3,5-DNA) Anion, 94 and p-Nitroaniline (PNA) Anion, 96

A thorough search of the current literature shows that no ^{1}H NMR data for the

3,5-dinitroanilide anion **94**, could be found. At the present time, far less data exists

that provides significant ^{1}H NMR structural evidence for various unsubstituted and

substituted aniline anions. In addition, we wanted to confirm by NMR that the 3,5-

dinitroanilide anion **94** from our UV-Vis studies was in fact a ground state singlet.

Discussed at length in the previous chapter, singlet anions generally show upfield

shifts or different chemical shifts from that of the conjugate acid in the ^{1}H NMR

spectrum. However, triplet diradicals which are paramagnetic, show either "NMR

silent" or extensive peak broadening in the proton NMR spectrum.[106] The analogous

in situ deprotonation experiments which were carried out to generate the dithiane

benzyl anion **79**, were again performed to obtain both the NMR spectrum for the 3,5-

dinitroanilide anion **94** and the *p*-nitroanilide anion **96** in a similar fashion.

Shown in Figure 5.5a-f is an NMR experiment whereby the *p*-nitroanilide (PNA) anion **96** and 3,5-dinitroanilide (3,5-DNA) anion **94**, were generated *in situ* with *n*-BuLi in *d₈*-THF. Spectrum (a) in Figure 5.5 represents that of the *p*-nitroaniline (PNA) **95**, in *d₈*-THF. Subsequent addition of base (Figure 5.5b) results in a small upfield shift (particularly of the aromatic protons) from the original proton resonances observed relative to the corresponding conjugate acid in Figure 5.5a. As discussed in section 5.2, the *p*-nitroaniline anion **96**, is predicted to be a ground state singlet. Therefore, on the basis of the experimental spectrum shown in Figure 5.5b, we feel that this prediction is in fact accurate for anion **96**. Unlike carbon acids
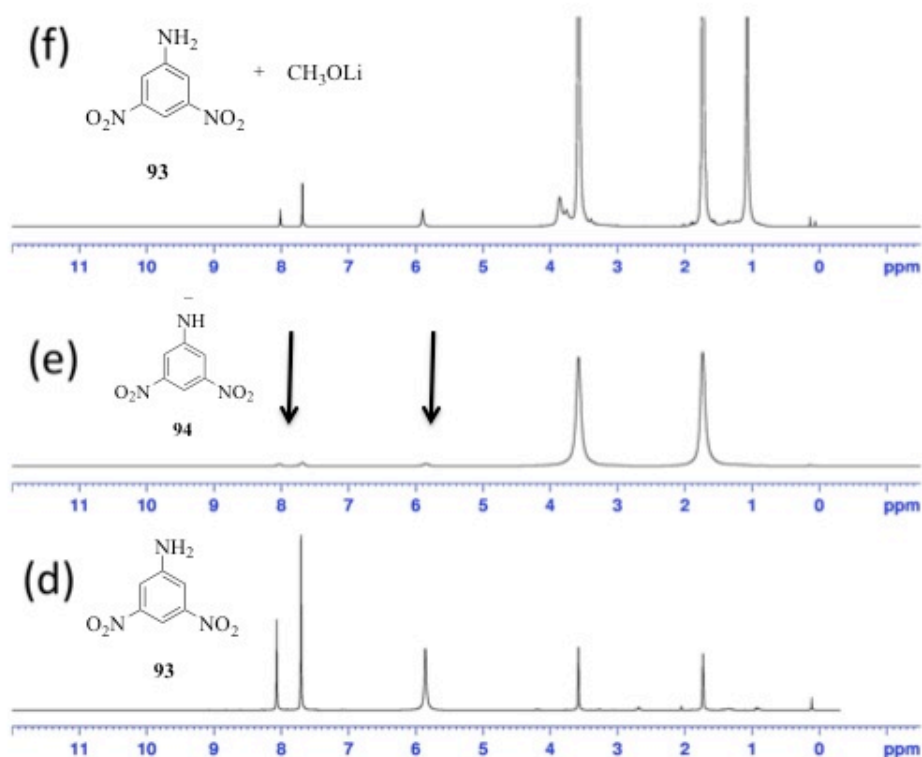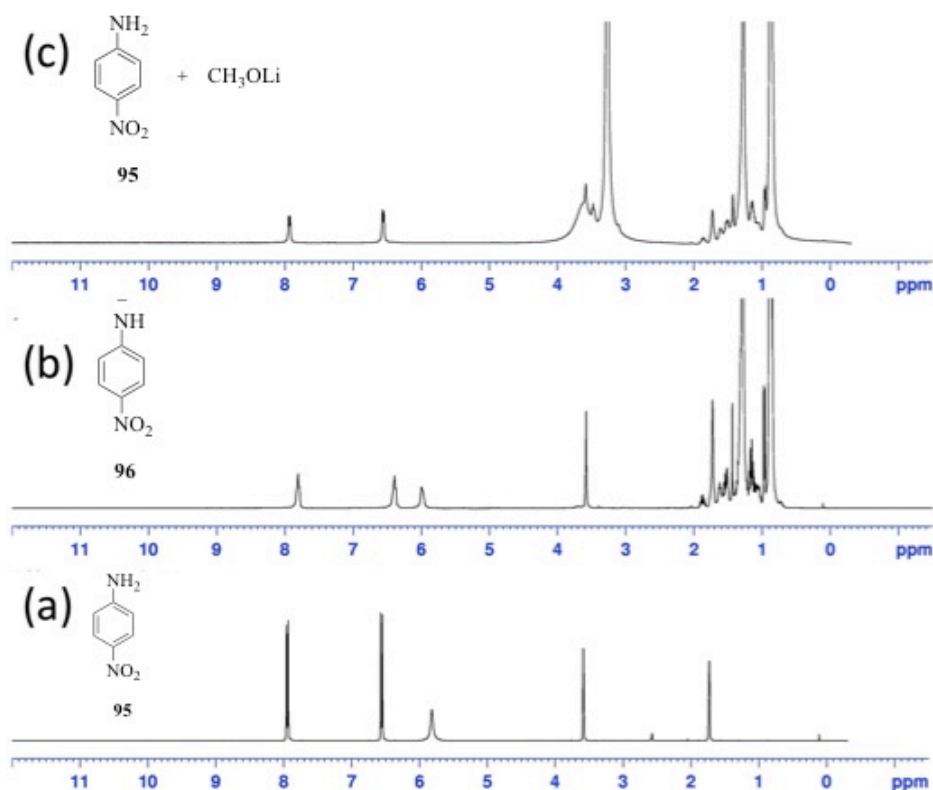
Figure 5.5. ^{1}H NMR (400 MHz) *in situ* generation of the 3,5-dinitroanilide anion **94** and the *p*-nitroanilide anion, **96** in d_8-THF with *n*-BuLi as base. (a) 162 mM *p*-nitroaniline, **95** in d_8-THF. (b) 162 mM *p*-nitroaniline, **95** in d_8-THF and the addition of 100 µL of 2.50 M *n*-BuLi/hexanes. (c) 162 mM *p*-nitroaniline, **95** in d_8-THF and the addition of 100 µL of 2.50 M *n*-BuLi/hexanes quenched with 150 µL of absolute MeOH. (d) 164 mM 3,5-dinitroaniline, **93** in d_8-THF. (e) 164 mM 3,5-dinitroaniline, **93** in d_8-THF and the addition 100 µL of 2.50 M *n*-BuLi/hexanes. (f) 164 mM 3,5-dinitroaniline, **93** in d_8-THF and the addition 100 µL of 2.50 M *n*-BuLi/hexanes quenched with 150 µL of absolute MeOH.

All experiments shown here were conducted in a sealed Young tube, under N_2. The arrow(s) in the figure represents significant change(s) that occur the NMR spectrum.

which we encountered in chapter 4, the conjugate acids to N-H, S-H, O-H, etc.

aromatic species rapidly exchange with the solvent on an NMR timescale. This is

reflected directly in the acidity associated with toluene, which is much lower than that

of its phenol or aniline analogs. Thus, exchange of a proton with the solvent becomes

less significant in the former case than the latter. Quenching of such anilide and phenoxy anions with a proton/deuterium source, would not yield an accurate assessment of H/D incorporation into the anion's structure due to this rapid exchange with the solvent.   Consequently, Figure 5.5c shows the quenching of the *p*-nitroanilide anion **96** with MeOH restores the aromatic resonances to their original chemical shifts in the ^{1}H NMR.

From on our preliminary calculations on the gas-phase anion and its lithium salt, as well as our UV-Vis results on the 3,5-dinitroanilide anion **94**, we expect to see similar NMR results to that of the *p*-nitroanilide anion **96** (Figure 5.5b). However, this was not the case. Instead, we again observe "NMR silent" or peak broadening of all aromatic proton resonances in the NMR (Figure 5.5e). Accordingly, we initially obtained a NMR spectrum of the 3,5-dinitroaniline (3,5-DNA), **93** in d_8-THF (Figure 5.5d). Titration of a slight excess of *n*-BuLi as base results in the loss of both the aromatic and N-H proton signals (Figure 5.5e). As discussed in chapter 4, there can be several causes to this peak broadening/"NMR silent" behavior. Nevertheless, quenching of the 3,5-dinitroanilide anion **94** with MeOH under nitrogen results in quantitative reformation of the aromatic and N-H proton signals in the NMR spectrum (Figure 5.5f).

The "NMR silent" or peak broadening due to the 3,5-dinitroanilide anion **94** is not solely confined to its formation in d_8-THF and *n*-BuLi as shown in Figure 5.5. One such example is shown in Figure 5.6. Here the 3,5-dinitroaniline **93**, was
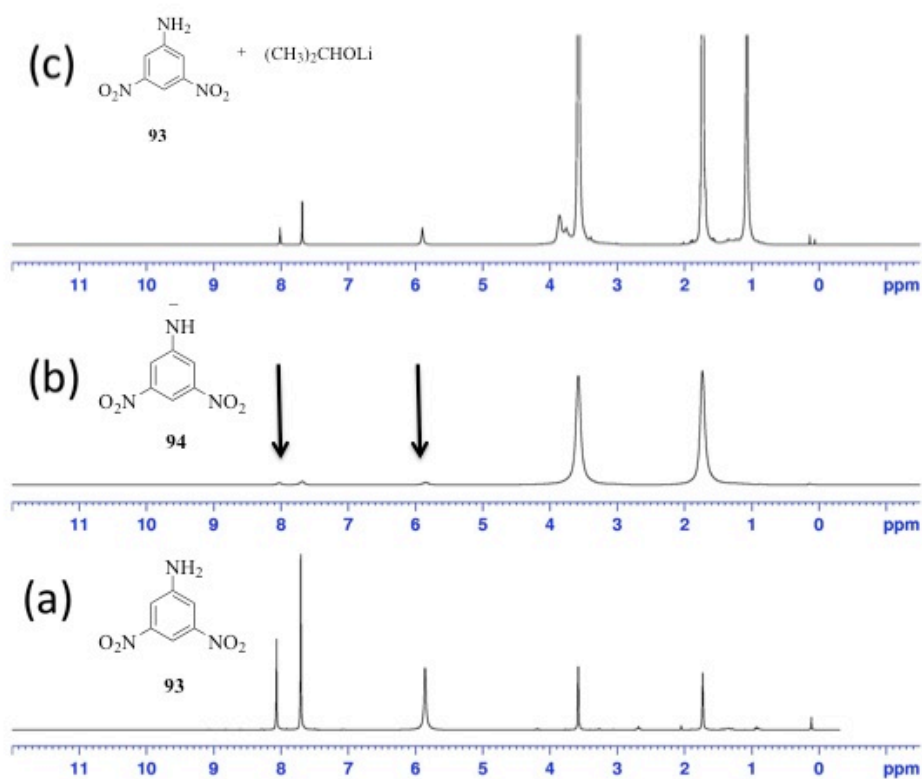
Figure 5.6. ^{1}H NMR (400 MHz) *in situ* generation of the 3,5-dinitroaniline anion **94** in d_8-THF/MeMgBr. (a) 166 mM 3,5-dinitroaniline, **93** in d_8-THF. (b) 166 mM 3,5-dinitroaniline, **93** in d_8-THF and the addition 280 μL of 1.00 M MeMgBr/THF. (c) 166 mM 3,5-dinitroaniline, **93** in d_8-THF and the addition 280 μL of 1.00 M MeMgBr/THF quenched with 120 μL of 2-propanol.

Experiments were conducted in a sealed Young tube under N_2. The arrow(s) in the figure represents significant change(s) that occur in the NMR spectrum.

deprotonated in a sealed Young tube under N_2 with MeMgBr as a base in d_8-THF

(Figure 5.6b). Similar to the results shown in Figure 5.5e, loss of the aromatic and N-

H proton signals for anion **94** was once again observed. Treatment of anion **94** with

2-propanol regenerates the aromatic and N-H resonances in the NMR (Figure 5.5c).

122

Other bases such as CH_3Li in d_8-THF yielded similar "NMR silent"/peak broadening NMR spectra for the 3,5-dinitroanilide anion **94**. The observed proton NMR data we obtained for the 3,5-dinitroanilide (3,5-DNA) anion **94**, seems to conflict with our computational and experimental UV-Vis data.

Therefore, we are able to make a few conclusions from our NMR results. First, deprotonation of the 3,5-dinitroaniline **93** yields an anionic species that is "NMR silent" and/or that shows extensive peak broadening. Secondly, the deprotonation and reformation of 3,5-dinitroaniline appears to be reversible under a variety of conditions. Lastly, the NMR data we have obtained for the 3,5-dinitroanilide anion **94**, suggests that a small amount of a paramagnetic triplet diradical species might exist on an NMR timescale at room temperature. Additionally, the 3,5-dinitroanilide anion **94** could posses a small percentage of triplet diradical character in solution that would be able to relax the large amount of singlet resonances present in that same NMR solution. Evans method magnetic susceptibility experiments in the following section will be used to further characterize the electronic spin state of the 3,5-dinitroanilide anion **94** intermediate.

5.5 Evans Method Magnetic Susceptibility Experiments on Anion, 94

We have discussed at length (chapter 1, section 1.7 and chapter 4, section 4.8) how the Evans method can be used to both identify and characterize weakly paramagnetic species. Also, the UV-Vis and computational data presented earlier in
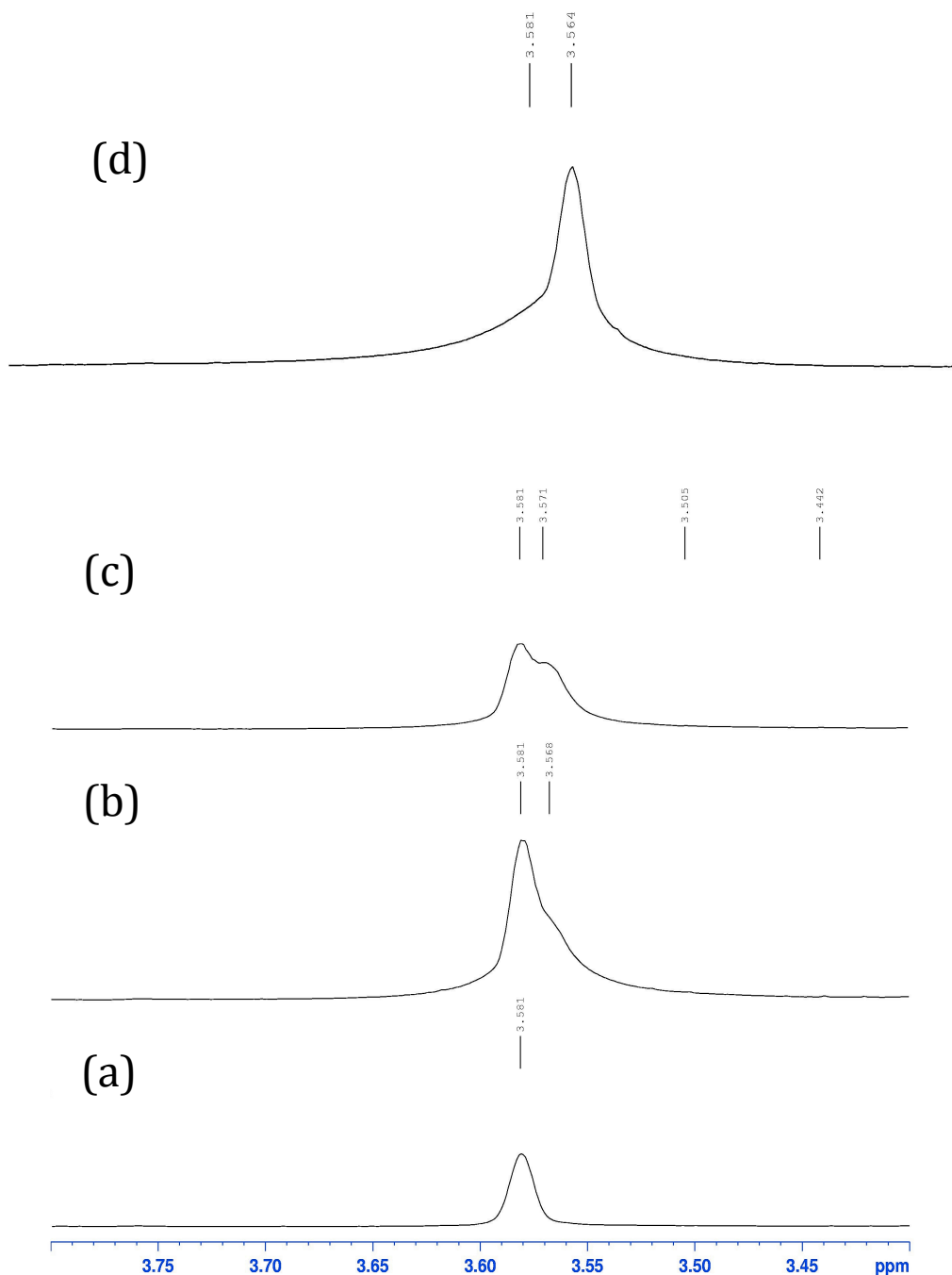
Figure 5.7. Representative ^{1}H NMR (400 MHz) Evans method experiments conducted at room temperature under N_2, expansions (3.8-3.4 ppm) for the 3,5-dinitroaniline, **93**/d_8-THF with *n*-BuLi as base. (a) 64.3 mM **93**/d_8-THF. (b) 64.3 mM **93**/d_8-THF and the addition of 60.0 μL of 2.50 M *n*-BuLi/hexanes. (c) 84.1 mM **93**/d_8-THF and the addition of 50.0 μL of 2.50 M *n*-BuLi/hexanes. (d) 104 mM **93**/d_8-THF and the addition of 70.0 μL of 2.50 M *n*-BuLi/hexanes.

this chapter (section 5.2 and 5.3), suggests that the singlet is favored as the ground state for the 3,5-dinitroanilide anion **94**. However, a number of NMR experiments we used to generate anion **94**, shows that this intermediate is either "NMR silent" or demonstrates paramagnetic peak broadening behavior. Unlike dithiane benzyl anion **79** which is predicted computationally to be a ground state triplet diradical, anilide anion **94** and its lithium salt are both expected to be ground state singlets, computationally. Therefore, based on all the current computational and experimental data that we have accumulated for the 3,5-dinitroanilide anion **94**, we would expect that this anion would show a very small, if any, Evans shift in the NMR spectrum.

Figure 5.7 represents a few Evans method results we obtained for the 3,5-dinitroanilide anion **94** in d_8-THF. Initially, there is only one peak for the solvent d_8-THF (Figure 5.7a). As one gradually increases both the concentration of aniline **93** and base (*n*-BuLi), the solvent peaks at *ca.* 3.58 ppm for d_8-THF begin to separate (Figure 5.7b-d). Similar Evans shifts can be seen for the other d_8-THF peak at 1.73 ppm, however these peaks are somewhat obscured by the signals from the base, *n*-BuLi (data not shown). Performing these Evans method experiments with concentrations > 104 mM of aniline **93**, yielded both inclusive and variable Evans shift results.

The Evans shifts shown in Figure 5.7, are unfortunately very small (the largest $\Delta\delta$ value in ppm is -0.017) when compared to that of dithiane benzyl anion **79** which

had Δδ values as high as -0.200 ppm.   Although the Evans shift Δδ values for the

3,5-dinitroanilide anion **94** is albeit small, just from fact that we even see any Evans

shift at all for this intermediate, indicates that it might possess some small degree of

paramagnetic character.

5.6 Summary, Furture Work, and Conclusions

Our computations and experimental UV-Vis data indicates that the 3,5-

dinitroanilide anion **94**, should be a ground state singlet. In contrast, the NMR and

Evans shift data on the 3,5-dintroanilide anion **94** suggests that this intermediate has

some small amount of paramagnetic character. Similar to dithiane benzyl anion **79**,

we had hoped that we could demonstrate an unambiguous chemical reactivity trend

between the *p*-nitroanilide anion **96** and the 3,5-dinitroanilide anion **94**. Experiments

like H/D exchange and chemical trapping studies involving anilide anions **94** and **96**

may not provide conclusive data on the overall reactivity of these intermediates.

However, future efforts could be done to develop reaction conditions in which both

the aniline and aniline anions of the *p*-nitroaniline and its 3,5-dinitro analog, shows

significant differences in their reactivity towards electrophiles. Although we have

obtained high quality IR spectra for the 3,5-dinitroanilide anion **94** (data not shown)

this seems to also yield inconclusive results with respects to this anion's electronic

ground state configuration. Additional research could also be done to characterize the

3,5-dinitroanilide anion **94**, by either X-ray crystallography or Raman spectroscopy.

In chapter 6, we will revisit carbanions that are clearly predicted to be ground state triplets by DFT. Moreover, in the next chapter we will show how one could develop future carbanion precursors and intermediates that could potentially lead to new ion-diradicals.

Chapter 6: An Experimental and Theoretical Study of the 3,5-Dinitrobenzyl Methoxy Ether Carbanion and Related Derivatives

6.1 Benzylic Carbanions With Alpha π-Donors and Meta Substituted Nitro Groups, Have Favorable Triplet Ground States

Recall from chapter 4 that several benzylic carbanion centers with 3,5-dinitro groups, bearing 2 of the same or different π-donating heteroatoms directly adjacent to the anionic center, have predicted positive ΔE_{ST} values by DFT (Scheme 4.1, **79-81**). These positive ΔE_{ST} values suggest that these carbanions have a triplet diradical ground state. We must ask ourselves why is this the case? There are two effects that directly contribute to the overall stability of the triplet state compared to that of the singlet state. First, the π-electron donating group(s) (i.e. OR, SR, NR_2, where R = alkyl or H) effectively raises the energy of the HOMO of the already filled *p*-orbital at the carbanion center. Therefore, the electron donation from such heteroatoms effectively destabilizes the carbanion center. Secondly, the overall LUMO of the carbanion is lowered compared to the ground state of benzyl anions with no π-electron withdrawing groups, since one has strong π-electron withdrawing groups at the *meta* positions. One of the NO_2 groups could thus serve as a good acceptor of an electron.

As a result of these two factors, the π,π^*-triplet state is favored due to the fact that the raised HOMO and the lowered LUMO of these systems makes the overall electron transfer process extremely favorable thermodynamically. Furthermore, analysis of the non-bonding molecular orbitals (NBMOs) computationally of similar

carbanion systems, shows that most of the electron density for these carbanions is localized on either the benzylic carbon or on one of the *meta* NO$_2$ group oxygen atoms (data not shown).

We will see in section 6.2 that it is not necessary to have two strong π-electron donating groups adjacent to the carbanionic center to yield a triplet ground state, computationally. Essentially having one strong π-donating group neighboring a benzylic carbanion center with disubstituted *meta* NO$_2$ groups, is sufficient enough to thermodynamically favor a triplet diradical ground state.

6.2 DFT Computations on Aryl Nitro Substituted Benzyl Carbanions With Alpha π-Donating Groups

We considered computationally some common benzylic carbanions that contain one or two alpha π-donating groups directly adjacent to the formally anionic center and also one or two aryl nitro groups. As we have seen earlier, cyclic glycols and 1,3-dithianes attached to an anionic benzylic carbon atom, which are also coupled with 3,5-disubstituted nitro groups, generally have triplet ground states computationally (see Scheme 4.1, compounds **79-81**). Additionally, precursors to anions **79-81** that were considered previously in chapter 4, can be easily synthesized from simple protection of the parent 3,5-dinitrobenzaldehyde. Subsequent deprotonation of such ketal or thioketal precursors by a suitable strong base such as an alkyllithium or metal hydride, should in principle result in quantitative formation of the target benzyl carbanions **79-81**. Our results show that only benzyl anion **79** can be formed by simple deprotonation by an appropriate base. Several attempts to

generate anions **80** and **81** *via* deprotonation of the hydrocarbon precursors resulted in

the deprotonation of the C-H aromatic proton between the two nitro groups (data not

shown). Though anions **80** and **81** are predicted to be ground state triplets by DFT

(ΔE_{ST} = +6.2 and +2.7 kcal/mol respectively), unfortunately they cannot be generated

by simple deprotonation of their hydrocarbon precursors.

Since previous experimental results showed that benzylic carbanions bearing

two alpha π-electron donating groups and aryl 3,5-dinitro groups could not be readily

generated, we therefore investigated whether a single alpha π-donor was sufficient to

favor a triplet ground state by DFT. Figure 6.1 shows several computed ΔE_{ST} values

for benzylic carbanions that contain a single alpha π-donor adjacent to the anionic

center. For comparison purposes, benzyl anion **80** that contains two alpha π-donating

groups is also shown in Figure 6.1. To our surprise, many of the simple benzyl

methoxy anions were predicted to be triplets by DFT. As expected, the *p*-nitrobenzyl

methoxy (PNBME) anion **98** is clearly a ground state singlet by -26.0 kcal/mol.

Because anion **98** is predicted to be a ground state singlet, it could serve as a viable

"anion control" that would likely show prototypical singlet anion behavior if

generated experimentally. As one might expect, adding steric bulk at the O center

that is adjacent to the benzyl anion, does not have a large impact on its overall ground

state electronic configuration. Therefore, the 3,5-dinitrobenzyl *tert*-butyl ether anion,

99 is also predicted to have a triplet ground state configuration by DFT (ΔE_{ST} = +2.38

kcal/mol). Adding a methyl group to increase the steric bulk around the anionic

center (**100**) still results in a favorable triplet ground state with a ΔE_{ST} value of +2.13

kcal/mol. Interestingly, the lithium salt of **97** (**97-Li$^+$**), has a drastic impact on raising the ΔE_{ST} value heavily in favor of the triplet state (ΔE_{ST} = +33.2 kcal/mol). Since **97-Li$^+$** is predicted to be a ground state triplet computationally (see Figure 6.1), we would thus anticipate that this salt if generated in solution should behave as a triplet diradical.

97
ΔE_{ST} = +2.81 kcal/mol

97-Li$^+$
ΔE_{ST} = +33.2 kcal/mol

80
ΔE_{ST} = +6.2 kcal/mol

98
ΔE_{ST} = -26.0 kcal/mol

99
ΔE_{ST} = +2.38 kcal/mol

100
ΔE_{ST} = + 2.13 kcal/mol
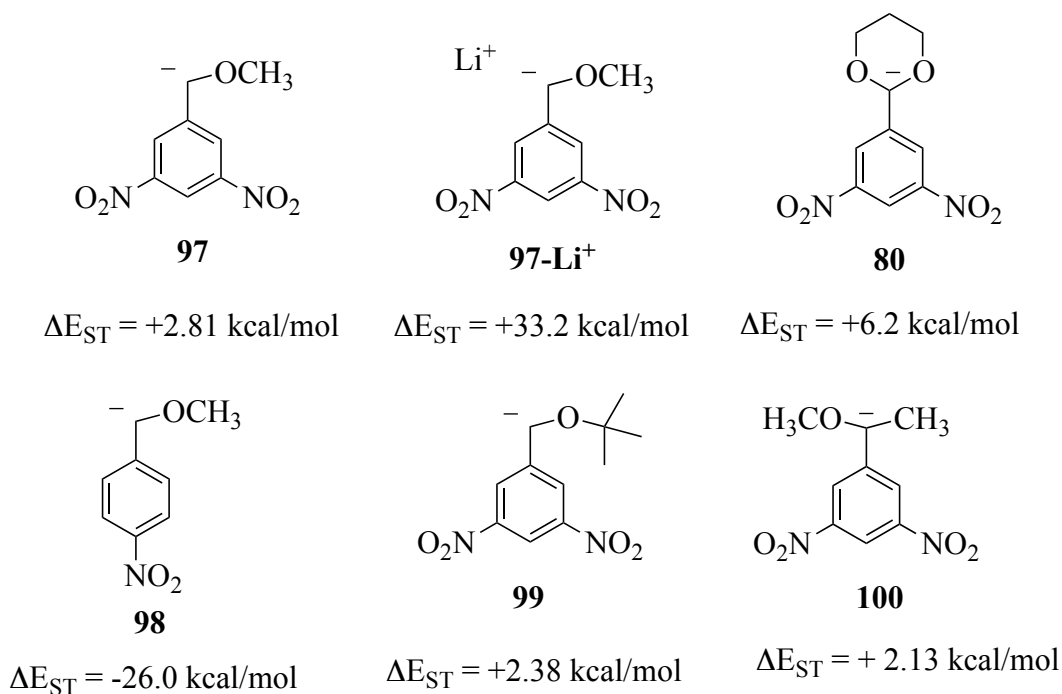
Figure 6.1. Computed DFT ΔE_{ST} values for various substituted nitroaryl, alpha π-donor benzylic carbanions. All computations were done using a B3LYP/6-31+G(d,p) basis set and all energies were calculated by both accounting for the electronic and zero-point vibrational energy (ZVPE) contributions from each state. The DFT singlet state energies for all anions were computed using a restricted basis set (i.e.(R)B3LYP/6-31+G(d,p)).

Examination of the optimized geometry of the 3,5-dinitrobenzyl methoxy ether anion singlet (**97S**) and triplet state (**97T**) shows a slight difference in the overall orientation of the methyl group attached to the oxygen atom (Figure 6.2a and b) by DFT. In the singlet state, the methyl group is slight skewed out the plane

relative to the oxygen in which it is attached (Figure 6.2a). Rotation of the molecule

on its side (not shown) shows that the oxygen atom, the benzylic C-H carbon, and the

(c)

(d)

97S-Li⁺

97T-Li⁺

(a)

(b)

97S
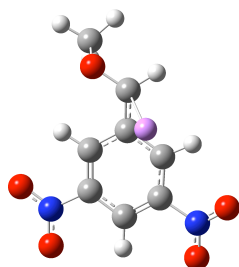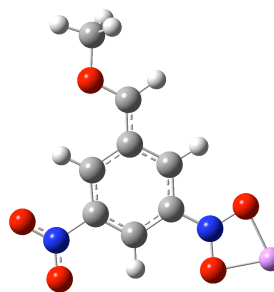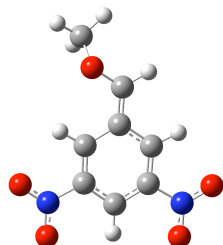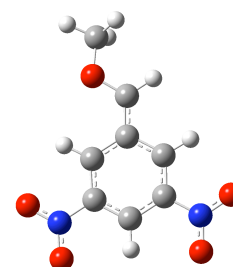
97T

Figure 6.2. DFT optimized structures for the 3,5-dinitrobenzyl methoxy ether anion and 3,5-dinitrobenzyl methoxy ether anion lithium salt. (a) 3,5-dinitrobenzyl methoxy ether anion singlet, **97S** (b) 3,5-dinitrobenzyl methoxy ether anion triplet, **97T** (c) 3,5-dinitrobenzyl methoxy ether anion lithium salt singlet, **97S-Li⁺** (d) 3,5-dinitrobenzyl methoxy ether anion lithium salt triplet, **97T-Li⁺**. All computations were performed using a B3LYP/6-31+G(d,p) basis set and all singlet geometries were optimized from the restricted singlet state.

aromatic ring (along with the NO$_2$ groups) are all in the same plane except for the methyl group attached to the ether oxygen atom. On the other hand, the triplet state has an optimized geometry in which all of the bonded atoms in the structure (including the C-O bond of the methoxy ether group), adopt a nearly planar geometry (Figure 6.2b). Similar optimized structures were obtained for the 3,5-dinitrobenzyl methoxy ether anion singlet and triplet lithium salts, **97S-Li$^+$** and **97T-Li$^+$** respectively by DFT computational methods (Figure 6.2c and d). Figure 6.2c and d clearly reflects a consistent picture for the singlet and triplet state benzylic anion lithium salts that we have seen earlier in both chapters 4 and 5. In the singlet state, (**97S-Li$^+$**) the lithium counterion is bound to the benzylic carbon, whereas in the triplet state (**97T-Li$^+$**) it is coordinated to one of the nitro groups (Figue 6.2c and d).

Sections 6.4-6.6 will mainly focus on our preliminary efforts to characterize and identify the 3,5-dinitrobenzyl methoxy ether carbanion **97** by NMR, IR, and UV-Vis spectroscopy.

6.3 The Synthesis of 3,5-Dinitrobenzyl Methoxy Ether and p-Nitrobenzyl Methoxy Ether Carbanion Precursors, 101 and 102

The synthesis of the 3,5-dintrobenzyl methoxy ether (**101**) and *p*-nitrobenzyl methoxy ether (**102**) can be achieved through a simple and straightforward Williamson ether synthesis (Scheme 6.1). Since both precursors **101** and its analog **102** are unsymmetrical ethers that can be constructed from a benzylic and primary methyl carbon fragments, there are two facile methods that one can impliment to synthesize these precursors (Method A and B for example in Scheme 6.1). Methoxy

ether **101** was synthesized *via* initial deprotonation of the 3,5-dinitrobenzyl alcohol,

followed by treatment with excess methyl iodide. The *p*-nitrobenzyl methoxy ether

can be either synthesized by heating the commercially available *p*-nitrobenzyl

Scheme 6.1. The synthesis of the 3,5-dinitrobenzyl methoxy ether, **101** and the *p*-nitrobenzyl methoxy ether, **102**

Method A

1. (1.5 equiv.) *n*-BuLi/THF, 0 ºC
1 h

2. (> 3 equiv.) MeI, r.t., 24 h
3. (3 equiv.) KO-*tert*-Bu, r.t. 24 h

101

1. excess NaNH$_2$ / THF
r.t, 2 h

2. excess MeI, r.t.
64 h

102

Method B

NaOMe / MeOH, 50 ºC
24 h

102
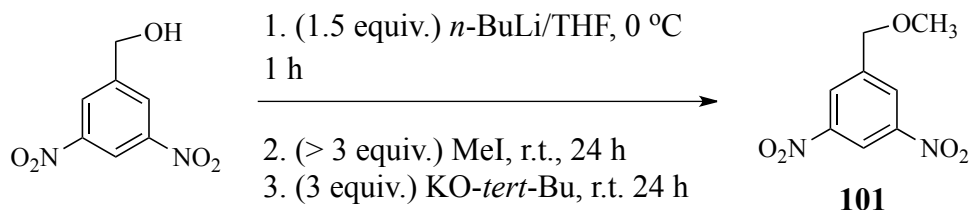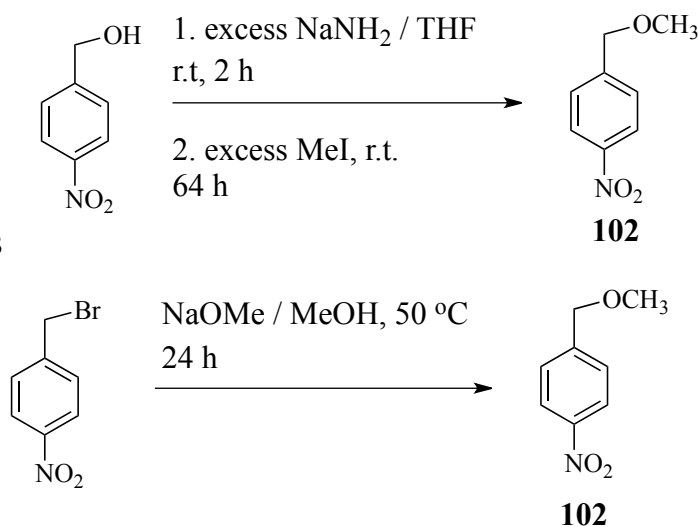
bromide with NaOMe in MeOH as solvent or by first deprotonating the *p*-nitrobenzyl

alcohol with NaNH$_2$/THF, which is then reacted with excess MeI. Both syntheses

effectively yield the *p*-nitrobenzyl methoxy ether, **102**. Notice that although the 3,5-

dinitrobenzyl methoxy ether **101** can in principle be synthesized from the treatment of

a 3,5-dinitrobenzyl halide with methoxide ion, we elected not to use this method.

This is primarily because it would involve the initial synthesis of a benzylic halide

from the 3,5-dinitrobenzyl alcohol and would therefore, add an extra synthetic step.

The purpose of this section is several fold. First, we will attempt to show that both the 3,5-dinitrobenzyl methoxy ether and *p*-nitrobenzyl methoxy ether carbanions can be generated and observed by NMR from the deprotonation of the parent ether precursors using alkyllithium bases. Secondly, we anticipated that the *p*-nitrobenzyl methoxy ether carbanion, which was predicted from our DFT computations to be a ground state singlet (ΔE_{ST} = -26.0 kcal/mol), should therefore show upfield chemical shifts in the NMR spectrum for this anion. Furthermore, because the 3,5-dinitrobenzyl methoxy ether carbanion **97** is predicted to be a ground state triplet diradical by our computations (ΔE_{ST} = +2.81 kcal/mol), we would expect from what we have seen in chapter 4, that this anion should show NMR silent or paramagnetic peak broadening, if generated in solution. We saw in chapter 4, how H/D exchange experiments can be used to indirectly demonstrate the formation of a benzylic anion intermediate. Hence, we also wanted to show that H/D incorporation could be achieved, and that the effective acid-base deprotonation and subsequent quenching of both the *p*-nitrobenzyl methoxy ether and 3,5-dinitrobenzyl methoxy ether is a reversible process.

Figure 6.3 shows the NMR spectra for the generation of the 3,5-dintrobenzyl methoxy ether (3,5-DNBME), **97** and *p*-nitrobenzyl methoxy ether (PNBME), **98** carbanions by deprotonation of the corresponding ether precursors with *n*-BuLi/d_8-THF. Initially, an NMR for the 3,5-dinitrobenzyl methoxy ether **101** and *p*-

nitrobenzyl methoxy ether **102**, were taken in d_8-THF (Figure 6.3a and d).

Unexpectedly, when excess base (*n*-BuLi) is added to the *p*-nitrobenzyl methoxy

ether, **102**/d_8-THF solution (Figure 6.3b) both the aromatic resonances at ~8.2 and 7.5

ppm as well as the benzylic CH$_2$ signal at ~4.7 ppm, broaden out nearly to the point

where no resonance appears for these protons in the NMR spectrum. This result is

surprising since the PNBME carbnion, **98** is clearly predicted to be a ground state

singlet anion from our DFT computations. Nonetheless, the PNBME anion solution

was subsequently quenched with CD$_3$OD, yielding 34 % H/D incorporation by NMR

(Figure 6.3c). Also, notice that the aromatic, benzylic and methoxy (δ = 3.4 ppm)

proton resonances are reformed, albeit broadened, likely from the quenching reaction
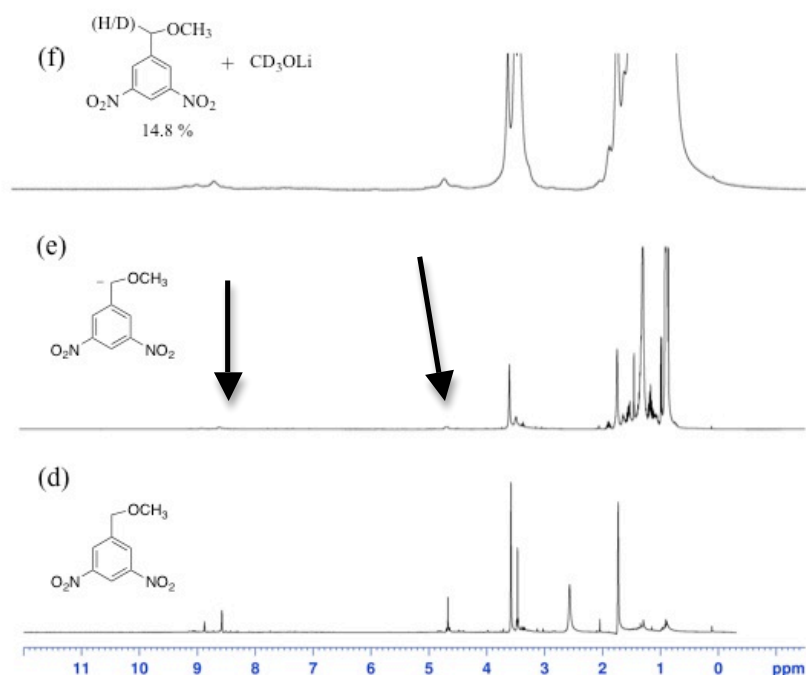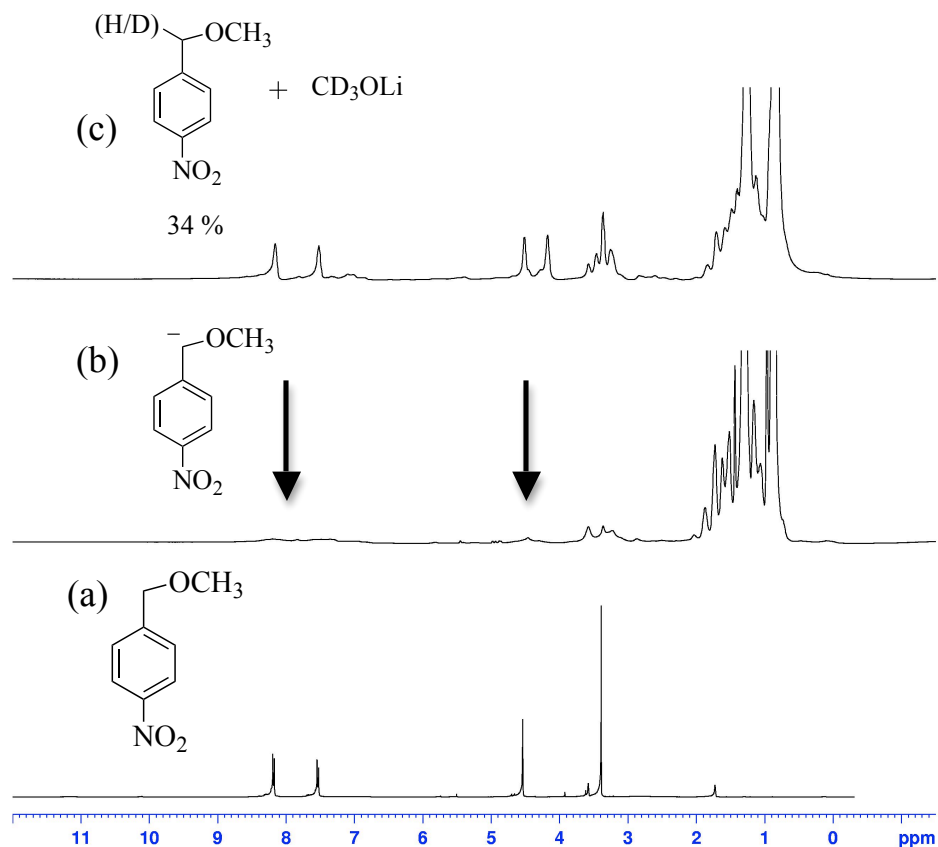
Figure 6.3. ^{1}H NMR (400 MHz) spectra of the *p*-nitrobenzyl methoxy ether (PNBME) carbanion, **98** and the 3,5-dinitrobenzyl methoxy ether (3,5-DNBME) carbanion, **97** generated *in situ* in a sealed Young tube under N$_2$, with *n*-BuLi as base. (a) 288 mM PNBME (**102**)/d_8-THF solution. (b) 288 mM PNBME (**102**)/d_8-THF solution and the addition of 110 μL of 2.50 M *n*-BuLi/hexanes. (c) 288 mM PNBME (**102**)/d_8-THF and the addition of 110 μL of 2.50 M *n*-BuLi/hexanes solution, which is quenched with 100 μL of CD$_3$OD. (d) 119 mM 3,5-DNBME (**101**)/d_8-THF. (e) 119 mM 3,5-DNBME (**101**)/d_8-THF solution and the addition of 130 μL of 2.50 M *n*-BuLi/hexanes. (f) 119 mM 3,5-DNBME (**101**)/d_8-THF and the addition of 130 μL of 2.50 M *n*-BuLi/hexanes solution, which is quenched with 200 μL of CD$_3$OD. Arrow(s) in the spectra indicate significant change(s) in the NMR spectra.

of the *p*-nitrobenzyl methoxy ether anion **98** with CD$_3$OD (Figure 6.3c). The residual singlet and multiplets observed at ~4.8 ppm and between ~3.6-3.2 ppm respectively, are likely attributed to CD$_3$OD/CD$_3$OLi, d_8-THF, and the OCH$_3$ singlet signal for benzyl methoxy ether **102**. As predicted, when excess base (*n*-BuLi) was added to

137

the 3,5-dinitrobenzyl methoxy ether (3,5-DNBME), **101**/d_8-THF solution, all the

aromatic, benzylic, and methoxy resonances for the parent ether (Figure 6.3d)

becomes essentially NMR silent (Figure 6.3e). The 3,5-dinitrobenzyl methoxy ether

carbanion **97**, is subsequently quenched with CH_3OD, and shows ~14.8 % H/D

incorporation by NMR (Figure 6.3f).   There are several possible explanations for the

small amount of H/D incorporation (14.8 %) observed in the NMR shown in Figure

6.3f. One explanation could be that a small amount of moisture contaminated the

CD_3OD we used to quench this reaction or that the NMR sample tube itself was

inadvertently exposed to some water during the process of quenching anion **97**.   In

addition, we are not entirely certain as to the extent in which benzyl methoxy ether

101 was fully deprotonated by *n*-BuLi in the NMR spectrum shown in Figure 6.3e.

Some other alternative explanations for the low H/D incorporation described in

Figure 6.3e, are that there may be more complicated chemical exchange phenomena

involved with either the deprotonation of **101** with *n*-BuLi (Figure 6.3e), or with the

quenching reaction between anion **97** and CD_3OD (Figure 6.3f).

Similar to the quenching reaction for the *p*-nitrobenzyl methoxy ether

carbanion (Figure 6.3c), we see that the aromatic resonances at ~8.8 and 8.5 ppm, the

benzylic proton signal at ~4.6 ppm, and the methoxy proton resonance at ~3.4 ppm

(note: this proton signal extensively overlaps with both d_8-THF and CD_3OD),
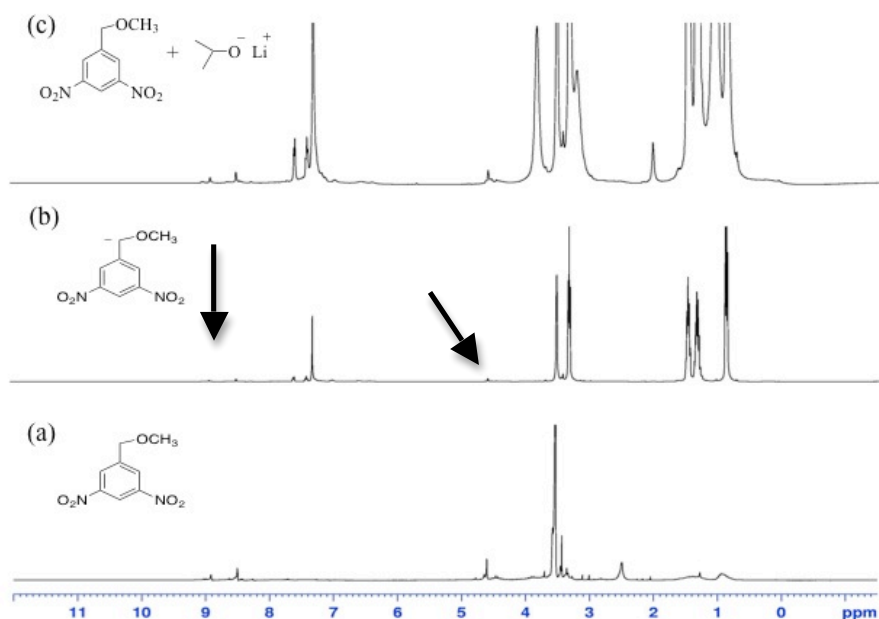
Figure 6.4. ¹H NMR (400 MHz) spectra of the 3,5-dinitrobenzyl methoxy ether (3,5-DNBME) carbanion, **97** generated *in situ* in a sealed Young tube under nitrogen, with PhLi as base. (a) 141 mM 3,5-DNBME (**101**)/d_8-dioxane (no base added). (b) 141 mM 3,5-DNBME (**101**)/d_8-dioxane and the addition of 80.0 μL of 1.80 M PhLi/DBE (dibutyl ether). (c) 141 mM 3,5-DNBME (**101**)/d_8-dioxane and the addition of 80.0 μL of 1.80 M PhLi/DBE (dibutyl ether) which is quenched with 50.0 μL of 2-propanol. Arrow(s) in the spectrum indicate significant change(s) in the NMR spectrum.

as well as all other signals for the 3,5-dinitrobenzyl methoxy ether **101** are reformed

from the quenching of carbanion **97** (Figure 6.3f). At the present time we do not

have a concrete explanation as to why the *p*-nitrobenzyl methoxy ether carbanion **98**

shows NMR silent/paramagnetic peak broadening behavior when generated under a

variety of conditions (*n*-BuLi/d_8-THF, *n*-BuLi/d_8-dioxane, and PhLi/d_8-THF). As

discussed in chapter 4, there are several reasons that can also explain the peak

broadening/NMR silent behavior observed for the *p*-nitrobenzyl methoxy ether in

these experiments. These again include chemical exchange, aggregation effects, and

the formation of precipitates in the NMR sample. However, we find it extremely

difficult to reconcile these arguments since quantitative regeneration of the parent *p-*

nitrobenzylmethoxy ether and H/D exchange seems to readily occur after the

quenching of this anion with a proton source.
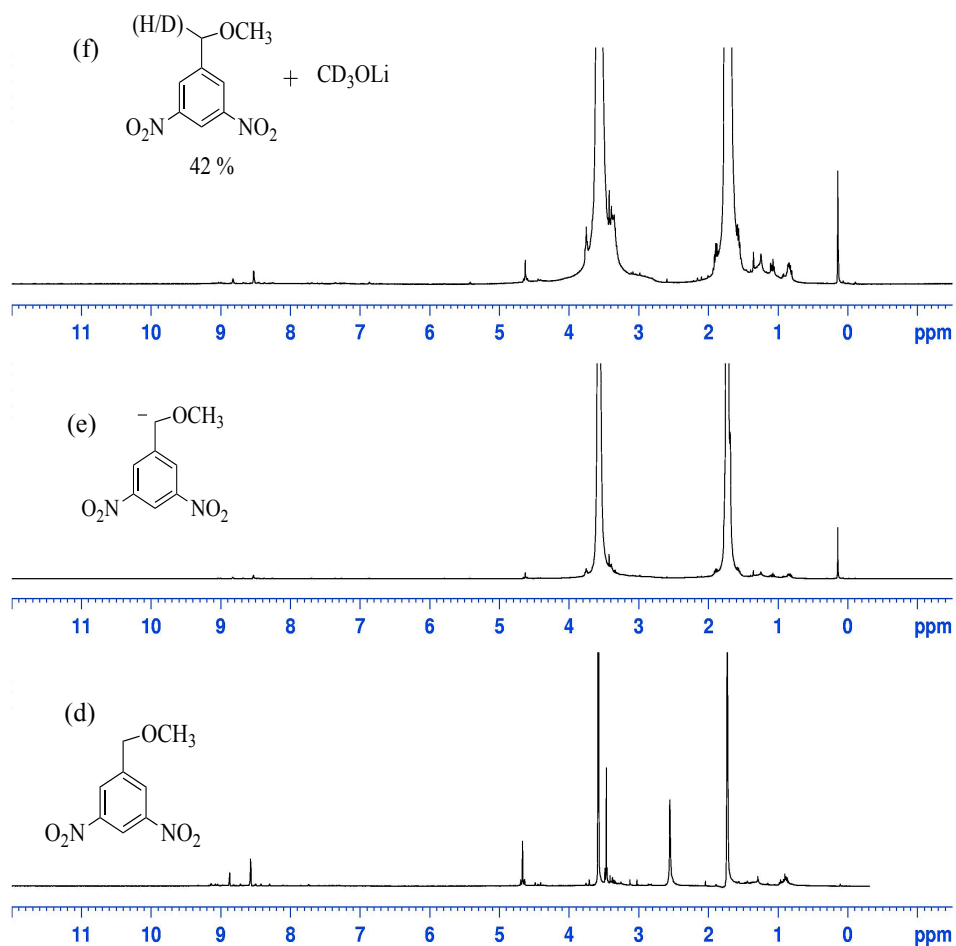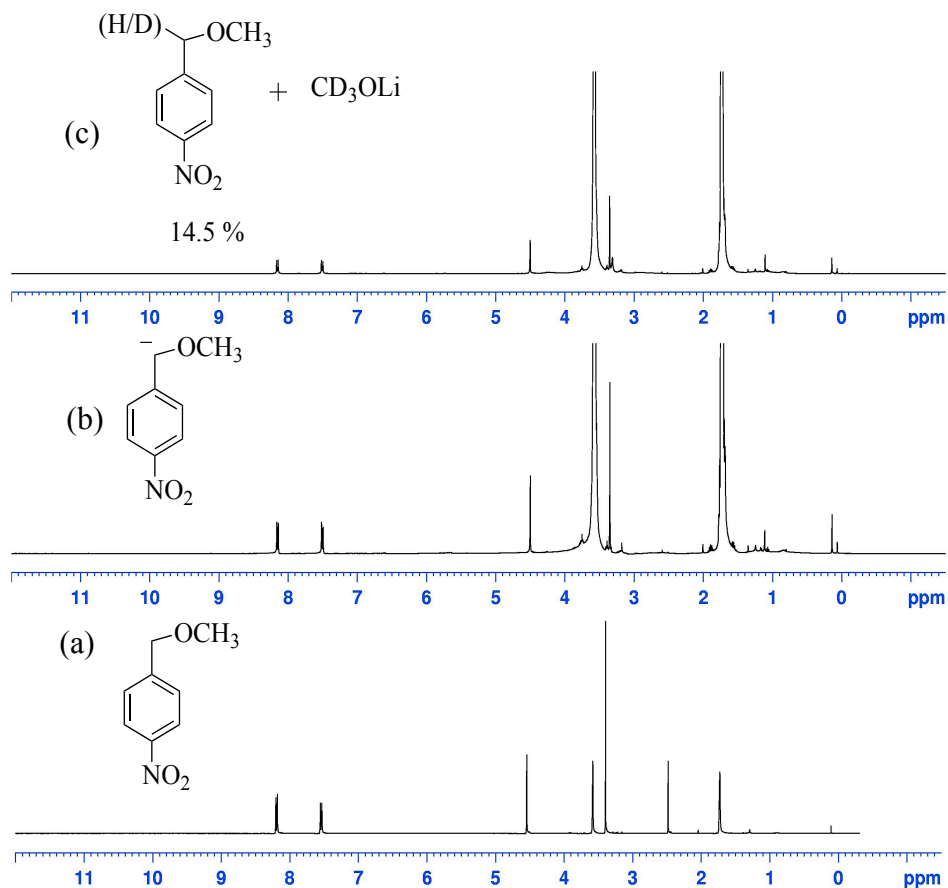
Figure 6.5. ^{1}H NMR (400 MHz) spectra of the *p*-nitrobenzyl methoxy ether (PNBME) carbanion, **98** and the 3,5-dinitrobenzyl methoxy ether (3,5-DNBME) carbanion, **97** generated *in situ* in a sealed Young tube under nitrogen, with MeMgBr as base. (a) 88.0 mM PNBME (**102**)/d_8-THF solution. (b) 88.0 mM PNBME (**102**)/d_8-THF and the addition of 240 μL of 1.00 M MeMgBr/THF solution. (c) 88.0 mM PNBME (**102**)/d_8-THF with the addition of 240 μL of 1.00 M MeMgBr/THF solution which is quenched with 100 μL of CD$_3$OD. (d) 103 mM 3,5-DNBME (**101**)/d_8-THF solution. (e) 103 mM 3,5-DNBME (**101**)/d_8-THF and the addition of 160 μL of 1.00 M MeMgBr/THF solution. (f) 103 mM 3,5-DNBME (**101**)/d_8-THF and the addition of 160 μL of 1.00 M MeMgBr/THF solution which is quenched with 100 μL of CH$_3$OD.

Analogous NMR results were observed for the 3,5-dinitrobenzyl methoxy ether carbanion **97**, when generated in PhLi/d_8-dioxane (Figure 6.4a-c), PhLi/d_8-THF

(not shown), *n*-BuLi/*d*$_8$-dioxane (data not shown), and MeMgBr/*d*$_8$-THF (Figure

6.5d-f). In all cases, the NMR spectrum for carbanion **97** showed either paramagnetic

peak broadening or NMR silent behavior when generated. Similarly, in each

experiment, anion **97** was quenched with a proton source or electrophile, and a

resulting NMR spectrum of this quenching reaction was obtained. In some of our

experiments, modest to extreme peak broadening was observed for certain NMR

signals as a result of the quenching reaction. More specifically, the aromatic

resonances at ~8.8 and 8.5 ppm were observed to be still broadened presumably due

to the formation of insoluble salts from the quenching reaction. The additional

signals between ~8-7 ppm observed in Figure 6.4b and c, is likely due to residual

impurities found in our PhLi solution. The triplet resonance likewise at ~3.5 ppm, the

other multiplets, and triplet signals located between 2-1 ppm in Figures 6.4b and c,

can be attributed the residual dibutyl ether present in PhLi. Thus, in a few of these

experiments, the reformation of the parent benzyl methoxy ethers **101** and **102** was

further verified by mass spectroscopy.

For instance, the generation of the 3,5-dinitrobenzyl methoxy ether carbanion,

which was carried out in *n*-BuLi/*d*$_8$-dioxane (data not shown) showed 45.5 % H/D

incorporation by NMR. To confirm that either the parent benzyl methoxy ether **101**

was reformed or H/D exchange occurred from the quenching of the corresponding

anion in this sample, a direct analysis in real time (DART) mass spectrum was taken.

In addition, we hypothesized that if deuterium were to be incorporated into **101**, that

the resulting compound would have a predicted mass of m/z = 213. Mass spectra

analysis of the quenched reaction mixture discussed above, would also rule out

whether dimers, polymers, or other side products were obtained from this experiment.

Although it is generally not possible to see molecular ion (M^+) peaks by DART (+/-)

mass spectroscopy, we were still able to see a significant M^+ - 2 peak at 211 and a

base peak fragment at 212 (M^+ - 1) (see Chapter 7, Supporting Information for

spectra). We unexpectedly observed a M^+ peak in this sample mixture of m/z = 213.

From this mass spectrum data, we considered that a singly deuterated 3,5-

dinitrobenzyl methoxy ether might be present in this NMR sample mixture. This

might suggests that if a single hydrogen was replaced with deuterium at the benzylic

position of ether **101**, the nominal parent peak for this compound should be M^+ = 213.

Hence, the M^+ - 1 and M^+- 2 peaks of 212 and 211 observed in our DART(-) analysis,

is consistent with the loss of a hydrogen and a deuterium atom from the parent M^+

ion, respectively. We also attempted to analyze this same sample by electron impact

(EI) or chemical impact (CI). A similar mass trace was obtained by these two

methods (data not shown). As a result, we concluded that these analyses did not

provide us with any new mass spectra information than that which we obtained from

our DART spectra analysis.

Regrettably, it is difficult to analyze and examine the mass spectra for the

replacement of a single hydrogen atom with a deuterium for either the 3,5-

dinitrobenzyl methoxy ether or *p*-nitrobenzyl methoxy ether. This is due to the fact

that it is probelmatic for one to determine whether the additional mass unit in the

mixture is attributed to a ^{13}C or a deuterium that is effectively incorporated into the ether.

Another example of how mass spectroscopy was used to verify our NMR results was when we performed the deprotonation of the *p*-nitrobenzyl methoxy ether, **102** in d_8-THF with *n*-BuLi as base. When the solution containing anion **98** was quenched with CD_3OD, and a DART(-) mass spectrum was taken, the results showed a M^+- 1 peak at m/z = 167 and a M^+- 2 peak at m/z = 166 (data not shown, see Chapter 7, Supporting Information for mass spectrum). The DART(-) mass spectrum results here suggests that the M^+ peak for the compound in the mixture has a nominal m/z = 168. It is likely that the M^+ peak at 168 that would give these two signature fragments, should rough correspond to the replacement of a single hydrogen with a deuterium at the benzylic position of ether **102**. Thus, our mass spectrum data here to some extent, reinforces our NMR results in this experiment (data not shown), which shows that 32 % H/D incorporation of the *p*-nitrobenzyl methoxy ether **102** was observed by NMR.

All of our NMR results show that anion **97** may possess some paramagnetic character and that the formation of this anion seems to be reversible under a variety of experimental conditions. More interesting is the NMR results we have also obtained for the generation of both anions **97** and **98** in d_8-THF with MeMgBr as the base (Figure 6.5). Figure 6.5a shows the initial NMR spectrum of a 88.0 mM *p*-nitrobenzyl methoxy ether, **102**/d_8-THF solution. When excess MeMgBr (240 μL)

was added to the solution containing methoxy ether **102**, a very subtle upfield shift is observed for the two aromatic doublets and the benzylic and methoxy protons in the NMR (Figure 6.5b) relative to the original *p*-nitrobenzyl methoxy ether signals (Figure 6.5a). The NMR spectrum shown in Figure 6.5b is indicative of the typical behavior for singlet anions, similar to that which was seen in chapters 4 and 5. One possible reason why the anion **98** shows NMR silent behavior when generated with alkyllithium bases (Figures 6.3b) rather than when it is generated with MeMgBr, could be that the MgBr$^+$ or Mg^{2+} salt to this anion is more soluble in ethereal solvents. A second reason could be that carbanion **98** might exist as more of a "free anion" in this solution, rather than when it is coordinated as a lithium salt in the former solution. When the *p*-nitrobenzyl methoxy ether carbanion, **98** is quenched with CD$_3$OD, the aromatic and aliphatic proton signals return to their original chemical shifts for that of the *p*-nitrobenzyl methoxy ether, **102** (Figure 6.5c).

Similar NMR spectra to what we have already seen in Figures 6.3d-f and 6.4a-c was observed for the 3,5-dinitrobenzyl methoxy ether anion **97**, which was also generated in *d$_8$*-THF/MeMgBr (Figure 6.5d-f). Additionally, 14.5 % and 42 % H/D incorporation was observed for the *p*-nitrobenzyl methoxy ether **102**, and 3,5-dinitrobenzyl methoxy ether **101**, respectively by NMR (Figure 6.5c and f).

There are several possible explanations for why we did not observe significant geminal H/D coupling for the benzylic methylene signal in the quenched proton NMR spectra in Figures 6.3c, f, 6.4c, and 6.5c, f. Typically, geminal hydrogen coupling

145

constants (J_{HH}) can be calculated by measuring the geminal coupling constant

obtained from replacement of a single geminal hydrogen with a deuterium (J_{HD}).

These values can be estimated by equation 6.1.[119] From equation 6.1, we can see that

the values for J_{HH} is 6.51 times the value for J_{HD}. Thus, the geminal coupling

$$J_{HH} = 6.51 J_{HD} \qquad \text{(eq. 6.1)}$$

constants for a given hydrogen and deuterium (J_{HD}), is generally much smaller than

J_{HH}. There are several factors that effect the value of J_{HH} such as the bond angle

between the geminal hydrogens and the groups bonded to the carbon bearing the

geminal hydrogens. For example, π-electron donating groups tend to donate electron

density and therefore make the value of J more positive (or less negative).[119]

However, π-electron withdrawing group makes J less positive.[119] Figure 6.6 provides

a few compounds that illustrate this trend.[119] The J_{HH} for the CH_3 hydrogens in

methanol with a single π-electron donating group (OH), has a value -10.8 Hz.[119]

Whereas if one adds a second oxygen π-electron donor as in the acetal shown in

Figure 6.6, the value increases to $J_{HH} = 1.5$ Hz.[119] We could therefore estimate the
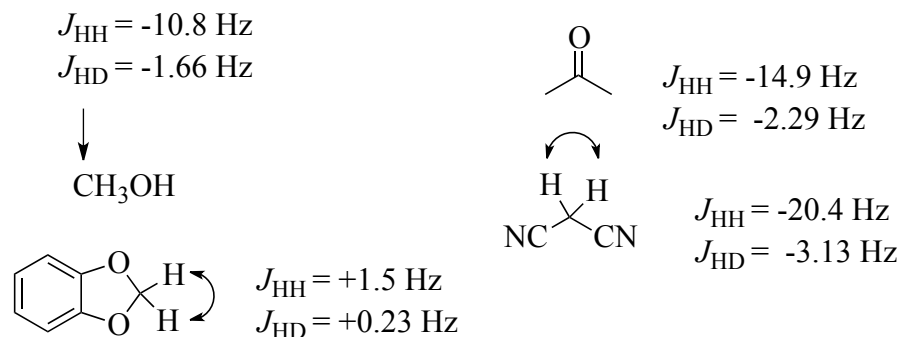
Figure 6.6. Some geminal J_{HH} and J_{HD} coupling constants for carbon atoms that contain π–electron donating groups and π-electron withdrawing groups.[120]

corresponding values for J_{HD} for methanol and the acetal shown in Figure 6.6, using

equation 6.1. These values are J_{HD} = -1.66 and 0.23 Hz accordingly. From the values

for J_{HD} for methanol and the acetal shown in Figure 6.6, we can estimate that the H/D

coupling constants for any of the partially deuterated benzyl methoxy ethers (**101** or

102), would have either very small values or might even be considered to be

negligible. As a result, we determined that the H/D geminal coupling for the benzylic

signal in Figures 6.3c, f, 6.4c, and 6.5c, f at ~4.6 ppm, is minute and thus the

resonances overall coalesce to give a single peak in the NMR.

Future Evans method or EPR spectra will be obtained for the 3,5-

dinitrobenzyl methoxy ether carbanion **97**, to verify the exact electron spin state of

this intermediate.

6.5 FT-IR Characterization of the 3,5-Dinitrobenzyl Methoxy Ether Carbanion, 97

Based solely on our NMR results, we have shown that the 3,5-dinitrobenzyl

methoxy ether carbanion **97**, may possess some small amount of triplet diradical

character. In hopes of further elucidating the ground state electronic configuration to

benzyl methoxy ether carbanion **97**, we carried out several FT-IR experiments where

we attempted to generate this anion under basic conditions. In addition, the NMR

data presented for carbanion **97** in section 6.4, provides us with a number of

conditions in which this anion could be formed. For instance, in the previous section

we have shown that the 3,5-dinitrobenzyl methoxy ether carbanion **97** can be

generated in THF or 1,4-dioxane as solvents, and by using the appropriate

alkyllithium or alkylmagnesium halide bases (i.e. PhLi, *n*-BuLi, CH$_3$MgBr).

Fortunately, computational chemistry allows us to also accurately predict the

FT-IR spectra for the electronic spin states to various anions and cations. As a result,

we predicted the gas-phase IR spectra for the 3,5-dinitrobenzyl methoxy ether anion

lithium salt, **97-Li$^+$** singlet and triplet states using DFT computations. The DFT IR

spectra for the 3,5-dinitrobenzyl methoxy ether anion lithium salt singlet and triplet

states are shown in Figure 6.7. Figure 6.7a shows the full IR spectrum from 400-

4000 cm^{-1} and Figure 6.7b shows mainly the fingerprint region of both spectra from

800-1900 cm^{-1}. Just by inspection, one can see that both the singlet and triplet IR

spectra have significant overlapping bands throughout the entire IR region (400-4000

cm^{-1}). However, a closer look at the fingerprint region (Figure 6.7b), shows that

some of the absorbance bands for both the singlet and triplet states of **97-Li$^+$** differ

slightly in the IR. For instance, the singlet state has the most intense IR absorptions

at ~1140, 1380, 1600 cm^{-1}. The triplet however has absorptions at ~1170, 1250,

1300, 1380, 1540 and 1570 cm^{-1}.

We also attempted to generate and obtain an experimental FT-IR transmission

spectrum for the 3,5-dinitrobenzyl methoxy ether carbanion, **97**. Consequently, we

generated anion **97** from the deprotonation of the parent 3,5-dinitrobenzyl methoxy

ether using various bases (PhLi, MeMgBr, *n*-BuLi) in a sealed CaF$_2$ IR cell with THF

or 1,4-dioxane as solvent. Each IR spectra for anion **97** under all of the above

conditions were reproduced at least three times and showed far less variation in the IR

148

absorbance bands. Only the overall intensities of the IR bands tended to vary to some

extent, between each experimentally generated spectrum. Figure 6.8 shows a set of

IR spectra for anion **97** which we obtained experimentally in 1,4-dioxane with excess

n-BuLi as base. Similar to all previous experiments where we generated carbanion

intermediates, we obtained an initial representative IR spectrum for a 2.01×10^{-2}

mmol aliquot of 3,5-dinitrobenzyl methoxy ether **101**, in 1,4-dioxane (Figure 6.8a,

pink spectrum). Accordingly, we obtained a transmission IR spectrum for anion **97**

(Figure 6.8b, red spectrum), which was obtained from the addition of excess *n*-BuLi

to the IR cell that contained a known amount of the 3,5-dinitrobenzyl methoxy ether,

101/1,4-dioxane. Anion **97** was then quenched (in this experiment) with 5 µL

(b)
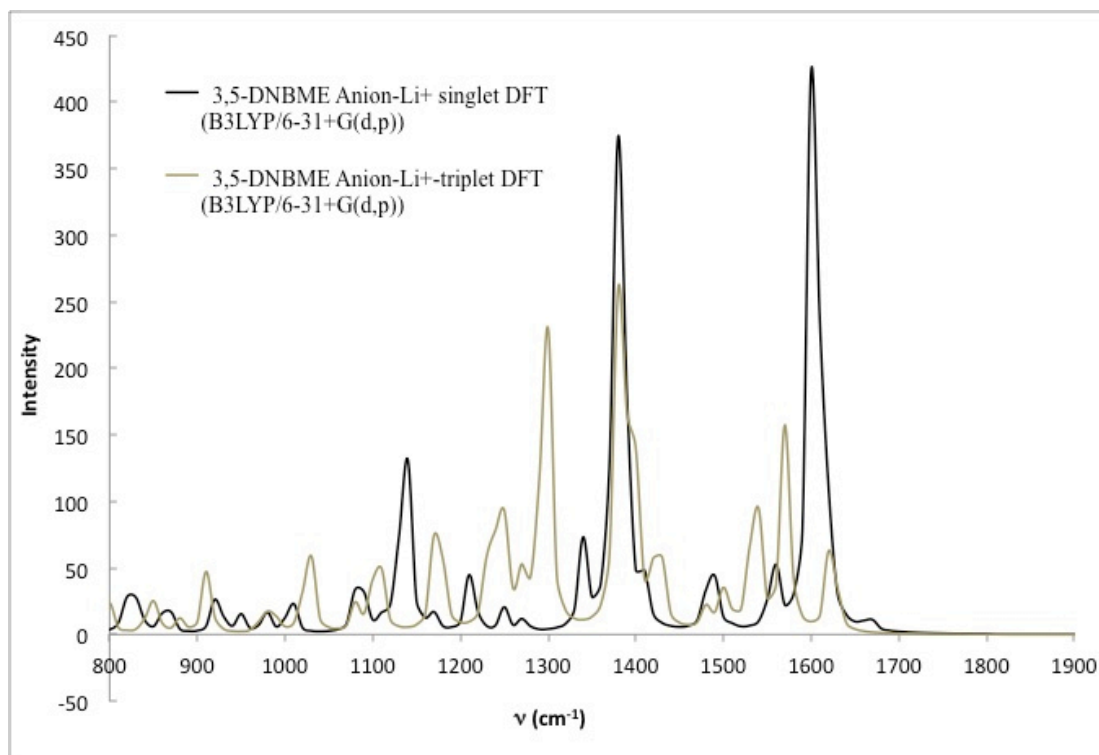
(a)
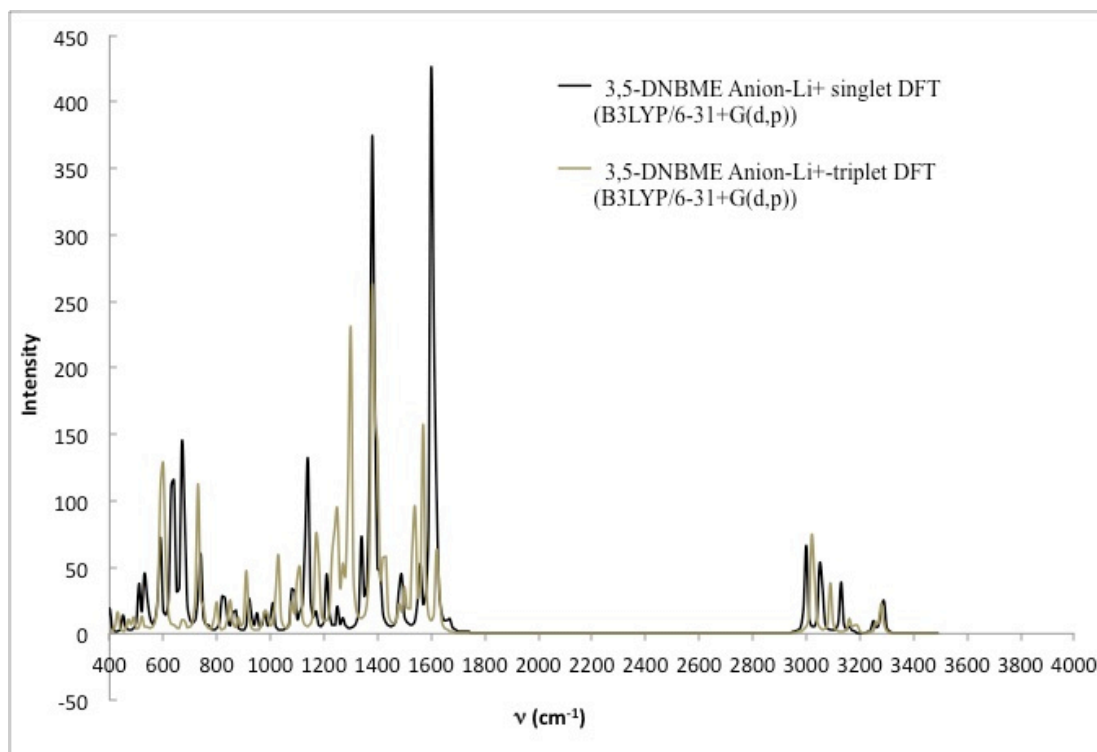
Figure 6.7. DFT predicted IR spectra for the 3,5-dinitrobenzyl methoxy ether carbanion lithium salt (**97-Li$^+$**) singlet and triplet states. (a) IR spectrum region between 400-4000 cm^{-1}. (b) IR spectrum region between 800-1900 cm^{-1}. All computed spectra where generated using a B3LYP/6-31+G(d,p) basis set and each of the energies associated with the IR absorptions generated in this figure, were corrected for zero-point vibrational energies (ZVPEs). The black spectrum represents the 3,5-dinitrobenzyl methoxy ether anion lithium singlet (**97S-Li$^+$**) and the brown spectrum represents the 3,5-dinitrobenzyl methoxy ether anion lithium triplet (**97T-Li$^+$**).

of H$_2$O and an IR spectrum was obtained (Figure 6.7c, light blue spectrum).   Like

our UV-Vis experiments discussed in chapters 4-5, we needed to generate a

difference spectrum for anion **97**. This was done by subtracting the initial 3,5-

dinitrobenzyl methoxy ether, **101**/1,4-dioxane IR spectrum (Figure 6.8a), and the IR

spectrum that only contained excess base (*n*-BuLi) in 1,4-dioxane (data not show)

from the IR spectrum we obtained in Figure 6.8b. The resulting subtracted IR

spectrum for anion **97** in *n*-BuLi/1,4-dioxane from this experiment is shown in Figure 6.8d.

There appears to be no significant changes in the IR bands associated with the initial 3,5-dinitrobenzyl methoxy ether **101**, in 1,4-dioxane either before any base is added (Figure 6.8a) or after the addition of excess base (Figure 6.8b). However, when the anion spectrum for the 3,5-dinitrobenzyl methoxy ether is quenched with H_2O (Figure 6.8c), one clearly can see that the resulting IR spectrum shows a large, broad band in the region of ~3600-2990 cm^{-1} which indicates that H_2O is present only when added to the anion **97** solution and is not present in a significant amount, prior to quenching (Figure 6.8a-b). The difference spectrum in Figure 6.8d, which we have

(d) difference IR spectrum: 3,5-dinitrobenzyl methoxy ehter carbanion 97 in 1,4-dioxane/n-BuLi
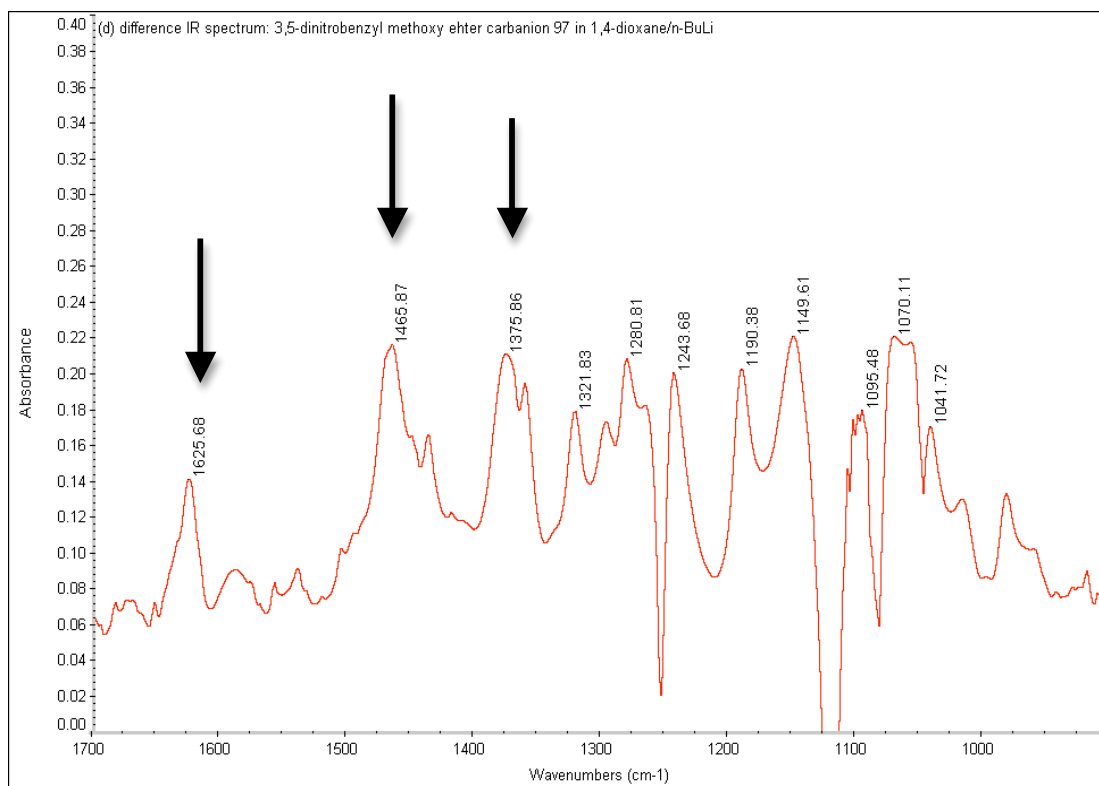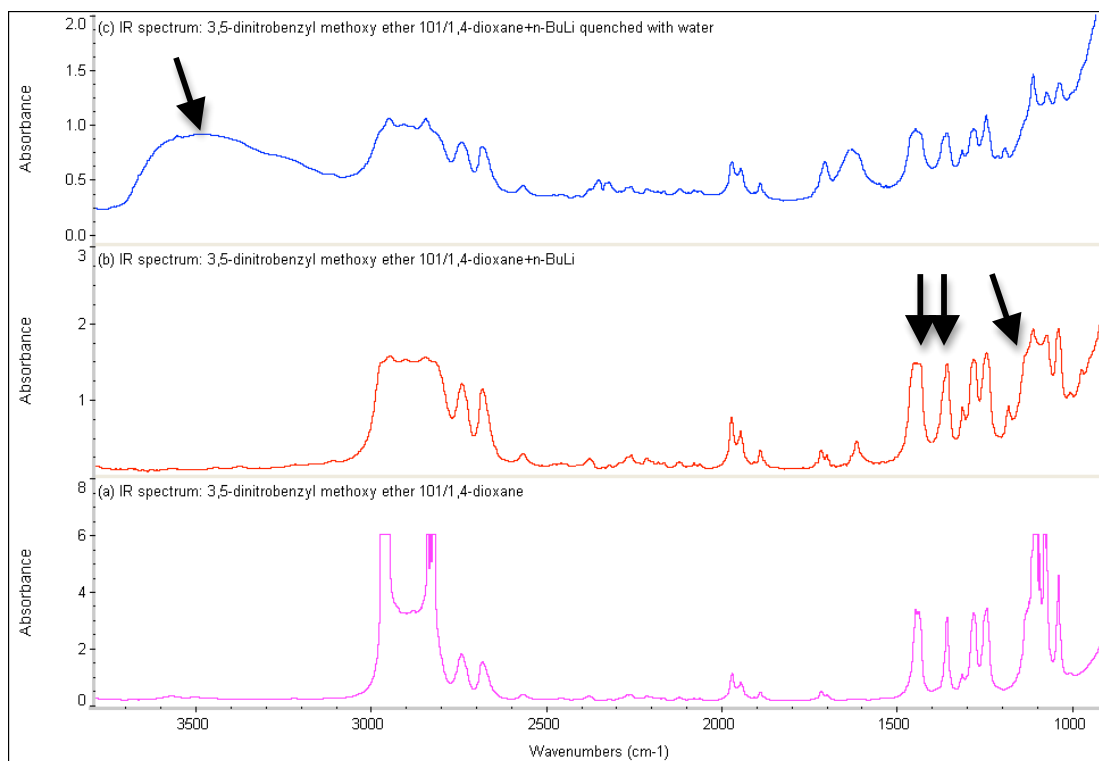
Figure 6.8. FT-IR spectra of the 3,5-dinitrobenzyl methoxy ether anion, **97** generated in 1,4-dioxane with addition of excess *n*-BuLi (2.50 M). (a) 2.01×10^{-2} mmol aliquot of 3,5-dinitrobenzyl methoxy ether, **101**/1,4-dioxane. (b) 1.79×10^{-2} mmol aliquot of 3,5-dinitrobenzyl methoxy ether, **101**/1,4-dioxane and a 3.75×10^{-2} mmol aliquot of *n*-BuLi added. (c) 1.79×10^{-2} mmol aliquot of 3,5-dinitrobenzyl methoxy ether, **101**/1,4-dioxane and a 3.75×10^{-2} mmol aliquot of *n*-BuLi + the addition of 5.00 μL of H_2O to the IR cell. (d) IR difference spectrum of anion **97** (fingerprint region between 800-1700 cm^{-1}): IR spectrum (b) - 2.01×10^{-2} mmol aliquot of 3,5-dinitrobenzyl methoxy ether, **101**/1,4-dioxane (a) – 3.33×10^{-2} mmol aliquot *n*-BuLi/1,4-dioxane (data not shown). Arrows in (d) indicated some of the prominent IR absorbances for the 3,5-dinitrobenzyl methoxy ether carbanion **97** that survive background subtraction. The arrow in IR spectrum (c) of this figure, indicates the significant O-H stretch frequency associated with the addition of water which is not present in the IR spectra in this region for (a) and (b). Arrow(s) in IR spectrum (b) indicate some characteristic peak(s) that change/shift in their absorbance in the IR when base is added to the solution containing 3,5-dinitrobenzyl methoxy ether **101**/1,4-dioxane in spectrum (a).

All IR spectra were collected using a sealed CaF_2 dispersive IR cell with a 0.10 mm path length, and was purged with nitrogen prior to the addition of any reagents, and before all sample collections. Each IR sample aliquot (*ca.* 80.0 μL) was taken from a stock solution of known concentration. Note that several difference spectra for anion **97** were collected, however spectrum (d) in the above figure, was the only spectrum that contained positive peaks after background subtraction.

tentatively assigned to be that of anion **97**, shows several modest bands that survive the rigorous subtraction discussed previously.

Since most of the intense IR bands for the predicted singlet and triplet states of the 3,5-dinitrobenzyl methoxy ether anion lithium salt appear in the fingerprint region between ~800-1700 cm^{-1}, we therefore focused our attention on comparing our computational and experimental data in this region of the spectrum. The difference spectrum shown in Figure 6.7d, has the strongest absorbances at ~1466, 1376, 1322, 1281, 1244, 1190, 1150, 1070 cm^{-1}. Because both the singlet and triplet states of the anion salt of **97** have an intense IR band at ~1380 cm^{-1}, the absorbances observed at or around this frequency, will not provide an unambiguous assignment of the electronic state for this anion. Thus, the peak at 1376 cm^{-1} is likely close enough to 1380 cm^{-1} to be attributed to either the IR bands of the singlet or triplet state of anion **97**. Furthermore, there are no significant IR absorbances for either the triplet and singlet state of anion **97** between 1400-1500 cm^{-1}. As a result, the IR band which we observed experimentally for anion **97** at ~1466 cm^{-1} does not seem to correspond to any of the IR bands for the singlet or the triplet state. The two IR bands for anion **97** at 1150 and 1190 cm^{-1} from our experimental spectrum (Figure 6.8d), both appear to match closely with a singlet absorbance at 1140 cm^{-1} and the triplet absorbance at 1170 cm^{-1} from our computed IR data (Figure 6.6b). More importantly, the triplet state to anion **97** has two IR bands at 1250 and 1300 cm^{-1} whereas the singlet state of anion **97** does not have any intense IR bands between 1200-1300 cm^{-1}. From our

experimental IR data on anion **97** (Figure 6.8d), we obtained three prominent IR

bands at 1322, 1281, and 1244 cm^{-1}. Although these bands do not show an exact

correlation to the IR peaks for the triplet anion of **97**, they are the only absorptions

observed in this region of the infared spectrum. In our experimental IR spectrum for

anion **97**, we did not observe any significant IR bands between 1500-1600 cm^{-1}.

However, there is a small absorbance observed at ~1626 cm^{-1} in the difference

spectrum for anion **97** (Figure 6.8d, indicated with an arrow). Despite the fact the

singlet has an intense IR band at *ca*. 1600 cm^{-1}, the triplet state has a very small

absorbance at ~1620 cm^{-1}. This absorbance closely resembles our experimental IR

band for anion **97** at ~1626 cm^{-1} here.

We do acknowledge that solvent effects and counterion binding in solution

can significantly impact the overall intensity and location of certain frequencies in the

IR spectrum.[2] Some factors that could advserely effect our experimental IR results

for the 3,5-dinitrobenzyl methoxy ether carbanion **97** described in Figure 6.8a-d,

could be changes in solvent reorganization, differential ion pairing, and complex

changes in aggregation states.[2]   Similar to our UV-Vis results discussed in previous

chapters, it is extremely difficult for one to obtain high-quality and accurate

transmission IR data/spectra particularly in the fingerprint region, due to the fact that

the solvent (THF, 1,4-dioxane) and the base (PhLi, *n*-BuLi, MeMgBr) also have

significant and intense IR absorptions in this region. Though we are confident that

we have in fact subtracted out many of these absorbances in our difference spectrum

for anion **97**, it may be possible that some of these signals might be, in part, attributed

to residual unsubtracted artifacts. It appears that the experimentally observed IR bands at 1626, 1244, 1280, and 1190 cm^{-1} match to some extent better with those predicted for the triplet state of anion **97**. Unfortunately, based on the discrepancies between these observed experimental IR bands and the computed IR bands for **97**, we cannot unambiguously identify the exact electronic state of this anion at this time. Therefore, we focused our efforts on obtaining UV-Vis data on the 3,5-dinitrobenzyl methoxy ether carbanion **97**, in hopes that we could better identify the electronic configuration to this anion using this spectroscopic method.

6.6 UV-Vis Spectra of the 3,5-Dinitrobenzyl Methoxy Ether and p-Nitrobenzyl Methoxy Ether Carbanions, 97 and 98.

Since we could not unambiguously identify the electronic spin state to carbanion **97** using FT-IR spectroscopy, we attempted to see if we could determine this anion's electronic spin state by UV-Vis spectroscopy. For comparison purposes, we also obtained UV-Vis spectra for the *p*-nitrobenzyl methoxy ether carbanion, **98** under similar conditions.

As discussed in chapter 5, TD-DFT computations allows us to predict the UV-Vis absorbances for the electronic states for various reactive intermediates. Therefore, we computed the singlet and triplet absorbance bands for the 3,5-dinitrobenzyl methoxy ether anion lithium salt (**97-Li$^+$**), and a table of these results is shown below (Table 6.1). We computed a total of 10 excited state absorbance frequencies for the singlet and triplet states for **97-Li$^+$**. It is also important to note

that the oscillator strength given for each excited state is proportional to the molar

absorptivity (ε) for that particular band (Table 6.1).

Table 6.1. TD-DFT UV-Vis Absorbance Bands for the 3,5-Dinitrobenzyl Methoxy Ether Anion Lithium Salt (**97-Li$^+$**) Singlet and Triplet States.

Excited State[a]	Singlet Absorbance (nm)	Oscillator Strength	Triplet Absorbance (nm)	Oscillator Strength
1	851.3	0.0114	798.7	0.0057
2	626.0	0.0185	736.6	0.0077
3	479.8	0.0271	436.5	0.0062
4	339.0	0.0030	430.0	0.0005
5	337.3	0.0010	389.6	0.0000
6	328.5	0.0067	382.0	0.0004
7	326.5	0.0128	353.8	0.0018
8	300.9	0.0291	329.0	0.0000
9	298.5	0.0019	324.3	0.0022
10	292.8	0.0749	322.4	0.0026

[a]Only 10 single-point excited states for both the singlet and triplet states of anion salt **97-Li$^+$** were calculated using a BLYP/6-31+G(d,p) basis set. Note that the oscillator strength given for each state is roughly proportional to the relative molar absorptivity (ε) for that absorbance band.

Our best experimental results for the UV-Vis spectrum for the *p*-nitrobenzyl

methoxy ether (PNBME) anion **98**, was obtained through the deprotonation of the

parent *p*-nitrobenzyl methoxy ether in THF with the use of excess PhLi as base

(Figure 6.9a). Similar to all previously reported UV-Vis experiments, we initial

obtained a UV-Vis spectrum for the *p*-nitrobenzyl methoxy ether in THF (Figure

6.9a, black spectrum). We then proceeded to titrate excess PhLi (in two portions)

into the solution that contained **102**/THF (Figure 6.9a, red and yellow spectra). As

one adds base to the solution that contains *p*-nitrobenzyl methoxy ether/THF, a low

intensity, broad band that begins to develop starting at ~570 nm and extends out until

450 nm and proceeds to go off-scale (Figure 6.9a, red and yellow spectra). After the two aliquots of base were added to the *p*-nitrobenzyl methoxy ether, **102**/THF solution, a small amount of 2-propanol was then combined with this resulting solution, and a UV-Vis spectrum was taken (Figure 6.9a, green spectrum). The green spectrum in Figure 6.9a is presumably the quenched spectrum for anion **98** in THF and clearly shows a decrease in the relative intensity of the broad band at ~570 nm seen from the addition of base and a large blue shift in the overall UV-Vis spectrum was also observed. This blue shift likely indicates that this solution is quenched and that the UV-Vis signals for *p*-nintrobenzyl methoxy ether **102** are regenerated from this reaction.

(b)
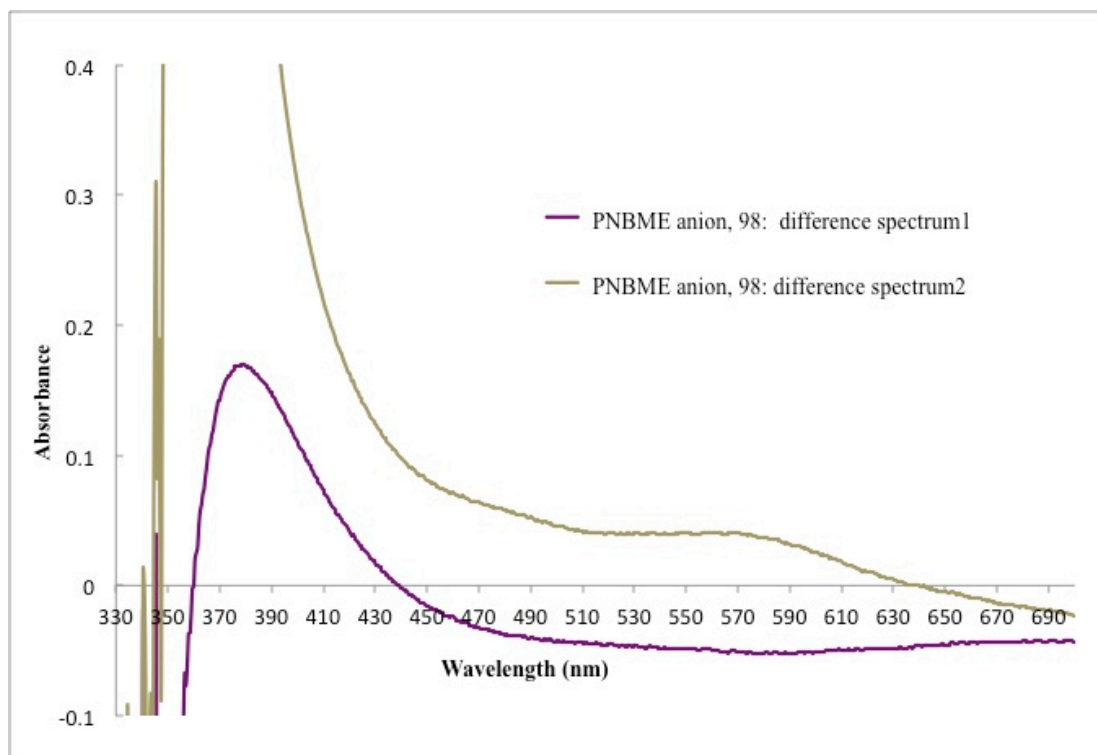
(a)
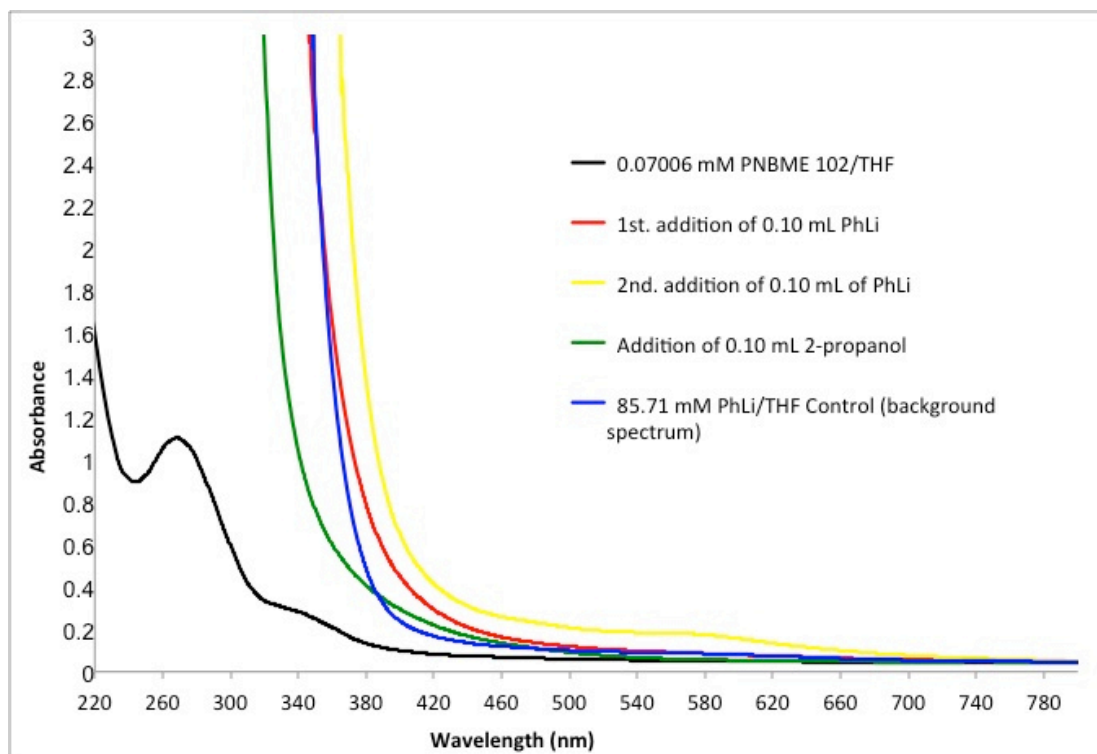
Figure 6.9. UV-Vis spectra of the *p*-nitrobenzyl methoxy ether (PNBME) carbanion, **98** generated in PhLi/THF. (a) 0.0701 mM PNBME, **102**/THF solution (black spectrum). 0.0701 mM PNBME, **102**/THF solution and the addition of the first aliquot of 0.100 mL of (1.80 M) PhLi/DBE (red spectrum). 0.0701 mM PNBME, **102**/THF solution with the addition of a second aliquot of 0.100 mL (0.200 mL total) of (1.80 M) PhLi/DBE (yellow spectrum). 0.0701 mM PNBME, **102**/THF and PhLi/DBE solution which is quenched with 0.100 mL of 2-propanol (green spectrum). 85.7 mM PhLi/THF background control spectrum (blue spectrum). (b) PNBME anion, **98** difference spectrum1 (purple spectrum): [red spectrum in (a) – blue spectrum in (a) - black spectrum in (a)]. PNBME anion, **98** difference spectrum2 (brown): [yellow spectrum in (a) – blue spectrum in (a) - black spectrum in (a)].

Moreover, Figure 6.9a shows a background UV-Vis control spectrum that we obtained for a 85.7 mM PhLi/THF solution (blue spectrum). Similar to all other anion UV-Vis spectra, which we have reported in this dissertation, we obtained two difference spectra for the *p*-nitrobenzyl methoxy ether carbanion **98** (Figure 6.9b,

purple and brown spectra). Again we generated the resulting difference spectra for anion **98** by subtracting both the UV-Vis spectra for **102**/THF and the 85.7 mM PhLi/THF solutions from the UV-Vis spectra from the successive additions of PhLi to the original *p*-nitrobenzyl methoxy ether/THF solution. The difference spectra for anion **98** shows two main absorbance maxima consisting of a broad band that starts at ~580 nm and a sharp absorbance band at *ca.* 375 nm (Figure 6.9b, purple and brown spectra). The UV-Vis spectrum for anion **98** was also obtained in MeMgBr/THF (data not shown). However, we were unable to obtain good quality UV-Vis spectra for anion **98** in THF or 1,4-dioxane with *n*-BuLi.

Similar UV-Vis spectra for the 3,5-dinitrobenzyl methoxy ether (3,5-DNBME) carbanion **97**, were likewise obtained under a variety of different conditions. For example, a UV-Vis spectrum of the 3,5-DNBME carbanion **97** was generated in 1,4-dioxane through the addition of excess *n*-BuLi as base (Figure 6.10a and b). In the experiment described in Figure 6.10a, we initially obtained a UV-Vis spectrum for the 3,5-DNBME, **101** in 1,4-dioxane (black spectrum) which showed only a small shoulder absorbance in the UV-Vis spectrum at ~320 nm. Consequently, we proceeded to add two aliquots of excess base (*n*-BuLi) to the solution containing 3,5-DNBME, **101**/1,4-dioxane (Figure 6.10a, red and yellow spectra). When the first aliquot of base was added (red spectrum), only a small shoulder band at ~300 nm begins to form, and when the second aliquot of *n*-BuLi was titrated into this solution, a large band that goes off-scale at ~320 nm grows into the UV-Vis spectrum (yellow spectrum). The resulting solution containing base, and 3,5-dinitrobenzyl methoxy

ether, **101**/1,4-dioxane was then quenched with 100 μL of 2-propanol (Figure 6.10a, green spectrum). The green quenched spectrum in Figure 6.10a shows a significant blue shift relative to the yellow spectrum which contained excess base, thereby indicating that the UV-Vis signals attributed to the base and the 3,5-dinitrobenzyl methoxy ether carbanion **97** were effectively quenched by 2-propanol. The small shoulder absorbance at *ca*. 320 nm in the quenched UV-Vis spectrum (green spectrum, Figure 6.10a), also indicates that the 3,5-dinitrobenzyl methoxy ether **101**, is mostly reformed in this experiment, since benzyl methoxy ether **101** initially has a small absorbance in the UV-Vis spectrum near this wavelength.

(b)
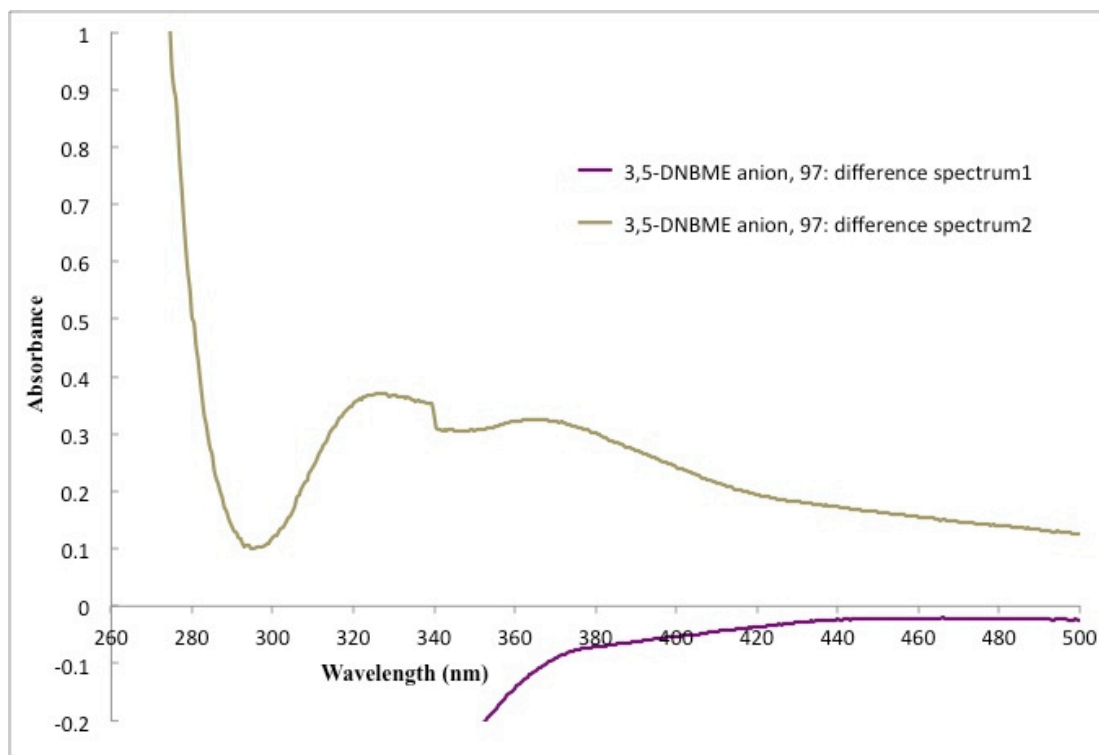
(a)
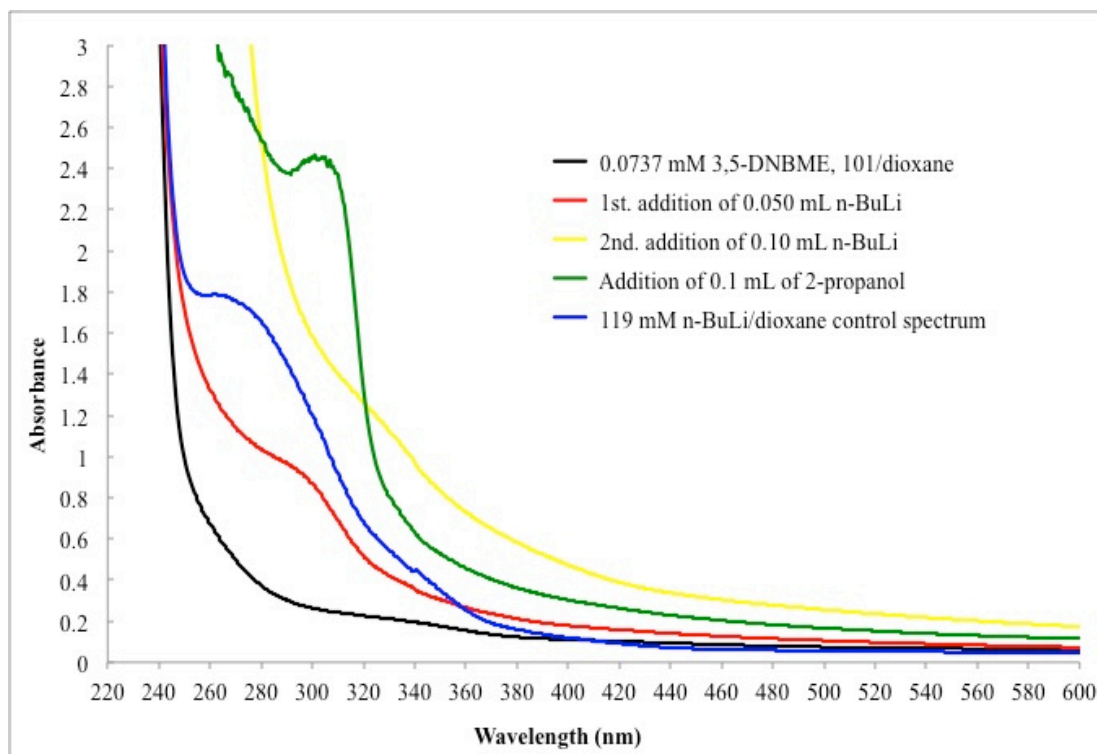
Figure 6.10. UV-Vis spectra of the 3,5-dinitrobenzyl methoxy ether (3,5-DNBME) carbanion, **97** generated in *n*-BuLi/1,4-dioxane. (a) 0.0737 mM 3,5-DNBME, **101**/1,4-dioxane (black spectrum). 0.0737 mM 3,5-DNBME, **101**/1,4-dioxane and the addition of the first aliquot of 50.0 μL of (2.50 M) *n*-BuLi/hexanes (red spectrum). 0.0737 mM 3,5-DNBME, **101**/1,4-dioxane and the addition of the second aliquot of 100 μL (150 μL total) of (2.50 M) *n*-BuLi/hexanes (yellow spectrum). 0.0737 mM 3,5-DNBME, **101**/1,4-dioxane and *n*-BuLi/hexanes solution quenched with 0.100 mL of 2-propanol (green spectrum). 119 mM *n*-BuLi/1,4-dioxane background control spectrum (blue). (b) 3,5-DNBME anion, **97** difference spectrum1 (purple): [red spectrum in (a) – blue spectrum in (a) - black spectrum in (a)]. 3,5-DNBME anion, **97** difference spectrum2 (brown): [yellow spectrum in (a) – blue spectrum in (a) - black spectrum in (a)].

Figure 6.10a additionally shows the UV-Vis spectrum for a 119 mM blank

solution containing solely *n*-BuLi/1,4-dioxane (blue spectrum). This blank or

background solution with *n*-BuLi/1,4-dioxane shows only one major shoulder

absorbance at *ca*. 280 nm. In order to accurately identify the absorbance band due

161

solely to carbanion **97**, we again subtracted out the UV-Vis absorbance from the

solution that only contained base (blue spectrum Figure 6.10a) and the UV-Vis bands

from the 3,5-dinitrobenzyl methoxy ether, **101** from the UV-Vis spectra in which we

obtained from the successive additions of excess base to the 3,5-dinitrobenzyl

methoxy ether, **101** in 1,4-dioxane (Figure 6.10a, red and yellow spectra). Figure

6.10b shows the resulting difference spectra we obtained for anion **97** in 1,4-dioxane.

Only the brown spectrum in Figure 6.10b shows positive absorbance bands at 327 and

367 nm that survive the rigorous background subtractions that was just discussed

previously.   The UV peaks at 327 and 367 nm for carbanion **97** obtained in this

experiment generally remained consistent when the analogous experiment was

repeated several times and the same background subtraction procedure was applied.

However, a few of the subtraction results from other experiments tended to show that

the band at 367 nm occasionally became indiscernible and simply coalesced with the

band at 327 nm, and as a result formed a larger shoulder band at ~327 nm.

We also obtained experimental UV-Vis absorbance spectra for the 3,5-

dinitrobenzyl methoxy ether carbanion, **97** with PhLi/THF, and MeMgBr/THF (data

nor shown, see Chapter 7, Supporting Information for spectra). Unfortunately, we

were unable to observe any significant UV-Vis abosrbance due to anion **97** with *n*-

BuLi/THF and PhLi/1,4-dioxane, even after careful subtraction of all unwanted

background absorbances. The UV-Vis spectrum for the 3,5-dinitrobenzyl methoxy

ether carbanion **97**, in PhLi/THF showed two broad bands at λ_{max} = ~485 and 566 nm

and with MeMgBr/THF showed a single shoulder band between 295-303 nm (note:

the difference spectrum for this result only involved background subtraction of absorbance due to MeMgBr/THF and not from the additional subtraction of 101/THF). As discussed with our results for the 3,5-dinitrobenzyl methoxy ether carbanion 97, in 1,4-dioxane/*n*-BuLi, the difficultly with assigning some of the bands for this anion, for the majority of our difference spectra, is due to the fact that many of these absorbances are very broad and may at times even coalesce with other peaks in the UV-Vis spectrum   Thus, some caution should be taken when interpreting the UV-Vis absorbances in which we are reporting for anion 97. Nonetheless, we are confident that the difference UV-Vis spectra for anion 97 which we have obtained under various conditions, is in fact accurate considering the extensive measures we have taken to subtract out all absorbances from the starting ether (101), the base, and solvent.

Comparing some of our UV-Vis experimental results with the TD-DFT data (Table 6.1) for anion 97, we see that the band at 327 nm we obtained in Figure 6.9b matches up well with the predicted singlet absorbances at 326.5 and 328.5 nm. Though we do not find any predicted bands for either the singlet or triplet in Table 6.1 for the second maxima at 367 nm, we must be aware that this band may be part of the broad band we observed experimentally at *ca*. 327 nm.   The two UV peaks we obtained for anion 97 in PhLi/THF at 485 and 566 nm do not directly correlate to any of the predicted UV-Vis bands for this anion. However, the absorbance band for the singlet anion at 479.5 nm is the only absorbance close enough to one of our observed UV-Vis maxima for anion 97 in PhLi/THF. Lastly, the single broad shoulder

absorbance for anion **97** between 295-303 nm, which was obtained in MeMgBr/THF, corresponds almost perfectly with a cluster of three intense singlet absorbances at 292.8, 298.5, and 300.9 nm from our predicted TD-DFT computations.   As a whole, we can conclude that the UV-Vis bands for the 3,5-dinitrobenzyl methoxy ether carbanion **97**, is nominally most consistent with the predicted singlet TD-DFT absorbances rather than that of the triplet.

Future work will be done to identify the electronic state of the 3,5-dinitrobenzyl methoxy ether carbanion **97**, by either X-ray crystallography, Raman spectroscopy, or EPR. Additional experiments should be conducted to further elucidate the unusual chemical behavior of anion **97**. These experiments might include chemical trapping studies, H/D exchange, and Evans method magnetic susceptibility experiments.

6.7 How to Design Future Carbanion Precursors?

This section will discuss how one could design, synthesize, and characterize

Scheme 6.2. General synthetic method for generating and studying carbanion based precursors

1. Mg / Et$_2$O
2. CO$_2$
3. aq. workup

base / THF
hν

observe anion by LFP
NMR or other spectroscopic method

R$_1$ = H or alkyl
R$_2$ = aryl

1. *n*-BuLi
2. CO$_2$
3. aq. workup
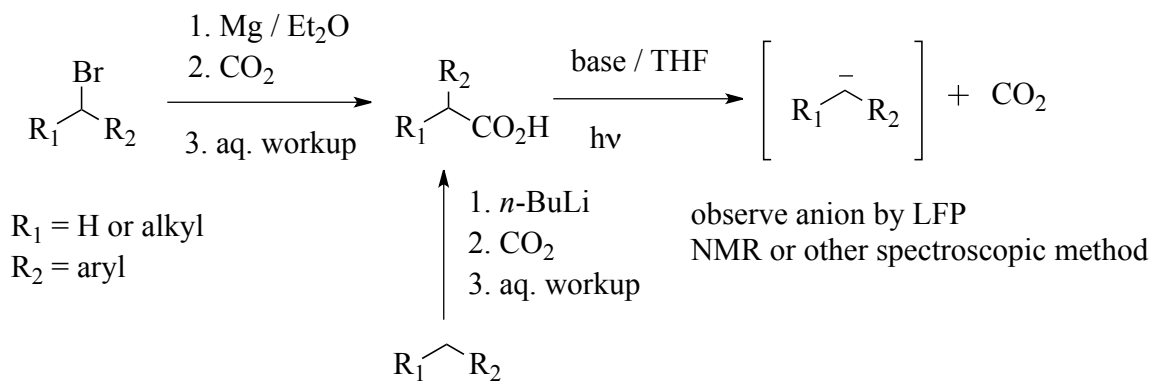
carbanion precursors and their corresponding carbanions. The first question we need

to ask ourselves when exploring a new method for generating a target carbanion

intermediate is: are there other precursors that could lead to a carbanion intermediate?

We have seen in this chapter as well as in chapters 4-5, that most carbanions

can be effectively generated and studied by a variety of spectroscopic methods *via* the

deprotonation of the respective hydrocarbon precusors. However, are there other

more practical methods for generating anions other than using very strong

alkyllithium bases? The answer to these questions is yes. One can envision

synthesizing a carboxylic acid homolog directly adjacent to the carbon center in

which the target carbanion would be generated (Scheme 6.2). If decarboxylation

could be efficiently achieved under an inert environment, then the target carbanion

would be formed. Scheme 6.2 shows exactly this concept. The carboxylic acid

precursor to the desired carbanion could be synthesized *via* either formation of an

alkyl Gringard followed by carboxylation or by deprotonation of the starting alkane

with *n*-BuLi followed by carboxylation (Scheme 6.2). Thus, these carboxylic acids

can be decarboxylated under mildly basic conditions using a suitable light source

(photodecarboxylation). Decarboxylation would then almost certainly lead to the

formation of the target anion intermediate and carbon dioxide as the other byproduct

from this reaction (Scheme 6.2). The desired carbanion intermediate in Scheme 6.2,

if long-lived, could be analyzed using a variety of spectroscopic methods, which

might include LFP, NMR, IR, UV-Vis, etc.

The carboxylic acid precursor in Scheme 6.2, essentially serves as an effective photoremovable protecting group for generating the target anion under basic conditions, in aprotic media. In principle, the method shown in Scheme 6.2, demonstrates a milder process for generating the corresponding carbanion intermediate in which one would like to study. If photodecarboxylation were to occur, and depending on the nature of the R_2 aryl group adjacent to the carbanion center, one can see that this might potentially lead to a very long-lived carbanion intermediate if the conditions are just right.

Additionally, the photodecarboxylation and identification of stable carbanions by the method shown in Scheme 6.2, is not a new concept. Scaiano, *et al.* and others have recently used this photodecarboxylation concept to generate and study stable

Scheme 6.3. Recent example of a stable carbanion generated from photodecarboxylation

Ketoprofen

Long-lived anion
observed by LFP
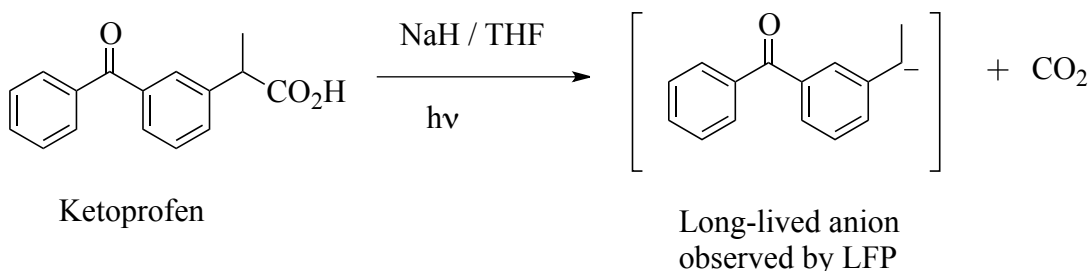
benzylic carbanions by LFP (Scheme 6.3).[120-123] Scaiano's work showed that the benzyl carbanion generated from the photodecarboxylation of ketoprofen in basic THF (Scheme 6.3), is stable for several minutes to even hours.[120] Following the general blueprint presented in work by Scaiano, Wan, and others, one might imagine that we could also derive similar carboxylic acid photoprecursors to many of the

anions discussed in this chapter and in chapter 4. Hence, Scheme 6.4 shows five such

carboxylic acid precursors. As discussed previously, the benzyl anion to ketoprofen

was reported by Scaiano to be unusually long-lived.[120] This is extremely fascinating

considering that the benzyl anion derived from the photodecarboxylation of

ketoprofen, is a simple aliphatic benzyl carbanion which is only able to delocalize

Scheme 6.4. Potential carbanion precursors (**103-106**) and how to generate the
corresponding anions by photodecarboxylation
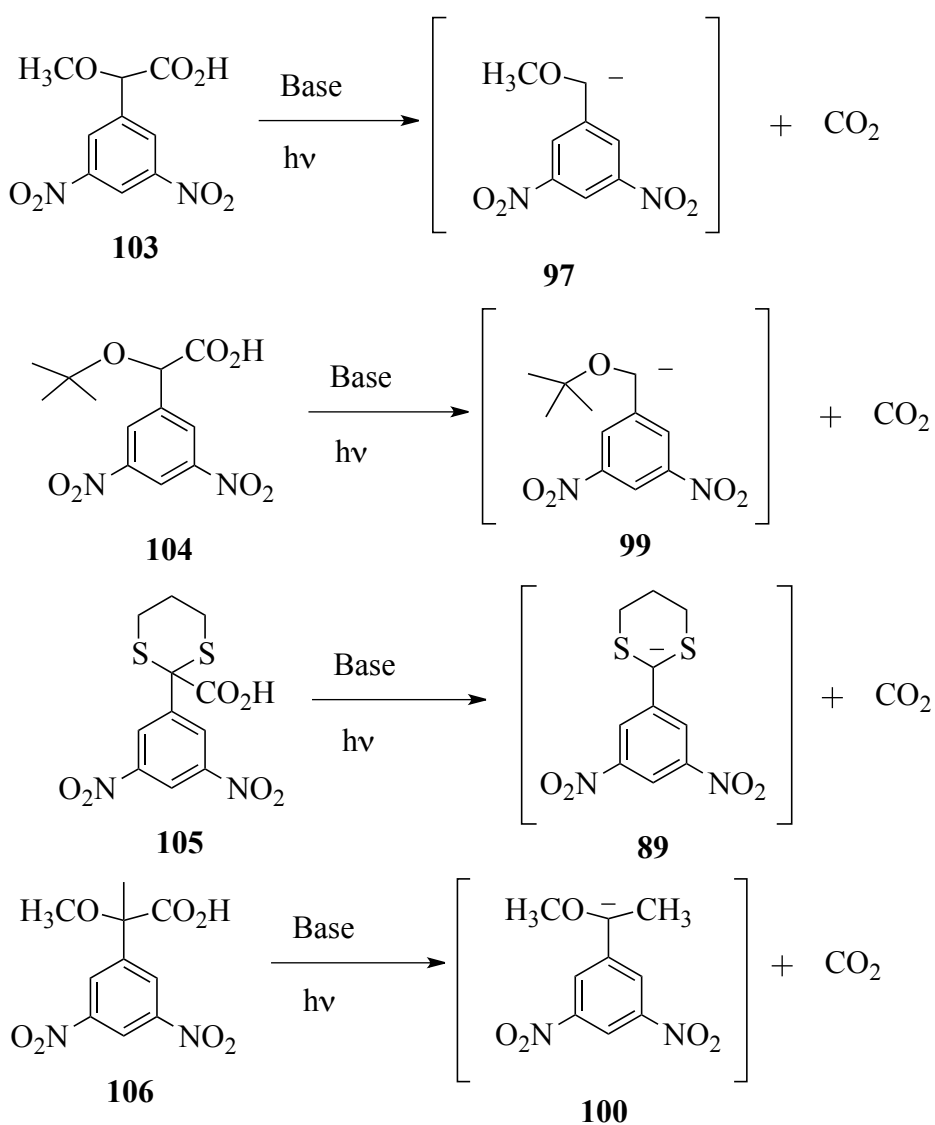
into the adjacent phenyl ring. Moreover, the ketoprofen benzyl anion has only one potential electron withdrawing group that could stabilize such an anion, albeit not through direct resonance delocalization of the anionic charge.

Interestingly, anions **97**, **99**, **89**, and **100** all possess two strong, π-electron withdrawing groups (e.g. NO_2 groups) *meta* with respects to the formally anionic center. By this logic, and from the data presented throughout this dissertation with regards to the overall stability of these carbanions, we would almost certainly predict that these anions should be also very long-lived intermediates. Although precursors **103-106** seem to be extremely feasible candidates for photodecarboxylation under basic conditions, there are however a few drawbacks that one must consider. In Scaiano's work, the carbanion precursor, ketoprofen is a natural product and therefore did not require extensive synthetic procdures to obtain this carboxylic acid precursor. Similar carboxylic acid precursors presented by Scaiano, *et al.*[122] usually required one trivial step to obtain the desired acid and in addition at least one of the coupling partners already contained the carboxylic acid moiety. Since Scaiano and others did not have to rigorously synthesize such phenyl acetic acid precursors, we must anticipate that the synthesis of the carboxylic acids shown in Scheme 6.4 may prove to be somewhat challenging. Likewise, none of the carboxylic acids **103-106** have been previously synthesized. Some insight into a possible synthetic route to at least a few of the carboxylic acid precursors shown in Scheme 6.4, may come from research reported by Nakai, *et al.*[124] Nakai reported that a simple benzyl methoxy ether could be deprotonated with either *tert*-butyl lithium or *sec*-butyl lithium in hexane and

subsequently carboxylated to yield the corresponding alpha-methoxy phenyl acetic acid, in modest to high yields (note: the yields obtained in this work ranged from > 5 % to 95 %).[124]

Despite the variable yields presented in Nakai's work, this synthesis provides us with a good starting point in the pursuit of synthesizing carbanion precursors such as **103-106**. As a whole, Scaiano's findings demonstrate that we might be able to develop a similar synthetic scheme to obtain suitable future carbanion precursors. Furthermore, we are somewhat confident that if such carboxylic acid precursors could be synthesized, that the photodecarboxylation of these precursors under mildly basic conditions, should proceed smoothly to form very stable carbanions (**97**, **99**, **100**, and **89**). Carbanions **97**, **99**, **89**, and **100** are all predicted to be ground state triplet diradicals, computationally. Therefore, generating and studying these carbanion intermediates *via* this photodecarboxylation method, may present some new and interesting insights into their chemistry.

6.8 Summary and Outlook

The placement of a single π-electron donating OR group adjacent to a benzylic carbanion center bearing two *meta* NO_2 groups, strongly favors a triplet ground state for these carbanions, computationally. In this chapter, we have chosen to focus our experimental efforts to characterize and identify the electronic ground state of the 3,5-dintrobenzyl methoxy ether carbanion, **97** and its corresponding lithium salt, **97-Li$^+$**. Our ^{1}H NMR experiments shows that the 3,5-dinitrobenzyl methoxy ether carbanion **97**, either exhibits paramagnetic peak broadening or NMR

silent behavior. Though we were able to obtain good quality FT-IR spectra for carbanion **97**, we could not conclusively match our predicted DFT values for the singlet or triplet states for this anion. Our UV-Vis spectroscopic data on the 3,5-dinitrobenzyl methoxy ether carbanion **97**, shows that the absorbances due to this anion is mostly consistent with the absorbances associated with the singlet state bands predicted by our TD-DFT data. One possible explanation for the discrepancy between our NMR and UV-Vis results, could be that in our UV-Vis studies, the majority of the 3,5-dinitrobenzyl methoxy ether carbanion **97**, is in the singlet state. However, our NMR studies indicate that the 3,5-dinitrobenzyl methoxy ether carbanion **97**, appears to show a small percentage of triplet diradical character.   The observed triplet diradical behavior for anion **97** in our NMR experiments, might be explained by the fact that in these NMR solutions, a small number of triplet diradicals of anion **97** that are present, are able to effectively relax the large amount of singlet anions in the same solution on a NMR timescale. Future experiments will be done to unambiguously identify the electronic ground state configuration of carbanion, **97**.

Additional research efforts will be done to synthesize carboxylic acid derivatives that could yield carbanions effectively after undergoing photodecarboxylation. It is our hope that if these carbanions (**97**, **99**, **100**, and **89**) can be generated under these conditions, that these anions should be stable and long-lived enough to be accurately characterized by a known spectroscopic method (NMR, laser flash photolysis, UV-Vis, IR, etc.).

In all, the research described in this dissertation shows that certain benzylic carbenium ions and carbanions behave as triplet diradicals. Most of these small molecule, organic intermediates discussed in our research (Chapters 2-6), were designed similar to the *m*-xylylene diradical, which has been reported both experimentally and computationally to have a triplet ground state.[12a,24] For example, in chapter 2 we demonstrated through photoproduct studies and NMR analysis, that the 3,5-bis(dimethylamino)benzyl carbenium ion **42** can be generated from the photoheterolysis of 3,5-bis(dimethylamino)benzyl alcohols and esters in alcoholic solvents. Furthermore, we have provided both experimental and computational results in chapter 2 that show carbenium ion **42** has a degenerate electronic state. More specifically, in all of our photoproduct studies, we observed solvent incorporated products (**49-51**, singlet state products), as well as a reduction product (**52**, triplet state product).

Chapters 4-6 investigated whether ion-diradicals could be generated from anionic groups attached to a benzene ring containing *meta* disubstituted π-acceptor groups such as NO_2, CN, CO_2H, etc. For instance, the 2-(3,5-dinitrophenyl)-1,3-dithiane carbanion **79**, and its corresponding lithium and potassium salts, has been shown through extensive experimental and computational studies to have an accessible triplet ground state (Chapter 4). NMR and Evans method magnetic susceptibility studies show that the 2-(3,5-dinitrophenyl)-1,3-dithiane carbanion **79** is

a persistent and paramagnetic species at room temperature. Moreover, DFT

computations, NMR and UV experiments in chapter 6, demonstrate that the 3,5-

dinitrobenzyl methoxy ether carbanion **97**, could also be another anionic intermediate

with a triplet ground state.

As a whole, we anticipate that ion-diradical intermediates can be added to the

list of known organic high-spin building blocks (diradicals, carbenes, and nitrenes) in

the near future. The computational and experimental studies presented throughout

this dissertation on ion-diradical intermediates, should provide a robust

guideline/blueprint towards the future development and characterization of these

unusual intermediates.

Chapter 7: Supporting Information

7.1 Computational Data

Singlet to triplet geometry optimizations and energy calculations for all structures were obtained with the use of Gaussian 2003 software package. The method used was density functional theory with the Becke, three-parameter, Lee-Yang-Parr exchange-correlation functional at the 6-31+G(d,p) level. The singlet-triplet energy gaps for compounds **79**, **81**, and **82** involved optimization and frequency calculation of the singlet at the RB3LYP level followed by a single point energy calculation of the restricted singlet geometry at UB3LYP level. The correction from the restricted frequency calculation was applied to the unrestricted energy. Then the difference between singlet and triplets were taken to obtain the respective numbers. For all other compounds, the singlet to triplet energy gaps were simply calculated by the difference of restricted singlets and triplets without doing a re-calculation for the unrestricted singlet. The compounds with reference numbers, ΔE_{ST} values, zero point vibrational energy corrections, standard orientation z-matrices, and graphical representations of optimized geometries from GaussView (version 3.0, 2000-2003, Semichem, Inc.) software package and this information/data is provided in the Supporting Information section of Perrotta, *et al.*[106] (note that some of these compounds were numbered differently in this document from the numbering scheme used throughout this dissertation for these compounds). A list of TD-DFT calculated UV-Vis absorbance values for anion **79** is provided in section 7.4 of this chapter. The predicted IR spectra generated for anion **97** and **97-Li$^+$** were done using the optimized singlet and triplet geometries and included all frequency energies associated with their respective zero-point vibrational energy contributions.

All chemicals and solvents for any synthesis and/or spectroscopic experiments were used without any further purification unless otherwise stated. 2-Phenyl-1,3-dithiane (**90**) was purchased from the Aldrich, Co. and was used without further purification. Dichloromethane was distilled over calcium hydride before use. Tetrahydrofuran for synthetic reactions was distilled prior to use under nitrogen with sodium metal and benzophenone. 3,5-Dinitrobenzyl alcohol was purchased from Aldrich and Alfa Aesar and was used without any further purification. Benzene (GR ACS, EMD Chemical, U.S.A.) was transferred to an oven dried amber bottle (1 L), and was dried using 4Å Linde molecular sieves, and purged with nitrogen until use. Anhydrous THF that was inhibitor free ($\geq$ 99%) was purchased from Sigma-Aldrich and anhydrous 1,4-dioxane (99.8%, Alfa Aesar) were used as received for all spectroscopic experiments. Additives potassium bis(trimethylsilyl)amide (KHMDS) 0.5 M solution in toluene (Aldrich) and potassium *tert*-butoxide (Acros Organic, 98+% pure) were both used without purification.

3,5-Diaminobenzoic acid (98%) was purchased from the Aldrich Chemical Co. Solvents were purchased from J.T. Baker, Fischer Scientific or Acros vendors. Anhydrous dichloromethane and acetonitrile were distilled over calcium hydride under an inert nitrogen environment prior to use. 1,4-Dioxane, reagent grade, 98% (Fischer Scientific), cyclohexane (J.T. Baker), and triethylamine reagent grade (Fischer Scientific) were used without any prior purification. 37% Formalin solution in water

(Fischer Scientific), 98% phenyl acetyl chloride, 97% (Aldrich Chemical Co.), 1,4-cyclohexadiene, stabilized 97% (Acros), sodium borohydride, reagent grade, ≥98.5% (Aldrich Chemical Co.), acetyl chloride, P.A. (Acros), lithium aluminum hydride, 97% dispersion in mineral oil (Alfa Aesar), anhydrous nickel (II) chloride, 98% (Aldrich Chemical Co.), absolute ethanol 100 proof ACS/USP reagent grade (Pharmaco), absolute methanol (J. T. Baker), sulfuric acid (Fischer Scientific), 2-propanol, reagent grade (Fischer Scientific), and 2,2,2-trifluoroethanol (TFE), reagent grade, 99.8% (Acros) were used without purification. Chemical standards, heptane, extra low UV-cut-off (EMD, Omni-Solv), 98% (triphenylene, 98% (Aldrich Chemical Co.), toluene, reagent grade/HPLC grade (J. T. Baker), bibenzyl, 98% (Aldrich Chemical Co.), and methyl *tert*-butyl ether, HPLC grade, 98% (Aldrich Chemical Co.) were also used without any further purification.

Alkylation reagents iodomethane, (Acros Organic, 99% stabilized with copper) and 1-bromopropane, (Aldrich, Co., 99%) were transferred in small aliquots (*ca.* 1-3 mL) to oven dried vials containing 4Å Linde molecular sieves and the vials were purged with nitrogen prior to their use. *N,N,N',N'*-Tetramethyl ethylenediamine (TMEDA) Ultrapure Bioreagent catalyst for polyacrylamide gels (J.T. Baker) was dried with 4Å Linde molecular sieves and was purged with nitrogen before use for all experiments. NMR solvents CD_3OD (Cambridge Isotope Laboratories, Inc.) and CH_3OD (Aldrich) were dried with 4Å Linde molecular sieves and were purged with nitrogen before use. C_6D_6 (Cambridge Isotope Laboratories, Inc.) was dried using 4Å Linde molecular sieves prior to use and d_8-dioxane (Cambridge Isotope Laboratories, Inc.) were used without further purification. Bases KH (Aldrich, 30% by weight in

mineral oil), 2.5 M *n*-butyllithium in hexanes (Aldrich), and 3.0 M methyllithium in 1,1-diethoxymethane (Aldrich), 1.0 M CH$_3$MgBr/THF solution (Acros Organic), 1.8 M PhLi/DBU (Aldrich) were used as received. Solvents methanol abs. (J. T. Baker), 2-propanol (BDH, Chemical), ethanol abs. (Pharmaco) were used without any further purification. 3,5-Dimethoxybenzoic acid (Acros Organic, 99%), *p*-nitroaniline (Aldrich, ≥99 %), 3,5-dinitroaniline (Acros Organic, 98%), 3,5-diaminobenzoic acid (Aldrich, 98%), 4-nitrobenzyl bromide (Aldrich, 99%), 4-nitrobenzyl alcohol (Aldrich, 99%), tetramethylammonium fluoride (Aldrich, 97%), Ruppert's reagnet (trifluoromethyl)trimethylsilane, (98%, purchased in 1 g quantities, Alfa Aesar), NaOCH$_3$ (Fischer Scientific), 1,2-dimethoxyethane (anhydrous. Sigma-Aldrich, 99.5%)

All NMR titration experiments and routine ^{1}H and ^{13}C characterization data for all compounds and mixtures was done using a Bruker DRX 400 and Bruker AV-400 (400 MHz) instruments. Chemical shifts (δ) for the NMR data for all products and compounds provided in section 7.3 of this chapter, are reported in ppm unless otherwise stated. Both NMR titration experiments and Evans method experiments on **89**, **90**, **93**, **95**, **101**, and **102** were done either in a sealed NMR tube with a screw top teflon/silcon rubber septum or a J.Young tube with a control atmosphere valve (CAV).[125] The sealed NMR/J. Young tubes were purchased either from Quark Enterprises or from New Era NMR tubes. Each sample tube was oven dried prior to use. During and before the addition of any reagents, the NMR tubes were purged with dry nitrogen (5-10 min.). The sealed NMR sample tubes consisted of threaded cap (8 mm) lined with a silicon/tefon septum and the NMR tube of 8 mm O.D., 168 mm in total length, and a 20 mm reservoir. The typical J. Young tube used for these NMR experiments consisted of

176

a tube (210 mm), 40 mm reservoir, and a sample tube 0.38 mm wall. Each Young tube

was sealed using a CAV TFE plug with a Viton o-ring seal (65 mm in length from the

reservoir to the end of the CAV). When reagents were added to the Young tube (*via*

dried gas-tight syringes), an oven dried glass CAV adapter (9.0 mm O.D., 7.0 mm I.D.,

and 45 mm in length) was added with a septum and was purged with nitrogen before and

during use. For Evans method experiments, a sealed capillary inner tube containing 100

μL of C_6D_6 or other specified solvent (O.D. = 2.5 mm) was carefully placed into the

Young or septum sealed NMR tube prior to the addition of any reagents. All samples

were analyzed by using either 32 or 64 scans.

Mass spectra data was collected on a JEOL AccuTOF-CS using ESI-TOF or

Direct Analysis in Real Time (DART) analysis.   All solids and oils that were

characterized by DART MS analysis were performed neat (solvent free) unless

otherwise indicated. A select number of compounds failed to ionize using ESI-TOF or

DART analysis, and were thus analyzed using a GC-MS system consisting of a Varian

3900 (GC) and Saturn 2100T (MS). The GC column that was used for all analyses was

a Supelco 24034 capilary column SPB-5 with dimensions of 30 m X 0.22 mm and 0.25

μm film thickness.   Samples were analyzed using an EI method that had a temperature

ramp between 100-280 °C and a split ratio of 5 : 1.   The GC method specifications for

each sample run were as follows: column flow = 1.2 mL/min., linear velocity = 43.3

cm/s, total flow = 10.4 mL/min., actual pressure = 23.8 psi, injector temperature was 250

°C, injectors initial split ratio was 5 : 1, after 0.01 minutes, 50 : 1 and 0.5 minutes, 5 : 1.

Masses of m/z = 40-650 were analyzed from 0-3 minutes and m/z = 50-450 from 3-

20.67 minutes. GC column ramp was as follows for the indicated method: 60 °C, hold

177

time 2 minutes, 15 °C/min., 15 °C/min., 180 °C, hold time 0 minutes, total run time of 7.33 minutes total time, and 30 °C/min., 280 °C, hold time of 10 minutes, and a total sample run time of 20.67 minutes.

All GC experiments and samples were taken using a Shimadzu GC-17A, containing a RTX-5 stationary phase column (length = 15 m, inner diameter (i.d.) = 0.25 mm, film thickness = 0.25 μm), equipped with a FID detection system, and using the following method specifications: column temperature = 60 °C, injection temperature = 280 °C, and detector temperature = 300 °C, with a temperature/pressure profile for injection of: 67 kPa, 3.0 minutes, 3.9 mL/minute, 98 kPa, 9.0 minutes, column of: 60 °C, 3 minutes, 30 mL/minute, 300 °C, 9.0 minutes, injector pressure of 60 kPa, total flow of 31 mL/min., column flow of 1.45 mL/min., linear velocity of 39.1 cm/s, and a split ratio of 19 : 1.

UV-Vis data in chapter 4 was collected using a Perkin Elmer Lambda 2S UV/Vis spectrometer. The raw UV-Vis data was collected using the Perkin-Elmer PECESS software package for Lambda 2, 11, 15/17, 9, version 4.3 (1993) and was subsequently exported as a text file into the Microsoft Office Excel 2003 spreadsheet software package where the final UV-Vis data was processed (this was done for all other UV-Vis raw data in this dissertation, regardless of the instrument where the data was initially collected). The UV-Vis spectra in chapter 5 was obtained using a Hewlett Packard (HP)/Aglient 8456 spectrometer. UV-Vis sepectra in chapter 6 was obtained using a Shimadzu, UV-1800 spectrometer, and data was initially collected using the UVProbe version 2.35 (2012) software package/interface. All UV-Vis spectra were collected using a standard fluorometer cuvette with 4-sided quartz polished windows.

The cuvette had the following specifications: O.D. 8 mm X I.D. 6 mm (top opening), height = 125 mm, light path length = 10 mm, outer length = 12.5 mm, outer width = 12.5 mm, outer height = 45 mm, inner length = 10 mm, inner width = 10 mm, and a 3.5 mL volume capacity. All UV-Vis experiments were taken by scanning from 800 nm-190 nm and with an absorbance scale between 0-3.0. Each UV-Vis measurement involved first purging the sample headspace for 5 minutes and the sample solution for the duration of 10 minutes. Nitrogen gas was bubbled into the sample cuvette before and during the addition of any given reagent. Unless otherwise indicated, all UV-Vis data presented throughout this dissertation and in this chapter, were conducted at room temperature

Transmission FT-IR experiments presented in chapter 6 was performed using a Thermo Nicolet 670 FTIR using the OMNIC software interface. Each FT-IR was performed using a sealed liquid CaF_2 IR cell (Buck Scientific) with a 0.10 mm path length. All transmission IR data were collected in frequencies that ranged from 4000-400 cm^{-1}. Generally, between 64-256 scans were performed on each sample to give the best resolution. Each IR measurement was taken at least 3 separate times to verify that the data collected was reproducible and prior to each measurement the IR cell was thoroughly cleaned and purged with nitrogen. All IR samples were purged with nitrogen prior and during the addition of all solutions to the IR cell, and each IR sample was prepared by transferring a *ca.* 80 μL aliquot from a pre-made stock solution (of a known concentration) using an oven dried gas-tight syringe.

ethyl 3,5-diaminobenzoate (44)-To an oven dried 250 mL round bottom flask containing a magnetic stir bar, was added 3,5-diaminobenzoic acid (5.0 g, 33 mmol) and 125 mL of absolute ethanol and was allowed to stir vigorously at room temperature in an oil bath. To the solution of 3,5-diaminobenzoic acid and ethanol was slowly added in small portions (3-5 mL) of a total of 30 mL of concentrated sulfuric acid. Vigorous bubbling proceeded when sulfuric acid was added to the reaction mixture and the solution turned a homogenous deep purple color. The reaction mixture was slowly heated at which time a reflux condenser was added to the top of the round bottom flask. The mixture was refluxed for 72 hours. Accordingly, the mixture was concentrated down (10-20 mL) *in vacuo* so that little to no ethanol remained. The viscous purple liquid was decanted into a large 4 L Erlenmeyer flask equipped with a magnetic stir bar, 50 mL of ethyl acetate was used to wash the reaction mixture into the 4 L Erlenmeyer flask. The purple concentrate was allowed to stir vigorously, and 200 mL of water was added. The mixture was made basic using 50-100 mL of saturated NaOH or until the pH > 7. Once basic the mixture was poured into a separatory funnel and 100-150 mL of EtOAc was added. An additional 100 mL of water was added to a 1 L separatory funnel as well. The EtOAc organic layer was collected, and the aqueous layer was washed 3-4 times with 100-150 mL of EtOAc. The organic extracts were combined and dried (MgSO$_4$). The dried extracts were then filter and the EtOAc was evaporated *in vacuo* to yield a viscous black to dark purple oil (5.60 g, 94%) that solidified when stored at 4 °C. The oil was stored at *ca*. 4 °C to avoid rapid decomposition. The oil was not further purified since its NMR spectrum was identical with the spectrum of an authentic

sample.[126] ^{1}H NMR (400 MHz, d_6-DMSO) δ: 6.42, 2H, d (J = 2.0 Hz), 6.01, 1H, t (J = 2.0 Hz), 4.98, 4H, s, 4.21, 2H, q. (J = 7.0 Hz), 1.26, 3H, t (J = 7.0 Hz).

ethyl 3,5-bis(dimethylamino)benzoate (45)-An oven dried 250 mL round bottom flask was charge with a magnetic stir bar which was placed in a dry ice/acetonitrile bath (*ca.* -41 °C) and was allowed to stir vigorously. To this round bottom flask, 14 mL of 37% formalin was added and 23 mL of 3 M H_2SO_4 was slowly added. In a separate oven dried round bottom flask that was purged with nitrogen, 1.10 g (6.11 mmol) of ethyl 3, 5-diaminobenzoate (**44**), was added and 48 mL of freshly distilled anhydrous THF and was gently mixed to dissolve all of the ethyl 3,5-diaminobenzoate (red-orange solution). The ethyl 3,5-diaminobenzoate/THF solution was placed under nitrogen. To the solution of ethyl 3,5-diaminobenzoate/THF, 7.68 g (202 mmol) of $NaBH_4$ (≥98.5%, reagent grade) was added slowly. This suspension was gently mixed in an attempt to dissolve as much $NaBH_4$ into the solution as possible and was placed under N_2. The suspension containing ethyl 3,5-dimaminobenzoate was very slowly added *via* 1-5 mL portions, to the round bottom flask containing 37% formalin/3 M H_2SO_4 which was stirring in a dry ice/acetonitrile bath. Vigorous evolution of hydrogen gas was observed (especially during the first few additions) of the ethyl 3,5-diaminobenzoate/THF/$NaBH_4$ solution to the solution containing 37% formalin/3 M H_2SO_4. Small portions of ethyl 3,5-diaminobenzoate/THF/$NaBH_4$ solution was added over the course of 1 hour. The reaction mixture was allowed to stir at *ca.* -41 °C for 2-3 hours. After 2-3 hours, 95 mL of wet THF was added to the stirring reaction mixture at *ca.* -41 °C for an additional 30 minutes. At this time, the reaction mixture was made basic with sat. NaOH and was diluted with 100 mL of water. The reaction mixture was immediately transferred to a

separatory funnel either by gravimetric filtration or by decanting the reaction mixture to remove large quantities of unwanted sodium borate or boron based salts. Ether (100 mL) was added to the separatory funnel and the organic layer (brown-orange) was extracted 3 times with 100 mL of ether and was combined and dried with $MgSO_4$. The combined orange-brown organic extracts was filtered and evaporated *in vacuo* to yield a gummy orange to brown solid (1.05 g, 73%) that frequently became a highly viscous oil at room temperature. Impurities in the orange-brown solid ethyl 3,5-bis(dimethylamino)benzoate were removed by recrystalization using absolute EtOH. Recrystalization yielded ethyl 3,5-bis(dimethylamino)benzoate **45**, as a orange to brown gummy solid (0.853 g, 60%), which was stored at *ca*. 4 °C to avoid oxidative decomposition. ^{1}H NMR (400 MHz, CD_3CN) δ: 6.75, 2H, d (J = 4.0 Hz), 6.25, 1H, t (J = 4.0 Hz), 4.30, 2H, q. (J = 8.0 Hz), 1.33, 3H, t (J = 8.0 Hz); MS (HRMS) 237.1602 (M^+ + 1), (calc. M^+ + 1, 237.1603).

3,5-bis(dimethylamino)benzyl alcohol (46)-A nitrogen purged 100 mL round bottom flask was charged with a magnetic stir bar, ester **45** (0.850 g, 3.60 mmol), and 6 mL of freshly distilled anhydrous THF. The reaction mixture was placed under N_2 and was stirred in an ice bath (*ca*. 0 °C) vigorously until the solution became homogenous. In an oven dried vial that was dried with nitrogen, (0.342 g, 9.01 mmol) of lithium aluminum hydride (dispersion in mineral oil, 97%) was added to the vial, which was immediately placed in an ice bath under nitrogen. To the vial containing lithium aluminum hydride, 6 mL of freshly distilled anhydrous THF was slowly added and the solution was gently mixed, and kept in an ice bath. The lithium aluminum hydride/THF slurry was slowly added to the 100 mL round bottom flask containing the ester in small portions. The

reaction mixture was allowed to stir at 0 °C for 1 hour and then overnight at room temperature, under N_2. To the crude reaction mixture, 50 mL of wet THF was added and allowed to stir at room temperature for 30 minutes. Then, 5% H_2SO_4 in water was added slowly to quench any unreacted lithium aluminum hydride, and was done until bubbling ceased. The brown to black crude reaction mixture was made basic by the addition of sat. NaOH and was transferred to a 250 mL separatory funnel. The crude mixture was then made biphasic by the addition of 100 mL of ether. The organic layers were separated and extracted. The aqueous layer was washed 2-3 times with 100 mL portions of ether. The organic extracts were combined and dried with $MgSO_4$. The orange-brown organic extracts were filtered and the solvent was evaporated to yield a black to dark orange oil (0.492 g, 70%) at room temperature. The crude oil was initially stored at *ca*. 4 °C and was subsequently chromatographed under nitrogen using first 1 : 1 hexanes : EtOAc and finally 100% EtOAc as eluent. The first fractions yielded the remaining unreacted ester (R_f = 0.9) by TLC (1 : 1 hexanes : EtOAc) and the latter fractions yielded the desired alcohol (R_f = 0.3) in 1 : 1 hexanes : EtOAc. The fractions were concentrated *in vacuo* and yielded 3,5-bis(dimethylamino)benzyl alcohol (**46**) (0.320 g, 46%), as a dark brown-orange oil that solidified at *ca*. 4 °C. Again 3,5-bis(dimethylamino)benzyl alcohol was stored at *ca*. 4 °C. ^{1}H NMR (400 MHz, CD_3CN) δ: 6.14, 2H, d (*J* = 2.4 Hz), 5.99, 3H, t (*J* = 2.4 Hz), 4.41, 2H, s, 2.89, 12H, s; ^{13}C NMR (400 MHz, CD_3CN) δ: 153.1, 144.2, 101.9, 97.6, 65.9, 41.1; MS (HRMS) 195.1492 (M^+ + 1), (calc. M^+ + 1, 195.1497).

3,5-bis(dimethylamino)benzyl acetate ester (47)-To an oven dried vial that was flushed with nitrogen, was added a magnetic stir bar and (0.200 g, 1.03 mmol) of 3,5-

bis(dimethylamino)benzyl alcohol **46.**   To alcohol **46**, 2.7 mL of anhydrous

dichloromethane and (0.16 mL, 1.1 mmol) of triethylamine was added. The reaction

mixture was stirred vigorously under nitrogen at room temperature. In a separate oven

dried vial or flask that was dried with nitrogen, (0.11 mL, 1.5 mmol) of acetyl chloride,

P.A. (Acros) was added and 2.7 mL of freshly distilled CH_2Cl_2 and was placed under

nitrogen also at room temperature. The solution containing acetyl chloride and CH_2Cl_2

was added to the solution containing alcohol **46**, in small portions. The reaction mixture

was allowed to stir at room temperature for 1 hour. During the 30 minutes-1 hour of

stirring, the reaction mixture turned from brown-orange to dark red.   The

progress/conversion of the reaction was determined by GC or TLC. After 1 hour the GC

of the reaction mixture indicated little to no alcohol (R_T = 8.7 min.) was present and a

new peak was observed at R_T = 9.0 min. which was presumed to be the desired benzyl

acetate product.   The reaction mixture was concentrated down and the solvent was

removed *in vacuo* to yield a red viscous oil (0.220 g, 91%), which was pure by ^{1}H NMR

and contained the correct mass.   3,5-bis(dimethylamino)benzyl acetate, **47** was stored at

ca. 4 $^\circ$C to prevent oxidative decomposition. ^{1}H NMR (400 MHz, CD_3CN) δ: 6.13, 2H,

d (*J* = 2.4 Hz), 6.02, 1H, t (*J* = 2.4 Hz), 4.95, 2H, 2.89, 12H, s, 2.04, 3H, s; ^{13}C NMR

(400 MHz, CD_3CN) δ: 171.7, 153.1, 138.6, 102.9, 98.1, 68.0, 41.0, 21.3; MS (ESI+)

237.1600 (M^+ + 1), (calc. M^+ + 1, 237.1603).

3,5-bis(dimethylamino)benzyl phenyl acetate ester (48)-0.106 g (0.546 mmol) of 3,5-

bis(dimethylamino)benzyl alcohol, **46** was added to an oven dried vial containing a

magnetic sitr bar under N_2. To the vial containing **46**, which was placed under N_2, 3 mL

of anhydrous CH_2Cl_2 was added and the mixture was allowed to stir at room

temperature. After 2 minutes, 91.0 μL (0.652 mmol) of triethylamine and (87.0 μL, 0.658 mmol) of phenyl acetyl chloride was added. The reaction mixture was allowed to stir vigorously at room temperature under nitrogen for 12 hours. After 1 hour the reaction mixture turned dark brown to red. The reaction mixture was worked up by first adding 4-5 mL of CH_2Cl_2 and 5 mL of water. The organic layer was extracted and the remaining aqueous layer was washed and extracted 2-3 times with 5 mL portions of CH_2Cl_2. The organic extracts were combined and dried using 4 Angstrom molecular sieves. The solvent was then evaporated to yield a pure red-brown oil (0.167 g, 97%) that was pure by ^1H NMR and GC (R_T = 11.0 min.). 3,5-bis(dimethylamino)benzyl phenyl acetate, **48** was stored at *ca*. 4 $°C$ to prevent oxidative decomposition. ^1H NMR (400 MHz, CD_3CN) δ: 7.35-7.25, 5H, m, 6.06, 2H, d (*J* = 4.0 Hz), 5.99, 1H, t (*J* = 4.0 Hz), 4.99, 2H, s, 3.68, 2H, s, 2.86, 12H, s; ^{13}C NMR (400 MHz, CD_3CN) δ: 172.4, 153.0, 138.5, 135.8, 130.2, 129.5, 128.0, 102.6, 98.1, 68.2, 55.4, 41.0; MS (ESI+), 313.2152 (M^+ + 1), (calc. M^+ + 1, 313.1838).

3,5-bis(dimethylamino)benzyl methoxy ether (49)-An oven dried vial was charged with (0.120 g, 0.619 mmol) of benzyl alcohol, **46**. Then, 4 mL of abs. MeOH was added to the vial containing **46**, to yield a 155 mM solution. An aliquot of 0.1 mL was taken from the original solution and diluted with 3 mL of abs. MeOH for GC analysis. The remaining solution containing **46** and abs. MeOH was photolyzed in a Rayonet reactor for 19.5 hours using a 4-sided quartz polished cuvette. Aliquots were taken for GC analysis during the course of the photolysis reaction. These aliquots were done for 17.5 hours and 19.5 hours of photolysis time to track reaction progress. Only ~60% of alcohol **46** was converted by GC after 17.5 hours, thus the mixture was irradiated at 254

185

nm for a longer period of time until additional conversion of **46**, to the desired benzyl methoxy ether (R_T = 8.5 minutes), **49** could be achieved. The crude photolysis mixture was then transferred to a vial and the solvent was evaporated to yield a red oily residue that indicated the presence of the benzyl methoxy ether by GC (R_T = 8.5 min.) as the major product in the mixture. TLC of the crude mixture in 5 : 1 hexnaes : EtOAc revealed 3 major UV active spots R_f = 0.53 and 0.29 and a residual baseline spot. Thus, the crude mixture was purified by prep TLC (5 : 1 hexnaes : EtOAc) and yielded 3 distinct bands, with R_f's of 0.5, 0.2 and a baseline band. All bands were UV active and stained light red to pink over time on the TLC plate. Each band was separated into 3 individual 125 mL Erlenmeyer flasks and each were dissolved with 50-100 mL of EtOAc and were allowed to stir vigorously at room temperature overnight. To each flask was also added 1-2 mL of triethylamine to neutralize the silica gel in each of the mixtures. The silica gel was removed by filtration for each flask and the filtrates were washed with copious amounts of EtOAc. The EtOAc was then evaporated from each band and each of the bands was analyzed by GC. It was determined from the GC analysis that the middle band contained the purest and largest amount of the methoxy ether, **49**. The crude middle band was a pink to off-white solid (~50 mg) that still contained a few impurities by GC and NMR. Thus, the crude pink solid was recrystalized in abs. MeOH to yield benzyl methoxy ether **49**, as a light red to pink oil (0.038 g, 29%) which was pure by GC and NMR. Compound **49** was stored at *ca.* 4 °C.

^{1}H NMR (400 MHz, d_6-acetone) δ: 6.11, 2H, d (J = 2.0 Hz), 5.99, 1H, t (J = 2.0 Hz), 4.29, 2H, s, 3.74 (d_6-acetone impurity), 3.27, 3H, s, 2.83, 12H, s; ^{13}C NMR (400 MHz,

d_6-acetone) δ: 153.2, 130.0, 98.2, 76.6, 69.9, 58.3, 41.4; MS (ESI+), 209.1389 (M^++1), (calc. $M^+ + 1$, 209.1576).

3,5-bis(dimethylamino)-((2,2,2-trifluoroethoxy)methyl)benzene (50)-Benzyl alcohol **46** (0.100 g, 0.515 mmol) was added to an oven dried vial and was dissolved in 5 mL of TFE, resulting in a concentrated 103 mM solution of **46** in TFE. From this solution a 0.1 mL aliquot was removed and diluted with 2.1 mL of TFE and was analyzed by GC to determine the retention time of the starting alcohol, **46**. Then, 4 mL of the solution was transferred to an oven dried 4-sided quartz cuvette and was purged with nitrogen for the duration of 15 minutes (5 minutes for the solution headspace and 10 minutes for the actual solution). The cuvette was then placed in a Rayonet reactor and was irradiated at 254 nm for 20 hours. The remaining amount of the original solution containing **46** in TFE, was stored for future use at *ca*. 4 °C. During the 20 hours of photolysis the solution turned from orange to dark red. The reaction progress was monitored by GC. This was done by initially taking aliquots of 0.1 mL from the photolysis mixture and diluting it with 2.1 mL of TFE. GC analysis of the photolysis mixture after 6 hours of irradiation at 254 nm showed only ~40 % of **46** was converted to the major product, the benzyl TFE ether adduct (R_T = 8.2 min.). Thus, the photolysis mixture in question was photolyzed for 20 hours at which time <5% of the starting alcohol **46** remained (by GC) in the crude mixture. The crude mixture was then transferred from the cuvette to a vial in which the solvent was evaporated *in vacuo* to yield a dark red oily residue. TLC of the crude mixture (5 : 1 hexanes : EtOAc) showed the presence of 3 UV active spots: R_f = 0.71, R_f = 0.51, and R_f = 0.21. Therefore, the crude benzyl TFE ether was flash chromotographed under nitrogen. The silica gel was pre-treated with 1% triethylamine

and the column was eluted with 100% hexanes followed by 5 : 1 and 1 : 1 hexanes : EtOAc. It was determined by GC and NMR, that the first fractions using 5 : 1 hexanes : EtOAc (R_f = 0.49-0.51) as eluant, yielded a moderately pure benzyl TFE ether, **50**. Thus, these fractions were combined and the solvent was evaporated to yield **50** as a red to pink oil (0.045 g, 32%) that was stored at *ca*. 4 °C. ^{1}H NMR (400 MHz, d_6-acetone) δ: 6.15, 2H, d (J = 2.0 Hz), 6.04, 1H, s, 4.57, 2H, s, 3.94, 2H, q. (J = 9.2 Hz), 2.88, 12H, s; ^{13}C NMR (400 MHz, d_6-acetone) δ: 153.3, 139.2, 127.8, 103.1, 98.4, 76.0, 67.5 (q., J = 130 Hz), 40.3; MS (HRMS), 277.1519 (M^+ + 1), (calc. M^+ + 1, 277.1449).

3,5-bis(dimethylamino)toluene (52)-The following procedure was adapted from He, Y., *et al.*[77] To an oven dried vial (0.063 g, 0.27 mmol) of 3,5-bis(dimethylamino)benzyl acetate **47** was added with a magnetic stir bar under N_2. Then, 2.7 mL of abs. MeOH was added and the reaction mixture was allowed to stir at room temperature. To the reaction mixture containing **47**, (0.243 g, 1.87 mmol) of anhydrous $NiCl_2$, 98% (Aldrich Chemical Co.) was added and was allowed to stir under nitrogen for 2-3 minutes. During the course of 10 minutes, (0.141 g, 3.74 mmol) of $NaBH_4$ was added to the reaction mixture in small portions. (Note, that the addition of $NaBH_4$ to the reaction mixture was generally exothermic, and was therefore typically done in small portions, particularly on a larger scale). The reaction mixture was allowed to stir under nitrogen for 2 hours at room temperature during which time the solution turned from red to black. After 2 hours the reaction mixture was concentrated down *via* rotary evaporator. The black residue was then diluted with 5 mL of water and 10 mL of ethyl acetate. The ethyl acetate layer was removed and the aqueous layer was extracted 3 times with 5-10 mL portions of EtOAc. The organic extracts were combined and dried with 4 Angstrom

molecular sieves and the solvent was evaporated to yield a pure red to pink oil (0.038 g, 79%), 3,5-bis(dimethylamino)toluene that was generally pure by GC, ESI or NMR. However, if the oil did in fact contain some unreacted acetate **47**, the crude red oil was chromatographed using 10 : 1 and 5 : 1 hexanes : EtOAc under nitrogen. The first few fractions generally yielded the desired 3,5-bis(dimethylamino)toluene. The fractions were concentrated down *in vacuo* to yield a pure red oil by GC/NMR and was stored at *ca*. 4 $^{\circ}$C. ^{1}H NMR (400 MHz, CD_3OD) δ: 6.09, 2H, s, 6.03, 1H, s, 2.87, 12H, s, 2.23, 3H, s; ^{13}C NMR (400 MHz, CD_3CN) δ: 153.2, 146.0, 104.6, 96.6, 41.3, 22.6; MS (ESI+), 179.1994 (M^++ 1), (calc. M^+ + 1, 179.1470).

3,5-dimethoxy benzoyl chloride (63)-The procedure to synthesize **63** was adapted from a previously reported synthesis of this benzoyl chloride by Ziessel *et al*.[127] To a stirring suspension of 3,5-dimethoxy benzoic acid (2.00 g, 11.0 mmol) (Acros Organic, 99%) in thionyl chloride (15 mL) was refluxed for 1 hour. Over the course of 1 hour, the reaction mixture turned from white to dark yellow to finally dark green. After 1 hour, the reaction was removed from heating and the excess thionyl chloride was removed by rotary evaporator to yield a dark green/grey oily solid. The crude solid was then dried under house vacuum overnight and then stored in a 4 °C freezer until further use (this is due to the fact that at room temperature the dark green/grey solid slowly begins to melt at room temperature). The crude solid (2.01 g, 91 %) was found to by pure by ^{1}H NMR and roughly matched the spectra data previously reported by Ziessel *et al*[127] Therefore, the 3,5-dimethoxy benzoyl chloride, **63** was used without further purification. ^{1}H NMR (400 MHz, $CDCl_3$), δ: 7.24, 2H, d (*J* = 2.4 Hz), 6.72, 1H, t (*J* = 2.4 Hz), 3.80, 6H, s.

2-(3,5-dimethoxyphenyl)-1,1,1,3,3,3-hexafluoro-2-propanol (64)-The synthesis of **64** was adapted from a procedure by Naumann, *et al.* to synthesize various bis(trifluoromethyl)carbinols from activated carboxylic acid derivatives or aldehydes.[82] A 3-neck 100 mL round bottom flask was charged with a stir bar, 1.00 g (4.99 mmol) of 3,5-dimethoxybenzoyl chloride, **63**, 12 mL of anhydrous 1,2-dimethoxyethane (DME), and ~3.0 equiv. (14.9 mmol, 1.39 g) $(CH_3)_4NF$ under nitrogen. The resulting light yellow solution was placed in a dry ice/acetonitrile bath (*ca*. -41 °C) and ~3.0 equiv. (2.2 mL, 15 mmol) TMS-CF_3 anhydrous was added rapidly under nitrogen. The reaction was kept at *ca*. -41 °C for 48 hours. After 48 hours, the crude reaction mixture was allowed to warm to room temperature and the DME was then removed by rotary evaporator. The yellow-brown residue was transferred to a 125 mL separatory funnel and 25 mL of 2 M HCl and 20 mL of Et_2O was used to separate the initial crude mixture. The contents in the separatory funnel were then extracted and the remaining aqueous layer was washed 2 more times and extracted with 20 mL portions of Et_2O. The combined organic extracts were dried with $MgSO_4$ and were vacuum filtered into a clean 100 mL round bottom flask. The solvent was then evaporated by rotary evaporator to yield a light brown solid, (1.13 g, 75%) **64**. ^1H NMR (400 MHz, CD_3CN) δ: 7.13, 1H, s (OH, exchanges), 6.82, 2H, s, 6.64, 1H, t (*J* = 4.0 Hz), 3.80, 6H, s; ^{13}C NMR (400 MHz, CD_3CN) δ: 162.4, 133.8, 108.5, 106.6, 106.5 (m), 102.8, 56.65; MS (DART+), 305.06 (intensity, 22079, $M^+ + 1$), (calc. $M^+ + 1$, 305.05).

2-(3,5-dimethoxyphenyl)-1,1,1,3,3,3-hexafluoro-2-propanyl acetate (65)-To an oven dried vial, which was dried under N_2, a magnetic stir bar and 0.500 g (1.64 mmol) of carbinol **64** was added. Consequently, 3.0 mL of freshly distilled (over CaH_2) CH_2Cl_2

was added to the vial containing carbinol **64** under N_2 using an oven dried gas-tight syringe. To the dark yellow-brown stiring solution of **64** in CH_2Cl_2 was added 1.2 equilvance (0.280 mL, 2.01 mmol) of triethylamine (Fischer Scientific, Reagent Grade) followed by 1.5 equivlance (0.175 mL, 2.46 mmol) of acetyl chloride (Acros Organic, ACS reagent) under N_2 at room temperature. Immediately after the addition of acetyl chloride, the reaction mixture turned from dark yellow-brown to dark red-brown. The reaction mixture was allowed to stir at room temperature and was monitored by GC. After roughly 96 hours of reaction time, the reaction was determined to be complete by GC (i.e. little to no peak due to alcohol **64** was observed in the GC trace thereby indicated nearly complete conversion of **64** to acetate **65**). As a result, the reaction mixture was removed from stiring and was diluted with 10-15 mL CH_2Cl_2 and 10-15 mL of water. The aqueous layer was removed. The organic layer was washed once more with 10-15 mL of water and the aqueous layer was again removed. The combined organic extracts were dried using oven dried 3 Angstrom molecular sieves. The solvent was then evaporated by rotary evaporator to yield acetate **65** (500.8 mg, 88%) as a dark red to orange viscous oil, which was shown to be pure by GC and ^1H NMR. ^1H NMR (400 MHz, $CDCl_3$) δ: 6.65, 1H, t (J = 4.0 Hz), 6.56, 2H, s, 3.81, 6H, s, 2.30, 3H, s; ^{13}C NMR (400 MHz, $CDCl_3$) δ: 166.1, 160.9, 129.4, 105.8, 101.5, 55.62, 30.28, 21.22; MS (DART+), 347.07 (intensity, 42726, M^+ + 1), (calc. M^+ + 1, 347.06).

3,5-dinitrobenzaldehyde (88)-A 250 mL round bottom flask that was dried under N_2 was charged with a magnetic stir bar, 2.00 g (10.1 mmol) of 3,5-dinitrobenzyl alcohol, **87** (98%, Aldrich, Co.), and 25 mL of freshly distilled (over CaH_2) CH_2Cl_2 was added. The mixture was allowed to stir at room temperature under nitrogen until most of the

alcohol was dissolved. Subsequently, 3.41 g (15.8 mmol) of pyridinium chlorochromate (PCC) (Aldrich, Co.) was added rapidly to the flask and an additional 25 mL of freshly distilled CH_2Cl_2 was also transferred to the reaction mixture. The flask was placed under nitrogen and was allowed to stir vigorously at room temperature overnight (*ca*. 12 hours). After the reaction mixture was allowed to stir overnight, the flask was observed to contain a large amount of brown to black precipitate on the sides of the flask. At this time a TLC (1 : 1 EtOAc : hexanes) was taken of the crude mixture. The TLC usually indicated nearly full conversion to a new spot (R_f = 0.95) which was presumed to correspond to the formation of the aldehyde. The reaction mixture was then removed from stirring and its contents were vacuum filtered over 1-2 inches of silica gel (pre-eluted with ~5-10 mL of anhydrous diethyl ether) with 100 mL of diethyl ether into a clean oven dried 250 mL round bottom flask. The tan brown crude mixture was rotary evaporated and dried under house vacuum to yield a powder like light brown solid (1.05 g, 53 %). The purity of the crude aldehyde was assessed by ^{1}H NMR and was compared to the literature or commercial available spectrum. If the crude 3,5-dinitrobenzaldehyde contained some amounts of impurities, then a recrystallization was performed using 100 % abs. EtOH, which usually yielded pure 3,5-dinitrobenzyaldehyde. ^{1}H NMR (400 MHz, $CDCl_3$) δ: 10.23, 1H, s, 9.31, 1H, t (*J* = 4.0 Hz), 9.06, 2H, d (*J* = 4.0 Hz); ^{13}C NMR (400 MHz, $CDCl_3$) δ: 187.4, 149.4, 138.7, 128.9, 123.5; GC-MS (EI) R_T = 8.06 min. 196.8 (M^+, 100 %), (calc. M^+, 196.0).

2-(3,5-dinitrophenyl)-1,3-dithiane (89)-A 100 mL round bottom flask with a magnetic stir bar, 4.00 g (20.4 mmol) 3,5-dinitrobenzaldehyde **88**, 0.320 g (1.684 mmol) of *p*-toluenesulfonic acid monohydrate (99%, Sigma-Aldrich), and 50 mL of toluene, was

allowed to stir at room temperature under N_2. To the stirring solution of aldehyde, 2.0 mL (20 mmol) of 1,3-propanedithiol (99%, Aldrich, Co.) was slowly added. After a few minutes the mixture turned from brown to dark green. The reaction mixture was placed in an oil bath and the nitrogen was removed and was replaced with a Dean-Stark trap and reflux condenser. The mixture was refluxed overnight in the oil bath to *ca*. 120 °C. The reaction completion was determined the following day by the accumulation of 2 layers in the Dean-Stark trap. At this time, the reaction mixture was removed from heating and all of the water in the Dean-Stark trap was removed. The crude reaction mixture was quenched with 2 portions of sat. $NaHCO_3$ and transferred to a 500 mL separatory funnel. The organic layer was extracted twice with 25 mL of diethyl ether. The combined organic extracts were washed with 2 portions of 25 mL of brine and were extracted twice with 50 mL of ethyl acetate. The combined organic extracts were dried with anhydrous $MgSO_4$ and were vacuum filtered into a 500 mL round bottom flask. The solvent was evaporated by rotary evaporator and was dried under house vacuum to yield a dark yellow chunky crude solid. The crude yellow solid was recrystalized using 50 : 50 abs. EtOH : water to yield **89** as a light yellow powder (3.65 g, 98%) which was pure by ^1H NMR and ESI/MS. ^1H NMR (400 MHz, CD_3CN) δ: 8.84, 1H, t (J = 4.0 Hz), 8.62, 2H, d (J = 4.0 Hz), 5.53, 1H, s, 3.10, 2H, ddd (J = 4.0 Hz, 12.0 Hz, 24 Hz), 2.96, 2H, dt, (J = 4.0 Hz, 8.0 Hz), 2.15, 1H, m, 1.85, 1H, m; ^{13}C NMR (400 MHz, CD_3CN) δ: 149.8, 144.8, 119.5, 118.3, 49.06, 31.80, 25.45; GC-MS (EI) R_T = 11.7 min. 286.9 (M^+, 94%), (calc. M^+, 286.0),

3,5-dinitrobenzyl methoxy ether (101)-0.501 g (2.53 mmol) of 3,5-dinitrobenzyl alcohol was added to an oven dried 100 mL round bottom flask with an almond sized

stir bar under N_2. Then, 5.0 mL of THF (anhydrous, no inhibitor) was added using a gas-tight syringe. The mixture of the alcohol and THF was allowed to stir and was then placed in an ice bath at which time 1.5 mL (1.50 equiv., 3.75 mmol) of 2.5 M n-BuLi/hexanes was slowly added over the course of a few minutes. The solution containing the 3,5-dinitrobenzyl alcohol/THF immediately turned from light orange to a deep burgundy color once the n-BuLi was completely added. The reaction mixture was kept at $ca.$ 0 °C for 1 hour, at which time 0.500 mL (3.20 equiv., 8.03 mmol) of CH_3I was added under nitrogen. The nitrogen line was then removed from the reaction mixture and the resulting mixture was then allowed to warm to room temperature. The reaction was monitored by TLC (5 : 1 hexanes : EtOAc) or by ^{1}H NMR. After the 50 hours of reaction time, it was determined by TLC, that reaction contained a mixture of 2 major products which were UV active by TLC, the alcohol (3,5-dinitrobenzyl alcohol) R_f = ~0.12 and the benzyl methoxy ether R_f = ~0.34. The NMR of the crude reaction mixture also indicated the presence of both the starting alcohol and the 3,5-dinitrobenzyl methoxy ether desired adduct. The aliquot removed for TLC/NMR analysis after 50 hours of reaction time was then dumped back into the reaction mixture under N_2. Based on the TLC results of the crude reaction mixture, 560 mg (2.00 equiv., 5.00 mmol) of potassium $tert$-butoxide as well as an additional 3.00 mL of anhydrous THF was added in one portion to the reaction mixture under N_2. The resulting mixture was allowed to stir at room temperature for 2 hours. After 2 hours, an additional 0.5000 mL (3.20 equiv., 8.03 mmol) of CH_3I was then added at room temperature under N_2. The reaction was determined by TLC and NMR to be complete after an additional 12 hours of stirring at room temperature. The solvent was then removed by rotary evaporator to yield 3,5-

dinitrobenzyl methoxy ether, **101** (0.525 g, 98%) as a dark brown-black chunky solid. In some cases, the crude reaction mixture still contained the benzyl methoxy ether, **101** and small amount of the 3,5-dinitrobenzyl alcohol. Therefore, the crude mixture was then purified by flash column chromatography and was eluted with initially 100 % hexanes, followed by 10 : 1 hexanes : EtOAc, and finally 5 : 1 hexanes : EtOAc. Most of ether **101** eluted smoothly after collecting several fractions from elution of 10 : 1 and 5 : 1 hexanes : EtOAc through the column. GC (in acetone) R_T = 10.5 min. (Shimadzu GC-17A, DB-5 column); ^{1}H NMR (400 MHz, CD$_3$CN) δ: 8.82, 1H, t (J = 2.4 Hz), 8.52, 2H, d (J = 2.0 Hz), 4.65, 2H, s, 3.45, 3H, s; ^{13}C NMR (400 MHz, d_6-acetone) δ: 145.2, 128.2, 118.6, 117.7, 73.0, 59.2; GC-MS, (EI) R_T = 11.2 min., 213.1 (M$^+$), 211.1 (M$^+$ - 1), 182.0 (M$^+$ - 31), (calc. M$^+$, 212.0).

_p_-nitrobenzyl methoxy ether (102), Method B-An oven dried 50 mL round bottom flask was charged with a small magnetic stir bar, 0.499 g (2.31 mmol) of _p_-nitrobenzyl bromide (Aldrich, 99 %), and 8.0 mL of abs. MeOH under N$_2$. The resulting solution was stirred at room temperature under N$_2$. To the mixture containing _p_-nitrobenzyl bromide/MeOH, was added 0.500 g (~4.00 equiv., 9.26 mmol) of NaOCH$_3$ (Fischer Scientific) in one portion. The reaction mixture was sealed with a septum and was placed in an oil bath and stirred and heated to _ca_. 50 °C for 24 hours. A ~200 μL aliquot was taken from the reaction mixture to monitor reaction progress after 24 hours. The solvent was removed from this aliquot to yield a crude milky white residue, which was dissolve in a small amount of EtOAc. TLC (10 : 1 hexanes : EtOAc) of the crude reaction mixture showed the presence of 2 UV active spots one with a R_f = ~0.43 and a baseline spot with a R_f = ~0. For comparison purposes a TLC in 10 : 1 hexanes : EtOAc

was obtained of the *p*-nitrobenzyl bromide (R_f = ~0.51) and *p*-nitrobenzyl alcohol (R_f = ~0, spot did not move from the baseline). From the TLC of the crude mixture, it was determined that reaction mixture did not contain a substantial amount of *p*-nitrobenzyl bromide, and that the mixture likely contained only *p*-nitrobenzyl alcohol and presumably the desired *p*-nitrobenzyl methoxy ether product (R_f = ~0.43). As a result, the remainder of the crude reaction mixture was removed from heated and the solvent was evaporated by rotary evaporator to yield a milky white residue. The crude residue was dissolved in 25 mL of 10 : 1 hexanes : EtOAc and 20 mL of water, and the biphasic mixture was then transferred to a 125 mL separatory funnel. The contents in the separatory funnel were extracted and the aqueous layer was washed with 2 x 25 mL portions of 10 : 1 hexanes : EtOAc. The combined organic layers were then dried with $MgSO_4$ and then filter into a clean 100 mL round bottom flask. The solvent was evaporated by rotary evaporator and then left overnight under the house vacuum to yield *p*-nitrobenzyl methoxy ether, **102** (270.7 mg, 70%) as a yellow-white viscous oil, which was pure by ^{1}H NMR/GC. GC (in CD_3CN) R_T = 9.2 min. (Shimadzu GC-17A, DB-5 column); ^{1}H NMR (400 MHz, CD_3CN) δ 8.19, 2H, d (J = 8.8 Hz), 7.54, 2H, d (J = 8.8 Hz), 4.55, 2H, s, 3.39, 3H, s; ^{13}C NMR (400 MHz, $CDCl_3$) δ: 146.1, 130.8, 127.8, 123.7, 73.46, 58.77; MS (DART-), 167.34 (M^+), 166.33 (M^+- 1), 333.58 (M^+ dimer), (calc. M^+- 1, 167.06).
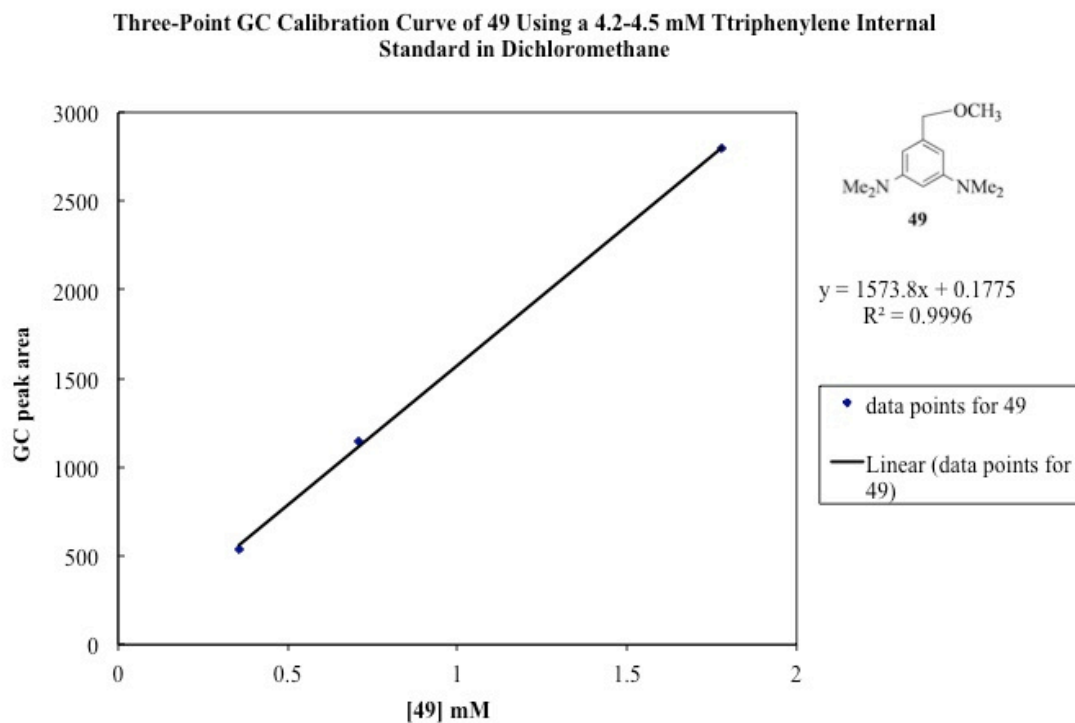
Figure 7.1. Three-point GC calibration curve for 3,5-bis(dimethylamino)benzyl methoxy ether, **49**.
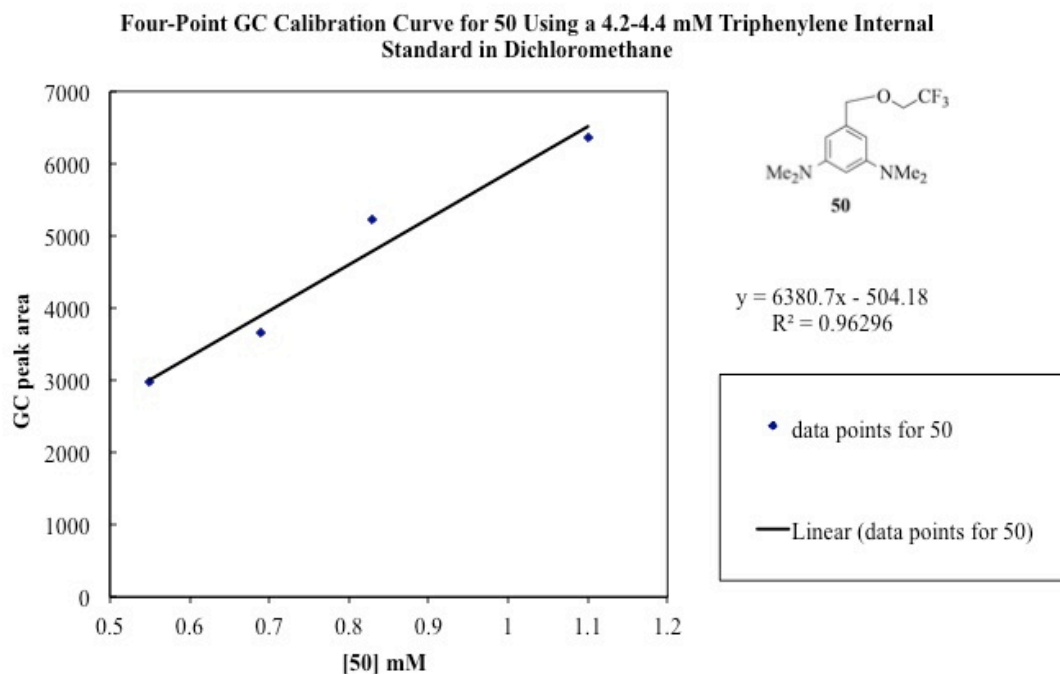
Figure 7.2. Four-point GC calibration curve for 3,5-bis(dimethylamino)-((2,2,2-trifluoroethoxy)methyl)benzene, **50**.
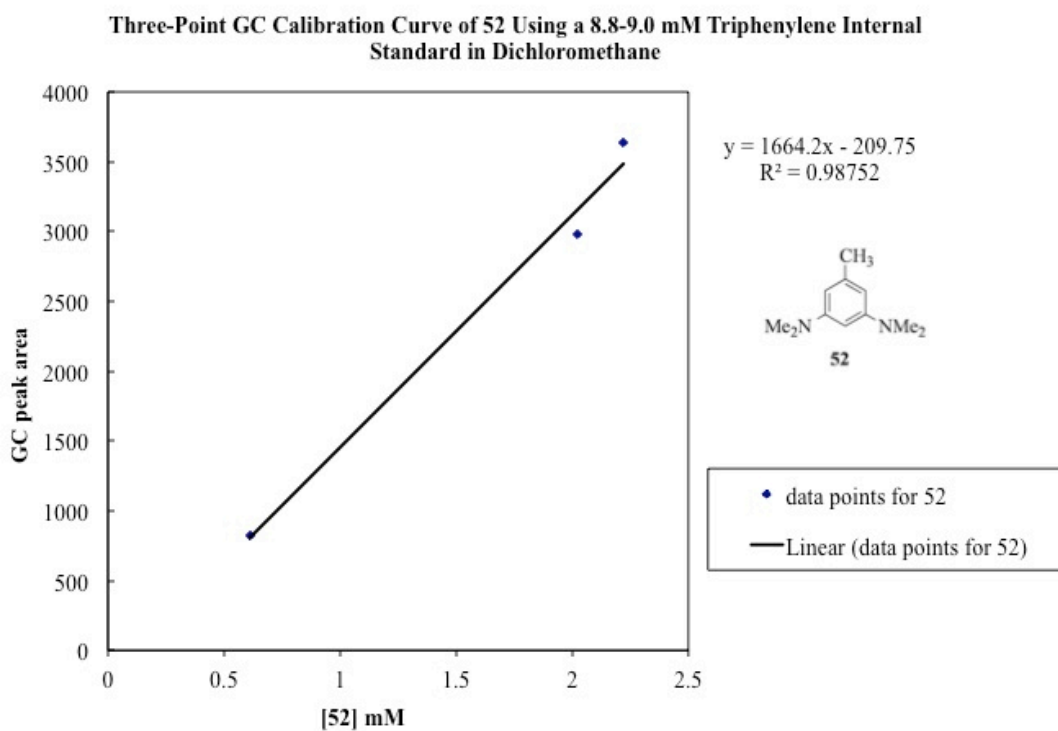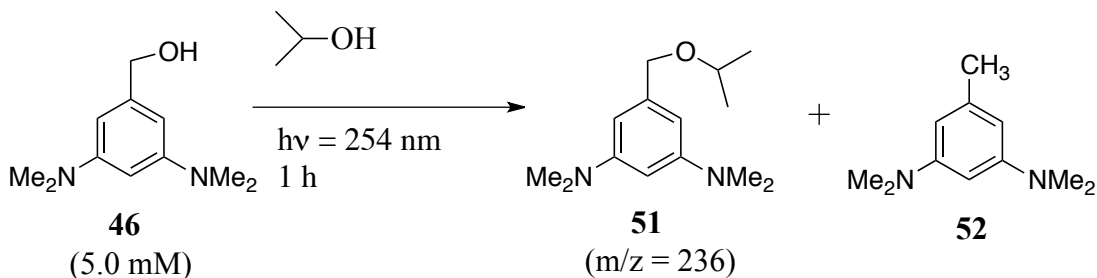

Figure 7.3. Three-point GC calibration curve for 3,5-bis(dimethylamino)toluene, **52**.

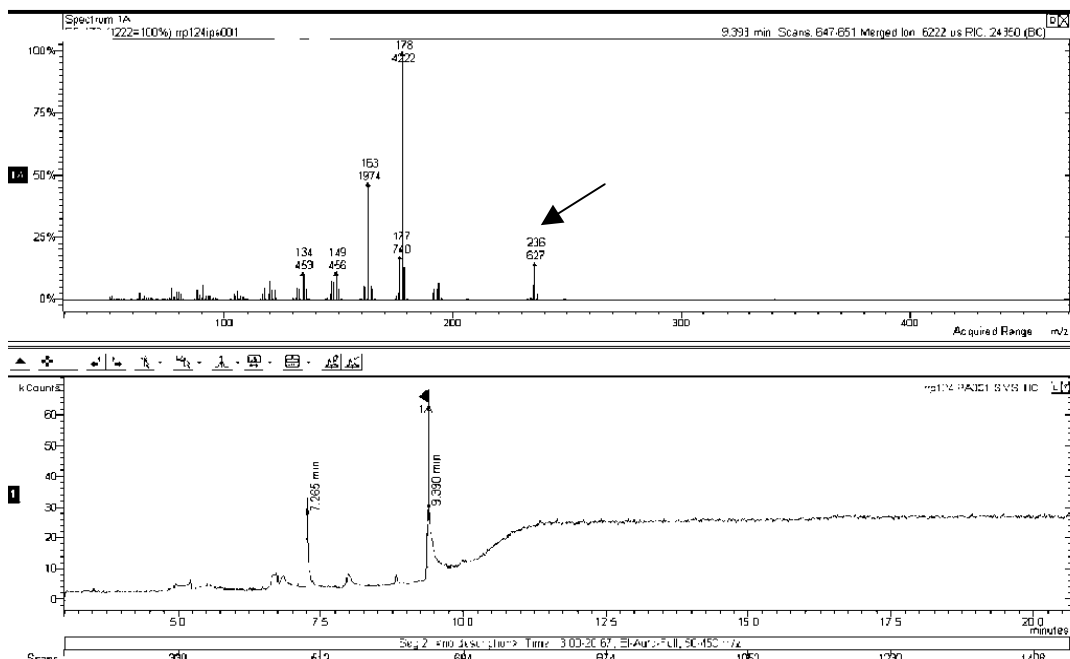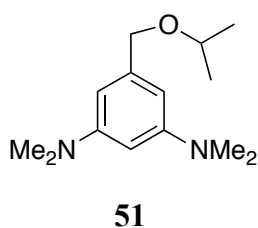**Scheme 7.1.** Photolysis of benzyl alcohol **46** in 2-propanol

Photolysis mixture with

51

Figure 7.4. Identification of benzyl ether photoproduct **51** by GC-MS. GC-MS trace for the photolysis of **46** (5.0 mM) at 254 nm in 2-propanol. A ~200 μL aliquot was taken from the photolysis mixture after 1 hour of irradiation at 254 nm. The peak with a retention time of 9.4 minutes was assigned to be that of benzyl ether **51**. The correct mass/charge (m/z) for the benzyl ether **51** of about 236 is also indicated in the above GC-MS trace.

Sample Photolysis Experiment

All photolysis experiments were carried out using a 3.5 mL four sided quartz cuvette. The photolysis experiments were performed in a Raynoet reactor with a merry-go-round array of 8 RMR-2537 Angstrom UV bulbs (35 W).

Photolysis of **46** in TFE: A solution of **46** and TFE was made by adding (11.0 mg, 0.0567 mmol) of alcohol **46**, to a vial and dissolving **46** with 11.0 mL of 2,2,2-trifluoroethanol (TFE), 99.8 %, reagent grade (Acros) to yield a yellow homogenous solution (5.20 mM). An aliquot was taken of this solution for GC analysis. Approximately 3.00 mL of the solution containing **46** and TFE, was transferred to an oven dried 4-sided quartz cuvette. The cuvette was purged with nitrogen for the duration of 15 minutes (5 minutes for the headspace and 10 minutes for the solution). The solution was then photolyzed in a Rayonet reactor as mentioned above. Aliquots of 100-200 μL were taken from the photolysis mixture for GC/GC-MS analysis after 30 minutes, 1 hour, and 1.5 hours of irradiation. From the GC analysis it was concluded that 1 hour of photolysis was necessary in this case to detect an appreciable amount of benzyl TFE ether adduct **50** (R_T = 8.2 minutes) and tolyl adduct **52** (R_T = 7.7 minutes). The photolysis aliquot for 1 hour of irradiation of **46** in TFE was co-injected with a solution containing the benzyl TFE ether authentic sample (**50**) in dichloromethane to verify the presence of the benzyl TFE ether adduct by GC. The GC co-injection with standard **50** of the photolysis mixture did show an increase in GC response for the peak observed at R_T = 8.2 minutes, thus demonstrating that in fact the TFE ether adduct **50** (see Table 2.1 in Chapter 2) is being generated from the photolysis of **46** in TFE.

Similar experiments were conducted in this fashion for benzyl cation substrates **46-48** in their respective alcoholic solvents.

Typical ^{1}H NMR Analysis/Photolysis Experiment

An oven dried vial was charged with 9.5 mg (0.030 mmol) of 3,5-bis(dimethylamino)benzyl phenyl acetate ester **48**. To the vial containing **48**, 5.0 mL of a ready made 3.0 mM MTBE/CD$_3$OD solution (this was done by adding 3.5 mL to 10 mL CD$_3$OD) was added and the contents were lightly mixed to yield a 6.1 mM solution containing **48**, in 3.0 mM MTBE/CD$_3$OD.   Roughly 0.80-1.0 mL of the solution was taken for ^{1}H NMR analysis and a 3.0 mL aliquot was then transferred to an oven dried, 4-sided quartz cuvette. The solution in the cuvette was purged with nitrogen for the duration of 15 minutes (5 minutes for the solution headspace and 10 minutes for the solution). The mixture containing **48**, and 3.0 mM MTBE/CD$_3$OD was irradiated in a Rayonet reactor at 254 nm. Aliquots of 0.80-1.0 mL were taken at after 1, 2, 3 and 4 hours of irradiation (via syringe), and were all transferred to separate oven dried NMR tubes for analysis. All NMR measurements were taken with either 32 or 64 scans of signal/noise, and were performed using a Bruker 400 MHz NMR. All samples shown in this work were calibrated to CD$_3$OD as a reference and all peak integration were calibrated towards the internal standard we used (MTBE).
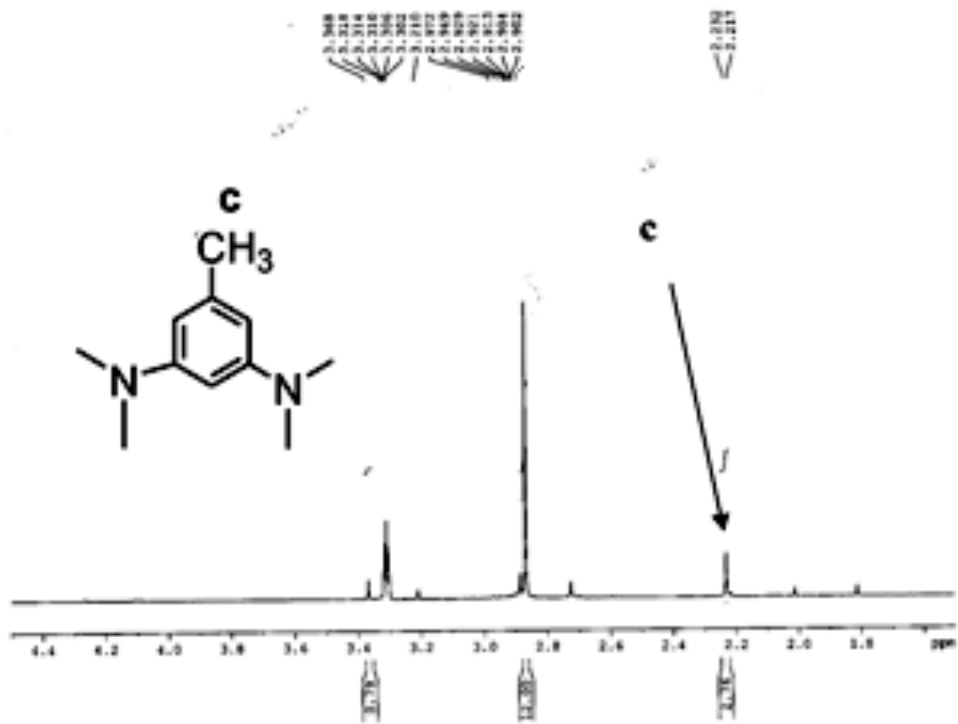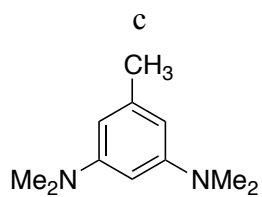
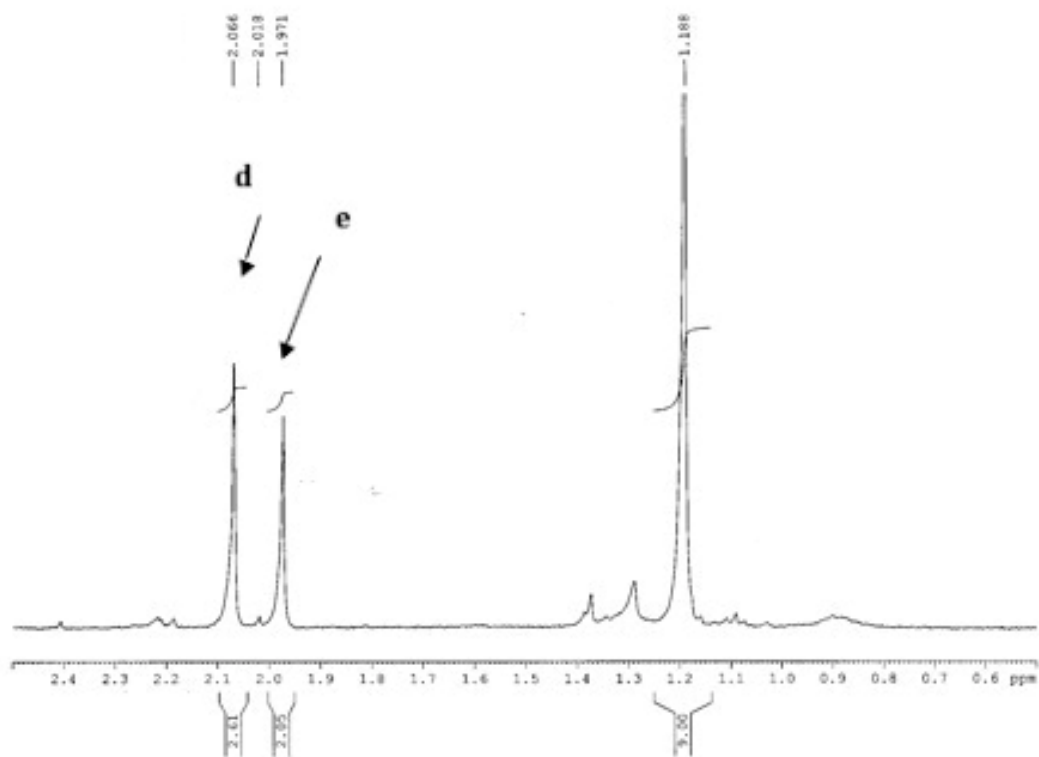**Scheme 7.2.** Photoproducts identified by ^{1}H NMR from the photolysis (hv = 254 nm) of acetate ester, **47** in CD$_3$OD/3.0 M MTBE
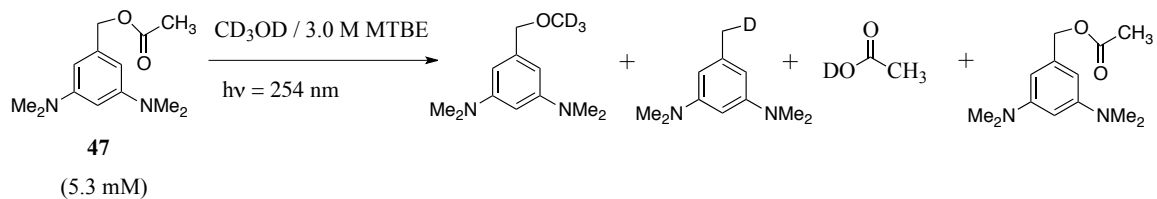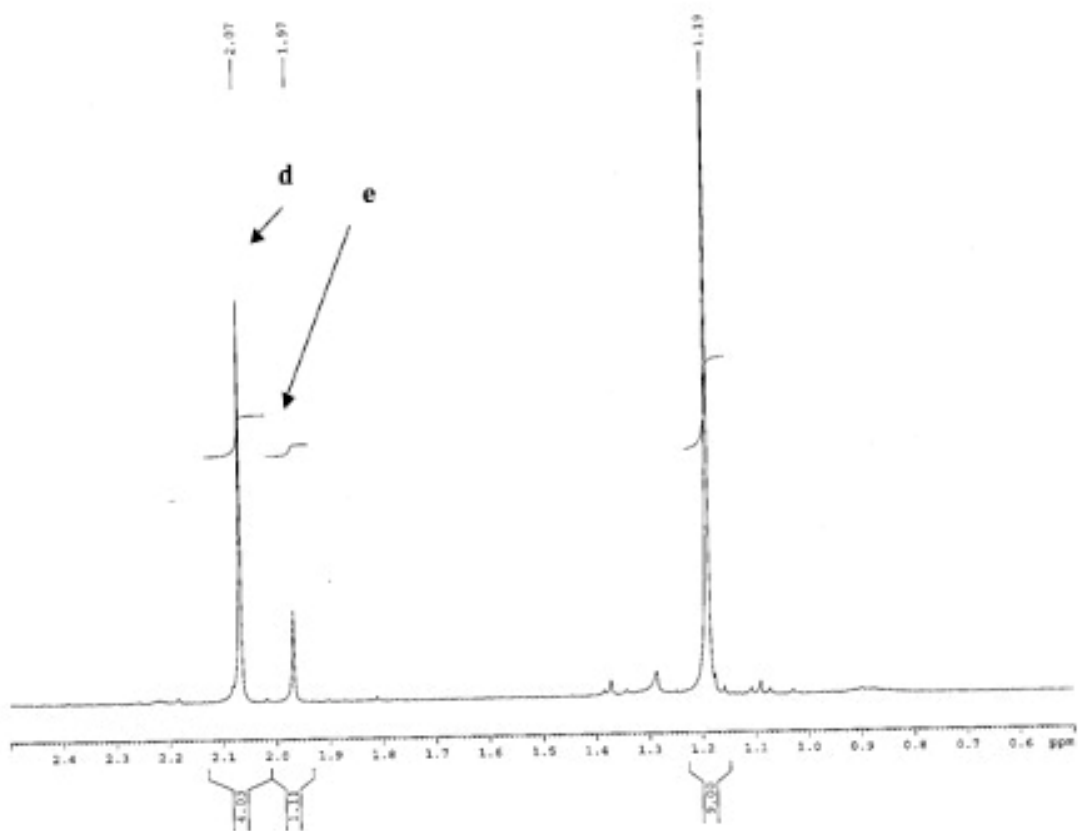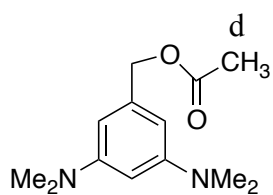

(f) t = 3 h
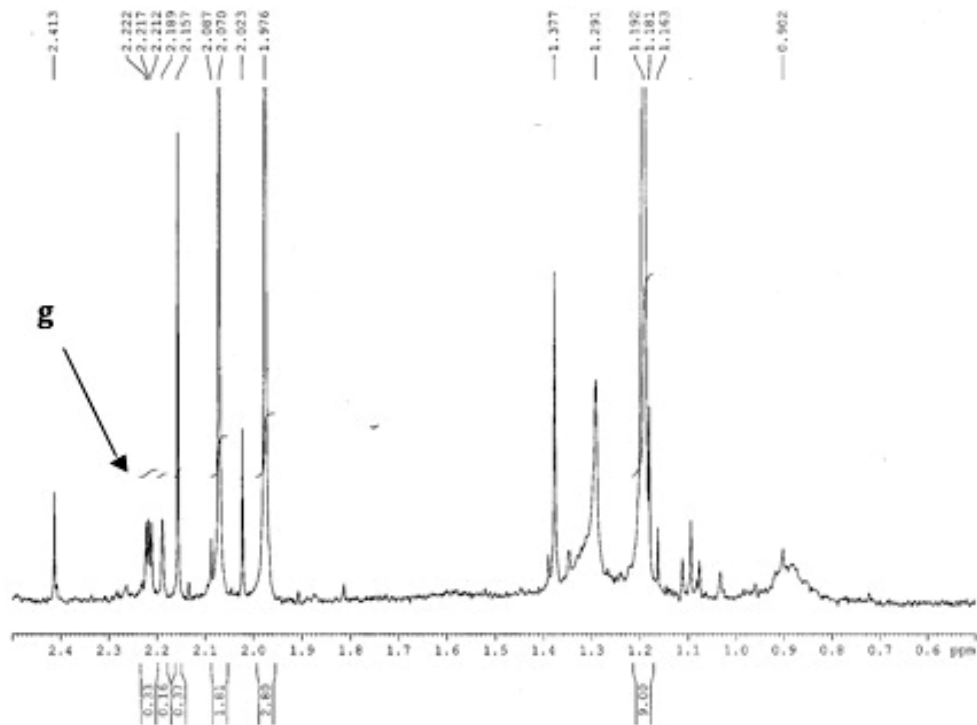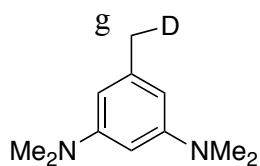
(e)

(d) t = 2 h

(c) t = 1 h

(b) t = 0 (no photolysis)

47

(a)

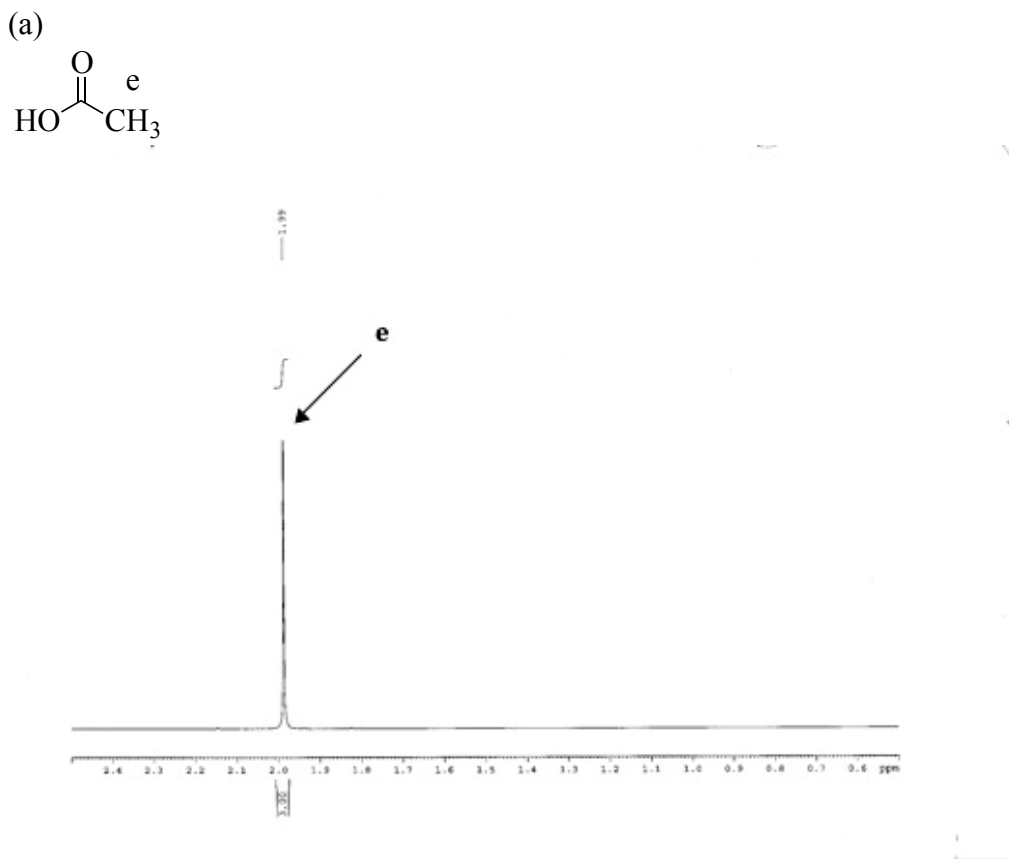$$\underset{HO}{\overset{O}{\parallel}}\overset{e}{\underset{}{C}}CH_3$$
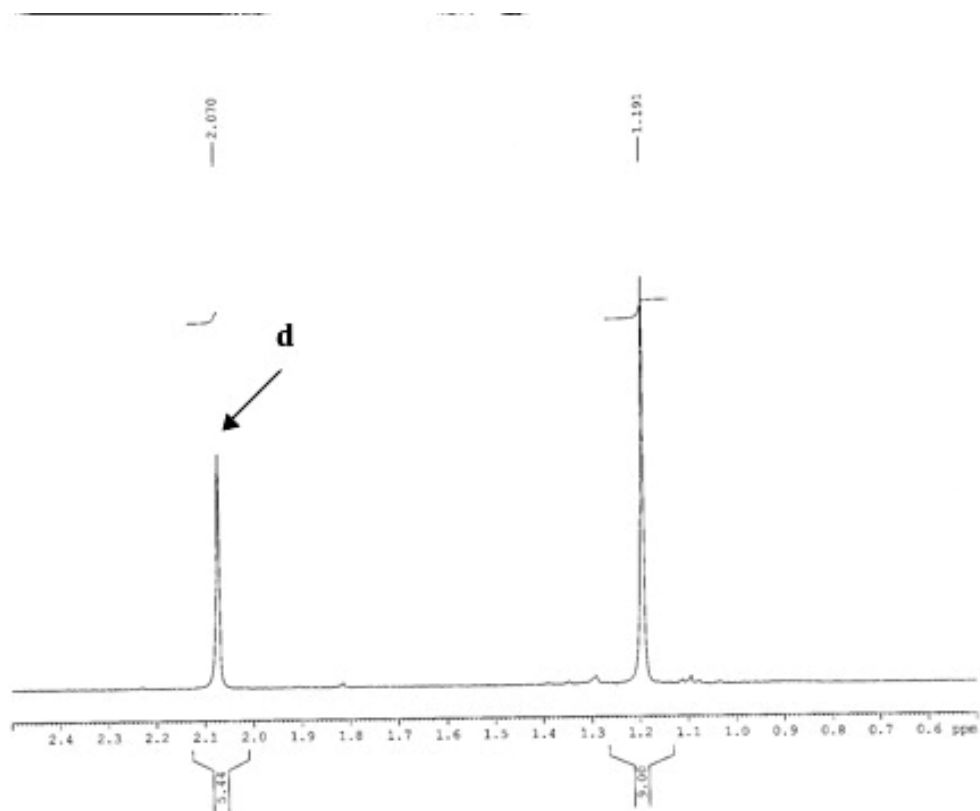
Figure 7.5. ^{1}H NMR (400 MHz) spectra for the photolysis of **47** (5.3 mM) in CD$_3$OD/3 mM MTBE irradiated at 254 nm. (a) Acetic acid standard NMR in CD$_3$OD/3 mM MTBE. Protons e indicates the corresponding CH$_3$ resonances in the acetic acid NMR spectrum. (b) 3,5-Bis(dimethylamino)benzyl acetate, **47** NMR spectrum taken prior to photolysis (t = 0). Protons d indicates the CH$_3$ resonances associated with the acetate group of **47** in CD$_3$OD/3 mM MTBE. (c) ^{1}H NMR spectrum in the region of 2.5-0.5 ppm of the photolysis mixture containing **47** in CD$_3$OD/3 mM MTBE after t = 1 h of irradiation at 254 nm. Shown in this spectrum is the formation of proton resonances for acetic acid indicated as protons e, are present as well as the original proton signals for the acetate CH$_3$ group for **47** (protons d). (d) ^{1}H NMR spectrum in the region of 2.5-0.5 ppm of the photolysis mixture containing **47** in CD$_3$OD/3 mM MTBE after t = 2 h of irradiation at 254 nm. Shown in this spectrum is the formation of proton resonances for acetic acid indicated as protons e, are present as well as the original proton signals for the acetate CH$_3$ group for **47** (protons d).   (e) Standard NMR spectrum of the authentic 3,5-bis(dimethylamino)toluene, **52** taken in CD$_3$OD/3 mM MTBE. Protons c in the spectrum corresponds to the CH$_3$ tolyl protons to **52**. (f) ^{1}H NMR spectrum in the region of 2.5-0.3 ppm of the photolysis mixture containing **47** in CD$_3$OD/3 mM MTBE after t = 3 h of irradiation at 254 nm. Shown in this spectrum is the proton resonances associated with the benzylic protons g that are coupled to a single germinal deuterium atom of the 3,5-bis(dimethylamino)tolyl photoproduct produced from this photolysis reaction.

*7.5 Typical H/D Exchange Experimental Procedure (Dithianes **89** and **90**)*

An oven dried vial (*ca.* 11 mL capacity) was charged with a magnetic stir bar and sealed with a septum was allowed to dry under nitrogen at room temperature. To the vial, 29.5 mg (0.103 mmol) of dithiane **89** and 2.0 mL of anhydrous THF was added under nitrogen. The solution containing **89**/THF was stirred vigorously at room temperature until all of dithiane **89** was dissolved. This yielded an initial concentration of 51.6 mM dithiane, **89** in THF. Subsequently, 70 µL (0.175 mmol) of 2.5 M *n*-BuLi/hexanes was added slowly at room temperature to the vial containing **89**THF under a steady stream of nitrogen. The solution immediately turned red to purple in color after *n*-BuLi was added. The resulting solution was stirred vigorously for 3-5 min. at room temperature, at which time 0.2 mL of CH_3OD (which was purged for 10 min. prior to use with nitrogen and was dried using 4Å Linde molecular sieves) was slowly added and the solution was allowed to stir under nitrogen for 2-3 min. No color change was observed after the addition of CH_3OD. The resulting red-purple solution was evaporated to dryness using a rotary evaporator to yield a red-orange solid residue. The solid residue was dissolved in 1-2 mL of C_6D_6 and was transferred to a dried NMR tube, and an NMR was taken. Each H/D exchange ^{1}H NMR spectrum was calibrated towards the integration of the aromatic doublet resonance at *ca.* 8.25 ppm. Therefore, all H/D incorporation values were calculated in reference to this proton resonance. Note some of the crude residue did not fully dissolve in C_6D_6 probably due to insoluble CH_3OLi precipitates or a high amount of dithiane **89**, which was present in the crude mixture.

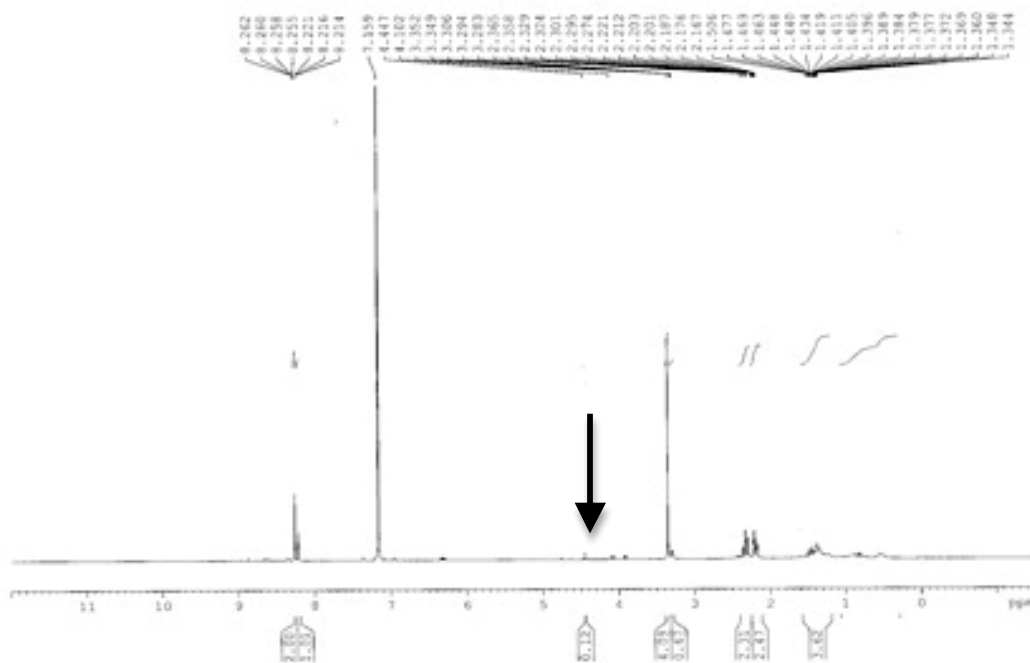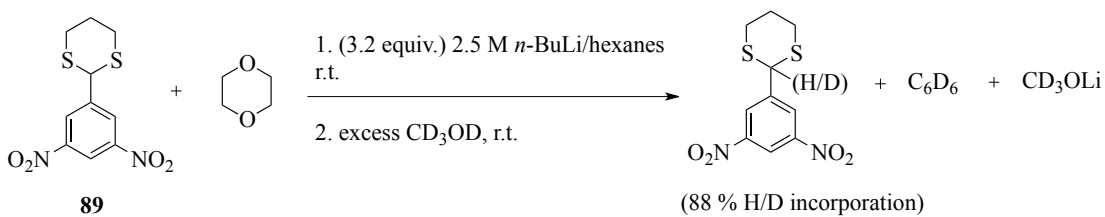**Scheme 7.3.** Room temperature H/D exchange experiment with dithiane **89**/1,4-dioxane and *n*-BuLi

Figure 7.6. ^{1}H NMR (400 MHz, C$_6$D$_6$) of **89** in anhydrous 1,4-dioxane with 3.2 equivalence of 2.5 M *n*-BuLi/hexanes, which is quenched with excess CD$_3$OD. The arrow in the figure indicates a decrease in the NMR integration for the benzylic proton signal for dithiane **89** at ~4.5 ppm. This decrease in the benzylic proton resonance for dithiane **89** signifies that sufficient H/D incorporation was achieved in this experiment.

Scheme 7.4. Room temperature H/D exchange experiment with dithiane **89**/THF and *n*-BuLi
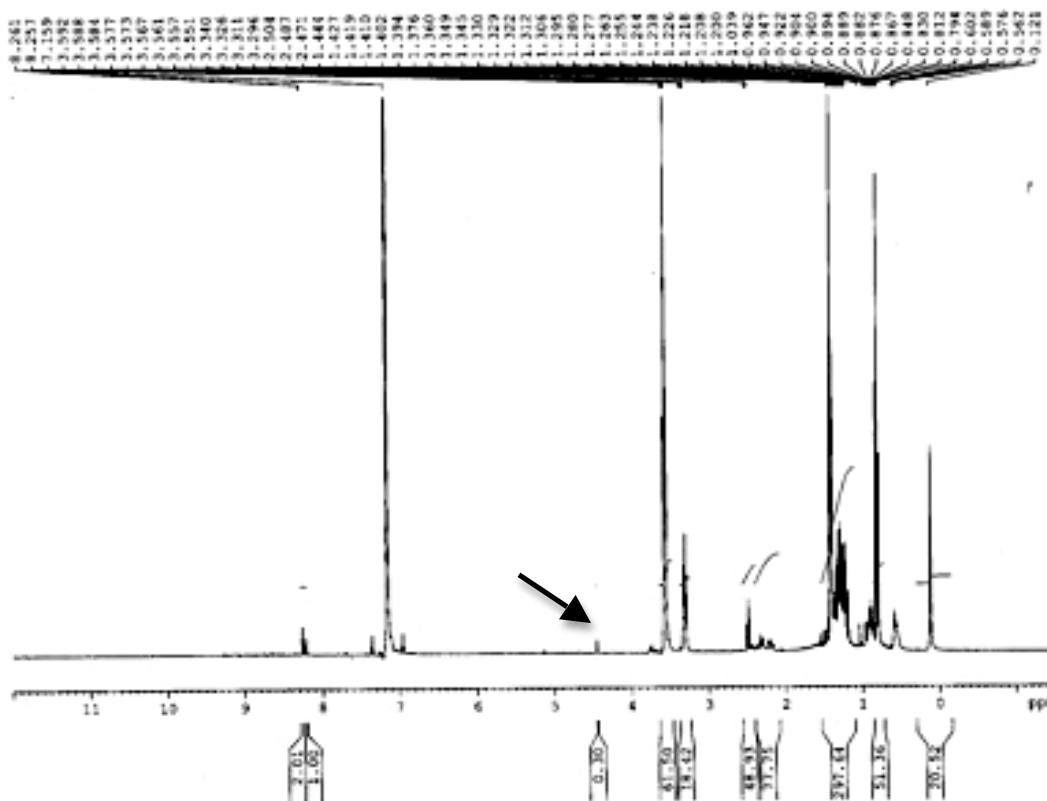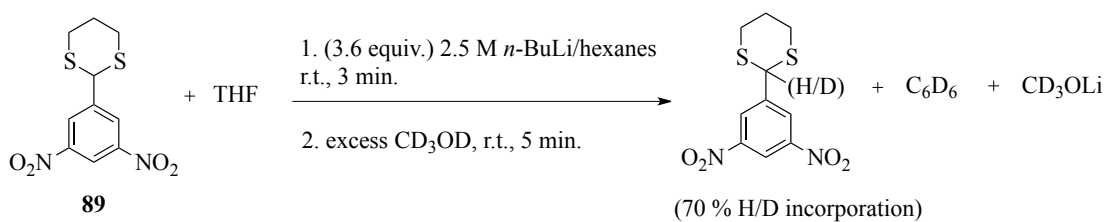

Figure 7.7. ^{1}H NMR (400 MHz, C$_6$D$_6$) of **89** in anhydrous THF with 3.6 equivalence of 2.5 M *n*-BuLi/hexanes, which is quenched with excess CD$_3$OD. The arrow in the figure indicates a decrease in the NMR integration for the benzylic proton signal for dithiane **89** at ~4.5 ppm. This decrease in the benzylic proton resonance for dithiane **89** signifies that sufficient H/D incorporation was achieved in this experiment.

Scheme 7.5. Room temperature H/D exchange experiment with dithiane **90** and KH/THF

90   (76 % H/D incorporation)

Figure 7.8. ^{1}H NMR (400 MHz, C$_6$D$_6$) of **90** in anhydrous THF with 25 equivalence of KH/THF, room temperature for 1 h, which is quenched with excess CD$_3$OD. The arrow in the figure indicates a decrease in the NMR integration for the benzylic proton signal for dithiane **90** at ~5.0 ppm. This decrease in the benzylic proton resonance for dithiane **90** signifies that sufficient H/D incorporation was achieved in this experiment.

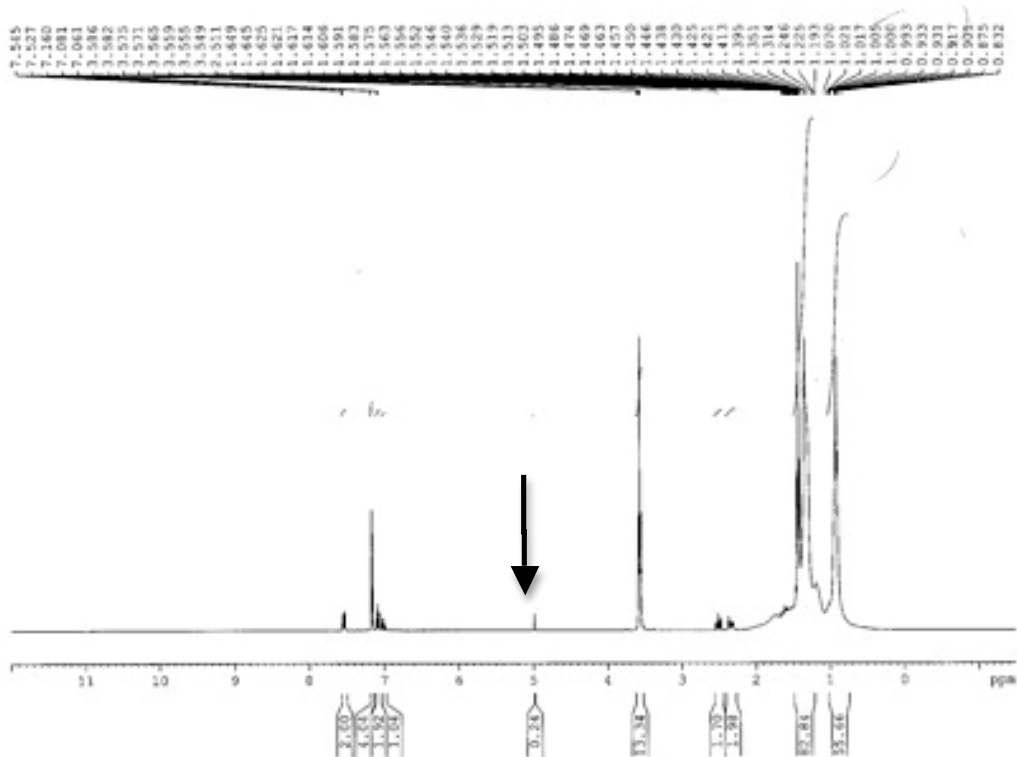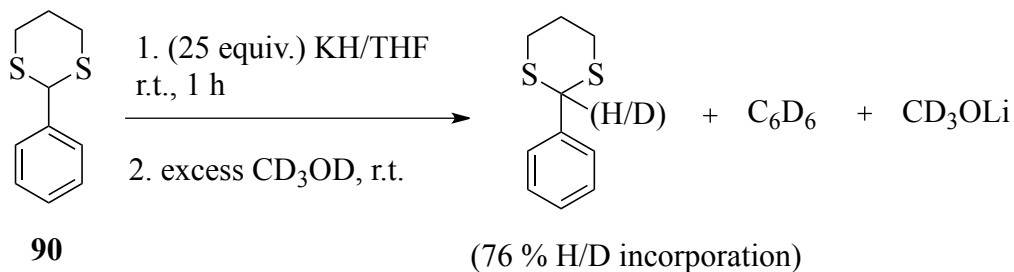**Scheme 7.6.** Room temperature H/D exchange experiment with dithiane **89** and KH/THF
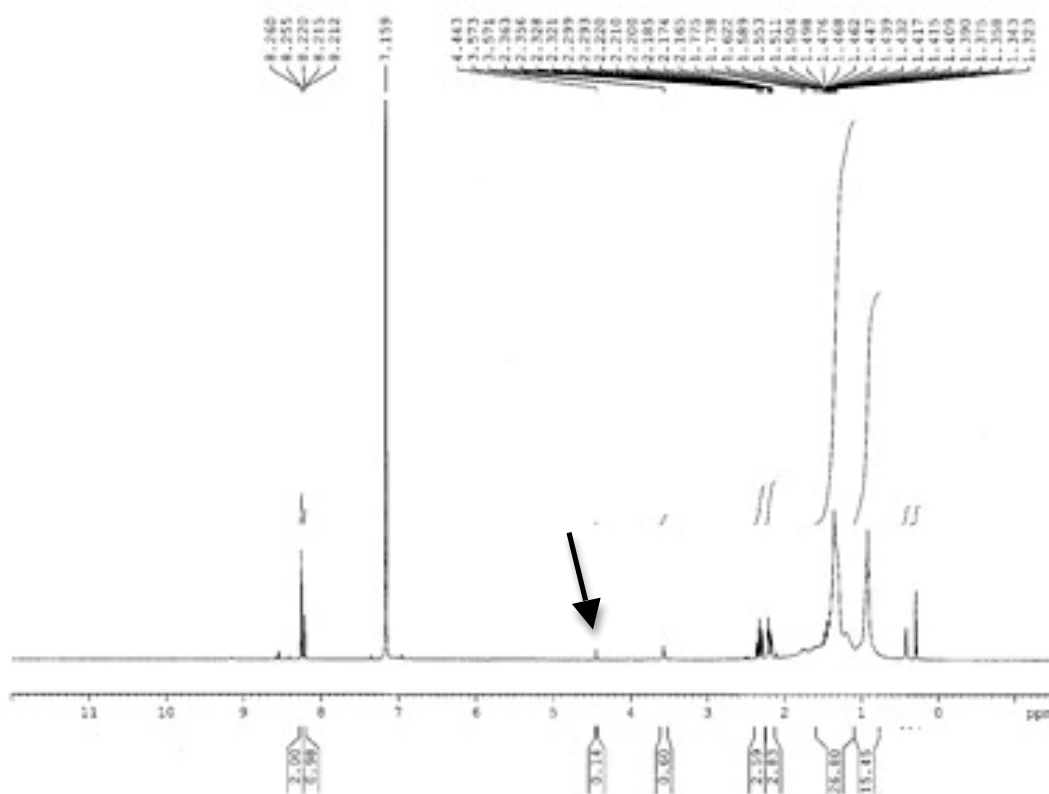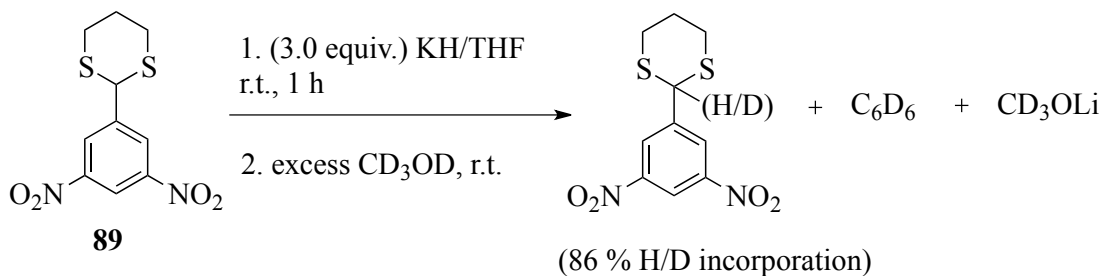

1. (3.0 equiv.) KH/THF
r.t., 1 h

2. excess CD$_3$OD, r.t.

(H/D)   +   C$_6$D$_6$ +   CD$_3$OLi

(86 % H/D incorporation)

89

Figure 7.9. ^{1}H NMR (400 MHz, C$_6$D$_6$) of **89** in anhydrous THF with 3.0 equivalence of KH/THF, room temperature for 1 h, which is quenched with excess CD$_3$OD. The arrow in the figure indicates a decrease in the NMR integration for the benzylic proton signal for dithiane **90** at ~5.0 ppm. This decrease in the benzylic proton resonance for dithiane **90** signifies that sufficient H/D incorporation was achieved in this experiment.

212

To an oven dried J. Young tube (as described on pg. 176) that was purged for 5-10 min. with dry nitrogen, was charged with 20.8 mg (0.106 mmol) of 2-phenyl-1,3-dithiane, **90**. A glass insert with a septum (see pp. 176-177) was added to the top of the Young tube CAV and a stream of dry nitrogen was allowed to flow through the entire sample tube. Subsequently, 25.0 μL (0.168 mmol) of TMEDA was transferred under nitrogen and 1.00 mL of C_6D_6 was also added. A stream of nitrogen was allowed to flow through the sample tube (*ca.* 5-10 min.) and the nitrogen line was remove and the CAV was quickly screwed closed. The sample tube was then gently agitated and inverted several times to ensure that the tube's contents were homogenous and mixed. This solution yielded an initial concentration of 104 mM of dithiane, **90** and 164 mM TMEDA in C_6D_6, respectively.

A ^{1}H NMR (400 MHz) was taken at *ca.* room temperature for each initial sample in these NMR experiments containing the dithiane **90**, C_6D_6, and TMEDA. This was done to verify that all signals due to dithiane **90** and TMEDA were present prior to base addition. After the initial NMR was taken, an oven dried glass adapter was again added to the CAV and was allowed to dry under a stream of N_2. Under N_2, 50 μL of 2.5 M *n*-BuLi/hexanes was added to the Young tube containing dithiane **90**/C_6D_6, and TMEDA at room temperature. A steady stream of nitrogen was allowed to flow through the sample tube for 2-3 minutes following the addition of *n*-BuLi and the CAV was quickly screwed closed and the nitrogen line was removed from the Young tube. The sample mixture in the Young tube was again lightly

agitated and was inverted several times to ensure that the tube's contents were homogenous and mixed. The NMR sample tube turned light yellow immediately after *n*-BuLi addition and mixing. The ^{1}H NMR (400 MHz) spectrum was obtained of this sample. After the addition of 50 μL of 2.5 M *n*-BuLi/hexanes, the ^{1}H NMR spectrum indicated that the benzylic proton due to dithiane, **90** was still present at *ca.* 5.0 ppm as well as no new proton resonances were observed in this NMR. Therefore, the oven dried glass adapter was again added to the CAV and was allowed to dry under a stream of N_2. Under N_2, 100 μL of 2.5 M *n*-BuLi/hexanes was added to the Young tube containing dithiane **90**/C_6D_6, and TMEDA at room temperature. A steady stream of nitrogen was allowed to flow through the sample tube for 2-3 minutes following the addition of *n*-BuLi and the CAV was quickly screwed closed and the nitrogen line was removed from the Young tube. The sample mixture in the Young tube was again lightly agitated and inverted several times to ensure that the tube's contents were homogenous and mixed. The NMR sample tube turned dark yellow immediately after *n*-BuLi addition and after mixing. The ^{1}H NMR (400 MHz) spectrum was obtained of this sample. Only after the addition of a total of 0.15 mL of *n*-BuLi does one see no benzylic proton at *ca.* 5.0 ppm and different NMR proton resonances appear in the aromatic (*ca.* 8.0-6.0 ppm) and aliphatic regions (*ca.* 3.0-0 ppm).

Since we were confident that the anion of dithiane **90** was generated under these conditions, the contents in the Young tube were subsequently quenched. This was done by first adding an oven dried glass adapter to the CAV which was allowed

to dry under a stream of N_2. Under N_2, 200 μL of CD_3OD was added slowly to the Young tube containing dithiane **90**/C_6D_6, TMEDA, and *n*-BuLi at room temperature. A steady stream of nitrogen was allowed to flow through the sample tube for 2-3 minutes following the addition of CD_3OD and the CAV was quickly screwed closed and the nitrogen line was removed from the Young tube. The resulting solution was carefully agitated and inverted several times to ensure that the tube's contents were homogenous and mixed. At which time the solution became colorless and a ^{1}H NMR (400 MHz) spectrum was obtained. Most of the original proton resonances for dithiane **90** appeared in the NMR spectrum, thus indicating that the anion of dithiane **90** was in fact quenched with CD_3OD.

A similar procedure and setup was used for dithiane **89**. In this experiment, 28.7 mg (0.100 mmol) of **89**, 25.0 μL (0.168 mmol) of TMEDA, and 1.00 mL of C_6D_6 was added to a Young tube under N_2. The initial concentrations of dithiane **89**, and TMEDA was 98.0 mM and 164 mM, respectively in the Young tube. The solution was then gently agitated and the Young tube was inverted several times to ensure that the initial solution was mixed and homogenous. A ^{1}H NMR (400 MHz) spectrum was obtained for this sample. This was again done to verify that all signals due to dithiane **89** and TMEDA were present prior to the addition of any base.

Similar to dithiane **90**, initially 50.0 μL (0.125 mmol) of 2.50 M *n*-BuLi/hexanes was added to the Young tube containing dithiane **89**, TMEDA, and C_6D_6 under N_2. The contents of the NMR tube were slightly agitated and the tube

was inverted several times. The NMR tube containing dithiane **89**/C_6D_6 and TMEDA turned dark red-purple immediately after *n*-BuLi addition and mixing at room temperature.   Since the resulting NMR spectrum showed a residual resonance for the benzyl proton for dithiane **89** at *ca.* 4.5 ppm, an additional 0.100 mL (0.250 mmol) of 2.50 M *n*-BuLi/hexanes was added. The NMR tube was again inverted several times and lightly agitated. The resulting NMR spectrum showed no resonance associated with the benzylic proton of dithiane **89**, as well as peak broadened or "NMR silent" signals for all aromatic (*ca.* 8.5-7.0 ppm) and most of the aliphatic resonances (*ca.* 3.0-0 ppm) for dithiane **89**.

Since we were confident that the anion of dithiane **89** was generated under these conditions, the contents in the Young tube were subsequently quenched. This was done by first adding an oven dried glass adapter to the CAV, which was allowed to dry under a stream of N_2. Under N_2, 200 μL of CD_3OD was added slowly to the Young tube containing dithiane **89**/C_6D_6, TMEDA, and *n*-BuLi at room temperature. A steady stream of nitrogen was allowed to flow through the sample tube for 2-3 minutes following the addition of CD_3OD and the CAV was quickly screwed closed and the nitrogen line was removed from the Young tube.   The resulting solution was carefully agitated and inverted several times to ensure that the tube's contents were homogenous and mixed. At which time a ^{1}H NMR (400 MHz) spectrum was obtained. Most of the original proton resonances for dithiane **89** were present in the NMR spectrum, thus indicating that the anion of dithiane **89** was in fact quenched with CD_3OD.
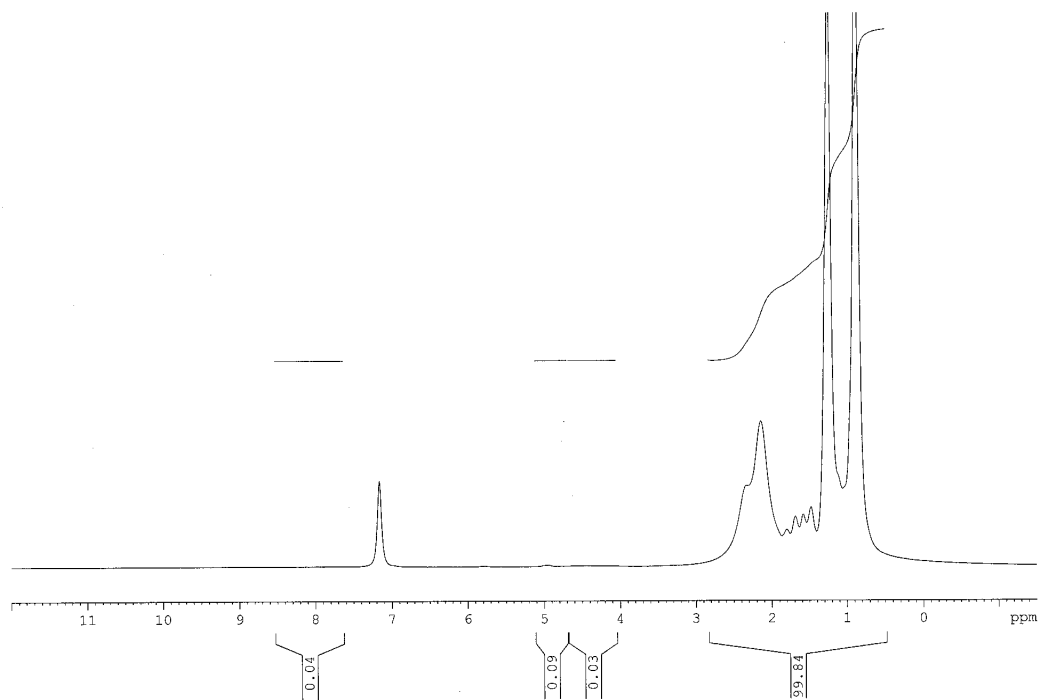
Scheme 7.7. *In situ* generation of dithiane benzyl anion **79** in C$_6$D$_6$/TMEDA and *n*-BuLi
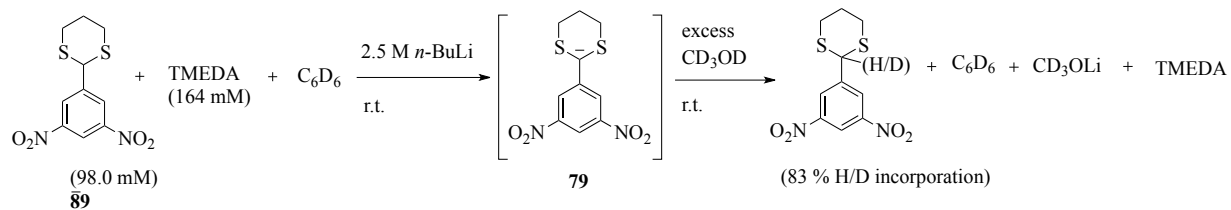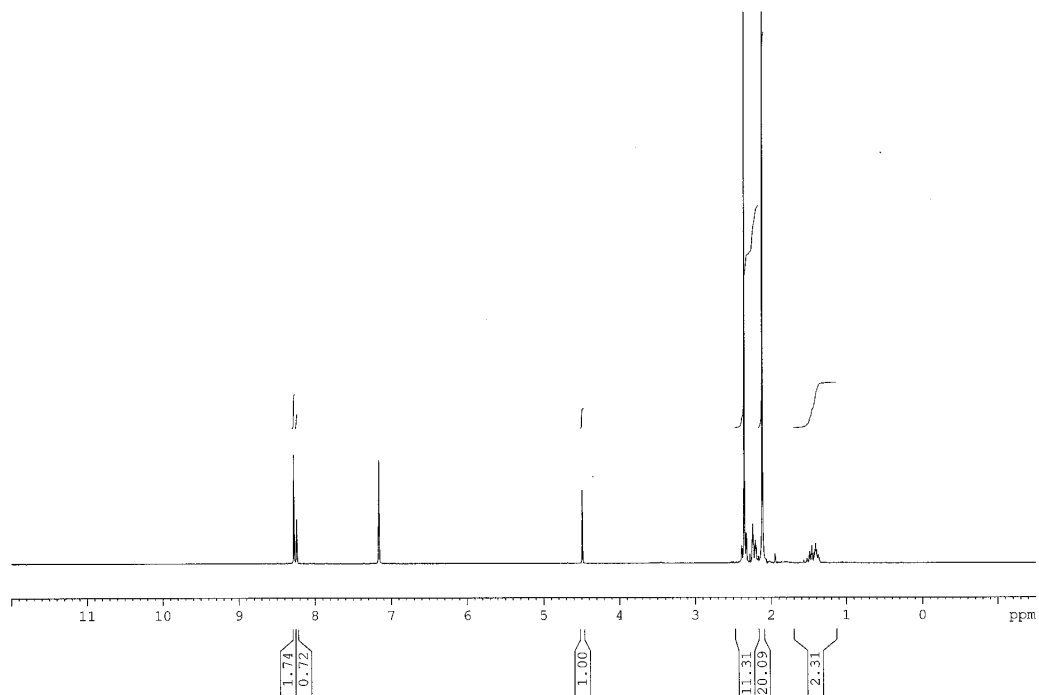

(c)
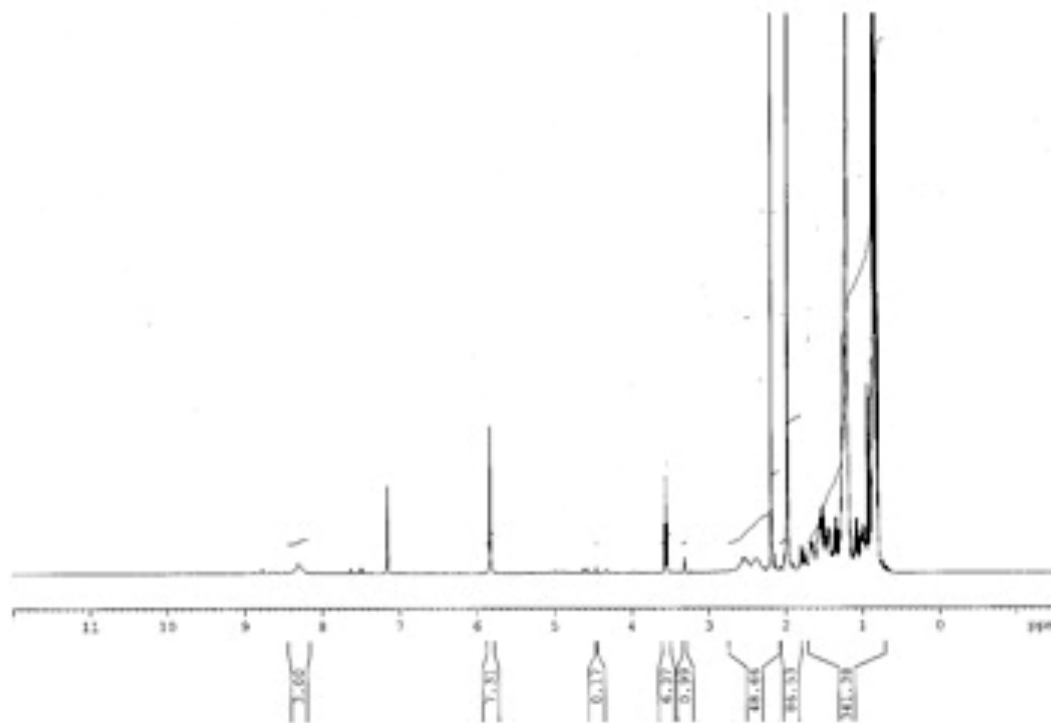
(b)

(a)

Figure 7.10. Room temperature ^{1}H NMR (400 MHz) spectra of the generation of the 2-(3,5-dinitrophenyl)-1,3-dithiane carbanion, **79** in C_6D_6/TMEDA with n-BuLi as a base. (a) **89** (98.0 mM)/C_6D_6 with 164 mM TMEDA solution (no base added). (b) **89** (98.0 mM)/C_6D_6 with 164 mM TMEDA and 50.0 μL of 2.50 M n-BuLi/hexanes added. (c) **89** (98.0 mM)/C_6D_6, 164 mM TMEDA, and 150 μL of 2.50 M n-BuLi/hexanes, which is quenched with 0.300 mL of CD_3OD.

Table 7.1. TD-DFT Predicted UV Absorbance Bands for Dithiane Benzyl Anion, **79** Singlet and Triplet States.

Excited State	Singlet, **79**		Triplet, **79**	
	Absorbance (nm)	Oscillator Strength	Absorbance (nm)	Oscillator Strength
1	2805.92	0.0001	1662.11	0.043
2	1553.34	0.0313	702	0.0016
3	579.06	0.00050	679.75	0.0124
4	481.93	0.036	549.33	0.0052
5	450.82	0.0026	529.77	0.0079
6	427.48	0.0083	478.05	0.003
7	408.48	0.002	456.72	0.0009
8	378.92	0.0001	438.2	0.0033
9	353.67	0.0290	422.76	0.0162
10	350.57	0.0025	411.84	0.000
11	350.07	0.0275	410.48	0.0043
12	347.04	0.0062	409.97	0.0005

Table 7.1 shows 12 computed states for both the singlet and triplet states for benzyl anion **79**. All computations were done using a B3LYP/6-31+G(d,p) basis set. The oscillator strengths provided in Table 7.1 are generally proportional to the molar absorptivity (ε) of each UV band.

Table 7.2. TD-DFT Predicted UV Absorbance Bands for the 3,5-Dinitroaniline Anion Lithium Salt, **94-Li⁺** Singlet and Triplet States.

Excited State	Singlet, **94-Li⁺**		Triplet, **94-Li⁺**	
	Absorbance (nm)	Oscillator Strength	Absorbance (nm)	Oscillator Strength
1	546.89	0.0234	768.86	0.0081
2	493.34	0.0088	546.00	0.0012
3	468.87	0.0068	465.15	0.0028
4	333.02	0.0000	428.95	0.0007
5	331.74	0.0000	398.22	0.0067
6	330.59	0.0025	388.92	0.0000
7	297.43	0.1458	380.66	0.0098
8	292.04	0.0004	352.41	0.0021
9	289.10	0.0001	335.28	0.0000
10	270.07	0.1205	334.63	0.0000
11	268.61	0.0015	333.61	0.0100
12	265.06	0.1382	328.84	0.0000

Table 7.2 shows 12 computed states for both the singlet and triplet states for 3,5-dinitroaniline anion lithium salto **94-Li⁺**. All computations were done using a B3LYP/6-31+G(d,p) basis set. The oscillator strengths provided in Table 7.2 are generally proportional to the molar absorptivity (ε) of each UV band.
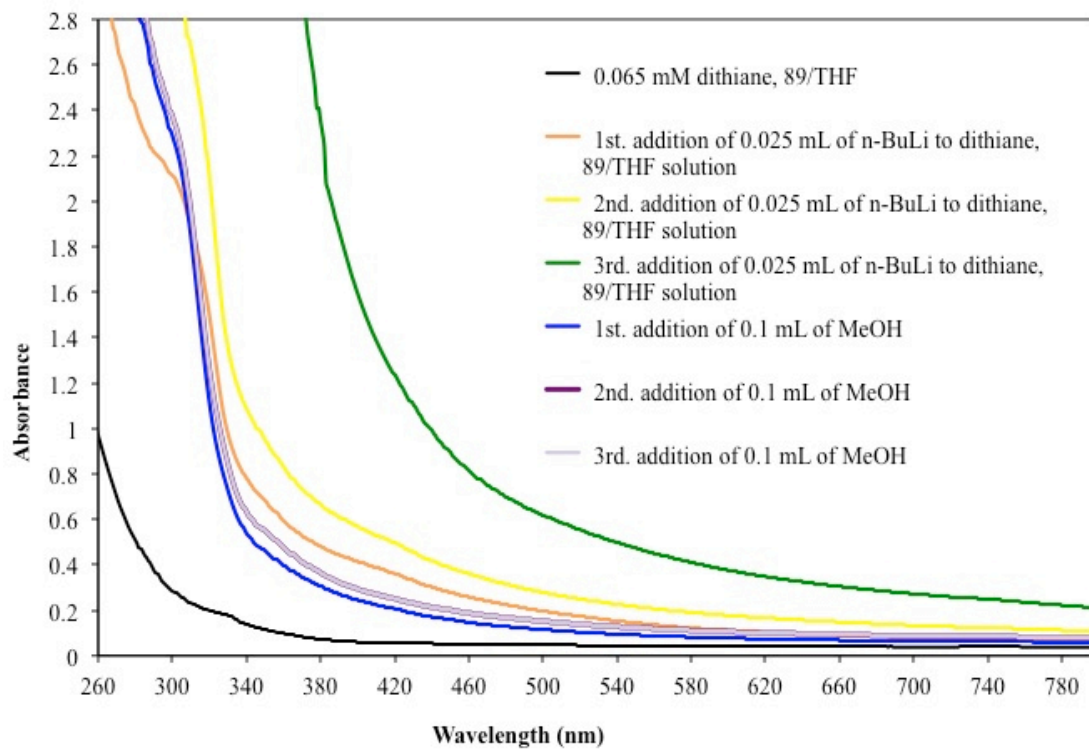
Figure 7.11. UV-Vis spectra of 0.065 mM dithiane, **89**/THF (black spectrum) and the addition of *n*-BuLi/hexanes (orange, yellow, and green spectra). The UV-Vis solution containing dithiane, **89**/THF and *n*-BuLi was subsequently quenched with successive additions of MeOH (blue, purple, and light purple spectra).
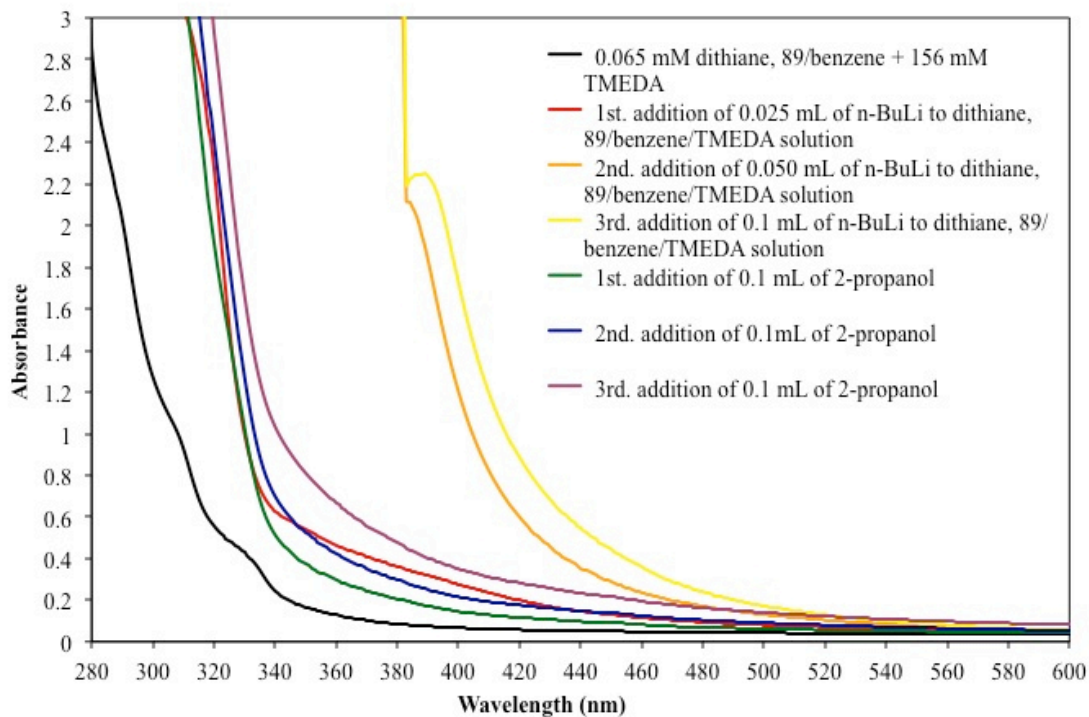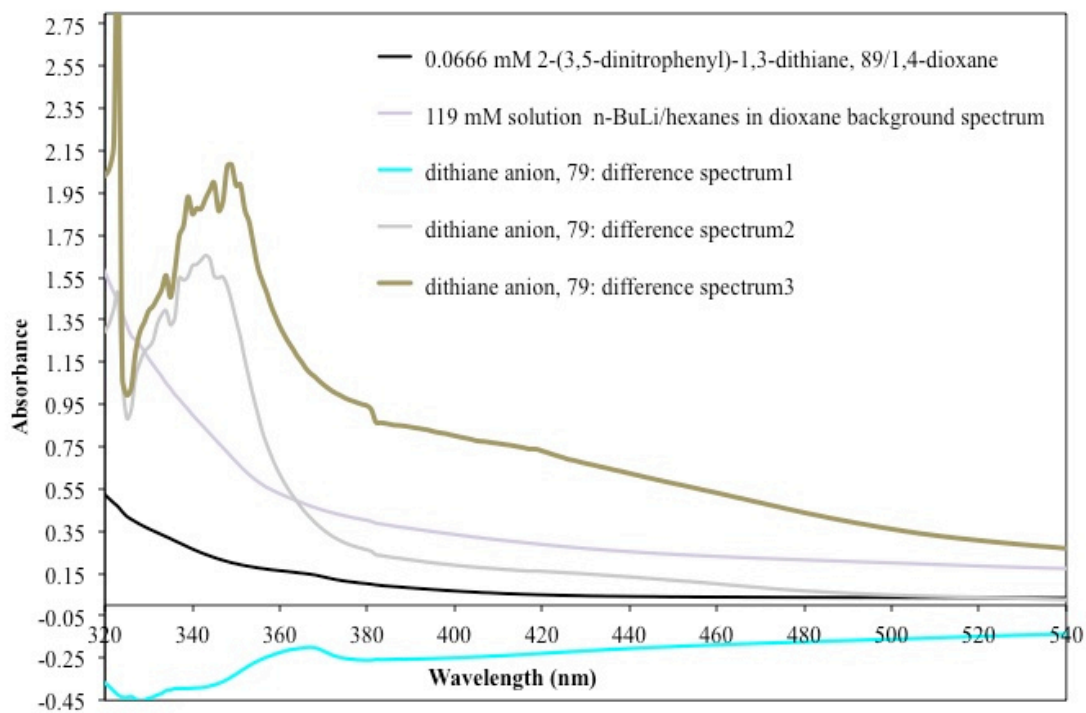
Figure 7.12. UV-Vis spectra of 0.0650 mM dithiane, **89**/benzene and 156 mM TMEDA (black spectrum) and the addition of *n*-BuLi/hexanes (red, yellow, and orange spectra). The UV-Vis solution containing dithiane, **89**/benzene/TMEDA and *n*-BuLi was subsequently quenched with successive additions of 2-propanol (blue, purple, and green spectra).
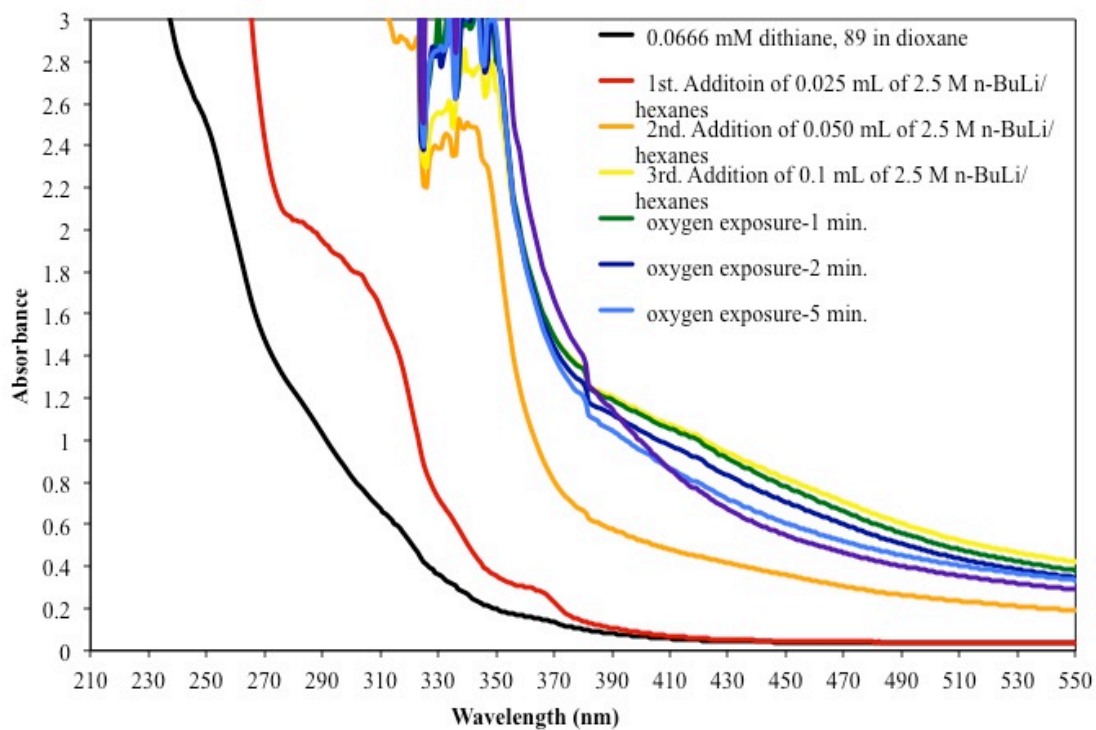
(b)

(a)

Figure 7.13. UV-Vis spectra of the generation of dithiane benzyl anion **79** in 1,4-dioxane with *n*-BuLi as base. (a) UV-Vis spectra of 0.0666 mM dithiane, **89**/1,4-dioxane (black spectrum) and the addition of *n*-BuLi/hexanes (red, yellow, and orange spectra). The UV-Vis solution containing dithiane, **89**/1,4-dioxane and *n*-BuLi was subsequently quenched with oxygen exposure at room temperature (light blue, blue, purple, and green spectra). (b) UV-Vis spectrum of 0.0666 mM dithiane, **89**/1,4-dioxane (black spectrum). 119 mM *n*-BuLi/hexanes solution in 1,4-dioxane background UV-Vis spectrum (light purple). Dithiane anion, **79** difference UV-Vis spectrum1 (cyan): [red UV-Vis spectrum in (a) – light purple UV-Vis spectrum in (b)}. Dithiane anion, **79** difference spectrum2 (light grey): [orange UV-Vis spectrum in (a) – light purple UV-Vis spectrum in (b)]. Dithiane anion, **79** difference UV-Vis spectrum3 (brown): [yellow UV-Vis spectrum in (a) – light purple UV-Vis spectrum in (b)].
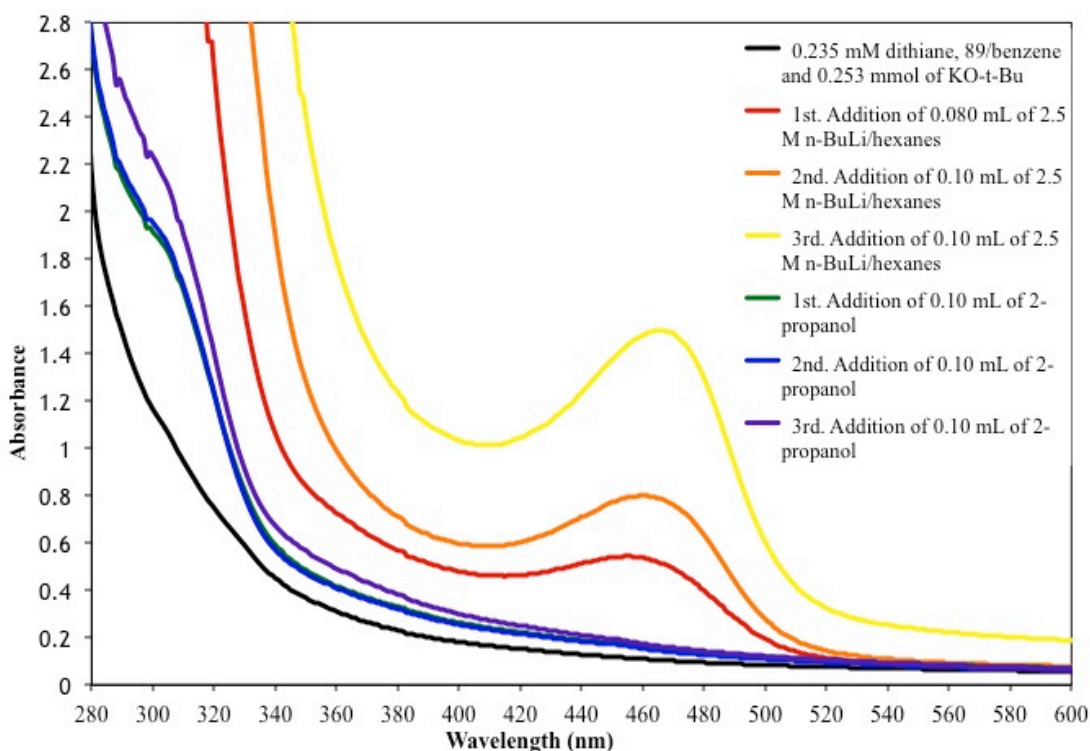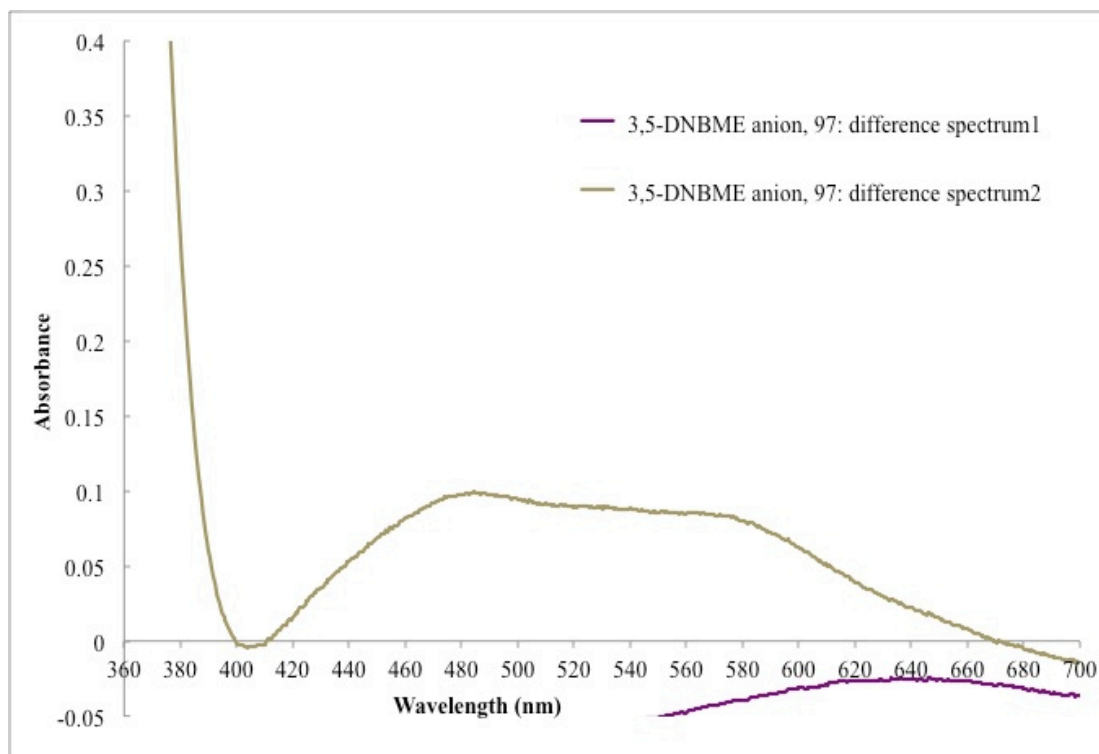

Figure 7.14. UV-Vis spectra of 0.235 mM dithiane, **89**/benzene and 0.253 mmol KO-*tert*-butoxide (black spectrum) and the addition of *n*-BuLi/hexanes (red, yellow, and orange spectra). The UV-Vis solution containing dithiane, **89**/benzene, 0.0253 mmol KO-*tert*-butoxide, and *n*-BuLi was subsequently quenched with successive additions of 2-propanol (blue, purple, and green spectra).
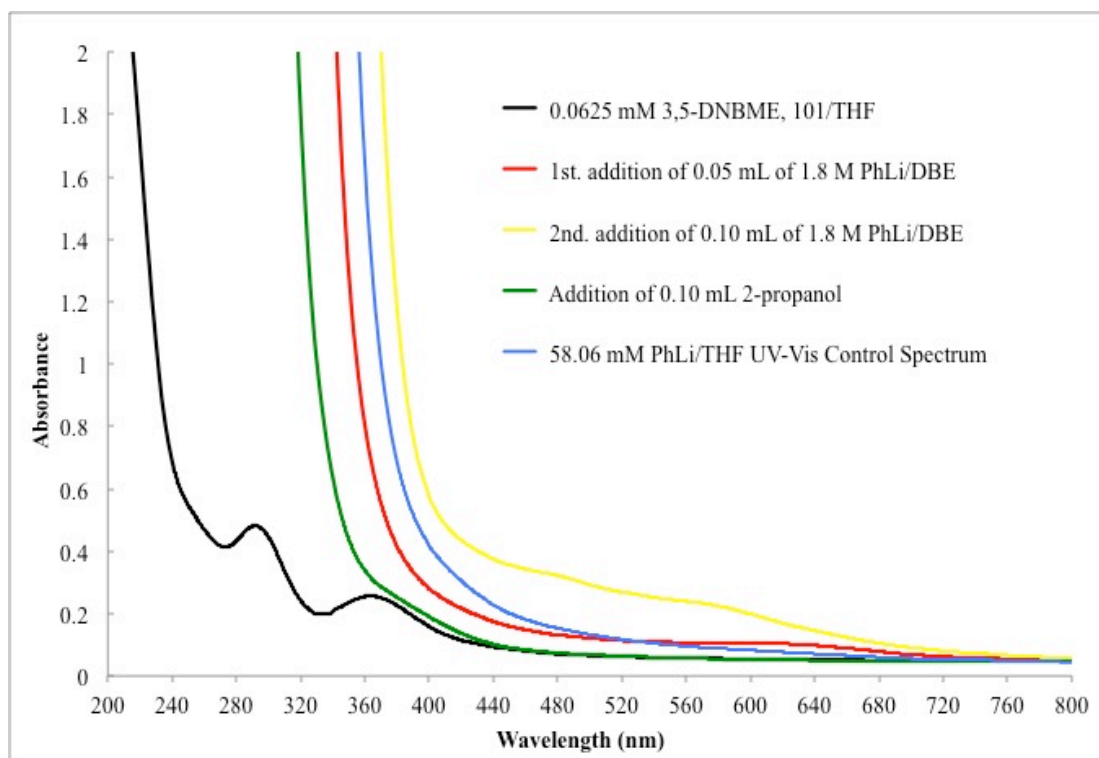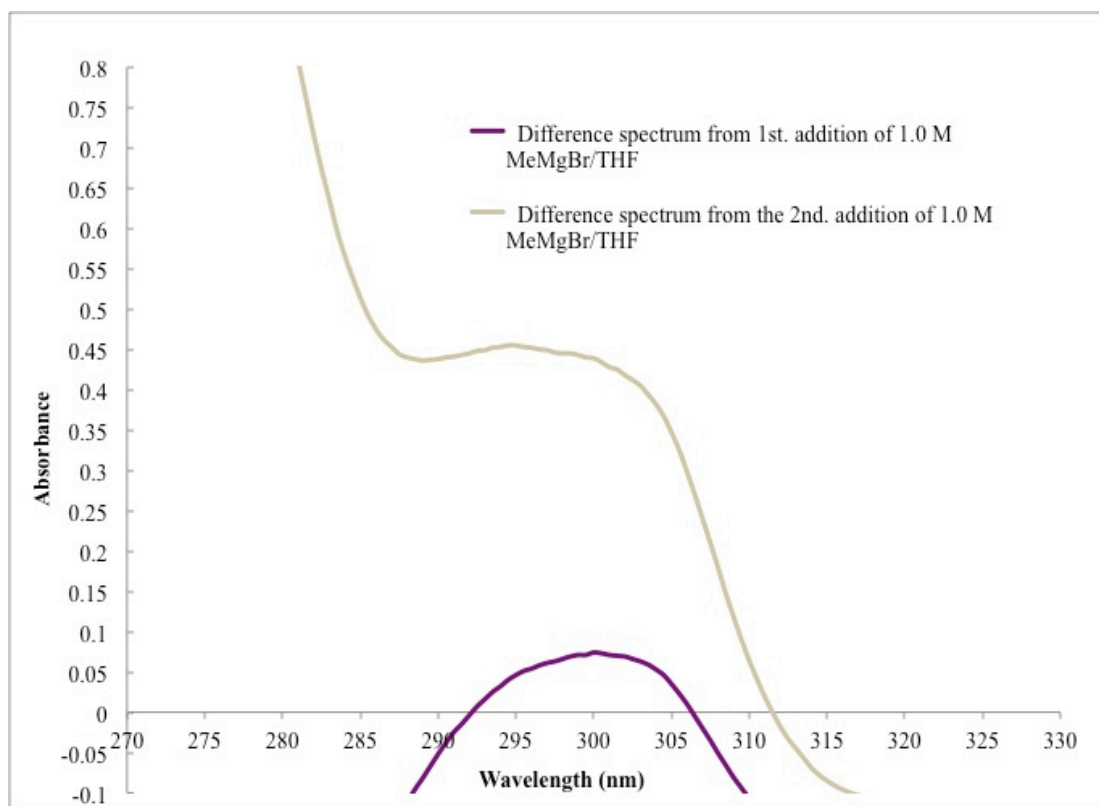
(b)

(a)

Figure 7.15. UV-Vis spectra of 3,5-dinitrobenzyl methoxy ether (3,5-DNBME), **101**/THF and the addition of 1.80 M PhLi/DBE. (a) 0.0625 mM 3,5-DNBME, **101**/THF solution (black spectrum). 0.0625 mM 3,5-DNBME, **101**/THF solution and the first addition of 50.0 μL of PhLi/DBE (red spectrum). 0.0625 mM 3,5-DNBME, **101**/THF solution and the second addition of 100 μL (total of 150 μL) of PhLi/DBE (yellow spectrum). 0.0625 mM 3,5-DNBME, **101**/THF solution and the addition of PhLi/DBE, which is quenched with 100 μL of 2-propanol (green spectrum). 58.06 mM PhLi/THF UV-Vis control spectrum (blue). (b) 3,5-DNBME anion, **97** difference spectrum1 (purple spectrum): [red spectrum in (a) – blue spectrum in (a) – black spectrum in (a)]. 3,5-DNBME anion, **97** difference spectrum2 (brown spectrum): [yellow spectrum in (a) – black spectrum in (a) – blue spectrum in (a)].
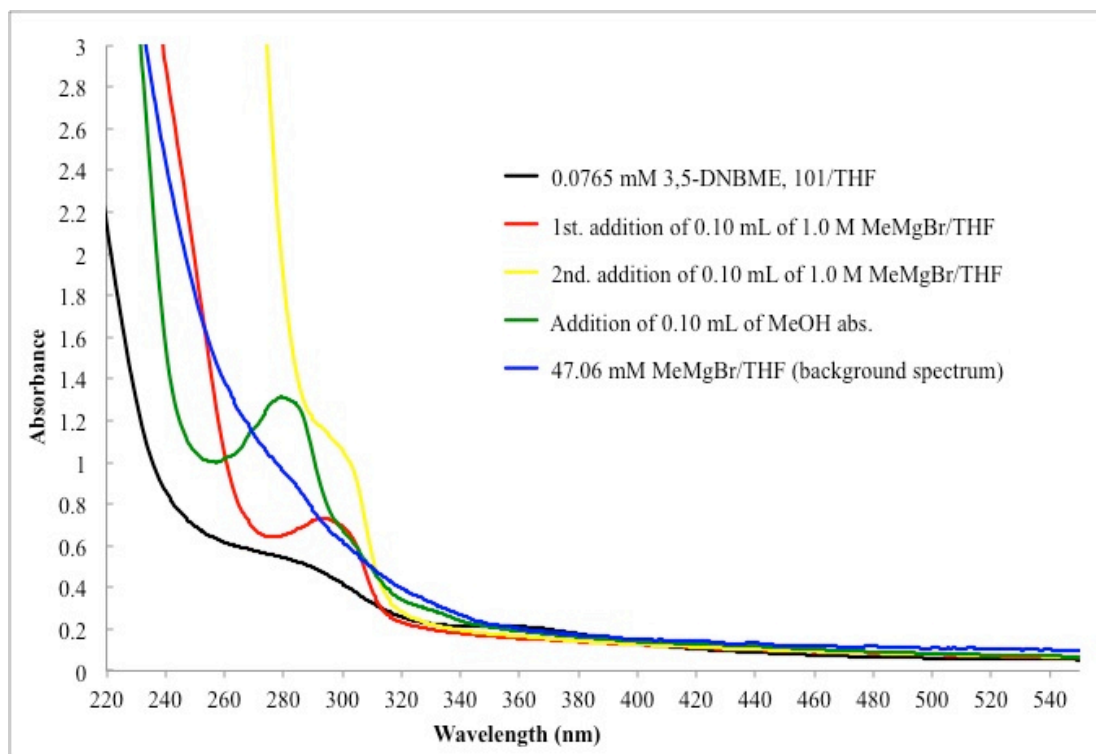
(b)

(a)

Figure 7.16. UV-Vis spectra of 3,5-dinitrobenzyl methoxy ether (3,5-DNBME), **101**/THF and the addition of 1.00 M MeMgBr/THF. (a) 0.0765 mM 3,5-DNBME, **101**/THF solution (black spectrum). 0.0765 mM 3,5-DNBME, **101**/THF solution and the first addition of 100 μL of 1.00 M MeMgBr/THF (red spectrum). 0.0765 mM 3,5-DNBME, **101**/THF solution and the second addition of 100 μL (200 μL total) of 1.0 M MeMgBr/THF (yellow spectrum). 0.0765 mM 3,5-DNBME, **101**/THF solution and the addition of 1.0 M MeMgBr/THF, which is quenched with 0.100 mL of MeOH abs. (green spectrum). 47.06 mM MeMgBr/THF UV-Vis background control spectrum (blue). (b) 3,5-DNBME anion, **97** difference spectrum 1 (purple spectrum): [red spectrum in (a) – blue spectrum in (a) – black spectrum in (a)]. 3,5-DNBME anion, **97** difference spectrum2 (brown spectrum): [yellow spectrum in (a) – black spectrum in (a) – blue spectrum in (a)].

7.7 Typical Evans Method Experiment

To an oven dried J. Young tube (as described on pp. 176-177) that was purged

for 5-10 min. with dry nitrogen, a sealed capillary (also described on pp. 176-177)

containing 100 μL of C_6D_6 (dried with 4Å Linde molecular sieves) was carefully

228

inserted into the outer Young tube with 19.9 mg (0.0664 mmol) of **89**. A glass insert

with a septum (see pp. 176-177) was added to the top of the Young tube CAV and a

stream of dry N_2 was allowed to flow through the entire sample tube. Consequently,

20.0 μL (0.134 mmol) of TMEDA was transferred under N_2 and 1.00 mL of C_6D_6

was also added. A stream of nitrogen was allowed to flow through the sample tube

(*ca.* 5-10 min.) and the nitrogen line was remove and the CAV was quickly screwed

closed. The sample tube was then gently agitated and inverted several times to ensure

that the outer tube's contents were homogenous and mixed.

A ^{1}H NMR (400 MHz) was taken at *ca.* room temperature for each initial

sample in these Evans method experiments containing the dithiane **89**, C_6D_6 in the

inner and outer NMR tubes, and TMEDA. This was done to verify that only one

C_6D_6 signal was present prior to base addition. After the initial NMR was taken, the

oven dried glass adapter was again added to the CAV and was allowed to dry under a

stream of N_2. Under N_2, 0.1 mL of 2.5 M *n*-BuLi/hexanes was added to the Young

tube containing dithiane **89** at room temperature. A steady stream of nitrogen was

allowed to flow through the sample tube for 2-3 minutes following the addition of *n*-

BuLi and the CAV was quickly screwed closed and the nitrogen line was removed

from the Young tube. The sample mixture in the Young tube was again lightly

agitated and was inverted several times to ensure that the outer tube's contents were

homogenous and mixed. The NMR sample tube turned orange to red-purple

immediately after *n*-BuLi addition and mixing. The ^{1}H NMR (400 MHz) spectrum

was obtained of this sample. As with all other Evans method experimental results, 2

NMR solvent peaks were observed for C_6D_6 and the most downfield shifted peak that closely had a chemical shift near 7.16 ppm for C_6D_6 was chosen for calibration of the chemical shifts in the resulting NMR spectrum. Furthermore, as in all other Evans method experiments, the NMR spectrum of the benzyl anion of dithiane **89** showed peak broadening and/or NMR silent behavior for the aromatic and benzylic proton resonances for **89**. It is important to note that in all Evans method experiments, the inner capillary tube was fully immersed in the outer tube solution (at all times) and that the entire inner capillary tube was located below the spinner when taking the NMR to allow proper spinning and shimming of the desired sample tube.
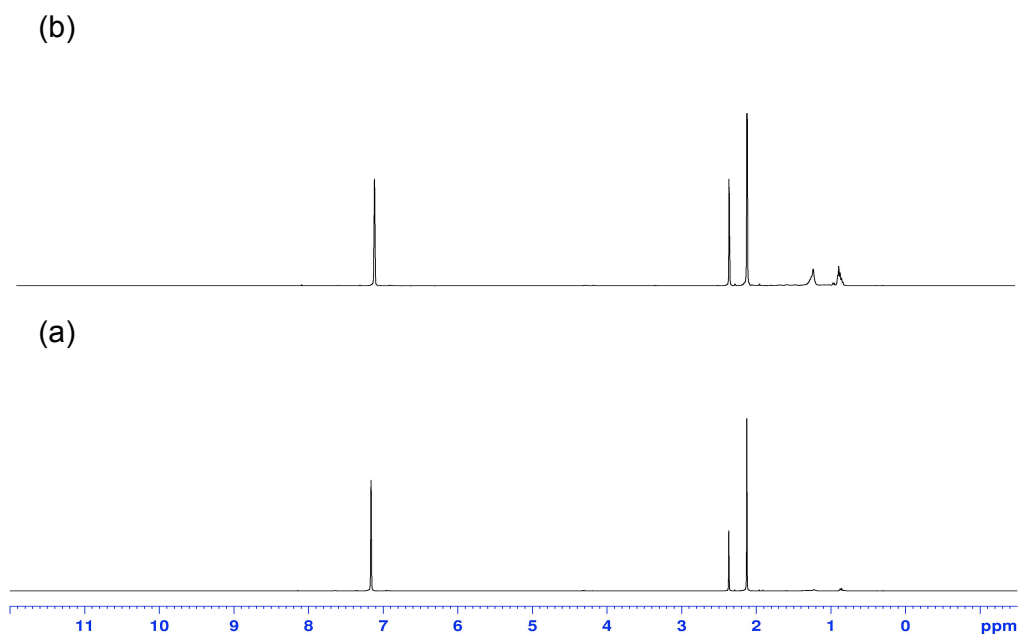
Figure 7.17. Evans method control experiment in a J. Young tube purged with nitrogen at room temperature. Inner tube contains 100 μL of C_6D_6 for both spectra (a) and (b). For further specification of the inner and outer tube Evans experiments see pp. 176-177 of this chapter. (a) ^{1}H NMR spectrum (400 MHz) of 40.0 μL (0.268 mmol) of TMEDA in 1.00 mL of C_6D_6 (258 mM solution of TMEDA). (b) ^{1}H NMR spectrum (400 MHz) of a solution containing 30.0 μL (0.201 mmol) of TMEDA in 1.00 mL of C_6D_6, and 0.100 mL (0.250 mmol) of 2.50 M *n*-BuLi/hexanes added to the J. Young tube at room temperature under N_2.
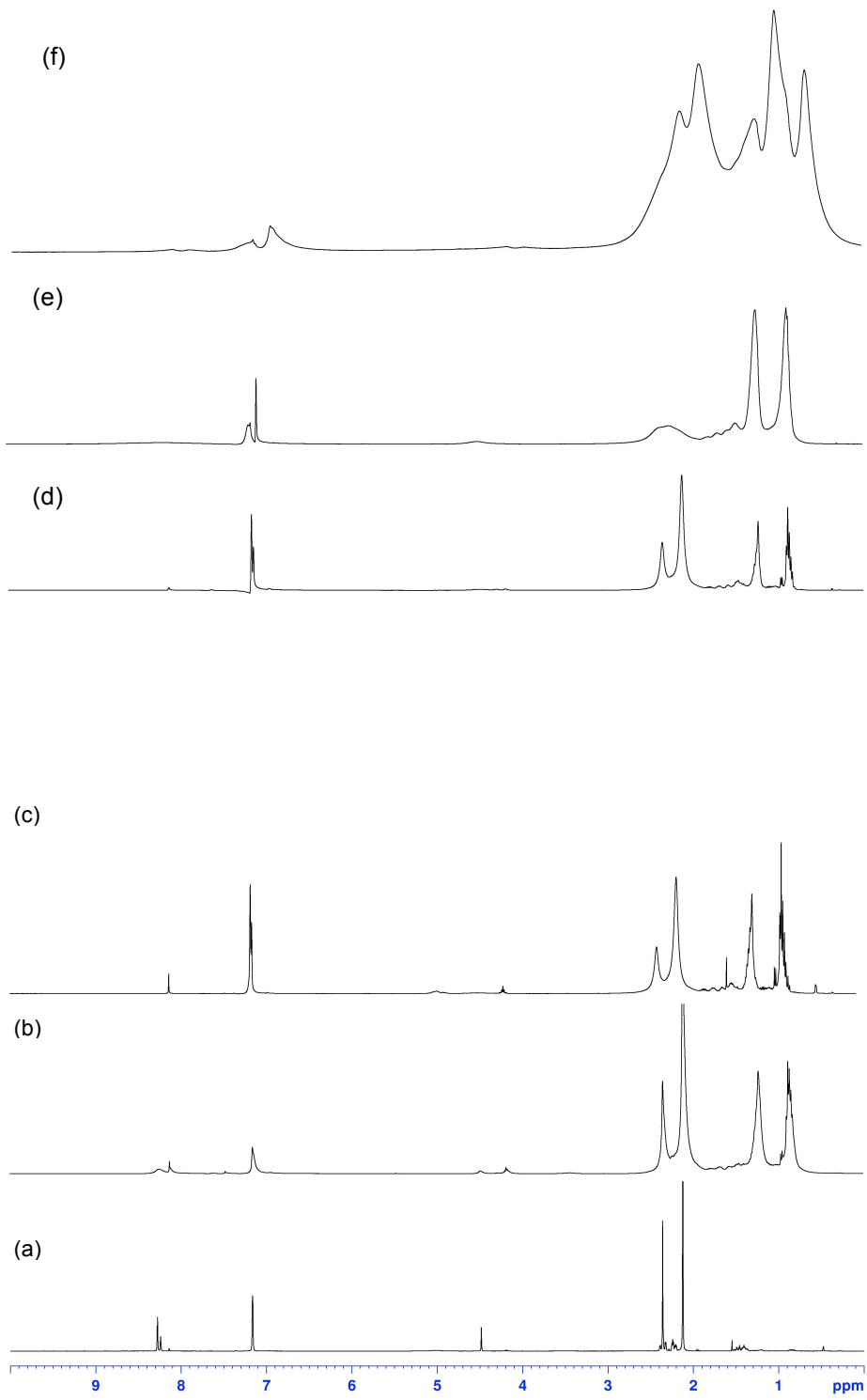
Figure 7.18. Representative ^{1}H NMR (400 MHz) Evans method experiments (full spectra) at room temperature of dithiane, **89**/C$_6$D$_6$/TMEDA with n-BuLi as base. (a) 85.0 mM **89** in C$_6$D$_6$ with 132 mM TMEDA. (b) 54.8 mM **89** in C$_6$D$_6$ with 132 mM TMEDA and 0.100 mmol of 2.50 M n-BuLi/hexanes. (c) 85.0 mM **89** in C$_6$D$_6$ with 132 mM TMEDA and 0.125 mmol of 2.50 M n-BuLi/hexanes. (d) 114 mM **89** in C$_6$D$_6$ with 258 mM TMEDA and 0.250 mmol of 2.50 M n-BuLi/hexanes. (e) 121 mM **89** in C$_6$D$_6$ with 258 mM TMEDA and 0.250 mmol of 2.50 M n-BuLi/hexanes. (f) 130 mM **89** in C$_6$D$_6$ with 258 mM TMEDA and 0.250 mmol of 2.50 M n-BuLi/hexanes.

All spectra were taken under an inert nitrogen environment in a J. Young tube or a septum sealed standard NMR tube (O.D. = 5 mm, length = ~168 mm) and a sealed capillary inner tube containing 100 μL of C$_6$D$_6$ (O.D. = 2.5 mm).

*7.8 Representative Chemical Trapping/Alkylation Experiments/Results Conducted on Dithianes **89** and **90***

Scheme 7.8. Benzylic alkylation S$_N$2 reaction of 2-phenyl-1,3-dithiane, **90** with methyl iodide

90

1. (1.5 equiv.) n-BuLi/hexanes
   r.t., 5 min.

2. (1.4 equiv.) MeI, r.t., 24 h

107
(60 %)^a

90
(40 %)^a
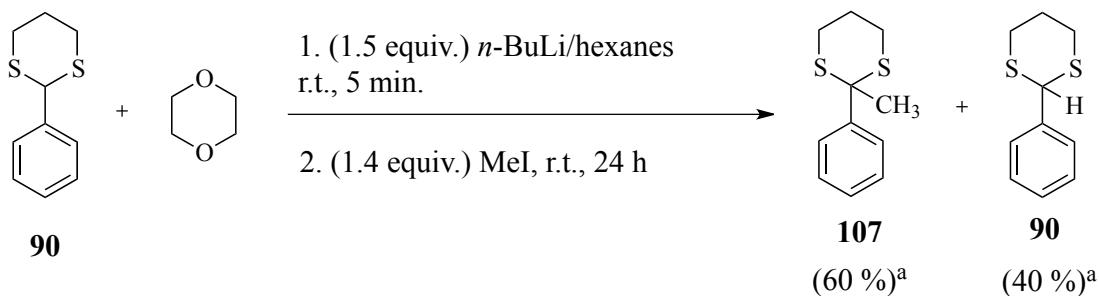
^{a} The yield of **90** was calculated from using a 4-point calibration curve of the crude mixture containing **90** and **107**. The yield of **107** was extrapolated through the use of an external standard.
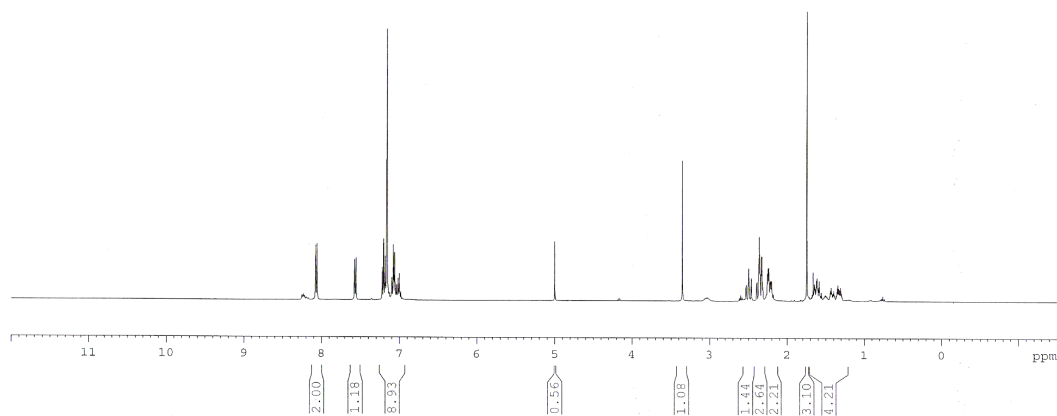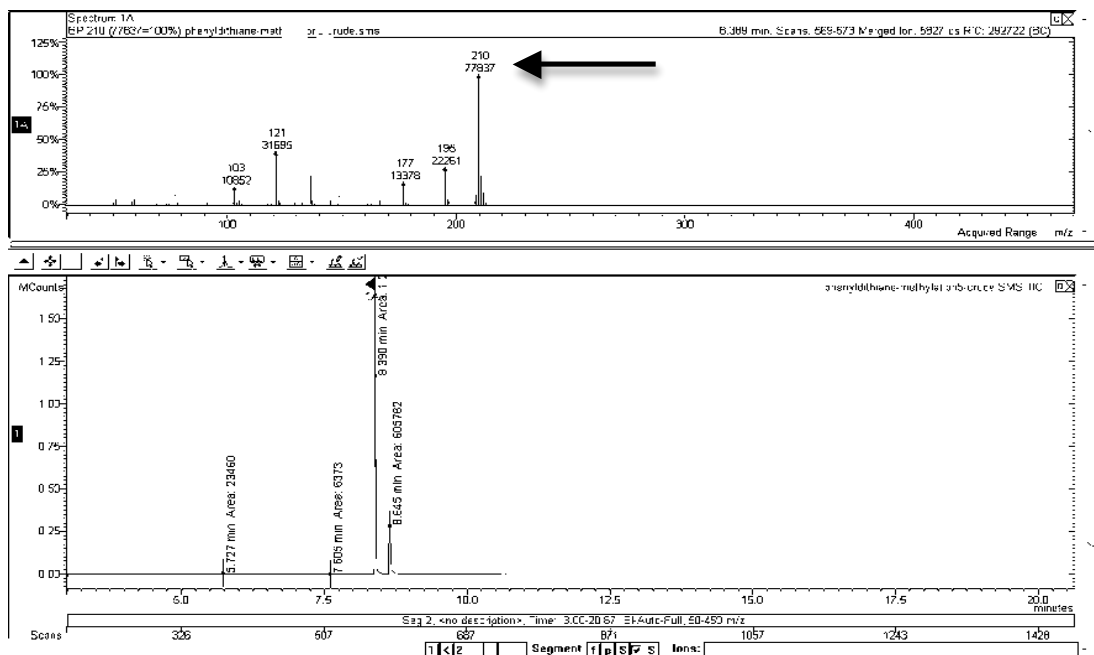
233

Figure 7.19. ^{1}H NMR (400 MHz) in C_6D_6 of the crude reaction mixture from the alkylation of **90** using methyl iodide.

Figure 7.20. GC-MS traces and mass spectra (EI) in CH$_3$CN of the crude NMR reaction mixture from the alkylation of **90** using methyl iodide shown in Figure 7.19.

Scheme 7.9. Benzylic alkylation S$_N$2 reaction of 2-(3,5-dinitrophenyl)-1,3-dithiane, **89** with methyl iodide

1. (1.5 equiv.) *n*-BuLi/hexanes
r.t., 5 min.

2. (1.4 equiv.) MeI, r.t., 24 h

89

(~ 100 %, only product observed)

235

Figure 7.21. ^{1}H NMR (400 MHz) in C_6D_6 of the crude reaction mixture from the alkylation of **89** using methyl iodide.
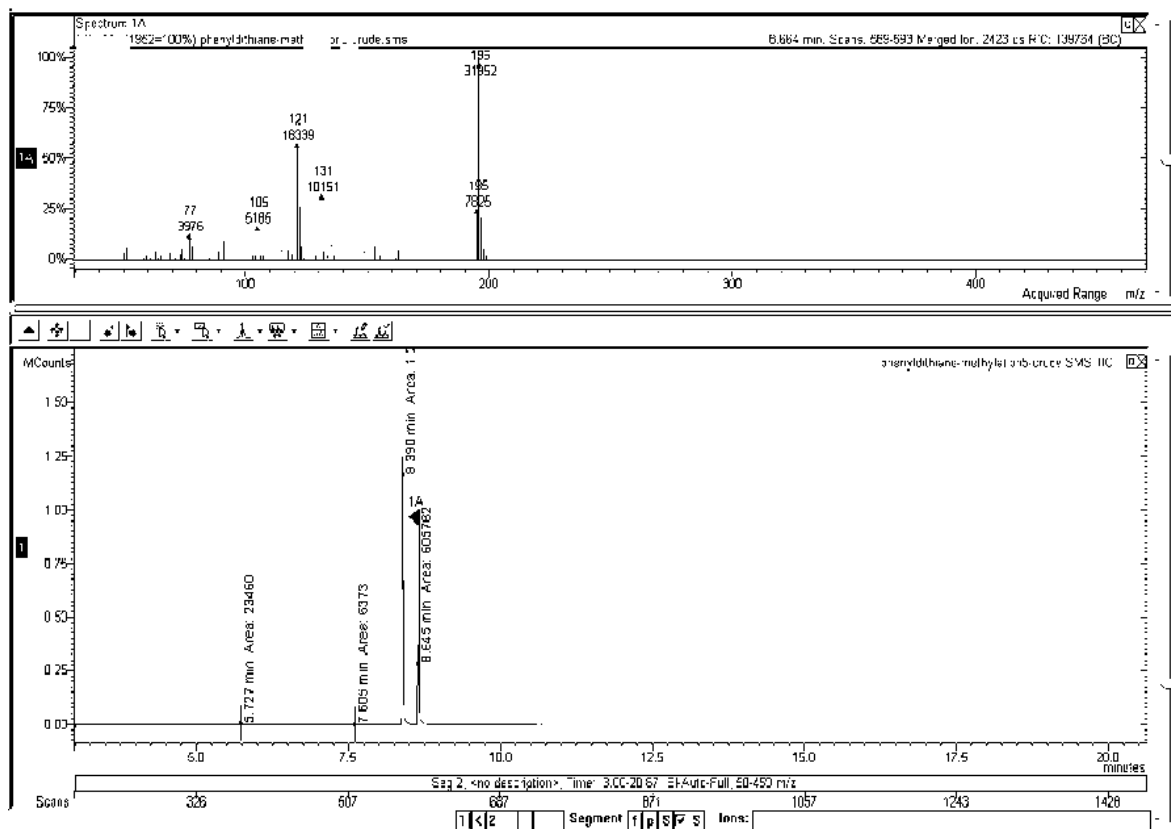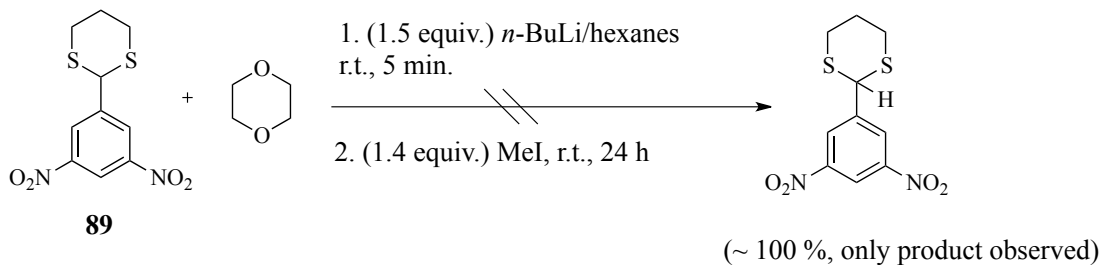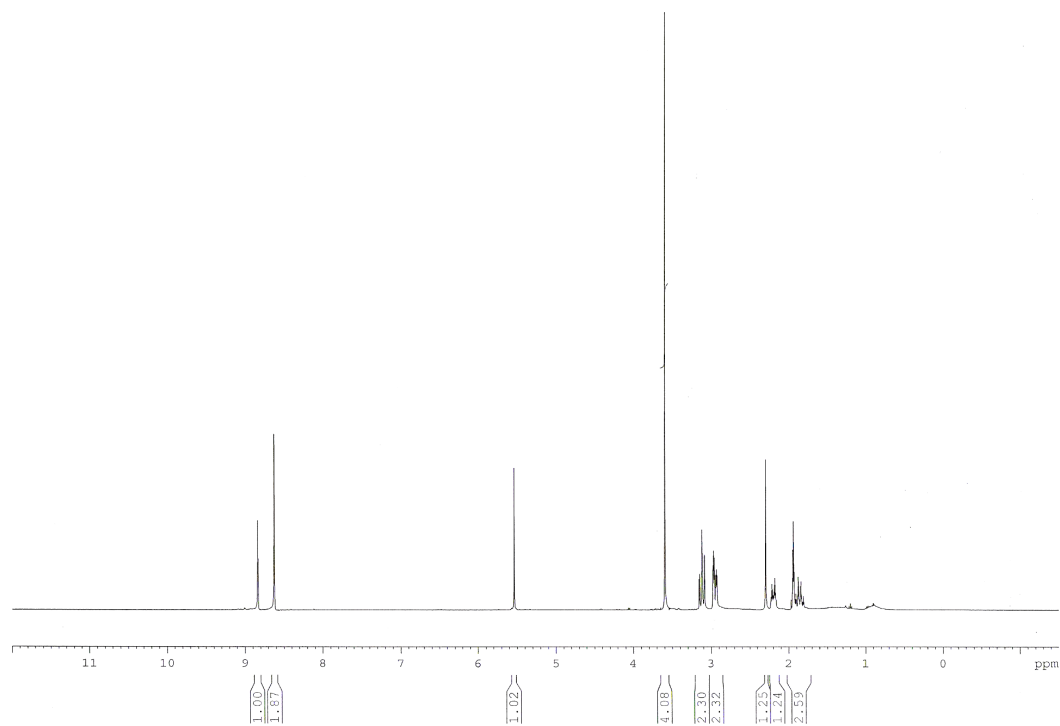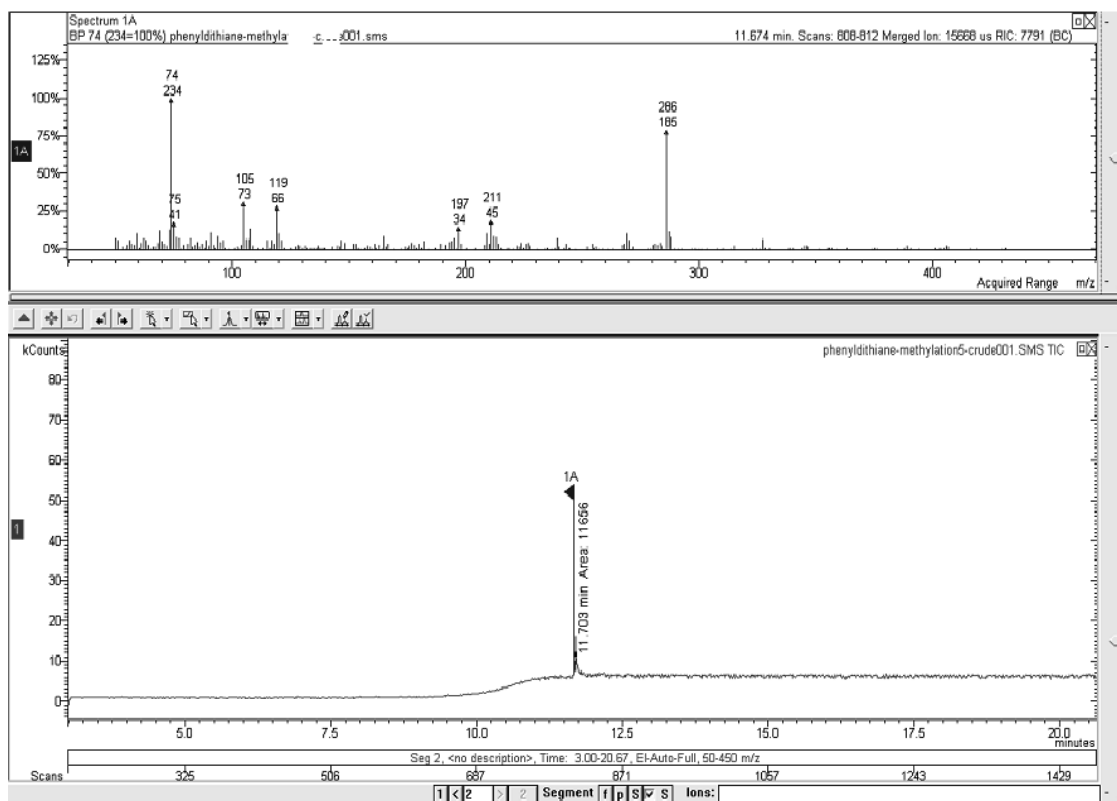
Figure 7.22. GC-MS traces and mass spectra (EI) in CH$_3$CN of the crude NMR reaction mixture from the alkylation of **89** using methyl iodide shown in Figure 7.21.
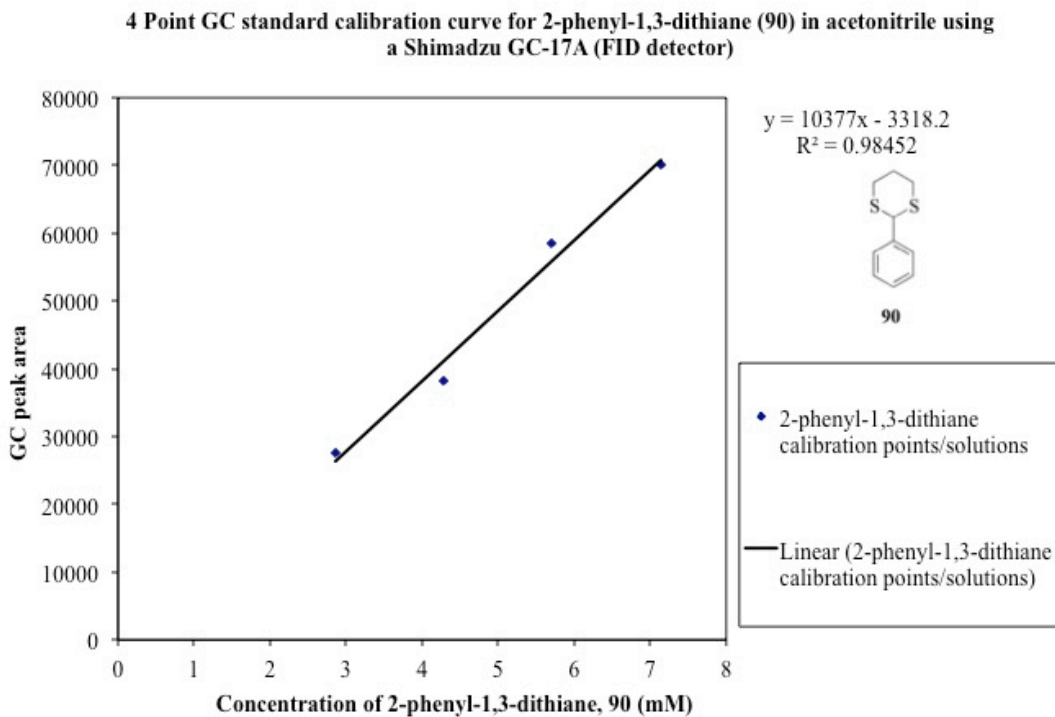
4 Point GC standard calibration curve for 2-phenyl-1,3-dithiane (90) in acetonitrile using a Shimadzu GC-17A (FID detector)

$y = 10377x - 3318.2$
$R^2 = 0.98452$

90

• 2-phenyl-1,3-dithiane calibration points/solutions

—Linear (2-phenyl-1,3-dithiane calibration points/solutions)

Figure 7.23. Four-point GC calibration curve of 2-phenyl-1,3-dithiane, **90**/CH$_3$CN.

Calculating the yield of 107 in the crude reaction mixture shown in Scheme 7.8.

Not shown here is the derivation of the concentrations of all values for **90** which were directly obtained from the chromatogram with the product mixtures and the 4-point calibration curve above (Figure 7.23). The concentrations in the reaction crude mixture of **107** was obtained from the following external standard equation (eq. 7.1).

$$C_x = \frac{A_x}{A_{st}} (C_{st}) \qquad\qquad (eq.\ 7.1)$$

Where C_x = concentration of the desired unknown in the mixture

A_x = GC peak area of the desired unknown in the mixture

C_{st} = concentration of the external standard used

A_{st} = GC peak area of the external standard

In this case, from the peak area of the mixture containing **90** and **107**, one obtains a concentration of 1.64 mM for **90** from the calibration curve in Figure 7.23. A 2.04 mM external standard was separately injected into the GC (at least 3-4 times). The peak area for the standard (A_{st}) was 16784 and the concentration of the external standard (C_{st} = 2.04 mM). The peak area for the unknown, **107** in the crude mixture was 19807 (i.e. A_x).

Therefore from eq. 7.1 we get the following results

$$C_x = \frac{19807}{16784} (2.04 \text{ mM}) = 2.41 \text{ mM}$$

2.41 mM is thus the concentration of **107** in the unknown crude mixture and again 1.64 mM is the concentration of **90** in the mixture that was determined from the calibration curve (Figure 7.23) of **90**. This therefore yields ~60 % for **107** and ~40 % for **90** respectively.
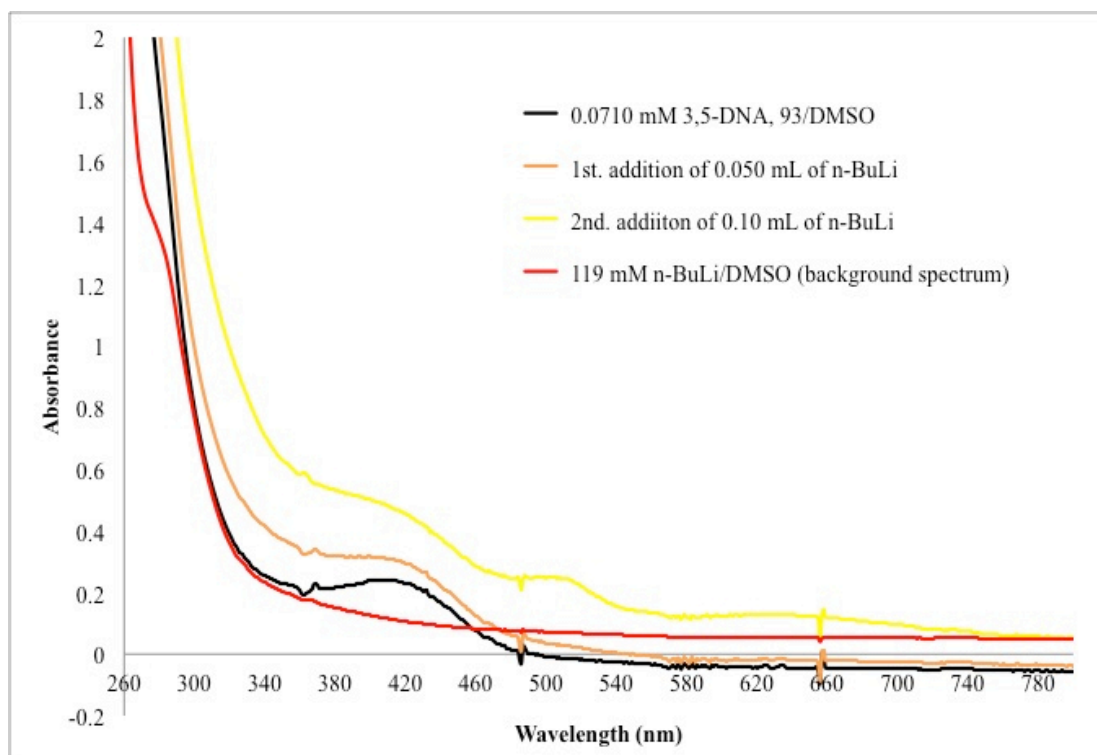
Figure 7.24. UV-Vis spectra of 0.0710 mM 3,5-dinitroaniline (3,5-DNA), **93**/DMSO (black spectrum) and the addition of 2.50 M *n*-BuLi/hexanes (yellow, and orange spectra). Also, shown is a background spectrum consisting of a 119 mM *n*-BuLi solution in DMSO (red spectrum).
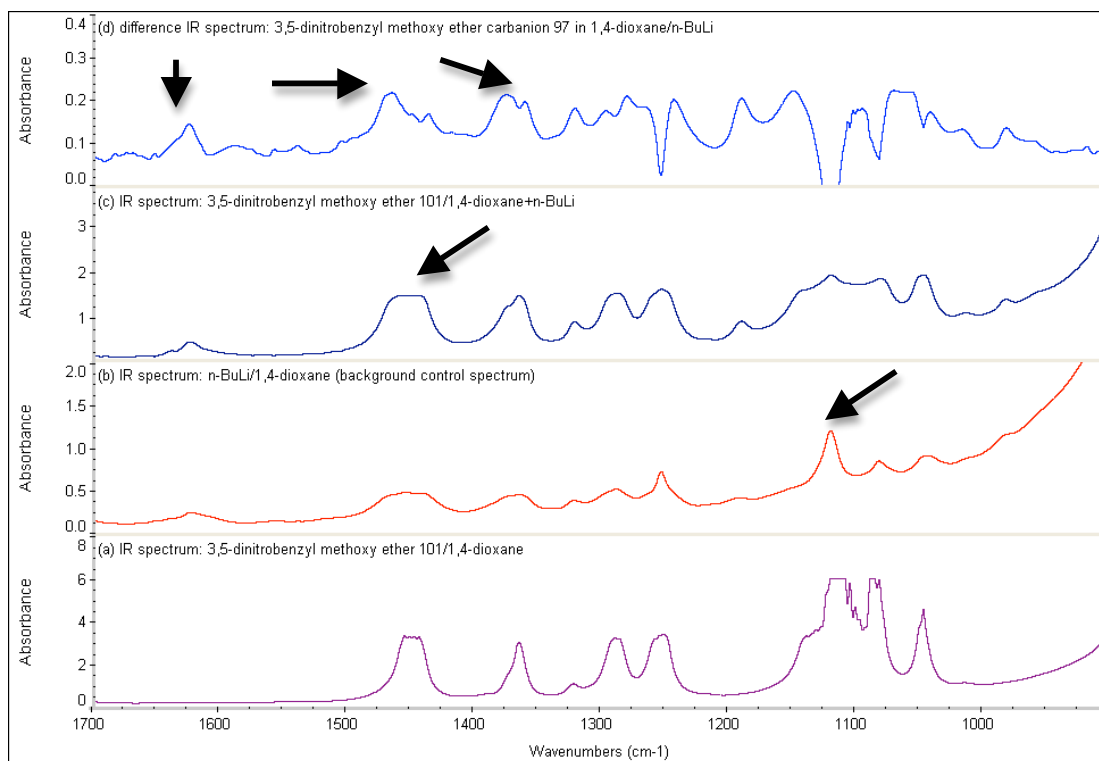
Figure 7.25. FT-IR spectra of the 3,5-dinitrobenzyl methoxy ether anion, **97** generated in 1,4-dioxane with the addition of excess *n*-BuLi (2.50 M), fingerprint region between 900-1700 cm^{-1}. Each IR sample was taken (*ca.* 80.0 μL aliquots) from a stock solution of known concentration. (a) 2.01×10^{-2} mmol aliquot of 3,5-dinitrobenzyl methoxy ether, **101**/1,4-dioxane. (b) 3.33×10^{-2} mmol *n*-BuLi/1,4-dioxane aliquot background IR spectrum. (c) 1.79×10^{-2} mmol aliquot of 3,5-dinitrobenzyl methoxy ether, **101**/1,4-dioxane and a 3.75×10^{-2} mmol aliquot of *n*-BuLi added. (d) Difference spectrum of anion **97**: IR spectrum (c) - 2.01×10^{-2} mmol aliquot of 3,5-dinitrobenzyl methoxy ether, **101**/1,4-dioxane (a) – 3.33×10^{-2} mmol aliquot *n*-BuLi/1,4-dioxane (b). Arrows in IR spectrum (d) indicate some prominent absorbance bands for the 3,5-dinitrobenzyl methoxy ether carbanion **97** that survive the subtraction of the IR bands associated with the original 3,5-dinitrobenzyl methoxy ether **101**, solvent (1,4-dioxane), and base (*n*-BuLi). The arrow in IR spectrum (c) indicates a change in the overall IR absorbance bands in this region compared to that shown in the IR spectra in (a) and (b). IR spectrum (b) has a single absorbance band attributed to the base (*n*-BuLi) in 1,4-dioxane, and an arrow depicts this specific band.
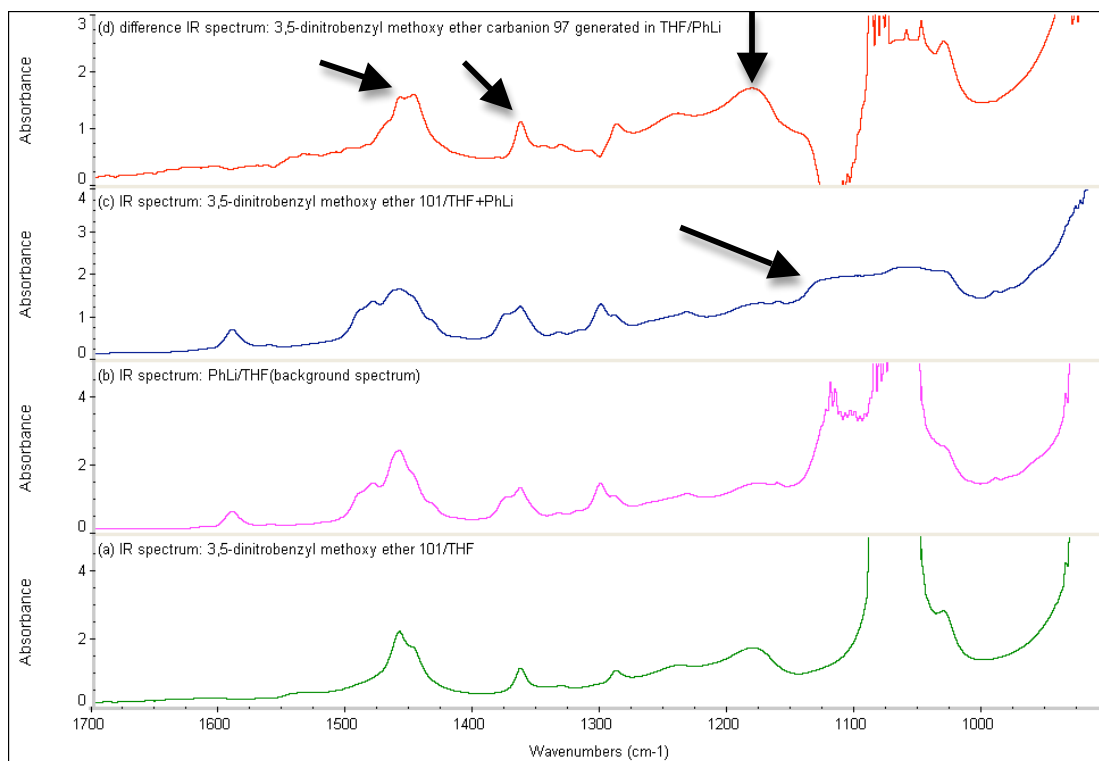
Figure 7.26. FT-IR spectra of the 3,5-dinitrobenzyl methoxy ether anion, **97** generated in THF with the addition of excess PhLi (1.80 M), fingerprint region between 900-1700 cm^{-1}. Each IR sample was taken (*ca.* 80.0 µL aliquots) from a stock solution of known concentraion. (a) 2.28×10^{-2} mmol aliquot of 3,5-dinitrobenzyl methoxy ether, **101**/THF. (b) 1.03×10^{-2} mmol PhLi/THF aliquot background IR spectrum. (c) 1.87×10^{-2} mmol aliquot of 3,5-dinitrobenzyl methoxy ether, **101**/THF and a 3.54×10^{-2} mmol aliquot of PhLi added. (d) Difference spectrum of anion **97**: IR spectrum (c) – 2.28×10^{-2} mmol aliquot of 3,5-dinitrobenzyl methoxy ether, **101**/THF (a) – 1.03×10^{-2} mmol aliquot PhLi/THF (b). Arrows in IR spectrum (d) indicate some prominent absorbance bands for the 3,5-dinitrobenzyl methoxy ether carbanion **97** that survive the subtraction of the IR bands associated with the original 3,5-dinitrobenzyl methoxy ether **101**, solvent (THF), and base (PhLi). The arrow in IR spectrum (c) indicates a change in the overall IR absorbance bands in this region compared to that shown in the IR spectra in (a) and (b).
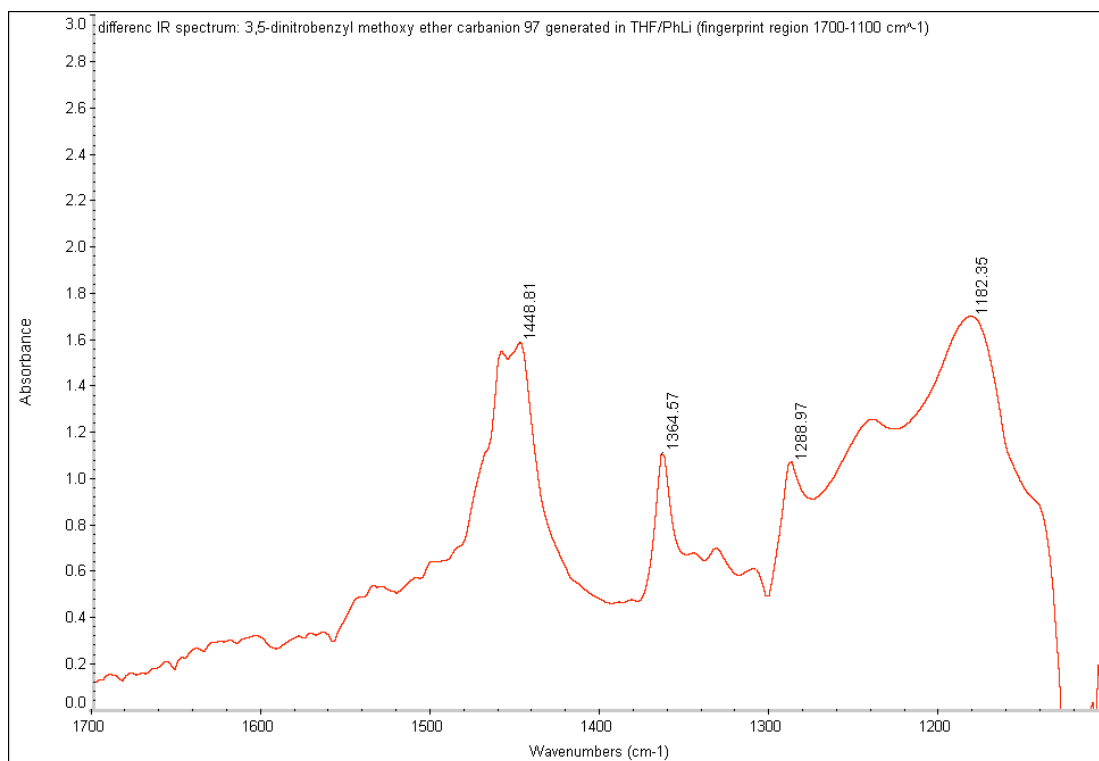
242

Figure 7.27. Enlarged difference IR spectrum of anion **97** shown in Figure 7.26d in the fingerprint region between 1100-1700 cm^{-1}. Key IR absorbance frequencies are marked which survive our background subtraction of the solvent (THF), base (PhLi), and the original 3,5-dinitrobenzyl methoxy ether **101**.
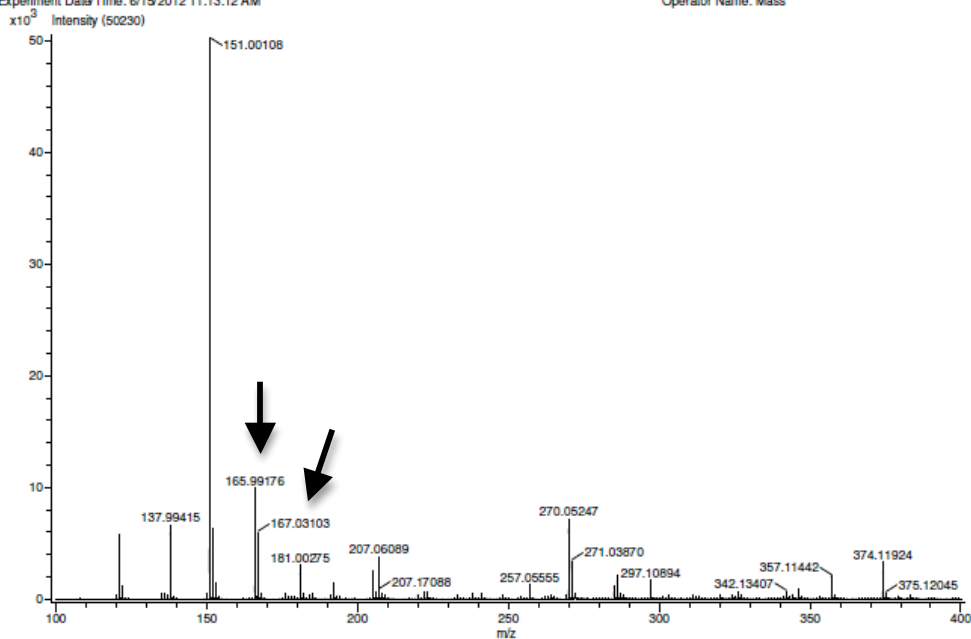
Figure 7.28. DART(-) mass spectrum of the resulting crude NMR mixture containing *p*-nitrobenzyl methoxy ether, **102**/*d₈*-THF, *n*-BuLi, and CD₃OD from the NMR experiment shown in Figure 6.3c. Arrows indicate the masses associated with the M⁺ - 1 peak of 167 and M⁺ - 2 peak of 165, which demonstrates that either the parent *p*-nitrobenzyl methoxy ether **102** (M⁺ = 167) or the monodeuterated *p*-nitrobenzyl methoxy ether **102** (M⁺ = 168) are present in this experimental reaction mixture.
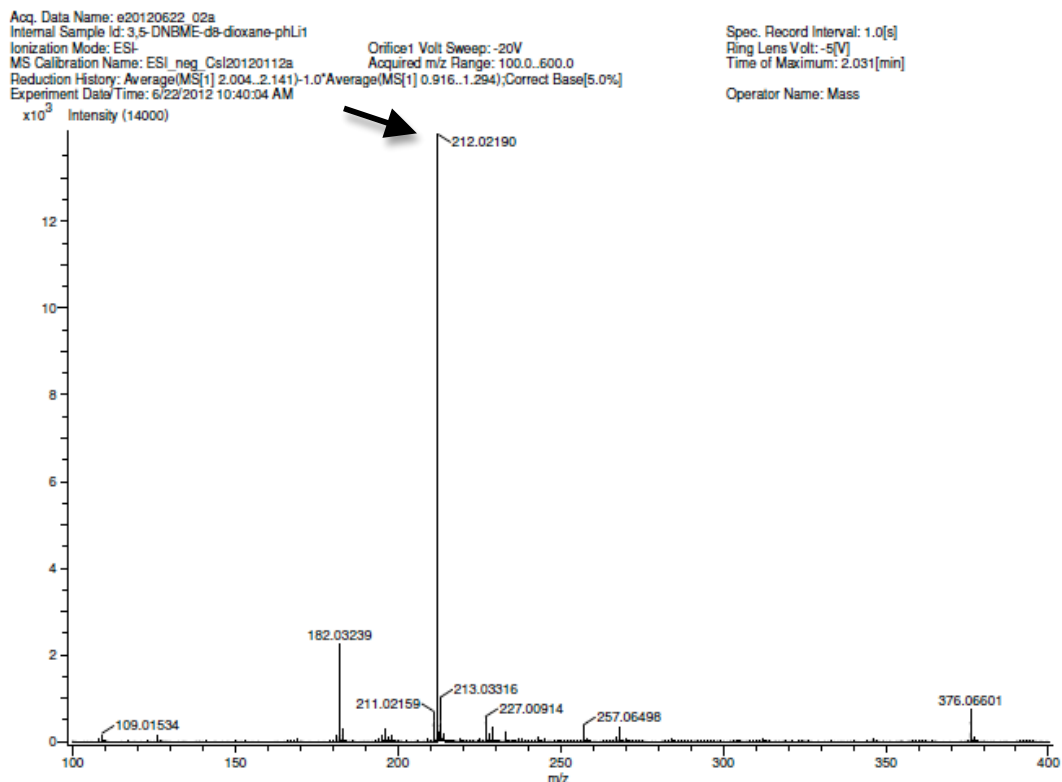
Figure 7.29. DART(-) mass spectrum of the resulting crude NMR mixture containing 3,5-dinitrobenzyl methoxy ether, **101**/d_8-dioxane, PhLi, and CD$_3$OD from the NMR experiment shown in Figure 6.4c. The arrow in this figure indicates the mass associated with the M$^+$ - 1 peak of 212, which demonstrates that the parent 3,5-dinitrobenzyl methoxy ether **101** (M$^+$ = 212) was reformed or is present as the major product in this experimental reaction mixture.

Bibliography

(1) Amyes, T. L.; Stevens, I. W.; Richard, J. P. *J. Org. Chem.* **1993**, *58*, 6057-6066.

(2) Lowry, T. H.; Richardson, K. S. *Mechanisms and Theory of Organic Chemistry*, 2nd Ed. ; Harper and Row: New York, 1981.

(3) Ansyln, E. V.; Dougherty, D. A. *Modern Physical Organic Chemistry*, Illustrative edition; University Science Books: California, 2005.

(4) Laube, T.; Olah, G. A.; Bau, R. *J. Am. Chem. Soc.* **1997**, *119*, 3087-3092.

(5) Olah, G. A.; Shamma, T.; Burrichter, A.; Rasul, G.; Surya Prakash, G. K. *J. Am. Chem. Soc.* **1997**, 119, 12923-12928.

(6) Bartl, J.; Steenken, S.; Mayr, H.; McClellend, R. A. *J. Am. Chem. Soc.* **1990**, *112*, 6918-6928.

(7) Kirmse, W.; Kilian, J. *J. Am. Chem. Soc.* **1990**, *112*, 6399-6400.

(8) Zimmerman, H. E.; Somasekhara, S. *J. Am. Chem. Soc.* **1963**, *85*, 922-927.

(9) Zimmerman, H. E.; Sandel, V. R. *J. Am. Chem. Soc.* **1963**, *85*, 915-921.

(10) Zimmerman, H. E. *J. Phys. Chem. A* **1998**, *102*, 5616-5621.

(11) Eliel, E. L.; Abatjoglou, A. G.; Kuyper, L. F. *J. Am. Chem. Soc.* **1977**, *99*, 8262-8269.

(12) (a) Borden, W. T. *Diradicals,* Wiley and Sons: New York, 1982. (b) Lahti, P. M. *Magnetic Properties of Organic Materials*, Ed.; Marcel Dekkar: New York, 1999. (c) Itoh, K.; Kinoshita, M. *Molecular Magnetisim*, Eds.; Kodansha, Tokyo, 1999. (d) Crayston, J. A.; Devine, J. N.; Walton, J. C. *Tetrahedron* **2000**, *56*, 7829. (e) Nozawa, T.; Nagata, M.; Ichinohe, M.; Sekiguchi, A. *J. Am. Chem. Soc.* **2011**, *133*, 5773-5775. (f) Shil, S.; Misra, A. *J. Phys. Chem. A* **2010**, *114*, 2022-2027. (g) Shultz, D. A.;

Fico, R. M.; Bodner, S. H.; Kumar, R. K.; Vostrikove, K. E.; Kampf, J. W.; Boyle, P.D. *J. Am. Chem. Soc.* **2003**, *125*, 11761-11771. (h) Oka, H. *Org. Lett.* **2010**, *12*, 448-451. (i) Rajca, A.; Wongsriratanakul, J.; Rajca, S. *Science*, **2001**, *294*, 1503-1505. (j) Lochmann, L.; Bauer, W. *J. Am. Chem. Soc.* **1992**, *114*, 7482-7489.

(13) Schlenk, W.; Brauns, M. *Chem. Ber.* **1915**, *48*, 716.

(14) Kothe, G.; Denkel, K-H; Summermann, W. *Angew. Chem. Intl. Ed. Engl.* **1970**, *9*, 906.

(15) Dowd, P. *J. Am. Chem. Soc.* **1966**, *88*, 2587.

(16) Goodman, J. L.; Berson, J. A. *J. Am. Chem. Soc.* **1984**, *106*, 1867-1868.

(17) Wright, B. B.; Platz, M. S. *J. Am. Chem. Soc.* **1983,** *105*, 628-630.

(18) Jordan, K. D.; Naghticall, P. *J. Am. Chem. Soc.* **1993**, *115*, 270-271.

(19) Flynn, C. R.; Michl, J. *J. Am. Chem. Soc.* **1974**, *96*, 3280-3288.

(20) Bakuzis, P.; Kochi, J. K.; Krusic, P. J. *J. Am. Chem. Soc.* **1970,** *92*, 1436-1438.

(21) Ovchinnikov, A. A. *Theor. Chim. Acta* **1978**, 47.

(22) Inglin, T. A.; Berson, J. A. *J. Am. Chem. Soc.* **1986**, *108*, 3394-3402.

(23) Rajca, A.; Olankitanit, A.; Rajca, S. *J. Am. Chem. Soc.* **2011**, *133*, 4750-4753.

(24) Moss, R. A.; Platz, M. S.; Jones, Jr., M. *Reactive Intermediate Chemistry*, Wiley and Sons, In.c: Hoboken, New Jersey, **2004**.

(25) Tomioka, H.; Okada, H.; Watanabe, T.; Kohji, B.; Komatsu, K.; Hirai, K. *J. Am. Chem. Soc.* **1997**, *119,* 1582-1593.

(26) Hirai, K.; Yasuda, K.; Tomioka, H. *Chem. Lett.* **2000**, 29, 398-399.

(27) Teki, Y.; Fujita, I.; Takui, T.; Kinoshita, T.; Itoh, K. *J. Am. Chem. Soc.* **1994**, *116*, 11499-11505.

(28) Hrovat, D. A.; Waali, E. E.; Borden, W. T. *J. Am. Chem. Soc.* **1992,** *114*, 8698.

(29) Kim, S.-J.; Hamilton, T. P.; Schaefer, H. F. *J. Am. Chem. Soc.* **1992**, *114*, 5349.

(30) Smith, P. A. S. *Azides and Nitrenes*, E. F. V. Scriven, Ed., Academic Press: New York, 1984, p. 8.

(31) Gritsan, N. P.; Gudmundsdottir, A.; Tigelaar, D.; Zhu, Z.; Karney, W. L., Hadad, C. M.; Platz, M. S. *J. Am. Chem. Soc.* **2001**, *123*, 1951-1962.

(32) Wasserman, E.; Murray, R. W.; Yager, W. A.; Trozzolo, A. M.; Smolinsky, G. *J. Am. Chem. Soc.* **1967**, *89*, 5076-5078.

(33) Kalgutkar, R. S.; Lahti, P. M. *J. Am. Chem. Soc.* **1997**, *119*, 4771-4772.

(34) Tomioka, H.; Sawai, S. *Org. Biomol. Chem.* **2003**, *1*, 4441-4450.

(35) Chapyshev, S. V.; Korchagin, D. V.; Budyka, M. F.; Gavrishova, T. N.; Neuhaus, P.; Sander, W. *J. Phys. Chem. A* **2011**, *115*, 8419-8425.

(36) Wright, B. B.; Platz, M. S. *J. Am Chem. Soc.* **1983**, *105*, 628-630.

(37) Wenthold, P. G.; Kim, J. B.; Lineberger, W. C. *J. Am. Chem. Soc.* **1997**, *119*, 1354-1359.

(38) Neuhaus, P.; Grote, D.; Sander, W. *J. Am. Chem. Soc.* **2008**, *130*, 2993-3000.

(39) Rajca, A.; Olankitwanit, A.; Rajca, S. *J. Am. Chem. Soc.* **2011**, *133*, 4750-4753.

(40) Winter, A. H.; Falvey, D. E.; Cramer, C. J. *J. Am. Chem. Soc.* **2004**, *126*, 9661-9668.

(41) Winter, A. H.; Falvey, D. E.; Cramer, C. J.; Gherman, B. F. *J. Am. Chem. Soc.* **2007**, *129*, 10113-10119.

(42) Winter, A. H.; Falvey, D. E. *J. Am. Chem. Soc.* **2010**, *132*, 215-222.

(43) Anderson, G. B.; Yang, L. L-N.; Falvey, D. E. *J. Am. Chem. Soc.* **1993**, *115*, 7254-7262.

(44) Robbins, R. J.; Laman, D. M.; Falvey, D. E. *J. Am. Chem. Soc.* **1996**, *118*, 8127-8135.

(45) Anderson, G. B.; Falvey, D. E. *J. Am. Chem. Soc.* **1993**, *115*, 9870-9871.

(46) Chiapperino, D.; Anderson, G. B.; Robbins, R. J.; Falvey, D. E. *J. Org. Chem.* **1996**, *61*, 3195-3199.

(47)   Robbins, R. J.; Laman, D. M.; Falvey, D. E. *J. Am. Chem. Soc.* **1995**, *117*, 6544-6552.

(48) Robbins, R. J.; Falvey, D. E. *Tetrahedron Lett.* **1994**, *35*, 4943-4946.

(49) Srivastava, S.; Falvey, D. E. *J. Am. Chem. Soc.* **1995**, *117*, 10186-10193.

(50) Stephens, P. J.; Dvlin, F. J.; Chabalowski, C. F.; Frisch, M. J. *J. Phys. Chem.* **1994**, *98*, 11623-11627.

(51) Perdew, J. P.; Yue, W.; *Phys. Rev. B.* **1996**, *33*, 8800-8802.

(52) Lee, C. T.; Yang, W. T.; Parr, R. G. *Phys. Rev. B.* **1988**, *37*, 785-789.

(53) Krylov, A. I. *Acc. Chem. Res.* **2006**, *39*, 83-91.

(54) Bally, T.; Borden, W. T. *Rev. Comput. Chem.* **1999**, *13*, 1-97.

(55) Becke, A. D. *J. Chem. Phys.* **1993**, *98*, 5648-5652.

(56) Poutsma, J. C.; Upshaw, S. D.; Squires, R. R.; Wenthold, P. G. *J. Phys. Chem. A* **2002**, *106*, 1067-1073.

(57) Cramer, C. J. *J. Am. Chem. Soc.* **1999**, *120*, 6261-62569.

(58) Anderson, K.; Malmqvist, P. A.; Ross, B. O. *J. Chem. Phys.* **1992**, *96*, 1218-1226.

(59) Ess, D. H.; Johnson, E. R.; Hu, X. Q.; Yang, W. T. *J. Phys. Chem. A* **2011**, *115*, 76-83.

(60) Wright, B. B.; Platz, M. S. *J. Am. Chem. Soc.* **1983**, *105*, 628-630.

(61) Gunther, H. *J. Braz. Chem. Soc.* **1999**, *10*, 241.

(62) Cupas, C. A.; Comisarow, M. B.; Olah, G. A. *J. Am. Chem. Soc.* **1966**, *88*, 361-362.

(63) Olah, G. A.; Porter, R. D.; Jeuell, C. L.; White, A. N. *J. Am. Chem. Soc.* **1972**, *94*, 2044-2052.

(64) Carlin, R. L. *Magnetochemistry*, Springer, Heidelberg, Germany, **1986**, pp. 5-18.

(65) Dowd, P. *J. Am. Chem. Soc.* **1966**, *88*, 2587.

(66) Dowd, P. *Acc. Chem. Res.* **1966**, *88*, 2587.

(67) Burns, G. *J. Appl. Phys.* **1961**, *32*, 2048.

(68) Wertz, J. E.; Bolton, , J. R. *Electron Spin Resonance Elementary Theory and Practial Applications*, McGraw Hill, New York, **1972**, Chapter 10.

(69) Wasserman, E.; Snyder, L. C.; Yager, W. A. *J. Chem. Phys.* **1964**, *41*, 1763.

(70) Gordy, W. *Theory and Applications of Electron Spin Resonance,* West, W., Ed., Wiley and Sons, Inc., New York, **1980**, vol. 15, p. 589 (A Weissberger series Ed.).

(71) Löliger, J.: Scheffold, R. *J. Chem. Ed.* **2972**, *49*, 646-647.

(72) Ostfeld, D.; Cohen, A. *J. Chem Ed.* **1972**, *49*, 829.

(73) Piguet, C. *J. Chem. Ed.* **1997**, *74*, 815-816.

(74) Crawford, T. H.; Swanson, J. *J. Chem. Ed.* **1971**, *48*, 382-386.

(75) Grant, D. H. *J. Chem. Educ.* **1995**, *72*, 39-40.

(76) Schubert, E. M. *J. Chem. Educ.* **1992**, *69*, 62.

(77) He, Y.; Pan, W.; Zhao, H.; Wang, S. *Synth. Commun.* **1999**, *19*, 3051-3054.

(78) Bordwell, F. G. *Acc. Chem. Res.* **1988**, *21*, 456-463.

(79) Hilborn, J. W.; Pincock, J. A. *J. Am. Chem. Soc.* **1991**, *113*, 2683-2686.

(80) Reichardt, C.; Schafer, G. *Liegis Ann.* **1995**, (8), 1579-1582.

(81) Ruane, P. H.; Bushan, K. M.; Pavlos, C. M.; D'Sa, R. A.; Toscano, J. P. *J. Am. Chem. Soc.* **2002**, *124*, 9806-9811. The one example where **42** is generated photochemically is complicated by competition between heterolysis to form the targeted cation and fragmentation within the diazeniumdiolate leaving group itself.

(82) Babadzhanova, L. A.; Kirij, N. V.; Yagupolskii, Y. L.; Tyrra, W.; Naumann, D. *Tetrahedron*, **2005**, *61*, 1813-1819.

(83) Fuji, K.; Ueda, M.; Sumi, K.; Kajiwara, K.; Fujita, E.; Iwashita, T.; Miura, I. *J. Org. Chem.* **1985**, *50*, 657-661.

(84) Eliel, E. L.; Jernigan, M. T. *J. Am. Chem. Soc.* **1995**, *117*, 9638-9644.

(85) Broaddus, C. D. *J. Am. Chem. Soc.* **1968**, *90*, 5504-5511.

(86) Mohrig, J. R.; Reiter, N. J.; Kirk, R.; Zawadski, M. R.; Lamarre-Vincent, N. *J. Am. Chem. Soc.* **2011**, *133*, 5124-5128.

(87) Buncel, E.; Menon, B. *J. Am. Chem. Soc.* **1977**, *99*, 4457-4461.

(88) Zoltewicz,, J. A.; Kauffman, G. M. *J. Org. Chem.* **1969**, *34*, 1405-1411.

(89) Corey, E. J.; Seebach, D. *Angew. Chem. Int. Engl.* **1965**, *4*, 1075-1077.

(90) Corey, E. J.; Seebach, D. *Angew. Chem. Int. Engl.* **1965**, *4*, 1077-1078.

(91) Corey, E. J.; Seebach, D. *J. Org. Chem.* **1966**, *31*, 4097-4099.

(92) Seebach, D.; Jones, N. R.; Corey, E. J. *J. Org. Chem.* **1968**, *33*, 300-305.

(93) Seebach, D.; Corey, E. J. *Org. Synth.* **1968**, *50*, 72.

(94) Seebach, D.; Corey, E. J. *J. Org. Chem.* **1975**, *40*, 231-237.

(95) Stowell, M. H.. B.; Rock, R. S.; Rees, D. C.; Chan, S. I. *Tetrahedron Lett.* **1996**, *37*, 307-810.

(96) Hassan, H. H. A. M.; Tamm, C. *Helv. Chim. Acta.* **1996**, *79*, 518-526.

(97) Lee, H. B.; Balasubramian, S. *J. Org. Chem.* **1999**, *64*, 3454-3460.

(98) Bräuer, M.; Weston, J.; Anders, E. *J. Org. Chem.* **2000**, *65*, 1193-1199.

(99) Okazaki, R.; O-oka, M.; Akiyama, T.; Inamoto, N.; Niwa, J.; Kato, S. *J. Am. Chem. Soc.* **1987**, *109*, 5413-5419.

(100) Hemberger, P.; Noller, B.; Steinbauer, M.; Fischer, K.; Fischer, I. *J. Phys. Chem Lett.* **2010**, *1*, 228-231.

(101) (a) Valentyna, V.; Wilson, R. M.; Panov, M.; Tamovsky, A. N.; Krause, J. A.; Vyas, S.; Winter, A. H.; Hadad, C. M. *J. Am. Chem. Soc.* **2009**, *131*, 11535-11547. (b) Winter, A. H.; Thomas, S. I.; Kung, A. C.; Falvey, D. E. *Org. Lett.* **2004**, *6*, 4671-4674. (c) Winter, A. H.; Gibson, H. H.; Falvey, D. E. *J. Org. Chem.* **2007**, *72*, 8186-8195.

(102) Klima, R. F.; Jadhav, A. V.; Singh, P. N. D.; Chang, M.; Vanos, C.; Sankaranarayaman, J.; Vu, M.; Ibrahim, N.; Ross, E.; McCloskey, S.; Murthy, R. S.; Rause, J. A.; Ault, B. S.; Gudmundsdóttir, A. D. *J. Org. Chem.* **2007**, *72*, 8186-8195.

(103) Cu, A.; Testa, A. C. *J. Am. Chem. Soc.* **1974**, *96*, 1963-1965.

(104)   Banik, B. K.; Mukhopadhyay, C.; Verkatraman, M.S.; Becker, F. F. *Tetrahedron Lett.* **1998**, *39*, 7243-7246.

(105) Anker, T.; Hilmerson, G. *Tetrahedron Lett.* **2007**, *48*, 5707-5710.

(106) Perrotta, R. R.; Winter, A. H.; Coldren, W. H.; Falvey, D. E. *J. Am. Chem. Soc.* **2011**, *133*, 15553-15558.

(107) Perrotta, R. R.; Winter, A. H.; Falvey, D. E. *Org. Lett.* **2011**, *13*, 212-215.

(108) Kemister, G.; Pross, A.; Radom, L.; Taft, R. W. *J. Org. Chm.* **1980**, *45*, 1056-1060.

(109) Krygowski, T. M.; Jezierka, A.; Panek, J. J.; Szatylowicz, H. *J. Phys. Chem. A* **2009**, *113*, 5800-5805.

(110)   Algrim, D.; Vanier, N. R.; Bordwell, F. G. *J. Org. Chem.* **1977**, *42*, 1817-1819.

(111) Algrim, D. J.; Bordwell, F. G. *J. Am. Chem. Soc.* **1988**, *110*, 2964-2968.

(112)   Fu, Y.; Liu, L.; Li, R-Q.; Liu, R.; Guo, G-X. *J. Am. Chem. Soc.* **2004**, *126*, 814-822.

(113)   Ando, R. A.; Borin, A. C.; Santos, P. S. *J. Phys. Chem. A*, **2007**, *111*, 7194-7199.

(114)   Vakula, N. I.; Kuramshina, G. M.; Makhmutova, S. F.; Pentin, Y. A. *Struct. Chem.* **2011**, *22*, 345-356.

(115)   Meyer, F. K.; Jasinski, J. M.; Rosenfeld, R. N.; Brauman, J. I. *J. Am. Chem. Soc.* **1982**, *104*, 663-667.

(116) Drzaic, P. S.; Brauman, J. I. *J. Phys. Chem.* **1984**, *88*, 5285-5290.

(117) Bowie, J. H.; Raftery, M. J. *Aust. J. Chem.* **1988**, *41*, 1477-1489.

(118) Matthews, W. S.; Bares, J. E.; Bartmess, J. E.; Bordwell, F. G.; Cornforth, F. J.; Drucker, G. E.; Margolin, Z.; McCallum, R. J.; McCollum, G. J.; Vanier, N. R. *J. Am. Chem. Soc.* **1975**, *97*, 7006-7014.

(119) Lambert, J. R.; Shurvell, H. F.; Lightner, D. A.; Cooks, R. G. *Organic Structural Spectroscopy*, Prentice-Hall, Inc.: Upper Saddle River, New Jersey, **1998**.

(120) Laferrière, M.; Sanramé, C. N.; Scaiano, J. C. *Org. Lett.* **2004**, *6*, 873-875.

(121) Cosa, G.; Llauger, L.; Scaiano, J. C.; Miranda, M. A. *Org. Lett.* **2002**, *4*, 3083-3085.

(122) Blake, J. A.; Gagnon, E.; Lukeman, M.; Scaiano, J. C.; *Org. Lett.* **2006**, *8*, 1057-1060.

(123) Xu, M.; Wan, P. *Chem. Commun.* **2000**, *21*, 2147-2148

(124) Komine, N.; Wang, L-F.; Tomooka, K.; Nakai, T. *Tetrahedron Lett.* **1999**, *40*, 6809-6812.

(125) Vicic, D. A.; Jones, G. D. *Comprehensive Organometallic Chemistry III, From Fundametals to Applications*, **2007**, vol. 1, 197-218.

(126) Mong, K.-K. T.; Niu, A.; Chow, H-F.; Wu, C.; Li, L.; Chen, R. *Chem. Eur. J.* **2001**, *7*, 686-699.

(127) Pickaert, G.; Cesario, M.; Ziessel, R. *J. Org. Chem.* **2004**, *69*, 5335-5341.